DOCTORAL THESIS

Interactions of Metal Ions with Peptides and Proteins Related to Alzheimer's Disease

Elina Berntsson

Interactions of Metal Ions with Peptides and Proteins Related to Alzheimer's Disease

ELINA BERNTSSON

TAL
TECH
PRESS

TALLINN UNIVERSITY OF TECHNOLOGY
School of Science
Department of Chemistry and Biotechnology
This dissertation was accepted for the defense of the degree of Doctor of Philosophy in Gene Technology on 20/12/2024

Supervisor:

Prof. Peep Palumaa
Department of Chemistry and Biotechnology
Tallinn University of Technology
Tallinn, Estonia

Co-supervisors:

PhD. Sebastian Wärmländer
Cellpept Sweden AB
Stockholm, Sweden

PhD. MD. Per M Roos
Department of Clinical Neuroscience
Karolinska Institute
Stockholm, Sweden

Opponents:

Prof. Jan Johansson
Department of Medicine
Karolinska Institute
Stockholm, Sweden

Prof. Ago Rinken
Institute of Chemistry
University of Tartu
Tartu, Estonia

Defence of the thesis: 31/01/2025, Tallinn

Declaration:
Hereby I declare that this doctoral thesis, my original investigation and achievement, submitted for the doctoral degree at Tallinn University of Technology has not been submitted for doctoral or equivalent academic degree.

Elina Berntsson

_____
signature

Metallioonide interaktsioonid Alzheimeri tõvega seotud peptiidide ja valkudega

ELINA BERNTSSON

Table of contents

List of publications

The list of author's publications, on the basis of which this thesis has been prepared:

I **Berntsson, E**., Sardis, M., Noormägi, A., Jarvet, J., Roos, P. M., Tõugu, V., Gräslund, A., Palumaa, P., & Wärmländer, S. (2022). Mercury Ion Binding to Apolipoprotein E Variants ApoE2, ApoE3, and ApoE4: Similar Binding Affinities but Different Structure Induction Effects. *ACS Omega*, *7*(33), 28924–28931.

II **Berntsson, E**., Vosough, F., Svantesson, T., Pansieri, J., Iashchishyn, I. A., Ostojic, L., Dong, X., Paul, S., Jarvet, J., Roos, P. M., Barth, A., Morozova-Roche, L. A., Gräslund, A., & Wärmländer, S. (2023). Residue-specific binding of Ni(II) ions influences the structure and aggregation of amyloid beta (Abeta) peptides. *Scientific Reports*, *13*(1), 3341.

III Noormägi, A., Golubeva, T., **Berntsson, E**., Wärmländer, S., Tõugu, V., & Palumaa, P. (2023). Direct Competition of ATCUN Peptides with Human Serum Albumin for Copper(II) Ions Determined by LC-ICP MS. *ACS Omega*, *8*(37), 33912–33919.

IV **Berntsson, E**., Vosough, F., Noormägi, A., Padari, K., Asplund, F., Gielnik, M., Paul, S., Jarvet, J., Tõugu, V., Roos, P. M., Kozak, M., Gräslund, A., Barth, A., Pooga, M., Palumaa, P., & Wärmländer, S. (2023). Characterization of Uranyl (UO_2^{2+}) Ion Binding to Amyloid Beta (Abeta) Peptides: Effects on Abeta Structure and Aggregation. *ACS Chem Neurosci*, *14*(15), 2618–2633.

Author's contribution to the publications

Contribution to the papers in this thesis are:

I The author performed and analyzed all the CD measurements and contributed to the fluorescence studies as well as participated in the manuscript preparation and writing.

II The author contributed to the planning of the study, analysis of the data, the preparation and the writing of the manuscript. Performed and analyzed the NMR, CD and fluorescence studies.

III The author participated in sample preparation, measurements and in the writing process.

IV The author conducted and analyzed the NMR, CD and fluorescence studies and contributed to the manuscript writing.

.

List of additional papers – not included in the thesis

Berntsson, E., Paul, S., Vosough, F., Sholts, S. B., Jarvet, J., Roos, P. M., Barth, A., Gräslund, A., & Wärmländer, S. (2021). Lithium ions display weak interaction with amyloid-beta (Abeta) peptides and have minor effects on their aggregation. Acta Biochimica Polonica, 68(2), 169–179.

Koski, L., Ronnevi, C., **Berntsson, E**., Wärmländer, S., & Roos, P. M. (2021). Metals in ALS TDP-43 Pathology. International Journal of Molecular Sciences, 22(22).

Paul, S., Jenistova, A., Vosough, F., **Berntsson, E**., Mörman, C., Jarvet, J., Gräslund, A., Wärmländer, S., & Barth, A. (2023). (13)C- and (15)N-labeling of amyloid-beta and inhibitory peptides to study their interaction via nanoscale infrared spectroscopy. Commun Chem, 6(1), 163.

Koski, L., **Berntsson, E**., Vikström, M., Wärmländer, S., & Roos, P. M. (2023). Metal ratios as possible biomarkers for amyotrophic lateral sclerosis. J Trace Elem Med Biol, 78, 127163.

Wärmländer, S., Lakela, A., **Berntsson, E**., Jarvet, J., Gräslund, A., (2024). Secondary structures of human calcitonin at different temperatures and in different membrane-mimicking environments, characterized by circular dichroism (CD) spectroscopy. *Accepted for publication in ACS Omega.*

Lakela, A., **Berntsson, E**., Vosough, F., Jarvet, J., Paul, S., Barth, A., Gräslund, A., Roos, P., Wärmländer, S. (2024). Molecular interactions, structural effects, and binding affinities between silver ions (Ag$^+$) and amyloid beta (Aβ) peptides. *Accepted for publication in Scientific Reports*.

Introduction

Alzheimer's disease (AD) is one of the most prevalent neurodegenerative disorders and the most common form of dementia worldwide. Despite decades of research, many details about AD pathogenesis remain unclear.

Aggregation of the amyloid-β (Aβ) peptide is one of the hallmarks of AD, and is believed to cause neurotoxicity and synaptic dysfunction, leading to neuronal death and cognitive decline. Aβ aggregates are formed when monomeric Aβ peptides misfold and convert from a random coil structure into a β-pleated-sheet-rich structure, which is more prone to aggregation. The peptides assemble from monomers into oligomers, protofibrils and finally into a mature fibril exhibiting cross-β structure, where the β-strands run perpendicular to the fibril axis.

Several factors have been implicated in the aggregation mechanism and toxicity of Aβ. One such possible factor is interactions with metal ions. Metals such as copper, iron and zinc are abundant in the brain and are required in many physiological processes. Importantly, dysregulation of metal homeostasis has been linked to AD pathogenesis. Maintaining metal homeostasis in the body is crucial, as increased metal ion levels can generate reactive oxygen species (ROS), leading to increased oxidative stress damaging cellular components and contribute to neurodegeneration. In addition, metal ions may directly interact with the Aβ and affect its aggregation.

It is well known that the Aβ aggregation process is sensitive to environmental changes. Minor variations in temperature, pH, peptide concentration, agitation, etc. may have large effects on the aggregation rate and the morphology of the formed aggregates. Therefore, it is not surprising that binding of charged metal ions typically affects the aggregation pathway of the peptide. Metal ions have been shown to modulate peptide aggregation by promoting aggregation of monomeric peptides into fibrils, but also by stabilizing aggregates in the most toxic oligomeric states. Metals such as copper and nickel ions have in this thesis been shown to bind to the Aβ N-terminal, where histidines are implicated as binding residues. In contrast, metal compounds such as the uranyl ion have been shown to interact with the peptide without residue-specific binding, instead affecting the peptide via electrostatic interactions.

Although the Aβ peptide is the most prevalent component of amyloid plaques in AD brains, other proteins such as Apolipoprotein E (ApoE) may also be relevant for the AD pathogenesis. One isoform of the ApoE protein, ApoE4, is known to increase the risk for developing AD, up to four-fold in heterozygotic carriers and up to twelve-fold in homozygotic carriers. Another isoform, ApoE2, seems to protect against the disease. A further interesting aspect of the ApoE protein, in relation to AD and metals, is that carriers of the ApoE4 allele have been shown to be more susceptible to mercury toxicity. It has therefore been suggested that the ApoE protein may play a role in the clearance of mercury, and perhaps also the Aβ peptide.

The aim of this study was to improve the understanding about the role of metal binding in AD pathology. A wide range of spectroscopic methods have been used to investigate the interactions between metal ions and AD related proteins. Although some metals in this study might not be required for biological function, they all occur in the environment and exposure is known to cause toxicity and interfere with normal neurological function. Obtained results widen our insight into the role of metal ions in AD pathology.

Abbreviations

Aβ	Amyloid-β
ACh	Acetylcholine
AD	Alzheimer's disease
AFM	Atomic force microscopy
ALS	Amyotrophic lateral sclerosis
ApoE	Apolipoprotein E
APP	Amyloid precursor protein
ATCUN	Amino-terminal Cu(II) and Ni(II) binding motif
BBB	Blood brain barrier
CAC	Critical aggregation concentration
CD	Circular dichroism
CNS	Central nervous system
CSF	Cerebrospinal fluid
fAD	Familial Alzheimer's disease
HD	Huntington's disease
HSA	Human serum albumin
NFT	Neurofibrillary tangle
NMR	Nuclear magnetic resonance
PD	Parkinsons disease
PSEN	Presenilin
ROS	Reactive oxygen species
sAD	Sporadic Alzheimer's disease
TBI	Traumatic Brain Injury
TEM	Transmission electron microscopy
ThT	Thioflavin T

1 Background

1.1 Folding of proteins

Understanding the basic properties of polypeptide chains is fundamental to comprehending how proteins achieve their diverse functions within biological systems. The primary structure of native proteins usually folds rapidly into a secondary structure, and then into a tertiary three-dimensional structure, largely affected by the properties of the amino acid residues and the surrounding environment to ensure functionality and achieve a state of lowest free energy. The secondary structure of a protein refers to the local folding patterns, where alpha helices and beta sheets are the two most common structures. Both are stabilized by hydrogen bonds between the backbone of the polypeptide chain(s). When a protein or a region of a protein does not form a stable, regular secondary structure, and instead exists in a flexible, disordered and irregular conformation, it is said to be in a random coil structure (Zorko, 2010).

Folding of proteins is driven by various molecular interactions. Van der Waals forces are weak interactions that occur between closely packed atoms, and they help to stabilize folded structures. Disulfide bridges, typically formed by oxidation of cysteine residues, can covalently link distant parts of polypeptide sidechains and thereby further enhance structural stability. Salt bridges can stabilize the structure of a protein by interactions between two oppositely charged amino acids, often arginine or lysine binding to aspartic or glutamic acid. Hydrophobic effects are crucial for reducing the free energy of a system, and it is common that proteins form a hydrophobic core, where nonpolar hydrophobic residues are shielded from the aqueous, polar environment.

Factors such as mutations, translational errors, environmental stress, aging etc. may interfere with the protein folding process. This interference may yield misfolded proteins, which are characterized by deviations from their native, functional three-dimensional conformation. Although human cells have multiple control systems that screen for misfolded proteins, and attempt to correct or degrade them, these systems can sometimes fail. When this happens, misfolded proteins can aggregate, disrupt cellular processes and contribute to the pathology of disease.

1.2 Neurodegeneration

Neurodegenerative diseases are a group of conditions which mainly impact neurons in the brain. The most frequently occurring examples of such diseases are Alzheimer's disease (AD), Parkinson's disease (PD), Huntington's disease (HD) and Amyotrophic lateral sclerosis (ALS). Although all neurodegenerative diseases are different in their specific features, they share several common pathological features, where progressive loss of neurons, synaptic dysfunction, and loss of synaptic connections are the most prominent (Ciurea et al., 2023; Hussain et al., 2018). As different diseases affect different areas of the brain, the symptoms will vary, although it is common to observe cognitive decline, motor dysfunction and behavioral changes in patients (Montero-Odasso et al., 2017; Trojsi et al., 2018). Many neurodegenerative diseases also have a long presymptomatic phase, when changes in the central nervous system (CNS) have started, but no symptoms are yet present in the patient. This makes it difficult to detect and treat the disease before substantial damage already has been made (Katsuno et al., 2018).

Extensive research has been conducted for decades in the field of neurodegeneration, but the underlying mechanisms and many details of the pathogenic mechanisms are for most diseases still not understood.

1.2.1 Proteinopathies

Many neurodegenerative diseases are categorized as proteinopathies, also known as protein conformational diseases. It is a class of diseases characterized by misfolding and aggregation of proteins, resulting in loss of function and/or toxic properties (Bayer, 2015; Noor et al., 2021). Proteinopathies primarily affect the CNS and manifest with a range of symptoms related to CNS dysfunction. Some proteinopathies involve multiple organs and peripheral tissues (Brito et al., 2023; Gertz, 2022; Sack, 2020), these will not be considered in this thesis.

In neurodegenerative proteinopathies (henceforth only called proteinopathies), proteins undergo structural modifications that lead to self-association, elongation, and aggregation into fibrillar structures that can accumulate in the CNS. Molecular processes such as disruptions in protein clearance, post-translational modifications or increased protein production can be observed in several proteinopathies (Bayer, 2015; Ciccocioppo et al., 2020). Many of the proteinopathies are complex and involve more than one type of aggregating protein, which often complicates diagnosis and the development of effective therapies. List of neurodegenerative proteinopathies and related proteins is presented in Table 1.

1.2.1.1 Amyloid formation

In the mid-19th century, researchers first described iodine stainable brain deposits found during autopsies. It was therefore assumed that the deposits consisted of starch, and they were consequently named "amyloid" (derived from the Latin word 'amylum', meaning starch). When the deposits were further studied, a high nitrogen content was detected, which prompted a re-interpretation that resulted in a suggestion that the deposits to a large extent consisted of proteins (Cohen, 1986; Sipe & Cohen, 2000).

Today the deposits are called amyloid plaques, and they are known to play a significant role in the pathogenesis of the diseases grouped as amyloidosis (some of which are listed in table 1). The plaques originate from normally soluble monomeric proteins which misfold, aggregate and assemble into insoluble fibrillar structures. The fibrils adopt a characteristic cross-β sheet structure, where the individual β-sheets run perpendicular to the fibril axis (Figure 1). The fibrils are unbranched and can reach lengths of several μm, with a diameter of approximately 7-12 nm (Chiti & Dobson, 2017; Sunde et al., 1997). Formation of amyloid structures can be monitored directly by transmission electron microscopy or indirectly via dyes, such as Congo red or Thioflavin T (ThT) where the intensity of these dyes is generally considered to correspond to the amount of amyloid material present in the sample (Malmos et al., 2017; Qin et al., 2017).
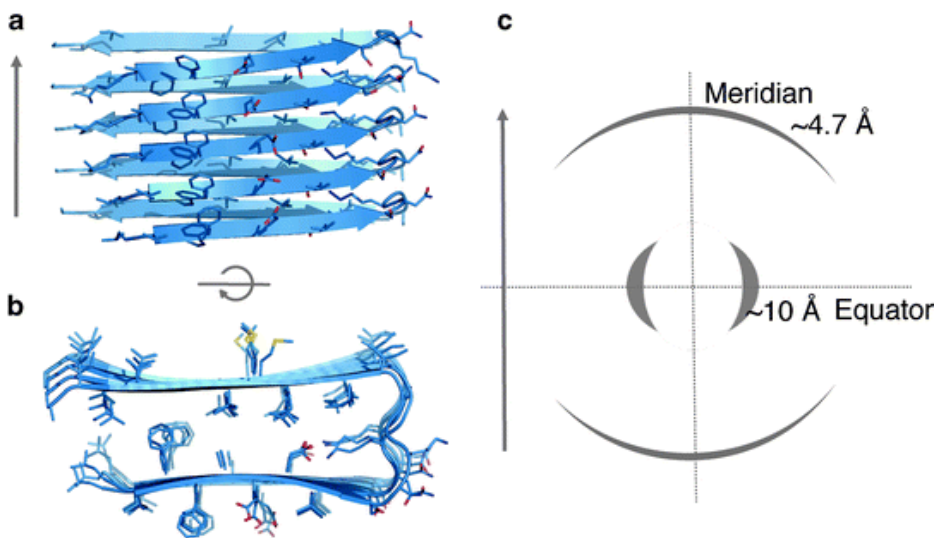
Figure 1. *Typical architecture of a cross-β structure. **a)** Side view of fibril structure composed of stacked β-sheets aligned perpendicular to the fibril axis. **b)** top view of a). **c)** Diffraction pattern of a typical amyloid fibril, where meridian ~4.7 Å corresponds to the regular spacing between β-strands within a β-sheet, and equator ~10 Å indicates the periodicity of β-sheets stacked on top of each other. By Morris and Serpell (2012), reprinted with permission from Springer Nature.*

Table 1. *List of proteinopathies, diseases and related proteins affecting the CNS.*

Type of proteinopathies	Diseases	Proteins involved	References
Amyloidosis	Alzheimer's disease, Cerebral amyloid angiopathy	Aβ	(Glenner & Wong, 1984; Qi & Ma, 2017; Selkoe, 2001)
	Creutzfeldt-Jakob disease, Kuru	Prion protein	(Collinge et al., 2006; Sitammagari & Masood, 2024)
	Type II diabetes	Amylin	(Marzban et al., 2003)
	TTR Amyloidosis	Transthyretin	(Manganelli et al., 2022)
Synucleinopathies	Parkinsons disease, Dementia with Lewy bodies, Multiple system atrophy	α-synuclein	(Ayers et al., 2022; Calabresi et al., 2023)
Tauopathies	Alzheimer's disease, Frontotemporal dementia, Corticobasal degeneration, Picks disease	Tau protein	(Hernandez & Avila, 2007; Medeiros et al., 2011; Probst et al., 1996; Zhang et al., 2020)
TDP-43 proteinopathies	Amyotrophic lateral sclerosis, Frontotemporal lobal degeneration	TDP-43	(Cairns et al., 2007; de Boer et al., 2020)
Huntingtinopathy	Huntington's disease	Huntingtin	(Byrne et al., 2018; Zheng & Diamond, 2012)
FUS Proteinopathies	Amyotrophic lateral sclerosis	FUS	(Assoni et al., 2023; Kamelgarn et al., 2018)
SOD1 Proteinopathies	Amyotrophic lateral sclerosis	Superoxide dismutase 1	(Berdynski et al., 2022; Ruffo et al., 2022)

1.3 Alzheimer's disease

Alzheimer's disease (AD) is a neurodegenerative disease characterized by the accumulation of proteinaceous aggregates in the brain. It is the most common form of dementia, with approximately 55 million cases worldwide (World Health Organization [WHO], 2023). The disease was first described by the German pathologist Alois Alzheimer in 1907 (Alzheimer, 1907). This article was later summarized and translated to English (Alzheimer et al., 1995). Dr. Alzheimer presented a case report of a woman who in her early 50's started to show symptoms of dementia. After her death in 1906 (aged 55). Dr. Alzheimer performed the post-mortem analysis of an atrophic brain with previously undescribed neuropathological features and deposits. The deposits are today called amyloid plaques and neurofibrillary tangles (NFTs), and are typical features that are associated with AD (Alzheimer et al., 1995). NFTs consist of hyperphosphorylated aggregates of the microtubule associated Tau proteins, which are assembled into strands and deposited within nerve cells (Zempel & Mandelkow, 2014). The amyloid plaques are instead primarily built up from the amyloid-β (Aβ) peptides and are mainly encountered extracellularly (Y. Zhang et al., 2023), (Aβ is further described in section 1.5).

A typical clinical presentation of AD starts with an asymptomatic period, where initial deposition of Aβ and NFTs starts the neuronal disruption, although the patient is not experiencing any symptoms. This period may last for many years or even decades (Jessen et al., 2022; Price & Morris, 1999). The first symptom of the disease is often mild memory loss, and at this stage are areas such as entorhinal cortex, hippocampus, cingulate cortex and parietotemporal cortex affected (Herholz et al., 2002; Hyman et al., 1984; Scheff & Price, 2001). As the disease progresses, language, reasoning and social behavior become affected. At a late stage, many brain areas do not function normally, and the progression of synaptic loss is highly correlated with the disease severity. The outcome is always fatal, even though the cause of death is usually not the disease itself, but rather secondary complications such as pneumonia, malnutrition, or heart failure (Alzheimers Association, 2023; Kukull et al., 1994; Terry et al., 1991).

The risk of developing AD increases with age, and AD is most common in people over the age of 65 (Reitz et al., 2011). As global life expectancy increases (WHO, 2024), it is expected that AD prevalence will increase. The disease does not only cause a lot of individual suffering, but also a great economic challenge for society. In 2019, the global cost of AD was estimated to be approximately 1.3 billion US $ (Wimo et al., 2023), and this number will increase in relation with the increasing number of patients.

The disease is divided into two subtypes: familial and sporadic Alzheimer's disease (fAD and sAD, respectively), where sAD is responsible for more than 95% of all cases (Chakrabarti et al., 2015; Reitz et al., 2011; van der Flier & Scheltens, 2005). The onset of the fAD usually occurs at an earlier age (age < 65 years), than sAD and numerous mutations in genes such as the amyloid precursor protein (APP), presenilin 1 (PSEN1), and presenilin 2 (PSEN2) have been linked to fAD (Cai et al., 2015; Kelleher & Shen, 2017; Li et al., 2019). The mutations typical for fAD often result in increased Aβ production and affect the length of the peptides produced, often increasing the levels of more toxic and aggregation-prone Aβ variants. Unlike fAD, sAD does not follow a clear inheritance pattern. Instead sAD is thought to be influenced by a complex interplay of genetic, environmental and lifestyle factors, such as air pollutions (PM$_{2.5}$, NO$_2$, NO) (Wilker et al., 2023) pesticides (Yan et al., 2016), metals (Babic Leko et al., 2023; Bakulski et al., 2020), cigarette smoking (Cataldo et al., 2010; Wallin et al., 2017), diet (Agarwal et al., 2023),

exercise (Meng et al., 2020), sleep (Sabia et al., 2021), and traumatic brain injury (TBI) (Mielke et al., 2022). Although the connections are not yet fully understood, several genetic risk factors have also been implicated in sAD and the primary genetic risk factor that has been identified is the apolipoprotein ε4 allele. It is, however, essential to note that carrying the apolipoprotein ε4 allele does not guarantee that an individual will develop the disease (further described in section 1.6). Mutations in genes involved in various biological processes such as the immune system, endocytosis and lipid transport may also be associated with the disease (De Roeck et al., 2019; Foster et al., 2019; Guerreiro & Hardy, 2014).

1.4 Molecular aspects of Alzheimer's disease

Understanding Alzheimer's disease is a major challenge in current research and healthcare. During many decades of research, considerable progress has been made regarding the clarification of biochemical and molecular mechanisms involved in the progression of AD, some of which are presented below.

1.4.1 The cholinergic hypothesis

An early hypothesis presented in the late 1970's and early 1980's to explain AD pathogenesis was the *cholinergic hypothesis* (Bartus et al., 1982; Davies & Maloney, 1976). The hypothesis suggests that loss of the cholinergic neurons and decreased levels of acetylcholine (ACh) have a central role in the cognitive deficits observed in AD. This was based on observations of reduced cholinergic activity in the brains of individuals with AD, in combination with the clinical efficacy of acetylcholinesterase inhibitors. Acetylcholinesterase inhibitors increase the ACh levels present and can (temporarily) improve function in the cognitive system of some AD patients (Nordberg & Svensson, 1998). Today it is widely accepted that the cholinergic hypothesis is not the sole explanation for the cognitive decline in AD, although acetylcholinesterase inhibitors are currently used for symptom relief in AD (Vaz & Silvestre, 2020).

1.4.2 Amyloid cascade hypothesis

In the early 1990's Hardy and Higgins (1992) first presented the *amyloid cascade hypothesis*, which suggests that the abnormal accumulation of Aβ in the brain is the initial cause of AD. It suggests that the peptide accumulation initiates a cascade of events that contributes to the progression of the disease. This was supported by the fact that individuals with Trisomy 21 (i.e. Downs syndrome) often develop AD at an early age, explained by the presence of an extra copy of the gene encoding Aβ precursor protein, located on chromosome 21 (Fortea et al., 2021; Strydom et al., 2018). Additionally, many mutations associated with fAD are associated with alterations in Aβ production, especially upregulation or shifting the production towards the more toxic peptide species (Selkoe, 2008).

There is currently an ongoing debate regarding the relevance of this hypothesis as it has been shown that Aβ content is not always correlated with the development and severity of AD and individuals may have a significant number of amyloid plaques in the brain, without showing symptoms of the disease (Aizenstein et al., 2008; Delaere et al., 1990; Dickson et al., 1992). Besides that, another argument against the hypothesis is the fact that therapies developed to target amyloid production, aggregation or clearance have failed to show significant effects (Ricciarelli & Fedele, 2017). The amyloid cascade

hypothesis might not be the sole or complete explanation for the pathogenesis of AD, yet there is no doubt that Aβ is linked to the disease and that it plays a significant role in AD pathology.

1.4.3 Tau hypothesis

The *tau hypothesis* states that abnormal hyperphosphorylation of Tau results in the formation of paired helical filaments (PHF-tau) and NFTs in AD (Iqbal et al., 2016; Kosik et al., 1986; Mohandas et al., 2009) which are highly toxic to neurons, disrupt microtubule stability, and as a result impair cellular transport, eventually leading to synaptic dysfunction and cell death (Gendreau & Hall, 2013; Kopeikina et al., 2012; Maccioni et al., 2010). The fact that the amount of NFTs generally correlates with the progression of the disease and that mutations in the tau-encoding gene (microtubule-associated protein tau, MAPT) lead to abnormal tau aggregation and neurodegeneration, are two arguments in favor of hypothesis that tau aggregates are the main toxic species in AD.

1.4.4 The oligomeric hypothesis

The oligomeric hypothesis suggests that the smaller, soluble oligomers of Aβ are the most neurotoxic forms and therefore the primary cause of onset and progression of AD. The hypothesis arose during the late 1990s when the amyloid cascade hypothesis started to be questioned, and focus was shifted towards these smaller Aβ aggregates. The oligomers have been shown to interfere with synaptic signaling pathways, disrupt long-term potentiation, interact with cellular membranes and as a result cause leakage. This hypothesis is also supported by the observation that there is a good correlation between the levels of soluble Aβ oligomers, cognitive deficits and synaptic dysfunction (Cline et al., 2018; Ferreira & Klein, 2011).

The oligomeric species are very unstable, and therefore difficult to study. Many protocols are used for the preparation of oligomers *in vitro*, and as a result a lot of variations have been observed. These inconsistencies complicate the studies of oligomers, as their function, structure and toxicity may be largely affected by minor changes in the experimental setup.

1.4.5 The metal hypothesis

The metal hypothesis argues that metal ion dysregulation plays a crucial role in AD. Particularly copper, iron and zinc have been suggested to contribute to AD pathogenesis. In early studies these metal ions showed interaction with the Aβ peptides and were found in elevated levels in amyloid plaques (Lovell et al., 1998; Miller et al., 2006). Metal homeostasis is important, and concentrations of metal ions must be tightly regulated to ensure proper cellular functioning and maintain essential processes such as redox balance and enzymatic activity (Alberts et al., 2008). However, patients with AD often display metal dyshomeostasis, which is considered to contribute to the aggregation of the Aβ peptide. Binding of metal ions can for example induce conformational changes in the peptide that facilitate aggregation. Metal ions are also known to contribute to oxidative stress by generating reactive oxygen species (ROS), which in turn interfere with biological processes, and potentially contribute to the disease. Additionally, metal ions affect Aβ production and the length of the peptide (by modulating APP cleavage) (De Benedictis et al., 2019; Maynard et al., 2005). It is worth noting that although metal dyshomeostasis in AD is widely accepted, it is not known if it is a cause of, or an effect of

the disease. Furthermore, it is not clear if metal ions contribute to the formation of amyloid plaques *in vivo*, or if the ions bind to the already formed plaques. Therefore, the metals may cause secondary effects instead of contributing to the initial disease pathogenesis. In either way, once bound to the plaques, the metal ions may contribute to neuronal damage through ROS formation. There are still many gaps in the metal hypothesis, and it is probably not the sole cause of the disease, however, metal ions likely play an important role in disease progression (Aaseth et al., 2016; Bush, 2013; Bush & Tanzi, 2008; Chen et al., 2023).

1.4.6 Mitochondrial dysfunction and oxidative stress in Alzheimer's disease

The functionality of the mitochondria has been recognized as a critical factor in AD. The mitochondria are considered the powerhouse of the cell and are essential for energy production, regulation of cellular metabolism, and maintenance of cellular health (Alberts et al., 2008). In AD brains, it has been shown that the mitochondrial dynamics is disturbed, resulting in a disruption of the morphology and functioning of the organelles. Neurons are highly energy-consuming cells, and mitochondrial dysfunction leads to decreased ATP production. Energy deficits may impair several cellular functions, including synaptic activity and plasticity, both of which are crucial processes for memory formation and cognitive functions (Cunnane et al., 2020). Mitochondria are also vital for neurotransmitter release in the presynaptic terminal, where they supply ATP, and also regulate intracellular calcium levels. In AD, this regulation is often disrupted, leading to elevated calcium levels which results in altered neuronal activity and may result in activation of cell death pathways (Guan et al., 2021). In addition, a dysfunctional mitochondrion may produce ROS and cause oxidative stress as a result of disturbances in the electron transport chain (Guo et al., 2013).

Oxidative stress refers to an imbalance between the production of ROS and the ability to detoxify these harmful compounds and repair the resulting damage. Under normal physiological conditions, a balance between ROS production and neutralizing antioxidative processes allows the cell to function normally. An overproduction of ROS disturbs this balance and leads to oxidative stress in the cell. ROS are natural byproducts of the cellular metabolism, particularly within the mitochondria during aerobic respiration but are also produced by macrophages and neutrophils in the immune system (Checa & Aran, 2020). Increased ROS levels may damage cellular components, including lipids, proteins and DNA which could impair cellular functions, induce apoptosis or contribute to the pathogenesis of various diseases (Shields et al., 2021). A wide range of diseases have been associated with oxidative stress, including cardiovascular diseases, diabetes, cancer, and aging, but also neurodegenerative diseases like PD and AD (Knott et al., 2008; Ray et al., 2012; Reddy et al., 2011; Wang et al., 2009). The mitochondrial dysfunctions often observed in AD patients are likely part of a vicious cycle, where dysfunctional mitochondria-induced oxidative stress causes even further damage which may damage additional mitochondria.

Both Aβ and hyperphosphorylated Tau have been shown to interact with and affect the mitochondria negatively. Aβ can interfere with the electron transport chain, thereby further increasing ROS production and reducing the efficiency of ATP production (Bobba et al., 2013; Spuch et al., 2012). Hyperphosphorylated tau, on the other hand, has been shown to disrupt the distribution of mitochondria inside the cell, which naturally affects the cell function (Isei et al., 2024). The Aβ peptides can induce ROS by themselves, and disrupt cellular membranes caused by lipid peroxidation (Cenini et al.,

2010; Cheignon et al., 2018; Harris et al., 1995). Moreover, Aβ peptides can induce ROS also through interactions with metal ions (extensively described in section 1.7).

Increased oxidative stress furthermore increases the risk of mutations in the mitochondrial DNA, which further results in defective mitochondrial proteins and contributes to additional mitochondrial dysfunction and the pathogenesis of AD (Druzhyna et al., 2008).

1.4.7 Neuroinflammation in Alzheimer's disease

Both Aβ aggregates and NFTs are thought to be able to activate an inflammatory response in the brain by activating glial cells (primarily microglia and astrocytes) (Hickman et al., 2018; Kim & Choi, 2015). Activated microglia release pro-inflammatory cytokines and chemokines, such as Interleukin-1, Interleukin-6 and tumor necrosis factor alpha, which in turn amplifies the inflammatory response by recruiting more immune cells (Gao et al., 2023). A chronic neuroinflammation may give rise to neuronal damage and further contributes to cognitive decline, and many inflammatory processes also lead to oxidative stress (Adamu et al., 2024; Mittal et al., 2014; W. Zhang et al., 2023).

AD is a complex and multifactorial disease, and the pathology of the disease is likely an interplay of multiple factors and pathological processes. The hypotheses presented in this section all contribute with different aspects of pathophysiology, adding pieces to the puzzle of AD (Figure 2).
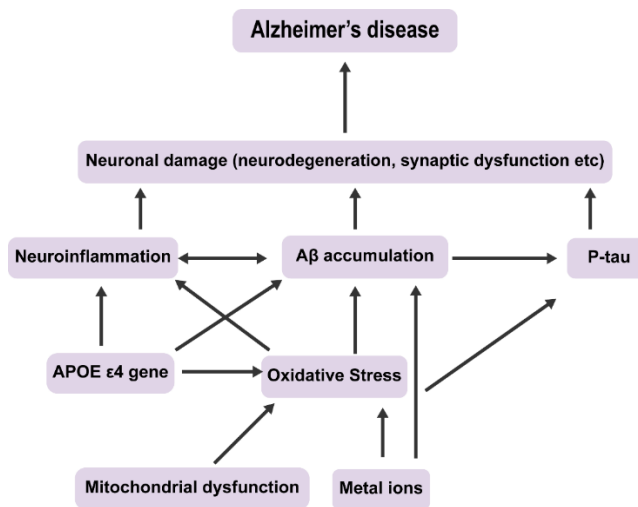
Figure 2. Simplified scheme of factors contributing to the progression of Alzheimer's disease. These (and many other) elements interact in a complex network, producing neuronal damage, synaptic loss, and cognitive decline.

1.5 Amyloid β

The 36-43 residues long amphipathic Aβ peptide is produced by enzymatic cleavage of the amyloid precursor protein, APP (Mawuenyega et al., 2013). Aβ was first described as a major component of the amyloid plaques found in the brains of AD patients in 1984 (Glenner & Wong, 1984). The Aβ peptide exists in different forms in humans, but also across various animal species. The variation in amino acid sequence affects how prone the peptides are to aggregate and thus, their possible contribution to AD pathology. In

humans, the Aβ$_{1-40}$ variant is the most common form of the peptide in the brain, whereas the Aβ$_{1-42}$ variant (Figure 3) shows a greater propensity for aggregation and is therefore considered to be more toxic (Mori et al., 1992; Naslund et al., 1994). In murine species, three amino acids are substituted, compared to human wild type Aβ, i.e. R5G, Y10P, and H13R. Additionally, rodent Aβ is also known to be less aggregation-prone than human Aβ (Xu et al., 2015). The Aβ peptide exists in many other species where there are variations in sequence, propensity to aggregate and structure. Although many species can display human-like amyloid aggregates, only few species are showing AD-like symptoms (Chen & Zhang, 2022; Walker & Jucker, 2017).

Although it is mostly associated with the pathogenesis of AD, it is important to note that Aβ is also present in healthy brains. It has been suggested to be involved in cell survival, memory formation, neuronal communication, and plasticity (Puzzo et al., 2015; Soucek et al., 2003). Studies have shown that knocking out the gene and enzymes involved in Aβ production leads to a significant reduction in Aβ, but also results in various neurological deficits and developmental problems (Dawson et al., 1999; Plant et al., 2003; Zheng et al., 1995). Thus, Aβ seems to have an important biological role in the brain, but the details are unclear.

In an aqueous solution at physiological pH values, the monomeric Aβ peptide is negatively charged, intrinsically disordered and adopting a random coil conformation. In a membrane or membrane-mimicking environment, the peptide adopts an α-helical secondary structure. In a detergent micelle, the C-terminal and central part of the peptide localizes inside, while the N-terminal remains unstructured outside the micelle (Tiiman et al., 2016). Upon aggregation, the peptide folds into β-sheets, which enable formation of amyloid fibrils (Rambaran & Serpell, 2008). The N-terminal part of the Aβ peptide contains three histidine residues (H6, H13, H14), where the nitrogen in the imidazole ring can coordinate metal ions. The central and C-terminal segments of the peptide are hydrophobic and may interact with membranes or fold into hairpin conformation, likely required for aggregation (Figure 3) (Abelein et al., 2014). The Aβ$_{1-42}$ peptide has two additional hydrophobic residues in the C-terminal (i.e. I41 and A42), making this variant less soluble in aqueous solution than Aβ$_{1-40}$, but also contributing to its aggregation propensity. The presence of these additional hydrophobic amino acids residues alters the molecular structure and, stabilizes the intermolecular interactions which drive aggregation (Sgourakis et al., 2007).

DAEFRHDSGY$_{10}$EVHHQKLVFF$_{20}$AEDVGSNKGA$_{30}$IIGLMVGGVV$_{40}$IA

Figure 3. *Amino acid sequence of Aβ$_{1-42}$. Blue: Histidine residues, mainly uncharged at neutral pH and protonated below pH ~6. Red: acidic, negatively charged residues at neutral pH. Purple: Positively charged residues at neutral pH. Amino acids that can be involved in metal coordination are marked with * and hydrophobic regions are overlined. Adapted from: (Wärmländer et al., 2019).*

1.5.1 Generation of Aβ

The Aβ peptide is produced by proteolytic cleavage of the amyloid precursor protein (APP) (Nunan & Small, 2000). APP is a transmembrane protein mainly located in the plasma membrane and is primarily expressed in neural tissues (O'Brien & Wong, 2011). The APP gene is in humans located on chromosome 21 (Korenberg et al., 1989; Patterson et al., 1988; Tosh et al., 2021) and is spliced into three variants of different lengths (APP$_{770}$, APP$_{751}$ and APP$_{695}$), where the APP$_{695}$ is the isoform most commonly found in the

brain (Delport & Hewer, 2022). APP contains a region that encodes for the Aβ peptide, and whether Aβ is produced or not depends on the specific enzymes involved in the enzymatic cleavage of APP (O'Brien & Wong, 2011). Under normal conditions, APP primarily follows the non-amyloidogenic pathway (Figure 4), where alpha (α)-secretases such as Disintegrin and Metalloprotease 10 (ADAM10) cleave APP within the Aβ fragment, resulting in a soluble amyloid precursor protein-alpha (sAPPα) fragment of 612 amino acids that is released into the extracellular space (Chasseigneaux & Allinquant, 2012; De Strooper et al., 2010). This, while an 83-residue long carboxyl-terminal fragment alpha (CTFα) is released intracellularly (Chen et al., 2017). The sPPα fragment is important in the brain development, involved in the regulation and proliferation of neuronal stem cells (Coronel et al., 2019). It is also thought to have a role in processes such as memory formation and synaptic plasticity in the mature brain (Ishida et al., 1997).

The subsequent cleavage of the CTFα fragment is performed by the gamma (γ)-secretase, a protein complex containing among other subunits also PSEN1 or PSEN2 (De Strooper et al., 2012). This cleavage results in the APP intracellular C-terminal domain (AICD) and the small P3 peptide (~3 kDa). The exact roles of these intracellularly released fragments are not yet elucidated. As the P3 peptide seems to be rapidly degraded, it suggests that P3 has no significant pathological or even biological function (Zhang et al., 2011).

In the amyloidogenic pathway, APP is instead cleaved by beta (β)-secretase which cuts APP and leaves the Aβ fragment complete and attached to the CTFβ fragment. One of the most common β-secretases are the Beta-Site APP cleaving enzyme 1 (BACE1), which belongs to the pepsin family of proteases and requires acidic conditions for optimal enzymatic activity (Cole & Vassar, 2007; Haass et al., 1993). The γ-secretase then cleaves the CTFβ fragment, leaving the AICD and an Aβ monomer (Figure 4). The main difference between the two pathways is that the α-secretase in the non-amyloidogenic pathway cuts within the Aβ sequence, hindering its production, while the β-secretase in the amyloidogenic pathway cleaves outside the Aβ site, making the formation of Aβ peptides possible (Nathalie & Jean-Noel, 2008).

The native role of APP is currently under discussion, but the evolutionary conservation of its gene family suggests that it serves an important function (Tharp & Sarkar, 2013; Zheng & Koo, 2011). APP is known to be involved in cell adhesion, neuronal guidance, synapse formation, to act as cell surface receptor, regulate synapse formation, and influence cell division (Ejaz et al., 2020; Nhan et al., 2015). Its importance is further confirmed by the negative effects observed in APP knockout mice (Mazinani et al., 2020; Senechal et al., 2008; Zheng et al., 1995). Additionally, APP have shown to bind Cu ions and are suggested to be implicated in iron metabolism (Wild et al., 2017).

Interestingly, it has been shown that the APP cleavage is not limited to the plasma membrane. APP can be transported into early endosomes by endocytosis, where β-secretase (especially BACE1) and γ-secretase, but less α-secretase is present. The lower pH in the early endosomes (approximately pH 6.5 (Hu et al., 2015)) promotes BACE1 cleavage, resulting in increased Aβ production. It has therefore been suggested that toxic Aβ may be produced intracellularly and then transported to the extracellular space (Fourriere et al., 2022; Iizuka et al., 1996; Skovronsky et al., 1998; Turner et al., 1996).
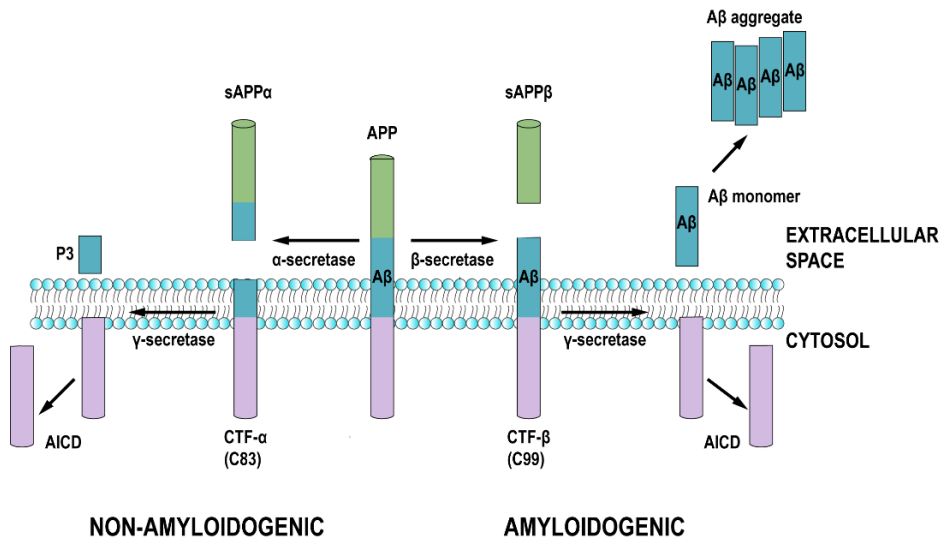
Figure 4. *Proteolytic cleavage of the APP by α-, β- or γ-secretase directs the protein into either the non-amyloidogenic or the amyloidogenic pathway. Adapted with permission from (Hampel et al., 2021).*

1.5.2 Aggregation of Aβ

The aggregation of Aβ is a complex and critical process in the pathogenesis of AD. The monomeric Aβ peptides undergo a series of structural changes and interactions which lead to the formation of aggregates and plaques in the brain.

To initiate aggregation, the Aβ peptides must exceed the critical aggregation concentration (CAC). While the CAC varies depending on the surrounding environment, it is estimated to be around 100 nM for $Aβ_{1-40}$ under physiological conditions, and even less for the more aggregation-prone $Aβ_{1-42}$ peptide (Brannstrom et al., 2014; Iljina et al., 2016).

The aggregation process can be divided into three stages (Figure 6). It begins with the lag phase, where monomers typically exist in a disordered state. As the concentration of Aβ peptides increases, some monomers undergo conformational changes and begin to associate with each other, forming small aggregates commonly known as oligomers during a process called primary nucleation. Once the critical threshold is reached, the aggregation process enters the transition into a rapid growth phase, called the elongation phase. Here, larger aggregates and fibrils are formed. During this phase, Aβ monomers are primarily added to existing fibril ends, leading to their elongation and growth. Finally, the aggregation process reaches the stationary phase, where a stable concentration of Aβ aggregates is reached. Although some fibrils may continue to grow, there will likely also be fragmentation of already formed structures and so-called secondary nucleation, resulting in a largely consistent aggregate concentration.

As mentioned in section 1.2.2.1, ThT fluorescence is a useful tool for monitoring the amyloid formation in a sample. ThT is a benzothiazole dye that contains a dimethylated benzothiazole ring connected to a dimethylamino benzyl ring via a single carbon-carbon bond (Figure 5). The single carbon-carbon bond makes rotation of the two rings possible which causes quenching of the fluorescence in unbound state. Upon binding to amyloid material, the free rotation is hindered and as a result the quenching is reduced.

This results in a great increase in fluorescence intensity. Therefore, the measured ThT fluorescence intensity roughly corresponds to the amount of amyloid material present in the sample (Biancalana & Koide, 2010; Malmos et al., 2017; Qin et al., 2017). The intensities can be plotted against time and produce a sigmoidal curve from which parameters such as lag time, growth rate and half time for aggregation can be determined (Figure 6). One limitation of the ThT dye is that aggregation of 50-70 monomers is required for the fluorescence to increase. That means that other techniques are required to monitor the initial aggregation steps (Tiiman et al., 2015).
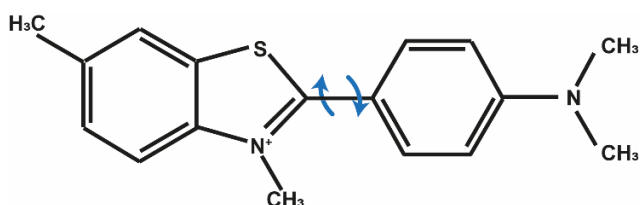
Figure 5. Chemical structure of Thioflavin T (ThT). A dimethylated benzothiazole ring connected to a dimethylamino benzyl ring by a single bond (denoted with arrows) which allows free rotation. Upon binding to amyloid material, the free rotation is hindered, and fluorescence can be detected.

The aggregation process is very sensitive to environmental conditions and factors like pH, temperature and presence of metal ions or other small molecules may have a large impact on the aggregation process, influencing both the rate of aggregation and the structural characteristics of the resulting aggregates. The different conditions may alter the balance between different aggregation steps, potentially affecting the stability and toxicity of the aggregates. For example, metal ions such as zinc (II) and copper (II) have been shown to be able to accelerate the aggregation, and variations in pH changes the intrinsic charge of the peptide. This sensitivity makes studies of Aβ peptides complicated and explains why large variations can be observed in similar studies performed by different authors.
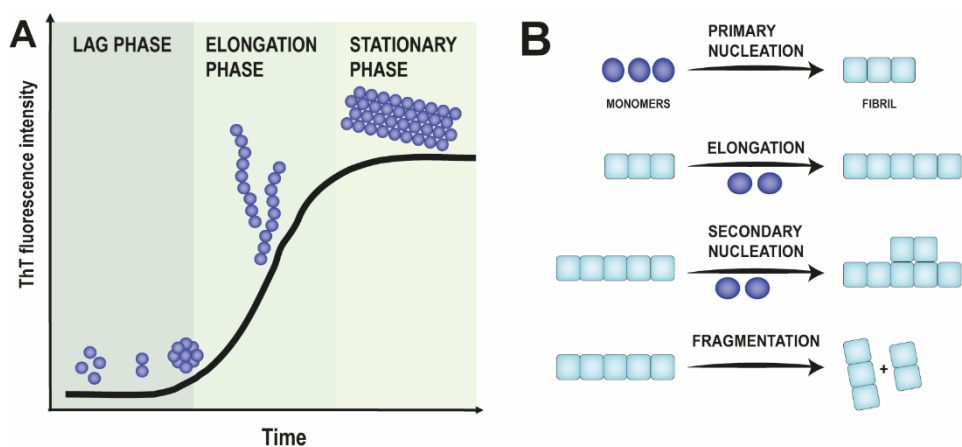
Figure 6. Aggregation kinetics of Aβ peptides. (A) shows a typical sigmoidal curve obtained from in vitro experiments, where the aggregation has been monitored by following the change in ThT fluorescence. (B) processes that takes places during the peptide aggregation. Adapted with permission from (Thacker et al., 2023) and (Kumar & Walter, 2011)

1.5.3 Structure of Aβ aggregates

The aggregation of Aβ peptides is central to the pathology of AD and as previously discussed, the monomeric Aβ peptide is soluble and typically adopts a random coil in aqueous solution and alpha helical structure in a membrane or membrane mimetic environment. The monomeric peptide does not exhibit significant toxicity on its own, although its interaction with other cellular components is suggested to be able to exacerbate pathological conditions (Tamagno et al., 2018). Upon initiation of aggregation, the monomers go through a conformational change, taking on a β-sheet structure which allows them to interact and form insoluble fibrils, characteristic of amyloid plaques. According to the amyloid cascade hypothesis, the aggregation of Aβ was causally linked to explain the pathogenesis of AD and this was initially supported by studies of brain tissues (Mann et al., 1985). However, a few years later the hypothesis started to be debated (Kepp et al., 2023). Researchers observed that the number of amyloid plaques in the brain of AD patients did not consistently correlate with severity of the disease. Some individuals with significant amyloid plaque deposits exhibited only mild symptoms or even normal cognitive function (Ricciarelli & Fedele, 2017). The focus was then shifted to the pre-fibrillar states, as the levels of soluble Aβ aggregates in the CNS of AD patients seemed to correlate better with the pathology (Viola & Klein, 2015). The pre-fibrillar state ranges from dimers to aggregates of hundreds of peptides, i.e. oligomers to protofibrils (Khaled et al., 2023).

1.5.3.1 Aβ oligomers

Aβ oligomers are small, prefibrillar, soluble aggregates that are currently considered to be the main toxic species in AD pathology (Cline et al., 2018; Lee et al., 2017; Walsh & Selkoe, 2004). Although they have been extensively studied for decades, no clear definition of their size has been stated, but it is common that dimers to dodecamers are considered oligomers, while larger and more fibrillar-like aggregates are called protofibrils (Cline et al., 2018; Sakono & Zako, 2010). Due to their instability, the secondary structure of the oligomers is not completely understood. They are thought to lack the highly ordered arrangements characteristic for mature fibrils and instead consist of mixed structures of β-sheets and random coil (Bitan et al., 2003; Ono et al., 2009).

Although the toxicity caused by oligomers is widely accepted, it is not yet completely understood how they exert their toxicity. For example, it has been suggested that the oligomers may have prion-like properties, meaning that they can be distributed between cells (Walker et al., 2016; Willbold et al., 2021). They are also thought to be able to disrupt cellular membranes, both intra- and extracellularly, thereby weakening membranes and inducing leakage. This may among other effects contribute to the Ca-dysregulation that is known to be associated with AD (Popugaeva et al., 2020; Serra-Batiste et al., 2016). Additionally, Aβ oligomers have been shown to bind to a variety of biomolecules, and thereby affect their natural function (Taniguchi et al., 2022; Wiatrak et al., 2021; Zhao et al., 2008).

1.5.3.2 Aβ fibrils and plaques

Mature Aβ fibrils are the end product of the fibrillogenic pathway. The fibrils display an elongated morphology which can reach several μm, with a diameter of approximately 7-12 nm (Chiti & Dobson, 2017; Sunde et al., 1997). X-ray diffraction has shown that fibrils are unbranched structures composed of cross-β sheets (Figure 1), a structure which many amyloid fibrils have in common (Fandrich, 2012; Sunde et al., 1997). Cross-β sheet structures are composed of hydrogen bonded β-strands that are packed perpendicular

to the fibril axis, creating highly ordered, stable aggregates that are resistant to proteolysis (Sabate & Ventura, 2013). The fibrils can aggregate into amyloid plaques, mainly through non-covalent interactions such as hydrogen bonding and hydrophobic interactions between fibrils. The plaques are mainly observed extracellularly (Jankovska et al., 2020). Although mature amyloid plaques are mainly composed of fibrils of the Aβ peptide, many other components are often also found within the plaques. Proteins such as Apolipoprotein E, proteoglycans, lipids and metal ions can also bind to the fibrils and might play a stabilizing role and might contribute to the plaque formation (Liao et al., 2004; McGeer et al., 1994; Stewart & Radford, 2017; Xiong et al., 2019).
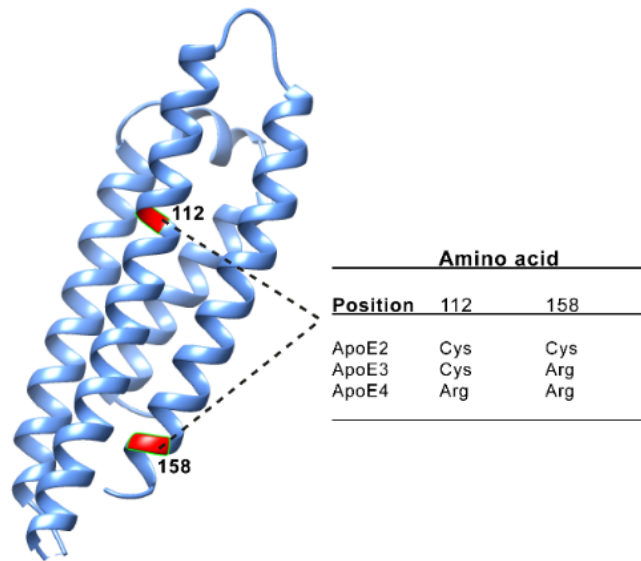
1.6 Apolipoprotein E

As mentioned in section 1.3, Apolipoprotein E (ApoE) has been shown to be a protein involved in AD. ApoE is a glycoprotein composed of 299 amino acid residues with a molecular mass of ~34kDa. It is involved in the transport and metabolism of lipids and contributes to lipid homeostasis in the body. The protein is encoded by the ApoE gene, located on chromosome 19 (Liu et al., 2013; Moreno-Grau et al., 2018). In CNS ApoE is mainly produced by astrocytes and the production has been shown to increase upon injury to the brain, suggesting its involvement in the repair of the nervous system (Chen et al., 1997) as well as in inflammatory responses in the brain (Lynch et al., 2003; Vitek et al., 2009).

The protein exists in three isoforms (ApoE2, ApoE3 and ApoE4), where ApoE3 is the most common and considered the normal form (Huang & Mahley, 2014). Only a single amino acid residue distinguishes ApoE2 and ApoE4 from ApoE3 (Figure 7). In ApoE2 the arginine at position 158 is exchanged to a cysteine, and in ApoE4 the cysteine at position 112 is exchanged to an arginine (ApoE2: C112 and C158, ApoE3: C112 and R158, ApoE4: R112 and R158).

The protein contains an N-terminal segment (residue 1-191) of mainly amphipathic alpha helices arranged in coiled-coils with the hydrophobic residues arranged in the protein's interior, while the polar, charged and hydrophilic residues are located on the protein surface. The N-terminus can bind to low-density lipoprotein (LDL) receptors and is therefore important for binding of lipoproteins. The C-terminus (residue 216-299) is also composed of amphipathic helices, and it is involved in lipid binding (Raussens et al., 1998; Segrest et al., 1992; Strittmatter et al., 1993; Weisgraber, 1994; Wilson et al., 1991; Yamauchi et al., 2008).

It has been shown that carriers of ApoE-ε4 allele are more susceptible to both mercury intoxication and at greater risk of developing AD (Corder et al., 1993; Farrer et al., 1997; Godfrey et al., 2003; Kim et al., 2009; Manelli et al., 2007). In contrast, the ApoE-ε2 isoform is considered "protective" against AD (Li et al., 2020). The underlaying reason remain unknown, but as the -SH groups of cysteines are known to bind metals, including Hg (Ajsuvakova et al., 2020; Mesterhazy et al., 2018), it has been suggested that the ApoE protein may be involved in removal of Hg from tissue and that the lacking cysteines in ApoE4 would result in a reduced capacity for metal removal. At the same time, the binding of Hg ions to ApoE proteins has not been studied.

Figure 7. Structure of Apolipoprotein E (residues 23-162) showing a predominance of alpha helices. Residues 112 and 158 are marked in red and indicate where the three ApoE variants differ. Structure was determined by X-ray diffraction. PDB ID: 1B68, protein structure is visualized with Chimera version 1.18 (Pettersen et al., 2004).

1.6.1 Relevance of Apolipoprotein E in Alzheimer's disease

Genetic analyses have shown that carrying an ApoE ε4 allele not only increases the risk of developing AD, but it also lowers the mean age of clinical onset (Bertram et al., 2007; Corder et al., 1993; Genin et al., 2011; Mishra et al., 2018; Rebeck et al., 1993; Roses, 1996). It is estimated that the risk of developing the disease increases 4-fold for heterozygotic carriers of the ε4 allele, and up to 12-fold for homozygotic carriers (Mahley & Huang, 2012). Interestingly, carrying the ε2 allele seems to have a protective effect and reducing the risk of developing AD (Corder et al., 1994; Li et al., 2020).

Exactly how the ApoE4 gene increases the risk of developing AD is not completely understood. It has been shown that compared to ApoE2 and ApoE3, the degradation and removal of Aβ from the brain are less effective in ApoE4 carriers, and ApoE4 can stabilize the Aβ peptide and to some extent increase the rate of its aggregation (Deane et al., 2008; Ma et al., 1994; Shackleton et al., 2019; Wisniewski et al., 1994). In a mice model, the ApoE4 isoform increased the half-life of Aβ peptides in the brain, and the ApoE4 mice also showed higher levels of amyloid-related gliosis, whereas ApoE3 reduced it (Liu et al., 2017). The ApoE4 isoform also increased Aβ production more than ApoE3 in cell cultures expressing APP (Ye et al., 2005).

Besides the interactions between the ApoE protein and Aβ peptide, ApoE4 is also associated with an increased inflammatory response in the brain, and is able to increase the inflammatory response by affecting the activation of microglial cells (Fernandez et al., 2019; Ferrari-Souza et al., 2023; Lee et al., 2023).

The blood brain barrier (BBB) is a highly selective semi-permeable membrane between the blood and the brain and controls trafficking of compounds into the brain, and it prevents entries of potentially toxic molecules and pathogens. The ApoE4 protein has been associated with a reduced integrity of the BBB, which may have a crucial effect

and result in a disrupted brain environment (Halliday et al., 2016; Jackson et al., 2022). The ApoE4 protein has also been shown to be less effective in lipid transport, which could negatively affect neuronal survival and plasticity (Yang et al., 2023).

1.7 Metal ions in Alzheimer's disease

More than 80% of the periodic table of elements consists of metals, many of which are essential for biological processes and crucial for the normal functioning of the human body. Metals such as iron (Fe), calcium (Ca), zinc (Zn), copper (Cu), manganese (Mn) and magnesium (Mg), are involved in enzymatic functions, transport of oxygen, DNA synthesis, regulation of oxidative stress and neuronal signaling (Majorek et al., 2024). As many physiological processes are dependent on metals, their proper regulation and homeostasis are crucial for health as both excess and deficiencies may lead to a variety of disorders (Wang & Zhang, 2015). Metals can directly affect proteins by breaking salt bridges, causing oxidative stress, inducing protein denaturation, and in the case of proteinopathies like AD, affect the aggregation processes. In AD and several other proteinopathies, metal dyshomeostasis is implicated and thought to be involved in the disease's progression, by inducing accumulation of peptides, increasing ROS production and impairing of biomolecular functions (Chen et al., 2023; Das et al., 2021). Already in the 1990's researchers showed that Zn(II) ions could affect Aβ aggregation (Bush et al., 1994), and that AD brains display abnormal metal concentrations (Babic Leko et al., 2023; Wang et al., 2020). In addition, amyloid plaques have shown to contain elevated levels of Zn, Cu and Fe (~mM concentration) (Beauchemin & Kisilevsky, 1998; Faller & Hureau, 2009; Lovell et al., 1998; Miller et al., 2006). The disrupted metal homeostasis in AD is a commonly recognized problem, however, the details are not yet fully understood. The published literature about this subject further highlights the complexity, as publications in many cases show contradictory results with both increased and decreased concentrations of metal ions in AD brains (Babic Leko et al., 2023; Brewer, 2014; Cicero et al., 2017; Lovell et al., 1998; Squitti et al., 2014).

Iron, copper and to some extent other transition metals such as manganese and nickel can participate in Fenton-type reactions where reactive hydroxyl radicals are formed by interaction between metal ions and hydrogen peroxide in redox reactions. The reactions happen when the metal ions recycle between different redox states, react with hydrogen peroxide, and create hydroxyl radicals which are highly reactive and contribute to oxidative stress (Gao et al., 2022; Lloyd & Phillips, 1999)

It is widely accepted that the metal homeostasis is disrupted in AD patients, but it is not yet elucidated whether the changes are a cause or an effect (or both) of the underlying pathology. Although it is not thought to be the sole cause of the disease, abnormal metal metabolism and homeostasis is believed to contribute to the disease's progression by, among other things, affecting the aggregation of AD-related proteins and contributing to oxidative stress and neurotoxicity (Babic Leko et al., 2023; Huat et al., 2019; Islam et al., 2022).

1.7.1 Metal binding properties of Aβ peptides
Metal binding to the Aβ peptide has been extensively studied for many years and the main focus has been on the most biologically relevant metals such as Cu, Ca, Zn and Fe, especially since these metals were found in elevated concentrations in amyloid plaques (Beauchemin & Kisilevsky, 1998; Lovell et al., 1998; Miller et al., 2006). The binding of metals ions to Aβ influences the net charge of the peptide, which affects the stability and

conformations of peptide regions and may destabilize the secondary structures in the peptide. This destabilization may induce a shift towards more stable conformations such as β-sheets, which in turn could facilitate the aggregation of peptides into amyloid fibrils. Metal ions have *in vitro* been shown to stabilize soluble oligomers, which could enhance their neurotoxicity if it would happen *in vivo* (Gonzalez Diaz et al., 2024; Ryan et al., 2015; Williams et al., 2016).

Interestingly, the metal: peptide ratio plays an important role and affects the rate of aggregation and morphology of aggregates. For example, the sub-equimolar concentrations of Cu(II) ions push the aggregation towards ThT-active, larger aggregates, whereas supra-equimolar concentrations promote formation of smaller oligomers and amorphous aggregates (Jin et al., 2011; Pedersen et al., 2011; D. P. Smith et al., 2007).

The Aβ peptide lacks cysteine residues (Figure 3), which are typical metal binding residues, however, the Aβ N-terminus contains aspartic acids and glutamic acids (D1, E3, D7 and E11). These residues are negatively charged and are likely to bind positively charged metal ions. Additionally, the peptide contains three histidine residues (H6, H13 and H14) which through their imidazole ring can contribute to the coordination of metal ions under physiological conditions. Histidine residues have a pKa of ~6, which makes their metal binding properties sensitive to pH variations.

Metal ions such as Ni(II), Cu(II), Pb(IV), Zn (II) have been shown to bind at specific sites on the Aβ peptide. This binding occurs in the N-terminal region by involving the His residues as binding ligands. The binding of metals to the Aβ peptide can also be non-specific, as in the case of uranyl, Mn(II) and Pb(II) ions. In these cases, it is proposed that the interactions occur via non-specific electrostatic interactions between negatively charged Aβ residues and the positively charged metal ions (Danielsson et al., 2007; Ghalebani et al., 2012; Wallin et al., 2016; Wallin et al., 2017). Copper is an essential trace element in the human body with several important roles. It is crucial for enzyme function, iron metabolism, the immune response and antioxidant defense (Council, 2000). In the brain and related neurological systems, Cu is a cofactor in several enzymes that are critical in production of neurotransmitters, in the electron transport chain, development and differentiation of neuronal cells and in antioxidant defense (D'Ambrosi & Rossi, 2015; Opazo et al., 2014; Zhiwu Zhu, 2000). The distribution of Cu ions varies in the brain, and areas such as hippocampus, cerebellum, subventricular zone and substantia nigra which are important for memory, motor control, neuronal generation and cognitive functions, have shown abnormal levels of Cu in AD patients (Bagheri et al., 2017; Fu et al., 2015; Magaki et al., 2007; Suryana et al., 2024). Gaier et al. (2013) explained that the levels of copper in synapses can change rapidly, as a result of neuronal activity and suggested that Cu is released to the synaptic cleft during neurotransmission. Interestingly, abnormal Cu homeostasis in the synapses has been linked to both Wilson's disease and AD.

Cu is a redox-active metal that is known to participate in Fenton-like reactions, resulting in the formation of ROS, which as previously discussed is likely a key process in AD. It has also been discussed whether Cu ions accelerate or inhibit Aβ aggregation, as contradictory results have been published. Interestingly, it has been suggested that Zn(II) ions are able to compete with Cu(II) ions for Aβ binding, and this effect may attenuate the amount of harmful redox chemistry caused by Cu interactions (D. G. Smith et al., 2007). It seems most likely that the toxicity of Aβ:Cu complexes in cell cultures is higher, as compared to free copper ions (Faller & Hureau, 2009)

The exact role of Cu in neurodegenerative diseases like AD, HD and PD is not yet understood, but the dysregulation indicates that it plays a role in pathology. It is well known that Cu ions are able to bind to Aβ with a high affinity, and although the exact binding affinity (K_D-values) varies depending on experimental setup and conditions, it is widely accepted that the Cu(II) ions bind to Aβ with a K_D value up to 0.1-1 nM (Alies et al., 2013; Conte-Daban et al., 2017; Young et al., 2014).

Metal binding to peptides and proteins can be studied by taking advantage of the intrinsic fluorescence in the aromatic amino acids, i.e. tyrosine, tryptophan and phenylalanine. The Aβ peptide contains one tyrosine residue (Y10), which is located in the N-terminus, in close proximity to the histidine residues at position 6,13 and 14. A decrease in fluorescence upon titration with a metal ion can therefore be assumed to reflect metal binding to the protein, resulting in quenching of the intrinsic fluorescence. Plotting the loss of intrinsic fluorescence against the concentration of added metal gives a binding curve, which can be fitted to e.g. the Morrison equation and an apparent binding affinity (K_D-value) can be obtained (Kuzmic, 2015). The Aβ peptide also contains three phenylalanine residues, but as the intrinsic fluorescence from these residues is very weak it can be considered negligible in the presence of tyrosine or tryptophan residues.

1.7.2 ATCUN-motif

The amino terminal Cu(II)- and Ni(II) binding (ATCUN) motif is a metal binding site, located in the N-terminus of many proteins. It requires a histidine residue at third position. The ATCUN complex consists of a four-nitrogen square-planar coordination mode, with a bound metal ion located in the center. One nitrogen atom is provided by the N-terminal amine, two from the protein backbone peptide bonds and one from the imidazole ring of the histidine residue (Maiti et al., 2020; Sankararamakrishnan et al., 2005).

Interestingly, truncated versions of the Aβ peptide have been found in amyloid plaques, especially Aβ$_{4-42}$, but also Aβ $_{11-x}$, both in patients with AD and in people with trisomy 21(Liu et al., 2006; Masters et al., 1985; Portelius et al., 2010).

As the Aβ peptide contains histidine residues at position 6, 13 and 14 (Figure 3), truncation into Aβ$_{4-42}$ and Aβ $_{11-x}$ puts a histidine residue in position three, forming ATCUN-motifs. The truncated Aβ peptides have been shown to bind Cu(II) ions several orders of magnitude stronger than the Aβ$_{1-40/42}$ peptide (Barritt & Viles, 2015; Mital et al., 2015), potentially explaining the increased metal content that have been found within amyloid plaques.

1.7.3 Dityrosine formation

Dityrosine is a dimeric form of the amino acid tyrosine and occurs when the two amino acids are linked together by a covalent bond between their aromatic rings. Dityrosine can be formed through both enzymatic and non-enzymatic processes, where in the latter case free radicals cause the oxidation of the tyrosine residue. A reactive tyrosyl radical is formed when the hydrogen of the hydroxyl group is removed. This process typically occurs under conditions of oxidative stress, where ROS can induce oxidation of tyrosine residues. Dityrosine crosslinks stabilize the structure of proteins/peptides. Although high levels of dityrosine often indicates oxidative stress and can act as a marker for some biochemical processes and pathological conditions, formation of dityrosine is in some processes thought to be required for proper biological function (Maina et al., 2023). The formation of dityrosine can be monitored *in vitro*, as it emits fluorescence around 350 nm (excited at 315 nm) (Radomska & Wolszczak, 2022).

In the case of Aβ, the peptide contains one tyrosine residue at position 10 (Y10), which can participate in dityrosine formation. Cross-linking of Aβ peptides promotes the formation of aggregates and these will be more resistant to degradation and potentially making normally soluble aggregates insoluble. Dityrosine-linked Aβ peptides have also been shown to be present in amyloid plaques in human AD brain and CSF (Al-Hilaly et al., 2013). Barnham et al. (2004) concluded that in oligomers formed mainly from Aβ peptides where the Y10 residue were exchanged for an alanine (Y10A), showed less toxicity compared to the oligomers of WT peptide. It was therefore suggested that the toxicity of oligomers might be dependent on the cross-linking of Y10 residues. This conclusion is further supported by the fact that murine Aβ, which lacks the tyrosine residue at position 10 (Y10P) generally has less Aβ deposits in their brains.

1.7.4 Interactions of Aβ peptides with non-essential metals

It has been shown that some non-biologically essential metals are able to accumulate in the brain and contribute to neurotoxicity (Carmona et al., 2021; Ijomone et al., 2020). Understanding the interactions between AD related proteins and metals that are prevalent in industrial and environmental settings such as nickel (Ni), mercury (Hg) and uranium (U) is important, as they may affect the disease progression.

The role of metal ions in AD has been discussed for decades, and as repeatedly mentioned in this thesis, it is still far from elucidated. Therefore, it is important to continue the studies to, if possible, reach a consensus if and how metals are involved in AD pathogenesis.

1.7.4.1 Mercury

Mercury is a chemical element with the atomic number 80. It occurs in three forms: elemental/metallic (Hg), inorganic (including Hg(I), which typically occurs as diatomic Hg_2^{2+} and Hg(II)) and organic (such as methyl- or ethyl mercury, CH_3Hg^+ and $C_2H_5Hg^+$, respectively). Humans are primarily exposed to Hg from industrial sources and through consumption of seafood. In 2021, the World Health Organization (WHO) placed mercury on the top ten list of "chemicals of major public health concern" and according to the Global Mercury Assessment 2018, the atmospheric Hg increased by 20% between 2010 and 2015, indicating a growing problem (UNEP, 2019; WHO, 2021).

It is well known that Hg is a toxic metal with a wide range of adverse health effects, affecting organs such as the lungs, kidneys, brain and nervous system (Arrifano et al., 2018; Bernhoft, 2012; Rice et al., 2014). Methyl mercury and mercury vapor are especially toxic as they can cross membranes, including the BBB. They are also able to accumulate in the brain and disrupt cellular functions and components through the generation of ROS and oxidative stress, inhibit enzyme function, disrupt Ca homeostasis and as a result interfere with the release of neurotransmitters (Carvalho et al., 2019; Farina et al., 2013; Kerper et al., 1992; Paduraru et al., 2022; Roos et al., 2012). The neurotoxicity of organic mercury such as MeHg is not completely understood. However, important targets for MeHg are sulfhydryl groups, which are present in larger proteins but also in the amino acid cysteine. By modifying the state of the SH-groups, the protein function may become perturbed (Farina et al., 2013).

1.7.4.2 Nickel

Nickel is a ferromagnetic metal that occurs naturally in the earth's crust in many minerals. It is a common metal in the industrialized world and is used mainly in Ni-Cd batteries, stainless steel and coins. Ni is not an essential metal in humans, although it

seems to be essential for some bacteria and plants (Eskew et al., 1983; Fischer et al., 2016). Nickel can be toxic for humans and may affect the cardiovascular system, have dermatological effects and be neurotoxic. The metal can reach the brain via the olfactory neurons in rats, and thereby circumvent the BBB (Henriksson et al., 1997). It contributes to neurotoxicity through ROS formation, inflammation and mitochondrial dysfunction. It also disrupts neurotransmitter systems, negatively affecting synaptic transmission and plasticity (He et al., 2011; Ijomone, 2021; Marchetti, 2014). One study showed that mice brains exposed to Ni nanoparticles exposed higher concentrations of both $A\beta_{40}$ and $A\beta_{42}$ than the controls (Kim et al., 2012). Although Ni is not the metal of primary focus in AD, it is a metal commonly occurring in the environment and as a result, many people are exposed and its potential contribution to neurogenerative processes should not be overlooked.

1.7.4.3 Uranium

Uranium is a metal with atomic number 92. It occurs in several isotopes, with uranium 238 being the most common. Depending on the chemical form, the toxicity of uranium varies. For example, natural uranium is very weakly radioactive, and its toxicity is primarily exerted through its chemical properties as a heavy metal. Enriched and depleted uranium is most commonly used as fuel in nuclear reactors and in military ammunition, respectively. Uranium is not a very common metal in the environment; however, uranium is a natural component of the earth's crust and activities like mining, volcanoes or industrial work may lead to its release. Therefore, the primary way of uranium exposure is through contaminated soil or water. Uranium mainly affects kidneys and bones, where it can accumulate and cause damage. Its role in neurotoxicity is not very well studied, but it is known to induce ROS, disrupt neurotransmitter release and damage mitochondria. In animal studies, it has been shown that the memory of the uranium exposed animals is affected, and a chronic exposure to uranium can result in depression-like symptoms and sleep disturbances (Lestaevel et al., 2005; Vellingiri, 2023). In this thesis, the metallic oxycation uranyl has been studied, and although the U ion is bound to oxygen, uranium ion is dominant in the molecule. The uranyl ion is soluble in water, and it is the most common form of U found in nature.

1.8 Therapeutic strategies for Alzheimer's disease

AD poses a significant challenge to both healthcare systems and researchers worldwide due to its complex pathology. Despite extensive research, where various aspects and molecular pathways of AD have been targeted, no effective disease-modifying treatment has yet been developed.

Traditionally, AD treatment has focused on symptom management rather than modifying the disease progression (Sheikh et al., 2023). As the cholinergic hypothesis suggest that a decrease in ACh is implicated in the cognitive decline, acetylcholinesterase inhibitors (such as Donepezil, Rivastigmine and Galantamine) have been developed and are used to treat mild to moderate AD by increasing levels of ACh (Annicchiarico et al., 2007). These drugs are often used in combination with NMDA receptor antagonists that can modulate the activity of glutamate which at high concentrations may cause neuronal damage (Hansen et al., 2008; Vaz & Silvestre, 2020).

Since the amyloid cascade hypothesis and the role of APP was proposed and widely accepted in the 1990s (Hardy & Higgins, 1992), a natural target for drug development has been the Aβ peptide. One strategy has been to target the secretases involved in the

proteolytic cleavage of APP, to reduce the amount of Aβ produced. Initially the focus was on inhibiting the main β-secretase (BACE1), but early compounds of BACE1-inhibitors faced challenges with selectivity and exposed an insufficient clinical effect on cognitive and functional decline. In addition, when the amyloid cascade hypothesis started to be debated, many companies shifted their focus towards other targets, resulting in a reduction of BACE inhibitors in clinical trials (Bazzari & Bazzari, 2022; Cummings et al., 2024; Egan et al., 2018). Another strategy is to instead upregulate the α-secretase (particularly ADAM10) to promote the non-amyloidogenic pathway. This approach showed promising results in a pilot study back in 2014 (Endres et al., 2014) and today two α-secretase modulator drugs are in phase 2 clinical trials (Cummings et al., 2024; Endres & Deller, 2017).

A problem with targeting the secretases for APP cleavage (α-,β- and γ-secretase) is that they have other important physiological functions and target also other substrates than APP. Therefore, their targeting may have some severe side effects (Hartmann et al., 2002; Hur, 2022).

In recent years, monoclonal antibodies (mAbs) have emerged as a leading and promising strategy in AD treatment as well as in other neurodegenerative diseases such as multiple sclerosis (Freeman & Zephir, 2024). The mAbs are designed to bind Aβ peptides at different stages of aggregation, facilitate their clearance from the brain and thereby might slow down disease progression. In 2021, the mAb Aducanumab was approved for AD treatment in the USA (U.S Food and Drug Administration, 2021). It is the first disease-modifying therapy that has been approved for AD treatment and was followed by the approval of Lecanemab in the USA in 2023 (U.S Food and Drug Administration, 2023). Additionally, several mAbs (Donanemab, Gantenerumab, Solanezumab etc.) are currently in clinical trials (Cummings et al., 2024).

Another type of drug for AD that has been suggested is the use of metal chelators. Metal chelators are chemical compounds that bind to metal ions and modulate the metal balance in the body. In AD, the chelators may play a role by affecting pathological processes related to metals, especially those that involve copper, zinc and iron. The principle of chelators is that they bind specifically and create complexes which redistribute metal ions or excrete them. In AD the aim would be to reduce or redistribute the levels of metal ions such as iron, copper and zinc which are most associated with aggregation of Aβ, oxidative stress, and also found in elevated levels in amyloid plaques. A few drugs have been suggested: Clioquinol and PBT2 bind specifically to Cu and Zn and have been shown to reduce number of Aβ aggregates and improve cognitive function in animal models. Additionally, iron and zinc chelators have also been tested (deferoxamine, deferasirox and TMEDA) to reduce the oxidative stress caused by the metal ions. However, none of the metal chelators mentioned above are available for the treatment of AD, as more studies are needed to ensure safety and minimize the side effects. Since the role of metals in AD is not yet fully understood, new insights are likely required before treatments with metal chelators can be used in AD (Budimir, 2011; Kenche & Barnham, 2011; Sharma et al., 2018). Additionally lipoic acid, which is a strong antioxidant that has been shown to have metal-chelating properties and have been suggested as a potential redistributor of copper in AD (Kirss et al., 2024).

2 Aims of the study

During the last decades, the connection between Alzheimer's disease and metals has been extensively studied. The aim of the current thesis has been to further examine the effect of metals on AD related proteins and peptides.

I. To investigate the interaction of inorganic mercury with different isoforms of the Apolipoprotein E protein and examine how the secondary structure of the protein is affected.

II. To investigate the interactions between Ni(II) ions and Aβ peptides, focusing on the metal-binding properties, the effects on Aβ structure and aggregation.

III. To determine if different ATCUN motifs show different Cu(II)-binding affinities under the conditions of direct competition with HSA and elucidate whether truncated Aβ peptides with ATCUN motifs can compete with HSA for the binding of Cu(II) ions.

IV. To monitor the effects of uranyl ions on the structure and aggregation of different Aβ species.

3 Materials and methods

Publication I: Mercury Ion Binding to Apolipoprotein E Variants ApoE2, ApoE3, and ApoE4: Similar Binding Affinities but Different Structure Induction Effects

- Fluorescence measurements: titration of Hg ions to monitor changes in intrinsic tryptophan fluorescence.
- Circular dichroism: titration of Hg ions to ApoE variants to determine the effect on secondary structure.

Publication II: Residue-specific binding of Ni(II) ions influences the structure and aggregation of amyloid beta (Aβ) peptides

- NMR spectroscopy: molecular details of Ni(II) binding to Aβ monomer and estimation of Ni binding affinity to Aβ.
- Circular dichroism: monitoring change in secondary structure of Aβ upon addition of Ni(II) ions.
- ThT fluorescence assay: effect of Ni(II) ions on kinetics of Aβ40 aggregation
- AFM imaging: characterization of morphology of Aβ40 aggregates.
- BN-PAGE analysis.
- FTIR spectroscopy of Aβ oligomers.
- Fluorescence microscopy: monitoring formation of dityrosine crosslinks.

Publication III: Direct Competition of ATCUN Peptides with Human Serum Albumin for Copper(II) Ions Determined by LC-ICP MS

- Competition of ATCUN Peptides with Human Serum Albumin for Cu(II) ions.
- LCP-ICP MS analysis.
- Data analysis for determination of relative dissociation constants.

Publication IV: Characterization of Uranyl (UO_2^2) Ion Binding to Amyloid Beta (Aβ) Peptides: Effects on Aβ Structure and Aggregation

- Monitoring of Aβ aggregation by ThT fluorescence.
- TEM imaging of aggregated Aβ40 peptides.
- NMR spectroscopy: binding of uranyl to Aβ40 monomers.
- Fluorescence measurements to determine binding affinity of uranyl to Aβ via quenching of Tyr10 fluorescence.
- Circular dichroism: monitoring changes in the secondary structure of Aβ upon addition of UO_2^2 ions.
- BN-PAGE analysis.
- FTIR spectroscopy.

4 Results

Publication I: Mercury Ion Binding to Apolipoprotein E Variants ApoE2, ApoE3, and ApoE4: Similar Binding Affinities but Different Structure Induction Effects

- Hg(II) ions have similar binding affinity to all three Apolipoprotein E variants ApoE2, ApoE3 and ApoE4, indicating that the cysteine residues in position 112 and 158 are not involved in binding of metal ions.
- Titration to the ApoE peptide with Hg(II) ions affects their secondary structure differently, the largest change can be observed in ApoE4.

Publication II: Residue-specific binding of Ni (II) ions influences the structure and aggregation of amyloid beta (Abeta) peptides

- Specific binding of Ni(II) ions to the N-terminal region of the $A\beta_{40}$ peptide was observed at neutral pH (7.3) but not at acidic pH (5.1). In the presence of a membrane-mimicking system (SDS micelles), no effect was observed on the C-terminal, while the N-terminal was largely affected.
- Addition of Ni (II) ions to Aβ peptides in aqueous buffer reduces intensity while the shape of CD spectra remains unaffected. This suggests that Ni(II) ions induce precipitation and reduce Aβ in solution.
- Ni(II) ions induce structural changes in $A\beta_{40}$ WT and $A\beta_{4-40}$ in aqueous buffer solution, indicating the transition of polyproline II helix structures into random coil structures.
- In membrane mimicking environment the peptide takes an alpha helical structure. Titration of Ni(II) ions reduce the intensity at 208nm but not at 222nm, indicating an increase in superhelicity.
- The estimated dissociation constant for the $A\beta_{40} \cdot$Ni(II) complex is in the low µM range.
- At sub-stoichiometric Ni(II):$A\beta_{40}$ ratios, the Ni(II) ions slow down the $A\beta_{40}$ fibrillization kinetics in a concentration-dependent manner.
- Results of IR and PAGE studies indicate that the addition of Ni(II) ions appears to interfere with the SDS-induced conversion of $A\beta_{42}$ monomers into homogenous and stable oligomeric structures, instead favoring the formation of larger and more heterogenous oligomer populations.
- Incubation of $A\beta_{40}$ and Ni(II) ions induces formation of dityrosine crosslinks.

Publication III: Direct Competition of ATCUN Peptides with Human Serum Albumin for Copper(II) Ions Determined by LC-ICP MS

- ATCUN and truncated Aβ peptides ($A\beta_{4-16}$ and $A\beta_{11-15}$) bind Cu(II) ions with an affinity similar to that for human serum albumin.
- Other ATCUN-containing peptides also have similar Cu(II)-binding affinities.

Publication IV: Characterization of Uranyl UO_2^{2+} Ion Binding to Amyloid Beta (Abeta) Peptides: Effects on Abeta Structure and Aggregation

- UO_2^{2+} ions inhibit the formation of Aβ amyloid fibrils in a concentration-dependent manner, with complete inhibition at stoichiometric uranyl/Aβ$_{40}$ ratios.
- Uniformly distributed, concentration dependent intensity loss of amide-cross-peak intensity in NMR spectra occurs at both pH 7.3 and 5.1.
- UO_2^{2+} ions bind with higher affinity to Aβ$_{40}$ WT and Aβ$_{40}$ NoHis at a lower pH.
- A structural transition in Aβ from random coil to β-sheets occurs upon titration of UO_2^{2+} ions at pH 5.1.
- UO_2^{2+} ions are not able to induce dityrosine crosslinks under the experimental conditions used.

5 Discussion

Alzheimer's disease is characterized by progressive cognitive decline and memory impairment, with an inevitable fatal outcome. It is a challenging disorder that places a great emotional burden on the patients and their families as well as a significant economic burden on society. Despite extensive investigation over several decades, many details regarding the pathogenesis of AD are still unknown.

The Aβ peptides are considered central to AD pathology and most likely play a critical role in the development and progression of the disease. Although the amyloid cascade hypothesis and the role of Aβ in AD pathogenesis is under debate, it is generally accepted that peptide plays an important role in AD pathogenesis. However, there is still disagreement about whether Aβ aggregation is the cause of the disease, or a consequence contributing to disease progression. It has been shown that the Aβ peptide exerts toxicity to cells during the aggregation process while preformed mature fibrillar aggregates show little or no toxicity (Krishtal et al., 2017). Therefore, understanding the aggregation process and the behavior of the Aβ peptide is crucial to understanding AD. Today, the oligomeric forms of Aβ are considered the most toxic species. Although the toxic mechanism is still unclear, it is believed to involve membrane disruption and induction of Ca-leakage (Wärmländer et al., 2019). Studying oligomeric Aβ species is therefore of great importance. However, as the oligomeric species are very unstable, their studies are complicated. To stabilize the oligomers detergents or fatty acids are often used (Vosough & Barth, 2021). Because there are many ways to prepare Aβ oligomers, there is also considerable variation in their reported properties, which makes it difficult to compare results and reach a consensus. It should be mentioned that Aβ peptides are in general extremely sensitive to variations in the experimental conditions. Factors such as pH, temperature, concentration, agitation, and access to surfaces or other interfaces may have large effects on the peptide's behavior. It is imperative to consider this when performing experiments and comparing results.

Metal ions such as copper, zinc and iron have for a long time been implicated in AD pathology, although their exact role remains unclear. They have been shown to interact with the Aβ peptide, influence aggregation, and possibly also promote the formation of toxic oligomeric species. Redox-active metal ions are furthermore known to induce ROS, which may cause further cellular and molecular damage. It is not yet clear if metal dyshomeostasis is a cause or an effect of the disease. It is also not clear if the formation of large aggregates is formed as a result of metal ions influencing the Aβ-peptide, or if the already formed aggregates attract metal ions. Either way, the metal ions seem to be involved in the pathological processes of AD, and possibly exacerbate it.

Metal binding to the Aβ peptide has been the focus in three of the papers in this thesis. Variants of the full length Aβ-peptide were the main focus in paper II and IV. Paper III instead focused on shorter, truncated segments of the peptide (Aβ$_{4-16}$ and Aβ$_{11-15}$), which have a histidine residue at the third position, thereby forming ATCUN-motifs (NH2-X-Z-H). ATCUN-motifs are known to bind certain metal ions with high affinity through square planar geometry coordination involving-terminal amino group, two adjacent peptide nitrogens, and nitrogen from the histidine residue at position three.

The truncated, ATCUN motif-containing Aβ$_{4-42}$ and Aβ$_{11-42}$ peptide fragments have been found in high concentrations in plaques of AD brains (Liu et al., 2006; Naslund et al., 1994; Portelius et al., 2010). The ATCUN configurations likely allow high-affinity metal binding to these peptide fragments, thereby probably altering the metal-peptide

interactions compared to the full-length peptide. Removal of the first three amino acids (Asp1, Ala2, Glu3) of the Aβ peptide furthermore reduces the overall negative charge of the peptide. It has been suggested that truncation of the N-terminal might increase the aggregation rate of the peptide, although the overall toxicity seems to be similar for Aβ$_{4-x}$ peptides and full-length peptides (Bouter et al., 2013; Pike et al., 1995; Wirths et al., 2019). The truncation also affects the conformation of the peptide. Aβ$_{4-x}$ peptides may have a stronger propensity to form β-sheets, due to the increased hydrophobicity (Karkisaval et al., 2020; Pike et al., 1995). In this thesis, structural studies have been performed on the Aβ$_{4-40}$ peptide with CD spectroscopy. No significant structural differences between the truncated- and full-length peptides were observed with this method (Figure 3, paper II). It should be pointed out that CD measurements are not very exact, as they report on the average secondary structure content in the sample. The truncated Aβ$_{4-16}$ peptide has been reported to bind Cu(II) ions with similar affinity than human serum albumin (HSA), where the latter normally binds a substantial amount of the body's circulating copper in the body (Kirsipuu et al., 2020). Interestingly, we showed that short peptides with ATCUN motifs could not remove substantial amounts of Cu(II) ions from excess HSA in blood and CSF environments (Paper III). We also investigated the interactions between full-length Aβ peptides, nickel(II) and uranyl ions, respectively. Interestingly, both Ni(II) and UO$_2^{2+}$ ions induce structural changes and inhibit the fibrillation pathway of the peptide, although through different mechanisms. The uranyl ions did not show residue-specific binding to Aβ. Instead, the observed interaction effects are likely caused by electrostatic interactions between the cationic uranyl ion and the anionic peptide. For the Ni(II) ion, on the other hand, we observed specific binding to N-terminal residues, especially histidines. This result shows that metal ions can affect the peptides via various modes of interaction. For example, when the peptide is in membrane-mimicking environments, the Aβ peptide typically adopts α-helical conformations. CD spectroscopy can then be used to measure the characteristic CD intensities at 208 nm and 222 nm, where the θ$_{222}$/θ$_{208}$ ratio reflects the amount of superhelicity in the sample (Barbar & Nyarko, 2014). A clear increase in superhelicity, i.e. α-helices wound around each other as coiled-coils, can be observed in the Aβ$_{1-40}$ WT and Aβ$_{4-40}$ samples when Ni(II) ions are added. The coiled-coil conformation might enhance peptide stability and could therefore influence the aggregation process (Lupas & Bassler, 2017). The uranyl ion did not show a similar induction of superhelicity, although a structural transition from random coil into β-sheet structure was observed for Aβ peptides in aqueous solution. This structural change is thought to promote the Aβ aggregation, although the Thioflavin T fluorescence curves and images from transmission electron microscopy show that uranyl ions inhibit the fibrillization of the peptide by directing it towards non-fibrillar, amorphous aggregates in a concentration-dependent manner.

The Ni(II) ions were found to induce dityrosine cross-links, which is a common effect of ROS action. Thus, Ni(II) ions may affect the Aβ aggregation processes not only through direct interactions with the peptide, but also through ROS formation. Dityrosine-linked Aβ dimers have been found in amyloid plaques in AD brains, most likely formed from ROS interactions, where the oxygen radicals might be created by the redox-active metal ions bound to the plaques (Berntsson et al., 2023; D. P. Smith et al., 2007; Williams et al., 2016). Since Ni(II) ions bind to the Aβ N-terminal segment, mainly via histidine residues, it is possible that these metal ions can induce aggregation by coordinating histidine residues from several peptides. This would also position the Y10 residues in close

proximity, potentially facilitating the formation of dityrosine motifs. Aβ-dimers linked together via covalent dityrosine bonds are more stable and resistant to dissociation compared to other non-covalently linked Aβ dimers (Kok et al., 2013).

Although the Aβ peptide is in the primary focus of AD research, the Aβ peptide will probably not give us all the answers about the disease. Other proteins and biomolecules also play important roles in AD. For example, the lipoprotein ApoE has been found within the amyloid plaques of AD patients, and the ApoE4 isoform is today the main genetic risk factor for developing sAD (Corder et al., 1993; Liao et al., 2004; Mishra et al., 2018). Interestingly, ApoE has been suggested to be involved in the clearance of metal ions and/or Aβ peptides from the brain. This conclusion is supported by the facts that the carriers (homo-/heterozygotes) of the ApoE4 isoform are more susceptible to mercury toxicity and have a higher risk of developing AD. In paper I of this thesis, we studied the effect of mercury ions on ApoE by monitoring changes in the secondary structure of the protein, as well as determining the apparent binding affinity for Hg(II) ions. Earlier, it has been suggested that the ApoE4 isoform may be less effective in metal binding as this isoform lacks cysteine residues at positions 112 and 158. Interestingly, the binding affinities for Hg(II) ions turned out to be virtually the same for all three isoforms, showing that Cys112 and Cys158 are not involved in Hg (II)-binding. Yet, binding of Hg(II) ions affected the secondary structure of the ApoE variants differently - the superhelicity increased more in ApoE4 than in ApoE2 and ApoE3. A previous study has shown that the C-terminal ApoE segment has a propensity to form superhelices, stabilized by salt bridges, and our results may therefore be explained by structural changes in this segment (Choy et al., 2003). It should be mentioned that the three ApoE isoforms have different initial secondary structures, as the variations at position 112 and 158 affect the protein structure. For example, it has been suggested that interactions between Arg61 and Glu255 would pull the N- and C-terminal segments closer to each other. This interaction does not happen when Cys112 is present, due to interactions between Cys112 and Arg61. With this initial difference, it is reasonable that addition of Hg(II) ions induces different structural alterations in the different isoforms. It has furthermore been shown that when ApoE is in a lipid-free solution, then the C-terminal segment promotes tetramerization, as the hydrophobic residues are positioned in the center of the tetramer and become protected from the aqueous environment. Such structural effects could potentially also affect the metal-binding properties of the protein (Horn et al., 2023).

This thesis adds new knowledge about the interactions AD-related proteins and peptides with metal ions, which provides new insights into the disease mechanism, and thereby helps to solve the large puzzle of Alzheimer's disease.

Conclusions

I. All tree isoforms of Apolipoprotein E (ApoE2, ApoE3 and ApoE4) were found to bind mercury ions with similar binding affinities. Yet, the Hg(II) ions induce different structural changes in the isoforms, with the largest changes in ApoE4. The changes observed are interpreted as increased superhelicity, due to the effects on the $\theta_{222}/\theta_{208}$ ratio in CD spectra. The results show that Hg binding is likely coordinated by other amino acids than Cys112 and Cys158, which are present in ApoE2 (Cys112 and Cys158) and ApoE3 (Cys112). Weaker Hg (II) binding was seen at pH 5, indicating that histidines are involved (i.e., His140 and His 299), although multiple binding sites are likely present. The binding affinity of Hg(I) ions is much weaker than that of divalent Hg(II) ions which suggests that the potentially harmful interactions between ApoE and Hg are happening in the oxidizing extracellular environment.

II. Ni(II) ions bind to the N-terminal segment of Aβ, with a binding affinity in the low μM range. The binding of Ni(II) ions affects the fibrillization process, and at equimolar amounts directs the aggregation away from fibrillar structures and towards amorphous aggregates. The bound Ni ions induce the formation of dityrosine cross-links via redox chemistry, thereby creating covalent Aβ dimers. Secondary structure alterations are observed upon the addition of Ni(II) ions, both in an aqueous environment and in a membrane-mimicking environment. Stochiometric amounts of Ni(II) ions promote the formation of heterogeneous Aβ oligomers. Since the oligomers are considered the most toxic species of Aβ aggregates, this might contribute to AD brain pathology.

III. Cu ions bind to truncated ATCUN-containing Aβ peptides with similar affinity as to human serum albumin. The ATCUN motif-containing peptides do not remove substantial amounts of Cu(II) ions from excess human serum albumin in blood and CSF environments.

IV. Uranyl ions bind to the Aβ peptide via non-specific electrostatic interactions, with the strongest binding affinity observed at pH 5.1. Weaker binding was observed at physiological pH values, potentially explained by interference from His sidechains or by the presence of other uranyl species. The uranyl ions inhibit Aβ fibrillization already at sub-stochiometric concentrations and induce structural changes in both monomeric and oligomeric Aβ species.

References

Aaseth, J., Alexander, J., Bjorklund, G., Hestad, K., Dusek, P., Roos, P. M., & Alehagen, U. (2016). Treatment strategies in Alzheimer's disease: a review with focus on selenium supplementation. *Biometals*, *29*(5), 827-839. https://doi.org/10.1007/s10534-016-9959-8

Abelein, A., Abrahams, J. P., Danielsson, J., Gräslund, A., Jarvet, J., Luo, J., Tiiman, A., & Wärmländer, S. K. (2014). The hairpin conformation of the amyloid beta peptide is an important structural motif along the aggregation pathway. *J Biol Inorg Chem*, *19*(4-5), 623-634. https://doi.org/10.1007/s00775-014-1131-8

Adamu, A., Li, S., Gao, F., & Xue, G. (2024). The role of neuroinflammation in neurodegenerative diseases: current understanding and future therapeutic targets. *Frontiers in Aging Neuroscience*, *16*, 1347987. https://doi.org/10.3389/fnagi.2024.1347987

Agarwal, P., Leurgans, S. E., Agrawal, S., Aggarwal, N. T., Cherian, L. J., James, B. D., Dhana, K., Barnes, L. L., Bennett, D. A., & Schneider, J. A. (2023). Association of Mediterranean-DASH Intervention for Neurodegenerative Delay and Mediterranean Diets With Alzheimer Disease Pathology. *Neurology*, *100*(22), e2259-e2268. https://doi.org/10.1212/WNL.0000000000207176

Aizenstein, H. J., Nebes, R. D., Saxton, J. A., Price, J. C., Mathis, C. A., Tsopelas, N. D., Ziolko, S. K., James, J. A., Snitz, B. E., Houck, P. R., Bi, W., Cohen, A. D., Lopresti, B. J., DeKosky, S. T., Halligan, E. M., & Klunk, W. E. (2008). Frequent amyloid deposition without significant cognitive impairment among the elderly. *Arch Neurol*, *65*(11), 1509-1517. https://doi.org/10.1001/archneur.65.11.1509

Ajsuvakova, O. P., Tinkov, A. A., Aschner, M., Rocha, J. B. T., Michalke, B., Skalnaya, M. G., Skalny, A. V., Butnariu, M., Dadar, M., Sarac, I., Aaseth, J., & Bjorklund, G. (2020). Sulfhydryl groups as targets of mercury toxicity. *Coord Chem Rev*, *417*. https://doi.org/10.1016/j.ccr.2020.213343

Al-Hilaly, Y. K., Williams, T. L., Stewart-Parker, M., Ford, L., Skaria, E., Cole, M., Bucher, W. G., Morris, K. L., Sada, A. A., Thorpe, J. R., & Serpell, L. C. (2013). A central role for dityrosine crosslinking of Amyloid-beta in Alzheimer's disease. *Acta Neuropathol Commun*, *1*, 83. https://doi.org/10.1186/2051-5960-1-83

Alberts, B., Johnson, A., Lewis, J., Raff, M., Roberts, K., & Walter, P. (2008). *Molecular Biology of The Cell* (5 ed.). Garland science, Taylor & Francis Group.

Alies, B., Renaglia, E., Rozga, M., Bal, W., Faller, P., & Hureau, C. (2013). Cu(II) affinity for the Alzheimer's peptide: tyrosine fluorescence studies revisited. *Anal Chem*, *85*(3), 1501-1508. https://doi.org/10.1021/ac302629u

Alzheimer, A. (1907). Über eine eigenartige Erkrankung der Hirnrinde. *Allgemeine Zeitschrift fur Psychiatrie und Psychisch-gerichtliche Medizin*, *64*, 146-148.

Alzheimer, A., Stelzmann, R. A., Schnitzlein, H. N., & Murtagh, F. R. (1995). An English translation of Alzheimer's 1907 paper, "Uber eine eigenartige Erkankung der Hirnrinde". *Clin Anat*, *8*(6), 429-431. https://doi.org/10.1002/ca.980080612

Annicchiarico, R., Federici, A., Pettenati, C., & Caltagirone, C. (2007). Rivastigmine in Alzheimer's disease: Cognitive function and quality of life. *Ther Clin Risk Manag*, *3*(6), 1113-1123. https://www.ncbi.nlm.nih.gov/pubmed/18516265

Arrifano, G. P. F., Martin-Doimeadios, R. C. R., Jimenez-Moreno, M., Fernandez-Trujillo, S., Augusto-Oliveira, M., Souza-Monteiro, J. R., Macchi, B. M., Alvarez-Leite, J. I., do Nascimento, J. L. M., Amador, M. T., Santos, S., Ribeiro-Dos-Santos, A., Silva-Pereira, L. C., Oria, R. B., & Crespo-Lopez, M. E. (2018). Genetic Susceptibility to Neurodegeneration in Amazon: Apolipoprotein E Genotyping in Vulnerable Populations Exposed to Mercury. *Frontiers in Genetics*, *9*, 285. https://doi.org/10.3389/fgene.2018.00285

Association, A. (2023). 2023 Alzheimer's disease facts and figures. *Alzheimers Dement*, *19*(4), 1598-1695. https://doi.org/10.1002/alz.13016

Assoni, A. F., Foijer, F., & Zatz, M. (2023). Amyotrophic Lateral Sclerosis, FUS and Protein Synthesis Defects. *Stem Cell Rev Rep*, *19*(3), 625-638. https://doi.org/10.1007/s12015-022-10489-8

Ayers, J. I., Lee, J., Monteiro, O., Woerman, A. L., Lazar, A. A., Condello, C., Paras, N. A., & Prusiner, S. B. (2022). Different alpha-synuclein prion strains cause dementia with Lewy bodies and multiple system atrophy. *Proceedings of the National Academy of Sciences of the United States of America*, *119*(6). https://doi.org/10.1073/pnas.2113489119

Babic Leko, M., Langer Horvat, L., Spanic Popovacki, E., Zubcic, K., Hof, P. R., & Simic, G. (2023). Metals in Alzheimer's Disease. *Biomedicines*, *11*(4). https://doi.org/10.3390/biomedicines11041161

Bagheri, S., Squitti, R., Haertle, T., Siotto, M., & Saboury, A. A. (2017). Role of Copper in the Onset of Alzheimer's Disease Compared to Other Metals. *Frontiers in Aging Neuroscience*, *9*, 446. https://doi.org/10.3389/fnagi.2017.00446

Bakulski, K. M., Seo, Y. A., Hickman, R. C., Brandt, D., Vadari, H. S., Hu, H., & Park, S. K. (2020). Heavy Metals Exposure and Alzheimer's Disease and Related Dementias. *Journal of Alzheimer's disease : JAD*, *76*(4), 1215-1242. https://doi.org/10.3233/JAD-200282

Barbar, E., & Nyarko, A. (2014). NMR Characterization of Self-Association Domains Promoted by Interactions with LC8 Hub Protein. *Comput Struct Biotechnol J*, *9*, e201402003. https://doi.org/10.5936/csbj.201402003

Barnham, K. J., Haeffner, F., Ciccotosto, G. D., Curtain, C. C., Tew, D., Mavros, C., Beyreuther, K., Carrington, D., Masters, C. L., Cherny, R. A., Cappai, R., & Bush, A. I. (2004). Tyrosine gated electron transfer is key to the toxic mechanism of Alzheimer's disease beta-amyloid. *FASEB J*, *18*(12), 1427-1429. https://doi.org/10.1096/fj.04-1890fje

Barritt, J. D., & Viles, J. H. (2015). Truncated Amyloid-beta(11-40/42) from Alzheimer Disease Binds Cu2+ with a Femtomolar Affinity and Influences Fiber Assembly. *The Journal of Biological Chemistry*, *290*(46), 27791-27802. https://doi.org/10.1074/jbc.M115.684084

Bartus, R. T., Dean, R. L., 3rd, Beer, B., & Lippa, A. S. (1982). The cholinergic hypothesis of geriatric memory dysfunction. *Science*, *217*(4558), 408-414. https://doi.org/10.1126/science.7046051

Bayer, T. A. (2015). Proteinopathies, a core concept for understanding and ultimately treating degenerative disorders? *Eur Neuropsychopharmacol*, *25*(5), 713-724. https://doi.org/10.1016/j.euroneuro.2013.03.007

Bazzari, F. H., & Bazzari, A. H. (2022). BACE1 Inhibitors for Alzheimer's Disease: The Past, Present and Any Future? *Molecules*, *27*(24). https://doi.org/10.3390/molecules27248823

Beauchemin, D., & Kisilevsky, R. (1998). A method based on ICP-MS for the analysis of Alzheimer's amyloid plaques. *Anal Chem*, *70*(5), 1026-1029. https://doi.org/10.1021/ac970783f

Berdynski, M., Miszta, P., Safranow, K., Andersen, P. M., Morita, M., Filipek, S., Zekanowski, C., & Kuzma-Kozakiewicz, M. (2022). SOD1 mutations associated with amyotrophic lateral sclerosis analysis of variant severity. *Scientific Reports*, *12*(1), 103. https://doi.org/10.1038/s41598-021-03891-8

Bernhoft, R. A. (2012). Mercury toxicity and treatment: a review of the literature. *Journal of Environmental and Public Health*, *2012*, 460508. https://doi.org/10.1155/2012/460508

Berntsson, E., Vosough, F., Svantesson, T., Pansieri, J., Iashchishyn, I. A., Ostojic, L., Dong, X., Paul, S., Jarvet, J., Roos, P. M., Barth, A., Morozova-Roche, L. A., Graslund, A., & Warmlander, S. (2023). Residue-specific binding of Ni(II) ions influences the structure and aggregation of amyloid beta (Abeta) peptides. *Scientific Reports*, *13*(1), 3341. https://doi.org/10.1038/s41598-023-29901-5

Bertram, L., McQueen, M. B., Mullin, K., Blacker, D., & Tanzi, R. E. (2007). Systematic meta-analyses of Alzheimer disease genetic association studies: the AlzGene database. *Nature genetics*, *39*(1), 17-23. https://doi.org/10.1038/ng1934

Biancalana, M., & Koide, S. (2010). Molecular mechanism of Thioflavin-T binding to amyloid fibrils. *Biochimica et biophysica acta*, *1804*(7), 1405-1412. https://doi.org/10.1016/j.bbapap.2010.04.001

Bitan, G., Kirkitadze, M. D., Lomakin, A., Vollers, S. S., Benedek, G. B., & Teplow, D. B. (2003). Amyloid beta -protein (Abeta) assembly: Abeta 40 and Abeta 42 oligomerize through distinct pathways. *Proceedings of the National Academy of Sciences of the United States of America*, *100*(1), 330-335. https://doi.org/10.1073/pnas.222681699

Bobba, A., Amadoro, G., Valenti, D., Corsetti, V., Lassandro, R., & Atlante, A. (2013). Mitochondrial respiratory chain Complexes I and IV are impaired by beta-amyloid via direct interaction and through Complex I-dependent ROS production, respectively. *Mitochondrion*, *13*(4), 298-311. https://doi.org/10.1016/j.mito.2013.03.008

Bouter, Y., Dietrich, K., Wittnam, J. L., Rezaei-Ghaleh, N., Pillot, T., Papot-Couturier, S., Lefebvre, T., Sprenger, F., Wirths, O., Zweckstetter, M., & Bayer, T. A. (2013). N-truncated amyloid beta (Abeta) 4-42 forms stable aggregates and induces acute and long-lasting behavioral deficits. *Acta Neuropathologica*, *126*(2), 189-205. https://doi.org/10.1007/s00401-013-1129-2

Brannstrom, K., Ohman, A., Nilsson, L., Pihl, M., Sandblad, L., & Olofsson, A. (2014). The N-terminal region of amyloid beta controls the aggregation rate and fibril stability at low pH through a gain of function mechanism. *J Am Chem Soc*, *136*(31), 10956-10964. https://doi.org/10.1021/ja503535m

Brewer, G. J. (2014). Alzheimer's disease causation by copper toxicity and treatment with zinc. *Frontiers in Aging Neuroscience*, *6*, 92. https://doi.org/10.3389/fnagi.2014.00092

Brito, D., Albrecht, F. C., de Arenaza, D. P., Bart, N., Better, N., Carvajal-Juarez, I., Conceicao, I., Damy, T., Dorbala, S., Fidalgo, J. C., Garcia-Pavia, P., Ge, J., Gillmore, J. D., Grzybowski, J., Obici, L., Pinero, D., Rapezzi, C., Ueda, M., & Pinto, F. J. (2023). World Heart Federation Consensus on Transthyretin Amyloidosis Cardiomyopathy (ATTR-CM). *Glob Heart*, *18*(1), 59. https://doi.org/10.5334/gh.1262

Budimir, A. (2011). Metal ions, Alzheimer's disease and chelation therapy. *Acta Pharm*, *61*(1), 1-14. https://doi.org/10.2478/v10007-011-0006-6

Bush, A. I. (2013). The metal theory of Alzheimer's disease. *Journal of Alzheimer's disease : JAD*, *33 Suppl 1*, S277-281. https://doi.org/10.3233/JAD-2012-129011

Bush, A. I., Pettingell, W. H., Multhaup, G., d Paradis, M., Vonsattel, J. P., Gusella, J. F., Beyreuther, K., Masters, C. L., & Tanzi, R. E. (1994). Rapid induction of Alzheimer A beta amyloid formation by zinc. *Science*, *265*(5177), 1464-1467. https://doi.org/10.1126/science.8073293

Bush, A. I., & Tanzi, R. E. (2008). Therapeutics for Alzheimer's disease based on the metal hypothesis. *Neurotherapeutics*, *5*(3), 421-432. https://doi.org/10.1016/j.nurt.2008.05.001

Byrne, L. M., Rodrigues, F. B., Johnson, E. B., Wijeratne, P. A., De Vita, E., Alexander, D. C., Palermo, G., Czech, C., Schobel, S., Scahill, R. I., Heslegrave, A., Zetterberg, H., & Wild, E. J. (2018). Evaluation of mutant huntingtin and neurofilament proteins as potential markers in Huntington's disease. *Science translational medicine*, *10*(458). https://doi.org/10.1126/scitranslmed.aat7108

Cai, Y., An, S. S., & Kim, S. (2015). Mutations in presenilin 2 and its implications in Alzheimer's disease and other dementia-associated disorders. *Clin Interv Aging*, *10*, 1163-1172. https://doi.org/10.2147/CIA.S85808

Cairns, N. J., Neumann, M., Bigio, E. H., Holm, I. E., Troost, D., Hatanpaa, K. J., Foong, C., White, C. L., 3rd, Schneider, J. A., Kretzschmar, H. A., Carter, D., Taylor-Reinwald, L., Paulsmeyer, K., Strider, J., Gitcho, M., Goate, A. M., Morris, J. C., Mishra, M., Kwong, L. K., . . . Mackenzie, I. R. (2007). TDP-43 in familial and sporadic frontotemporal lobar degeneration with ubiquitin inclusions. *Am J Pathol*, *171*(1), 227-240. https://doi.org/10.2353/ajpath.2007.070182

Calabresi, P., Mechelli, A., Natale, G., Volpicelli-Daley, L., Di Lazzaro, G., & Ghiglieri, V. (2023). Alpha-synuclein in Parkinson's disease and other synucleinopathies: from overt neurodegeneration back to early synaptic dysfunction. *Cell Death Dis*, *14*(3), 176. https://doi.org/10.1038/s41419-023-05672-9

Carmona, A., Roudeau, S., & Ortega, R. (2021). Molecular Mechanisms of Environmental Metal Neurotoxicity: A Focus on the Interactions of Metals with Synapse Structure and Function. *Toxics*, *9*(9). https://doi.org/10.3390/toxics9090198

Carvalho, L. V. B., Hacon, S. S., Vega, C. M., Vieira, J. A., Larentis, A. L., Mattos, R., Valente, D., Costa-Amaral, I. C., Mourao, D. S., Silva, G. P., & Oliveira, B. F. A. (2019). Oxidative Stress Levels Induced by Mercury Exposure in Amazon Juvenile Populations in Brazil. *International Journal of Environmental Research and Public Health*, *16*(15). https://doi.org/10.3390/ijerph16152682

Cataldo, J. K., Prochaska, J. J., & Glantz, S. A. (2010). Cigarette smoking is a risk factor for Alzheimer's Disease: an analysis controlling for tobacco industry affiliation. *Journal of Alzheimer's disease : JAD*, *19*(2), 465-480. https://doi.org/10.3233/JAD-2010-1240

Cenini, G., Cecchi, C., Pensalfini, A., Bonini, S. A., Ferrari-Toninelli, G., Liguri, G., Memo, M., & Uberti, D. (2010). Generation of reactive oxygen species by beta amyloid fibrils and oligomers involves different intra/extracellular pathways. *Amino Acids*, *38*(4), 1101-1106. https://doi.org/10.1007/s00726-009-0319-7

Chakrabarti, S., Khemka, V. K., Banerjee, A., Chatterjee, G., Ganguly, A., & Biswas, A. (2015). Metabolic Risk Factors of Sporadic Alzheimer's Disease: Implications in the Pathology, Pathogenesis and Treatment. *Aging Dis*, *6*(4), 282-299. https://doi.org/10.14336/AD.2014.002

Chasseigneaux, S., & Allinquant, B. (2012). Functions of Abeta, sAPPalpha and sAPPbeta : similarities and differences. *J Neurochem*, *120 Suppl 1*, 99-108. https://doi.org/10.1111/j.1471-4159.2011.07584.x

Checa, J., & Aran, J. M. (2020). Reactive Oxygen Species: Drivers of Physiological and Pathological Processes. *J Inflamm Res*, *13*, 1057-1073. https://doi.org/10.2147/JIR.S275595

Cheignon, C., Tomas, M., Bonnefont-Rousselot, D., Faller, P., Hureau, C., & Collin, F. (2018). Oxidative stress and the amyloid beta peptide in Alzheimer's disease. *Redox Biol*, *14*, 450-464. https://doi.org/10.1016/j.redox.2017.10.014

Chen, G. F., Xu, T. H., Yan, Y., Zhou, Y. R., Jiang, Y., Melcher, K., & Xu, H. E. (2017). Amyloid beta: structure, biology and structure-based therapeutic development. *Acta Pharmacologica Sinica*, *38*(9), 1205-1235. https://doi.org/10.1038/aps.2017.28

Chen, L. L., Fan, Y. G., Zhao, L. X., Zhang, Q., & Wang, Z. Y. (2023). The metal ion hypothesis of Alzheimer's disease and the anti-neuroinflammatory effect of metal chelators. *Bioorg Chem*, *131*, 106301. https://doi.org/10.1016/j.bioorg.2022.106301

Chen, Y., Lomnitski, L., Michaelson, D. M., & Shohami, E. (1997). Motor and cognitive deficits in apolipoprotein E-deficient mice after closed head injury. *Neuroscience*, *80*(4), 1255-1262. https://doi.org/10.1016/s0306-4522(97)00007-9

Chen, Z. Y., & Zhang, Y. (2022). Animal models of Alzheimer's disease: Applications, evaluation, and perspectives. *Zool Res*, *43*(6), 1026-1040. https://doi.org/10.24272/j.issn.2095-8137.2022.289

Chiti, F., & Dobson, C. M. (2017). Protein Misfolding, Amyloid Formation, and Human Disease: A Summary of Progress Over the Last Decade. *Annu Rev Biochem*, *86*, 27-68. https://doi.org/10.1146/annurev-biochem-061516-045115

Choy, N., Raussens, V., & Narayanaswami, V. (2003). Inter-molecular coiled-coil formation in human apolipoprotein E C-terminal domain. *J Mol Biol*, *334*(3), 527-539. https://doi.org/10.1016/j.jmb.2003.09.059

Ciccocioppo, F., Bologna, G., Ercolino, E., Pierdomenico, L., Simeone, P., Lanuti, P., Pieragostino, D., Del Boccio, P., Marchisio, M., & Miscia, S. (2020). Neurodegenerative diseases as proteinopathies-driven immune disorders. *Neural Regen Res*, *15*(5), 850-856. https://doi.org/10.4103/1673-5374.268971

Cicero, C. E., Mostile, G., Vasta, R., Rapisarda, V., Signorelli, S. S., Ferrante, M., Zappia, M., & Nicoletti, A. (2017). Metals and neurodegenerative diseases. A systematic review. *Environ Res*, *159*, 82-94. https://doi.org/10.1016/j.envres.2017.07.048

Ciurea, A. V., Mohan, A. G., Covache-Busuioc, R. A., Costin, H. P., Glavan, L. A., Corlatescu, A. D., & Saceleanu, V. M. (2023). Unraveling Molecular and Genetic Insights into Neurodegenerative Diseases: Advances in Understanding Alzheimer's, Parkinson's, and Huntington's Diseases and Amyotrophic Lateral Sclerosis. *International Journal of Molecular Sciences*, *24*(13). https://doi.org/10.3390/ijms241310809

Cline, E. N., Bicca, M. A., Viola, K. L., & Klein, W. L. (2018). The Amyloid-beta Oligomer Hypothesis: Beginning of the Third Decade. *Journal of Alzheimer's disease : JAD*, *64*(s1), S567-S610. https://doi.org/10.3233/JAD-179941

Cohen, A. S. (1986). General Introduction and a Brief History of Amyloidosis. In *Amyloidosis*. Dordrecht Springer. https://doi.org/https://doi.org/10.1007/978-94-009-4309-4_1

Cole, S. L., & Vassar, R. (2007). The Basic Biology of BACE1: A Key Therapeutic Target for Alzheimer's Disease. *Curr Genomics*, *8*(8), 509-530. https://doi.org/10.2174/138920207783769512

Collinge, J., Whitfield, J., McKintosh, E., Beck, J., Mead, S., Thomas, D. J., & Alpers, M. P. (2006). Kuru in the 21st century--an acquired human prion disease with very long incubation periods. *Lancet*, *367*(9528), 2068-2074. https://doi.org/10.1016/S0140-6736(06)68930-7

Conte-Daban, A., Borghesani, V., Sayen, S., Guillon, E., Journaux, Y., Gontard, G., Lisnard, L., & Hureau, C. (2017). Link between Affinity and Cu(II) Binding Sites to Amyloid-beta Peptides Evaluated by a New Water-Soluble UV-Visible Ratiometric Dye with a Moderate Cu(II) Affinity. *Anal Chem*, *89*(3), 2155-2162. https://doi.org/10.1021/acs.analchem.6b04979

Corder, E. H., Saunders, A. M., Risch, N. J., Strittmatter, W. J., Schmechel, D. E., Gaskell, P. C., Jr., Rimmler, J. B., Locke, P. A., Conneally, P. M., Schmader, K. E., & et al. (1994). Protective effect of apolipoprotein E type 2 allele for late onset Alzheimer disease. *Nature genetics*, *7*(2), 180-184. https://doi.org/10.1038/ng0694-180

Corder, E. H., Saunders, A. M., Strittmatter, W. J., Schmechel, D. E., Gaskell, P. C., Small, G. W., Roses, A. D., Haines, J. L., & Pericak-Vance, M. A. (1993). Gene dose of apolipoprotein E type 4 allele and the risk of Alzheimer's disease in late onset families. *Science*, *261*(5123), 921-923. https://doi.org/10.1126/science.8346443

Coronel, R., Palmer, C., Bernabeu-Zornoza, A., Monteagudo, M., Rosca, A., Zambrano, A., & Liste, I. (2019). Physiological effects of amyloid precursor protein and its derivatives on neural stem cell biology and signaling pathways involved. *Neural Regen Res*, *14*(10), 1661-1671. https://doi.org/10.4103/1673-5374.257511

Council, N. R. (2000). Physiological Role of Copper. In *Copper in Drinking Water*. National Academies Press (US). https://doi.org/10.17226/9782

Cummings, J., Zhou, Y., Lee, G., Zhong, K., Fonseca, J., & Cheng, F. (2024). Alzheimer's disease drug development pipeline: 2024. *Alzheimers Dement (N Y)*, *10*(2), e12465. https://doi.org/10.1002/trc2.12465 (Alzheimer's disease drug development pipeline: 2024.)

Cunnane, S. C., Trushina, E., Morland, C., Prigione, A., Casadesus, G., Andrews, Z. B., Beal, M. F., Bergersen, L. H., Brinton, R. D., de la Monte, S., Eckert, A., Harvey, J., Jeggo, R., Jhamandas, J. H., Kann, O., la Cour, C. M., Martin, W. F., Mithieux, G., Moreira, P. I., . . . Millan, M. J. (2020). Brain energy rescue: an emerging therapeutic concept for neurodegenerative disorders of ageing. *Nat Rev Drug Discov*, *19*(9), 609-633. https://doi.org/10.1038/s41573-020-0072-x

D'Ambrosi, N., & Rossi, L. (2015). Copper at synapse: Release, binding and modulation of neurotransmission. *Neurochem Int*, *90*, 36-45. https://doi.org/10.1016/j.neuint.2015.07.006

Danielsson, J., Pierattelli, R., Banci, L., & Gräslund, A. (2007). High-resolution NMR studies of the zinc-binding site of the Alzheimer's amyloid beta-peptide. *FEBS J*, *274*(1), 46-59. https://doi.org/10.1111/j.1742-4658.2006.05563.x

Das, N., Raymick, J., & Sarkar, S. (2021). Role of metals in Alzheimer's disease. *Metab Brain Dis*, *36*(7), 1627-1639. https://doi.org/10.1007/s11011-021-00765-w

Davies, P., & Maloney, A. J. (1976). Selective loss of central cholinergic neurons in Alzheimer's disease. *Lancet*, *2*(8000), 1403. https://doi.org/10.1016/s0140-6736(76)91936-x

Dawson, G. R., Seabrook, G. R., Zheng, H., Smith, D. W., Graham, S., O'Dowd, G., Bowery, B. J., Boyce, S., Trumbauer, M. E., Chen, H. Y., Van der Ploeg, L. H., & Sirinathsinghji, D. J. (1999). Age-related cognitive deficits, impaired long-term potentiation and reduction in synaptic marker density in mice lacking the beta-amyloid precursor protein. *Neuroscience*, *90*(1), 1-13. https://doi.org/10.1016/s0306-4522(98)00410-2

De Benedictis, C. A., Vilella, A., & Grabrucker, A. M. (2019). The Role of Trace Metals in Alzheimer's Disease. In (pp. 85-106). Codon Publications. https://doi.org/10.15586/alzheimersdisease.2019.ch6

de Boer, E. M. J., Orie, V. K., Williams, T., Baker, M. R., De Oliveira, H. M., Polvikoski, T., Silsby, M., Menon, P., van den Bos, M., Halliday, G. M., van den Berg, L. H., Van Den Bosch, L., van Damme, P., Kiernan, M. C., van Es, M. A., & Vucic, S. (2020). TDP-43 proteinopathies: a new wave of neurodegenerative diseases. *J Neurol Neurosurg Psychiatry*, *92*(1), 86-95. https://doi.org/10.1136/jnnp-2020-322983

De Roeck, A., Van Broeckhoven, C., & Sleegers, K. (2019). The role of ABCA7 in Alzheimer's disease: evidence from genomics, transcriptomics and methylomics. *Acta Neuropathologica*, *138*(2), 201-220. https://doi.org/10.1007/s00401-019-01994-1

De Strooper, B., Iwatsubo, T., & Wolfe, M. S. (2012). Presenilins and gamma-secretase: structure, function, and role in Alzheimer Disease. *Cold Spring Harb Perspect Med*, *2*(1), a006304. https://doi.org/10.1101/cshperspect.a006304

De Strooper, B., Vassar, R., & Golde, T. (2010). The secretases: enzymes with therapeutic potential in Alzheimer disease. *Nat Rev Neurol*, *6*(2), 99-107. https://doi.org/10.1038/nrneurol.2009.218

Deane, R., Sagare, A., Hamm, K., Parisi, M., Lane, S., Finn, M. B., Holtzman, D. M., & Zlokovic, B. V. (2008). apoE isoform-specific disruption of amyloid beta peptide clearance from mouse brain. *J Clin Invest*, *118*(12), 4002-4013. https://doi.org/10.1172/JCI36663

Delaere, P., Duyckaerts, C., Masters, C., Beyreuther, K., Piette, F., & Hauw, J. J. (1990). Large amounts of neocortical beta A4 deposits without neuritic plaques nor tangles in a psychometrically assessed, non-demented person. *Neuroscience letters*, *116*(1-2), 87-93. https://doi.org/10.1016/0304-3940(90)90391-l

Delport, A., & Hewer, R. (2022). The amyloid precursor protein: a converging point in Alzheimer's disease. *Mol Neurobiol*, *59*(7), 4501-4516. https://doi.org/10.1007/s12035-022-02863-x

Dickson, D. W., Crystal, H. A., Mattiace, L. A., Masur, D. M., Blau, A. D., Davies, P., Yen, S. H., & Aronson, M. K. (1992). Identification of normal and pathological aging in prospectively studied nondemented elderly humans. *Neurobiol Aging*, *13*(1), 179-189. https://doi.org/10.1016/0197-4580(92)90027-u

Druzhyna, N. M., Wilson, G. L., & LeDoux, S. P. (2008). Mitochondrial DNA repair in aging and disease. *Mech Ageing Dev*, *129*(7-8), 383-390. https://doi.org/10.1016/j.mad.2008.03.002

Egan, M. F., Kost, J., Tariot, P. N., Aisen, P. S., Cummings, J. L., Vellas, B., Sur, C., Mukai, Y., Voss, T., Furtek, C., Mahoney, E., Harper Mozley, L., Vandenberghe, R., Mo, Y., & Michelson, D. (2018). Randomized Trial of Verubecestat for Mild-to-Moderate Alzheimer's Disease. *The New England Journal of Medicine*, *378*(18), 1691-1703. https://doi.org/10.1056/NEJMoa1706441

Ejaz, H. W., Wang, W., & Lang, M. (2020). Copper Toxicity Links to Pathogenesis of Alzheimer's Disease and Therapeutics Approaches. *International Journal of Molecular Sciences*, *21*(20). https://doi.org/10.3390/ijms21207660

Endres, K., & Deller, T. (2017). Regulation of Alpha-Secretase ADAM10 In vitro and In vivo: Genetic, Epigenetic, and Protein-Based Mechanisms. *Front Mol Neurosci*, *10*, 56. https://doi.org/10.3389/fnmol.2017.00056

Endres, K., Fahrenholz, F., Lotz, J., Hiemke, C., Teipel, S., Lieb, K., Tuscher, O., & Fellgiebel, A. (2014). Increased CSF APPs-alpha levels in patients with Alzheimer disease treated with acitretin. *Neurology*, *83*(21), 1930-1935. https://doi.org/10.1212/WNL.0000000000001017

Eskew, D. L., Welch, R. M., & Cary, E. E. (1983). Nickel: an essential micronutrient for legumes and possibly all higher plants. *Science*, *222*(4624), 621-623. https://doi.org/10.1126/science.222.4624.621

Faller, P., & Hureau, C. (2009). Bioinorganic chemistry of copper and zinc ions coordinated to amyloid-beta peptide. *Dalton Trans*(7), 1080-1094. https://doi.org/10.1039/b813398k

Fandrich, M. (2012). Oligomeric intermediates in amyloid formation: structure determination and mechanisms of toxicity. *J Mol Biol*, *421*(4-5), 427-440. https://doi.org/10.1016/j.jmb.2012.01.006

Farina, M., Avila, D. S., da Rocha, J. B., & Aschner, M. (2013). Metals, oxidative stress and neurodegeneration: a focus on iron, manganese and mercury. *Neurochem Int*, *62*(5), 575-594. https://doi.org/10.1016/j.neuint.2012.12.006

Farrer, L. A., Cupples, L. A., Haines, J. L., Hyman, B., Kukull, W. A., Mayeux, R., Myers, R. H., Pericak-Vance, M. A., Risch, N., & van Duijn, C. M. (1997). Effects of age, sex, and ethnicity on the association between apolipoprotein E genotype and Alzheimer disease. A meta-analysis. APOE and Alzheimer Disease Meta Analysis Consortium. *JAMA*, *278*(16), 1349-1356. https://www.ncbi.nlm.nih.gov/pubmed/9343467

Fernandez, C. G., Hamby, M. E., McReynolds, M. L., & Ray, W. J. (2019). The Role of APOE4 in Disrupting the Homeostatic Functions of Astrocytes and Microglia in Aging and Alzheimer's Disease. *Frontiers in Aging Neuroscience*, *11*, 14. https://doi.org/10.3389/fnagi.2019.00014

Ferrari-Souza, J. P., Lussier, F. Z., Leffa, D. T., Therriault, J., Tissot, C., Bellaver, B., Ferreira, P. C. L., Malpetti, M., Wang, Y. T., Povala, G., Benedet, A. L., Ashton, N. J., Chamoun, M., Servaes, S., Bezgin, G., Kang, M. S., Stevenson, J., Rahmouni, N., Pallen, V., . . . Pascoal, T. A. (2023). APOEepsilon4 associates with microglial activation independently of Abeta plaques and tau tangles. *Sci Adv*, *9*(14), eade1474. https://doi.org/10.1126/sciadv.ade1474

Ferreira, S. T., & Klein, W. L. (2011). The Abeta oligomer hypothesis for synapse failure and memory loss in Alzheimer's disease. *Neurobiol Learn Mem*, *96*(4), 529-543. https://doi.org/10.1016/j.nlm.2011.08.003

Fischer, F., Robbe-Saule, M., Turlin, E., Mancuso, F., Michel, V., Richaud, P., Veyrier, F. J., De Reuse, H., & Vinella, D. (2016). Characterization in Helicobacter pylori of a Nickel Transporter Essential for Colonization That Was Acquired during Evolution by Gastric Helicobacter Species. *PLoS Pathog*, *12*(12), e1006018. https://doi.org/10.1371/journal.ppat.1006018

Fortea, J., Zaman, S. H., Hartley, S., Rafii, M. S., Head, E., & Carmona-Iragui, M. (2021). Alzheimer's disease associated with Down syndrome: a genetic form of dementia. *Lancet Neurol*, *20*(11), 930-942. https://doi.org/10.1016/S1474-4422(21)00245-3

Foster, E. M., Dangla-Valls, A., Lovestone, S., Ribe, E. M., & Buckley, N. J. (2019). Clusterin in Alzheimer's Disease: Mechanisms, Genetics, and Lessons From Other Pathologies. *Frontiers in Neuroscience*, *13*, 164. https://doi.org/10.3389/fnins.2019.00164

Fourriere, L., Cho, E. H., & Gleeson, P. A. (2022). Segregation of the membrane cargoes, BACE1 and amyloid precursor protein (APP) throughout the Golgi apparatus. *Traffic*, *23*(3), 158-173. https://doi.org/10.1111/tra.12831

Freeman, S. A., & Zephir, H. (2024). Anti-CD20 monoclonal antibodies in multiple sclerosis: Rethinking the current treatment strategy. *Rev Neurol (Paris)*. https://doi.org/10.1016/j.neurol.2023.12.013

Fu, S., Jiang, W., & Zheng, W. (2015). Age-dependent increase of brain copper levels and expressions of copper regulatory proteins in the subventricular zone and choroid plexus. *Front Mol Neurosci*, *8*, 22. https://doi.org/10.3389/fnmol.2015.00022

Gaier, E. D., Eipper, B. A., & Mains, R. E. (2013). Copper signaling in the mammalian nervous system: synaptic effects. *Journal of neuroscience research*, *91*(1), 2-19. https://doi.org/10.1002/jnr.23143

Gao, C., Jiang, J., Tan, Y., & Chen, S. (2023). Microglia in neurodegenerative diseases: mechanism and potential therapeutic targets. *Signal Transduct Target Ther*, *8*(1), 359. https://doi.org/10.1038/s41392-023-01588-0

Gao, F., Sun, M., Zhang, J., Chang, Y., Gao, W., Ma, G., Ma, X., & Guo, Y. (2022). Fenton-like reaction and glutathione depletion by chiral manganese dioxide nanoparticles for enhanced chemodynamic therapy and chemotherapy. *J Colloid Interface Sci*, *616*, 369-378. https://doi.org/10.1016/j.jcis.2022.02.060

Gendreau, K. L., & Hall, G. F. (2013). Tangles, Toxicity, and Tau Secretion in AD - New Approaches to a Vexing Problem. *Front Neurol*, *4*, 160. https://doi.org/10.3389/fneur.2013.00160

Genin, E., Hannequin, D., Wallon, D., Sleegers, K., Hiltunen, M., Combarros, O., Bullido, M. J., Engelborghs, S., De Deyn, P., Berr, C., Pasquier, F., Dubois, B., Tognoni, G., Fievet, N., Brouwers, N., Bettens, K., Arosio, B., Coto, E., Del Zompo, M., . . . Campion, D. (2011). APOE and Alzheimer disease: a major gene with semi-dominant inheritance. *Mol Psychiatry*, *16*(9), 903-907. https://doi.org/10.1038/mp.2011.52

Gertz, M. A. (2022). Immunoglobulin light chain amyloidosis: 2022 update on diagnosis, prognosis, and treatment. *Am J Hematol*, *97*(6), 818-829. https://doi.org/10.1002/ajh.26569

Ghalebani, L., Wahlstrom, A., Danielsson, J., Warmlander, S. K., & Graslund, A. (2012). pH-dependence of the specific binding of Cu(II) and Zn(II) ions to the amyloid-beta peptide. *Biochem Biophys Res Commun*, *421*(3), 554-560. https://doi.org/10.1016/j.bbrc.2012.04.043

Glenner, G. G., & Wong, C. W. (1984). Alzheimer's disease: initial report of the purification and characterization of a novel cerebrovascular amyloid protein. *Biochem Biophys Res Commun*, *120*(3), 885-890. https://doi.org/10.1016/s0006-291x(84)80190-4

Godfrey, M. E., Wojcik, D. P., & Krone, C. A. (2003). Apolipoprotein E genotyping as a potential biomarker for mercury neurotoxicity. *Journal of Alzheimer's disease : JAD*, *5*(3), 189-195. https://doi.org/10.3233/jad-2003-5303

Gonzalez Diaz, A., Cataldi, R., Mannini, B., & Vendruscolo, M. (2024). Preparation and Characterization of Zn(II)-Stabilized Abeta(42) Oligomers. *ACS Chem Neurosci*, *15*(14), 2586-2599. https://doi.org/10.1021/acschemneuro.4c00084

Guan, P. P., Cao, L. L., Yang, Y., & Wang, P. (2021). Calcium Ions Aggravate Alzheimer's Disease Through the Aberrant Activation of Neuronal Networks, Leading to Synaptic and Cognitive Deficits. *Front Mol Neurosci*, *14*, 757515. https://doi.org/10.3389/fnmol.2021.757515

Guerreiro, R., & Hardy, J. (2014). Genetics of Alzheimer's disease. *Neurotherapeutics*, *11*(4), 732-737. https://doi.org/10.1007/s13311-014-0295-9

Guo, C., Sun, L., Chen, X., & Zhang, D. (2013). Oxidative stress, mitochondrial damage and neurodegenerative diseases. *Neural Regen Res*, *8*(21), 2003-2014. https://doi.org/10.3969/j.issn.1673-5374.2013.21.009

Haass, C., Hung, A. Y., Schlossmacher, M. G., Teplow, D. B., & Selkoe, D. J. (1993). beta-Amyloid peptide and a 3-kDa fragment are derived by distinct cellular mechanisms. *The Journal of Biological Chemistry*, *268*(5), 3021-3024. https://www.ncbi.nlm.nih.gov/pubmed/8428976

Halliday, M. R., Rege, S. V., Ma, Q., Zhao, Z., Miller, C. A., Winkler, E. A., & Zlokovic, B. V. (2016). Accelerated pericyte degeneration and blood-brain barrier breakdown in apolipoprotein E4 carriers with Alzheimer's disease. *J Cereb Blood Flow Metab*, *36*(1), 216-227. https://doi.org/10.1038/jcbfm.2015.44

Hampel, H., Hardy, J., Blennow, K., Chen, C., Perry, G., Kim, S. H., Villemagne, V. L., Aisen, P., Vendruscolo, M., Iwatsubo, T., Masters, C. L., Cho, M., Lannfelt, L., Cummings, J. L., & Vergallo, A. (2021). The Amyloid-beta Pathway in Alzheimer's Disease. *Mol Psychiatry*, *26*(10), 5481-5503. https://doi.org/10.1038/s41380-021-01249-0

Hansen, R. A., Gartlehner, G., Webb, A. P., Morgan, L. C., Moore, C. G., & Jonas, D. E. (2008). Efficacy and safety of donepezil, galantamine, and rivastigmine for the treatment of Alzheimer's disease: a systematic review and meta-analysis. *Clin Interv Aging*, *3*(2), 211-225. https://www.ncbi.nlm.nih.gov/pubmed/18686744

Hardy, J. A., & Higgins, G. A. (1992). Alzheimer's disease: the amyloid cascade hypothesis. *Science*, *256*(5054), 184-185. https://doi.org/10.1126/science.1566067

Harris, M. E., Hensley, K., Butterfield, D. A., Leedle, R. A., & Carney, J. M. (1995). Direct evidence of oxidative injury produced by the Alzheimer's beta-amyloid peptide (1-40) in cultured hippocampal neurons. *Exp Neurol*, *131*(2), 193-202. https://doi.org/10.1016/0014-4886(95)90041-1

Hartmann, D., de Strooper, B., Serneels, L., Craessaerts, K., Herreman, A., Annaert, W., Umans, L., Lubke, T., Lena Illert, A., von Figura, K., & Saftig, P. (2002). The disintegrin/metalloprotease ADAM 10 is essential for Notch signalling but not for alpha-secretase activity in fibroblasts. *Human Molecular Genetics*, *11*(21), 2615-2624. https://doi.org/10.1093/hmg/11.21.2615

He, M. D., Xu, S. C., Lu, Y. H., Li, L., Zhong, M., Zhang, Y. W., Wang, Y., Li, M., Yang, J., Zhang, G. B., Yu, Z. P., & Zhou, Z. (2011). L-carnitine protects against nickel-induced neurotoxicity by maintaining mitochondrial function in Neuro-2a cells. *Toxicol Appl Pharmacol*, *253*(1), 38-44. https://doi.org/10.1016/j.taap.2011.03.008

Henriksson, J., Tallkvist, J., & Tjalve, H. (1997). Uptake of nickel into the brain via olfactory neurons in rats. *Toxicol Lett*, *91*(2), 153-162. https://doi.org/10.1016/s0378-4274(97)03885-x

Herholz, K., Salmon, E., Perani, D., Baron, J. C., Holthoff, V., Frolich, L., Schonknecht, P., Ito, K., Mielke, R., Kalbe, E., Zundorf, G., Delbeuck, X., Pelati, O., Anchisi, D., Fazio, F., Kerrouche, N., Desgranges, B., Eustache, F., Beuthien-Baumann, B., . . . Heiss, W. D. (2002). Discrimination between Alzheimer dementia and controls by automated analysis of multicenter FDG PET. *Neuroimage*, *17*(1), 302-316. https://doi.org/10.1006/nimg.2002.1208

Hernandez, F., & Avila, J. (2007). Tauopathies. *Cell Mol Life Sci*, *64*(17), 2219-2233. https://doi.org/10.1007/s00018-007-7220-x

Hickman, S., Izzy, S., Sen, P., Morsett, L., & El Khoury, J. (2018). Microglia in neurodegeneration. *Nat Neurosci*, *21*(10), 1359-1369. https://doi.org/10.1038/s41593-018-0242-x

Horn, J. V. C., Kakutani, L. M., Narayanaswami, V., & Weers, P. M. M. (2023). Insights into the C-terminal domain of apolipoprotein E from chimera studies with apolipophorin III. *Mol Cell Biochem*, *478*(1), 173-183. https://doi.org/10.1007/s11010-022-04497-y

Hu, Y. B., Dammer, E. B., Ren, R. J., & Wang, G. (2015). The endosomal-lysosomal system: from acidification and cargo sorting to neurodegeneration. *Translational Neurodegeneration*, *4*, 18. https://doi.org/10.1186/s40035-015-0041-1

Huang, Y., & Mahley, R. W. (2014). Apolipoprotein E: structure and function in lipid metabolism, neurobiology, and Alzheimer's diseases. *Neurobiol Dis*, *72 Pt A*, 3-12. https://doi.org/10.1016/j.nbd.2014.08.025

Huat, T. J., Camats-Perna, J., Newcombe, E. A., Valmas, N., Kitazawa, M., & Medeiros, R. (2019). Metal Toxicity Links to Alzheimer's Disease and Neuroinflammation. *J Mol Biol*, *431*(9), 1843-1868. https://doi.org/10.1016/j.jmb.2019.01.018

Hur, J. Y. (2022). gamma-Secretase in Alzheimer's disease. *Exp Mol Med*, *54*(4), 433-446. https://doi.org/10.1038/s12276-022-00754-8

Hussain, R., Zubair, H., Pursell, S., & Shahab, M. (2018). Neurodegenerative Diseases: Regenerative Mechanisms and Novel Therapeutic Approaches. *Brain Sci*, *8*(9). https://doi.org/10.3390/brainsci8090177

Hyman, B. T., Van Hoesen, G. W., Damasio, A. R., & Barnes, C. L. (1984). Alzheimer's disease: cell-specific pathology isolates the hippocampal formation. *Science*, *225*(4667), 1168-1170. https://doi.org/10.1126/science.6474172

Iizuka, T., Shoji, M., Kawarabayashi, T., Sato, M., Kobayashi, T., Tada, N., Kasai, K., Matsubara, E., Watanabe, M., Tomidokoro, Y., & Hirai, S. (1996). Intracellular generation of amyloid beta-protein from amyloid beta-protein precursor fragment by direct cleavage with beta- and gamma-secretase. *Biochem Biophys Res Commun*, *218*(1), 238-242. https://doi.org/10.1006/bbrc.1996.0042

Ijomone, O. (2021). Neurotoxicity of nickel. In L. G. C. Michael Aschner (Ed.), *Neurotoxicity of Metals: Old Issues and New Developments* (Vol. 5, pp. 263-280). Elsevier. https://doi.org/10.1016/bs.ant.2020.11.004.

Ijomone, O. M., Ijomone, O. K., Iroegbu, J. D., Ifenatuoha, C. W., Olung, N. F., & Aschner, M. (2020). Epigenetic influence of environmentally neurotoxic metals. *NeuroToxicology*, *81*, 51-65. https://doi.org/10.1016/j.neuro.2020.08.005

Iljina, M., Garcia, G. A., Dear, A. J., Flint, J., Narayan, P., Michaels, T. C., Dobson, C. M., Frenkel, D., Knowles, T. P., & Klenerman, D. (2016). Quantitative analysis of co-oligomer formation by amyloid-beta peptide isoforms. *Scientific Reports*, *6*, 28658. https://doi.org/10.1038/srep28658

Iqbal, K., Liu, F., & Gong, C. X. (2016). Tau and neurodegenerative disease: the story so far. *Nat Rev Neurol*, *12*(1), 15-27. https://doi.org/10.1038/nrneurol.2015.225

Isei, M. O., Girardi, P. A., Rodwell-Bullock, J., Nehrke, K., & Johnson, G. V. W. (2024). Site-specific phosphorylation of tau impacts mitochondrial function and response to stressors. *J Neurochem*, *168*(6), 1019-1029. https://doi.org/10.1111/jnc.15975

Ishida, A., Furukawa, K., Keller, J. N., & Mattson, M. P. (1997). Secreted form of beta-amyloid precursor protein shifts the frequency dependency for induction of LTD, and enhances LTP in hippocampal slices. *Neuroreport*, *8*(9-10), 2133-2137. https://doi.org/10.1097/00001756-199707070-00009

Islam, F., Shohag, S., Akhter, S., Islam, M. R., Sultana, S., Mitra, S., Chandran, D., Khandaker, M. U., Ashraf, G. M., Idris, A. M., Emran, T. B., & Cavalu, S. (2022). Exposure of metal toxicity in Alzheimer's disease: An extensive review. *Front Pharmacol*, *13*, 903099. https://doi.org/10.3389/fphar.2022.903099

Jackson, R. J., Meltzer, J. C., Nguyen, H., Commins, C., Bennett, R. E., Hudry, E., & Hyman, B. T. (2022). APOE4 derived from astrocytes leads to blood-brain barrier impairment. *Brain*, *145*(10), 3582-3593. https://doi.org/10.1093/brain/awab478

Jankovska, N., Olejar, T., & Matej, R. (2020). Extracellular Amyloid Deposits in Alzheimer's and Creutzfeldt-Jakob Disease: Similar Behavior of Different Proteins? *International Journal of Molecular Sciences*, *22*(1). https://doi.org/10.3390/ijms22010007

Jessen, F., Georges, J., Wortmann, M., & Benham-Hermetz, S. (2022). What Matters to Patients with Alzheimer's Disease and Their Care Partners? Implications for Understanding the Value of Future Interventions. *J Prev Alzheimers Dis*, *9*(3), 550-555. https://doi.org/10.14283/jpad.2022.22

Jin, L., Wu, W. H., Li, Q. Y., Zhao, Y. F., & Li, Y. M. (2011). Copper inducing Abeta42 rather than Abeta40 nanoscale oligomer formation is the key process for Abeta neurotoxicity. *Nanoscale*, *3*(11), 4746-4751. https://doi.org/10.1039/c1nr11029b

Kamelgarn, M., Chen, J., Kuang, L., Jin, H., Kasarskis, E. J., & Zhu, H. (2018). ALS mutations of FUS suppress protein translation and disrupt the regulation of nonsense-mediated decay. *Proceedings of the National Academy of Sciences of the United States of America*, *115*(51), E11904-E11913. https://doi.org/10.1073/pnas.1810413115

Karkisaval, A. G., Rostagno, A., Azimov, R., Ban, D. K., Ghiso, J., Kagan, B. L., & Lal, R. (2020). Ion channel formation by N-terminally truncated Abeta (4-42): relevance for the pathogenesis of Alzheimer's disease. *Nanomedicine*, *29*, 102235. https://doi.org/10.1016/j.nano.2020.102235

Katsuno, M., Sahashi, K., Iguchi, Y., & Hashizume, A. (2018). Preclinical progression of neurodegenerative diseases. *Nagoya J Med Sci*, *80*(3), 289-298. https://doi.org/10.18999/nagjms.80.3.289

Kelleher, R. J., 3rd, & Shen, J. (2017). Presenilin-1 mutations and Alzheimer's disease. *Proceedings of the National Academy of Sciences of the United States of America*, *114*(4), 629-631. https://doi.org/10.1073/pnas.1619574114

Kenche, V. B., & Barnham, K. J. (2011). Alzheimer's disease & metals: therapeutic opportunities. *British Journal of Pharmacology*, *163*(2), 211-219. https://doi.org/10.1111/j.1476-5381.2011.01221.x

Kepp, K. P., Robakis, N. K., Hoilund-Carlsen, P. F., Sensi, S. L., & Vissel, B. (2023). The amyloid cascade hypothesis: an updated critical review. *Brain*, *146*(10), 3969-3990. https://doi.org/10.1093/brain/awad159

Kerper, L. E., Ballatori, N., & Clarkson, T. W. (1992). Methylmercury transport across the blood-brain barrier by an amino acid carrier. *Am J Physiol*, *262*(5 Pt 2), R761-765. https://doi.org/10.1152/ajpregu.1992.262.5.R761

Khaled, M., Rönnbäck, I., Ilag, L. L., Gräslund, A., Strodel, B., & Österlund, N. (2023). A Hairpin Motif in the Amyloid-beta Peptide Is Important for Formation of Disease-Related Oligomers. *J Am Chem Soc*, *145*(33), 18340-18354. https://doi.org/10.1021/jacs.3c03980

Kim, E. K., & Choi, E. J. (2015). Compromised MAPK signaling in human diseases: an update. *Arch Toxicol*, *89*(6), 867-882. https://doi.org/10.1007/s00204-015-1472-2

Kim, J., Basak, J. M., & Holtzman, D. M. (2009). The role of apolipoprotein E in Alzheimer's disease. *Neuron*, *63*(3), 287-303. https://doi.org/10.1016/j.neuron.2009.06.026

Kim, S. H., Knight, E. M., Saunders, E. L., Cuevas, A. K., Popovech, M., Chen, L. C., & Gandy, S. (2012). Rapid doubling of Alzheimer's amyloid-beta40 and 42 levels in brains of mice exposed to a nickel nanoparticle model of air pollution. *F1000Res*, *1*, 70. https://doi.org/10.12688/f1000research.1-70.v1

Kirsipuu, T., Zadoroznaja, A., Smirnova, J., Friedemann, M., Plitz, T., Tougu, V., & Palumaa, P. (2020). Copper(II)-binding equilibria in human blood. *Scientific Reports*, *10*(1), 5686. https://doi.org/10.1038/s41598-020-62560-4

Kirss, S., Reinapu, A., Kabin, E., Smirnova, J., Tougu, V., & Palumaa, P. (2024). alpha-Lipoic acid: a potential regulator of copper metabolism in Alzheimer's disease. *Front Mol Biosci*, *11*, 1451536. https://doi.org/10.3389/fmolb.2024.1451536

Knott, A. B., Perkins, G., Schwarzenbacher, R., & Bossy-Wetzel, E. (2008). Mitochondrial fragmentation in neurodegeneration. *Nat Rev Neurosci*, *9*(7), 505-518. https://doi.org/10.1038/nrn2417

Kok, W. M., Cottam, J. M., Ciccotosto, G. D., Miles, L. A., Karas, J. A., Scanlon, D. B., Roberts, B. R., Parker, M. W., Cappai, R., Barnham, K. J., & Hutton, C. A. (2013). Synthetic dityrosine-linked β-amyloid dimers form stable, soluble, neurotoxic oligomers [10.1039/C3SC22295K]. *Chemical Science*, *4*(12), 4449-4454. https://doi.org/10.1039/C3SC22295K

Kopeikina, K. J., Hyman, B. T., & Spires-Jones, T. L. (2012). Soluble forms of tau are toxic in Alzheimer's disease. *Transl Neurosci*, *3*(3), 223-233. https://doi.org/10.2478/s13380-012-0032-y

Korenberg, J. R., Pulst, S. M., Neve, R. L., & West, R. (1989). The Alzheimer amyloid precursor protein maps to human chromosome 21 bands q21.105-q21.05. *Genomics*, *5*(1), 124-127. https://doi.org/10.1016/0888-7543(89)90095-5

Kosik, K. S., Joachim, C. L., & Selkoe, D. J. (1986). Microtubule-associated protein tau (tau) is a major antigenic component of paired helical filaments in Alzheimer disease. *Proceedings of the National Academy of Sciences of the United States of America*, *83*(11), 4044-4048. https://doi.org/10.1073/pnas.83.11.4044

Krishtal, J., Bragina, O., Metsla, K., Palumaa, P., & Tougu, V. (2017). In situ fibrillizing amyloid-beta 1-42 induces neurite degeneration and apoptosis of differentiated SH-SY5Y cells. *PLOS ONE*, *12*(10), e0186636. https://doi.org/10.1371/journal.pone.0186636

Kukull, W. A., Brenner, D. E., Speck, C. E., Nochlin, D., Bowen, J., McCormick, W., Teri, L., Pfanschmidt, M. L., & Larson, E. B. (1994). Causes of death associated with Alzheimer disease: variation by level of cognitive impairment before death. *J Am Geriatr Soc*, *42*(7), 723-726. https://doi.org/10.1111/j.1532-5415.1994.tb06531.x

Kumar, S., & Walter, J. (2011). Phosphorylation of amyloid beta (Abeta) peptides - a trigger for formation of toxic aggregates in Alzheimer's disease. *Aging (Albany NY)*, *3*(8), 803-812. https://doi.org/10.18632/aging.100362

Kuzmic, P. (2015). History, variants and usage of the "Morrison equation" in enzyme inhibition kinetics. *Biokin Technical Note*, *TN-2015-01*. http://www.biokin.com/publications/technotes/TN201501.html

Lee, S., Devanney, N. A., Golden, L. R., Smith, C. T., Schwartz, J. L., Walsh, A. E., Clarke, H. A., Goulding, D. S., Allenger, E. J., Morillo-Segovia, G., Friday, C. M., Gorman, A. A., Hawkinson, T. R., MacLean, S. M., Williams, H. C., Sun, R. C., Morganti, J. M., & Johnson, L. A. (2023). APOE modulates microglial immunometabolism in response to age, amyloid pathology, and inflammatory challenge. *Cell Rep*, *42*(3), 112196. https://doi.org/10.1016/j.celrep.2023.112196

Lee, S. J., Nam, E., Lee, H. J., Savelieff, M. G., & Lim, M. H. (2017). Towards an understanding of amyloid-beta oligomers: characterization, toxicity mechanisms, and inhibitors. *Chem Soc Rev*, *46*(2), 310-323. https://doi.org/10.1039/c6cs00731g

Lestaevel, P., Bussy, C., Paquet, F., Dhieux, B., Clarencon, D., Houpert, P., & Gourmelon, P. (2005). Changes in sleep-wake cycle after chronic exposure to uranium in rats. *Neurotoxicol Teratol*, *27*(6), 835-840. https://doi.org/10.1016/j.ntt.2005.07.005

Li, N. M., Liu, K. F., Qiu, Y. J., Zhang, H. H., Nakanishi, H., & Qing, H. (2019). Mutations of beta-amyloid precursor protein alter the consequence of Alzheimer's disease pathogenesis. *Neural Regen Res*, *14*(4), 658-665. https://doi.org/10.4103/1673-5374.247469

Li, Z., Shue, F., Zhao, N., Shinohara, M., & Bu, G. (2020). APOE2: protective mechanism and therapeutic implications for Alzheimer's disease. *Molecular Neurodegeneration*, *15*(1), 63. https://doi.org/10.1186/s13024-020-00413-4

Liao, L., Cheng, D., Wang, J., Duong, D. M., Losik, T. G., Gearing, M., Rees, H. D., Lah, J. J., Levey, A. I., & Peng, J. (2004). Proteomic characterization of postmortem amyloid plaques isolated by laser capture microdissection. *The Journal of Biological Chemistry*, *279*(35), 37061-37068. https://doi.org/10.1074/jbc.M403672200

Liu, C. C., Liu, C. C., Kanekiyo, T., Xu, H., & Bu, G. (2013). Apolipoprotein E and Alzheimer disease: risk, mechanisms and therapy. *Nat Rev Neurol*, *9*(2), 106-118. https://doi.org/10.1038/nrneurol.2012.263

Liu, C. C., Zhao, N., Fu, Y., Wang, N., Linares, C., Tsai, C. W., & Bu, G. (2017). ApoE4 Accelerates Early Seeding of Amyloid Pathology. *Neuron*, *96*(5), 1024-1032 e1023. https://doi.org/10.1016/j.neuron.2017.11.013

Liu, K., Solano, I., Mann, D., Lemere, C., Mercken, M., Trojanowski, J. Q., & Lee, V. M. (2006). Characterization of Abeta11-40/42 peptide deposition in Alzheimer's disease and young Down's syndrome brains: implication of N-terminally truncated Abeta species in the pathogenesis of Alzheimer's disease. *Acta Neuropathologica*, *112*(2), 163-174. https://doi.org/10.1007/s00401-006-0077-5

Lloyd, D. R., & Phillips, D. H. (1999). Oxidative DNA damage mediated by copper(II), iron(II) and nickel(II) fenton reactions: evidence for site-specific mechanisms in the formation of double-strand breaks, 8-hydroxydeoxyguanosine and putative intrastrand cross-links. *Mutat Res*, *424*(1-2), 23-36. https://doi.org/10.1016/s0027-5107(99)00005-6

Lovell, M. A., Robertson, J. D., Teesdale, W. J., Campbell, J. L., & Markesbery, W. R. (1998). Copper, iron and zinc in Alzheimer's disease senile plaques. *J Neurol Sci*, *158*(1), 47-52. https://doi.org/10.1016/s0022-510x(98)00092-6

Lupas, A. N., & Bassler, J. (2017). Coiled Coils - A Model System for the 21st Century. *Trends in Biochemical Sciences*, *42*(2), 130-140. https://doi.org/10.1016/j.tibs.2016.10.007

Lynch, J. R., Tang, W., Wang, H., Vitek, M. P., Bennett, E. R., Sullivan, P. M., Warner, D. S., & Laskowitz, D. T. (2003). APOE genotype and an ApoE-mimetic peptide modify the systemic and central nervous system inflammatory response. *The Journal of Biological Chemistry*, *278*(49), 48529-48533. https://doi.org/10.1074/jbc.M306923200

Ma, J., Yee, A., Brewer, H. B., Jr., Das, S., & Potter, H. (1994). Amyloid-associated proteins alpha 1-antichymotrypsin and apolipoprotein E promote assembly of Alzheimer beta-protein into filaments. *Nature*, *372*(6501), 92-94. https://doi.org/10.1038/372092a0

Maccioni, R. B., Farias, G., Morales, I., & Navarrete, L. (2010). The revitalized tau hypothesis on Alzheimer's disease. *Arch Med Res*, *41*(3), 226-231. https://doi.org/10.1016/j.arcmed.2010.03.007

Magaki, S., Raghavan, R., Mueller, C., Oberg, K. C., Vinters, H. V., & Kirsch, W. M. (2007). Iron, copper, and iron regulatory protein 2 in Alzheimer's disease and related dementias. *Neuroscience letters*, *418*(1), 72-76. https://doi.org/10.1016/j.neulet.2007.02.077

Mahley, R. W., & Huang, Y. (2012). Apolipoprotein e sets the stage: response to injury triggers neuropathology. *Neuron*, *76*(5), 871-885. https://doi.org/10.1016/j.neuron.2012.11.020

Maina, M. B., Al-Hilaly, Y. K., & Serpell, L. C. (2023). Dityrosine cross-linking and its potential roles in Alzheimer's disease. *Frontiers in Neuroscience*, *17*, 1132670. https://doi.org/10.3389/fnins.2023.1132670

Maiti, B. K., Govil, N., Kundu, T., & Moura, J. J. G. (2020). Designed Metal-ATCUN Derivatives: Redox- and Non-redox-Based Applications Relevant for Chemistry, Biology, and Medicine. *iScience*, *23*(12), 101792. https://doi.org/10.1016/j.isci.2020.101792

Majorek, K. A., Gucwa, M., Murzyn, K., & Minor, W. (2024). Metal ions in biomedically relevant macromolecular structures. *Front Chem*, *12*, 1426211. https://doi.org/10.3389/fchem.2024.1426211

Malmos, K. G., Blancas-Mejia, L. M., Weber, B., Buchner, J., Ramirez-Alvarado, M., Naiki, H., & Otzen, D. (2017). ThT 101: a primer on the use of thioflavin T to investigate amyloid formation. *Amyloid*, *24*(1), 1-16. https://doi.org/10.1080/13506129.2017.1304905

Manelli, A. M., Bulfinch, L. C., Sullivan, P. M., & LaDu, M. J. (2007). Abeta42 neurotoxicity in primary co-cultures: effect of apoE isoform and Abeta conformation. *Neurobiol Aging*, *28*(8), 1139-1147. https://doi.org/10.1016/j.neurobiolaging.2006.05.024

Manganelli, F., Fabrizi, G. M., Luigetti, M., Mandich, P., Mazzeo, A., & Pareyson, D. (2022). Hereditary transthyretin amyloidosis overview. *Neurological Sciences*, *43*(Suppl 2), 595-604. https://doi.org/10.1007/s10072-020-04889-2

Mann, D. M., Yates, P. O., & Marcyniuk, B. (1985). Correlation between senile plaque and neurofibrillary tangle counts in cerebral cortex and neuronal counts in cortex and subcortical structures in Alzheimer's disease. *Neuroscience letters*, *56*(1), 51-55. https://doi.org/10.1016/0304-3940(85)90439-2

Marchetti, C. (2014). Interaction of metal ions with neurotransmitter receptors and potential role in neurodiseases. *Biometals*, *27*(6), 1097-1113. https://doi.org/10.1007/s10534-014-9791-y

Marzban, L., Park, K., & Verchere, C. B. (2003). Islet amyloid polypeptide and type 2 diabetes. *Experimental gerontology*, *38*(4), 347-351. https://doi.org/10.1016/s0531-5565(03)00004-4

Masters, C. L., Simms, G., Weinman, N. A., Multhaup, G., McDonald, B. L., & Beyreuther, K. (1985). Amyloid plaque core protein in Alzheimer disease and Down syndrome. *Proceedings of the National Academy of Sciences of the United States of America*, *82*(12), 4245-4249. https://doi.org/10.1073/pnas.82.12.4245

Mawuenyega, K. G., Kasten, T., Sigurdson, W., & Bateman, R. J. (2013). Amyloid-beta isoform metabolism quantitation by stable isotope-labeled kinetics. *Anal Biochem*, *440*(1), 56-62. https://doi.org/10.1016/j.ab.2013.04.031

Maynard, C. J., Bush, A. I., Masters, C. L., Cappai, R., & Li, Q. X. (2005). Metals and amyloid-beta in Alzheimer's disease. *Int J Exp Pathol*, *86*(3), 147-159. https://doi.org/10.1111/j.0959-9673.2005.00434.x

Mazinani, N., Strilchuk, A. W., Baylis, J. R., Hur, W. S., Jefferies, W. A., & Kastrup, C. J. (2020). Bleeding is increased in amyloid precursor protein knockout mouse. *Res Pract Thromb Haemost*, *4*(5), 823-828. https://doi.org/10.1002/rth2.12375

McGeer, P. L., Klegeris, A., Walker, D. G., Yasuhara, O., & McGeer, E. G. (1994). Pathological proteins in senile plaques. *Tohoku J Exp Med*, *174*(3), 269-277. https://doi.org/10.1620/tjem.174.269

Medeiros, R., Baglietto-Vargas, D., & LaFerla, F. M. (2011). The role of tau in Alzheimer's disease and related disorders. *CNS Neurosci Ther*, *17*(5), 514-524. https://doi.org/10.1111/j.1755-5949.2010.00177.x

Meng, Q., Lin, M. S., & Tzeng, I. S. (2020). Relationship Between Exercise and Alzheimer's Disease: A Narrative Literature Review. *Frontiers in Neuroscience*, *14*, 131. https://doi.org/10.3389/fnins.2020.00131

Mesterhazy, E., Lebrun, C., Crouzy, S., Jancso, A., & Delangle, P. (2018). Short oligopeptides with three cysteine residues as models of sulphur-rich Cu(i)- and Hg(ii)-binding sites in proteins. *Metallomics*, *10*(9), 1232-1244. https://doi.org/10.1039/c8mt00113h

Mielke, M. M., Ransom, J. E., Mandrekar, J., Turcano, P., Savica, R., & Brown, A. W. (2022). Traumatic Brain Injury and Risk of Alzheimer's Disease and Related Dementias in the Population. *Journal of Alzheimer's disease : JAD*, *88*(3), 1049-1059. https://doi.org/10.3233/JAD-220159

Miller, L. M., Wang, Q., Telivala, T. P., Smith, R. J., Lanzirotti, A., & Miklossy, J. (2006). Synchrotron-based infrared and X-ray imaging shows focalized accumulation of Cu and Zn co-localized with beta-amyloid deposits in Alzheimer's disease. *J Struct Biol*, *155*(1), 30-37. https://doi.org/10.1016/j.jsb.2005.09.004

Mishra, S., Blazey, T. M., Holtzman, D. M., Cruchaga, C., Su, Y., Morris, J. C., Benzinger, T. L. S., & Gordon, B. A. (2018). Longitudinal brain imaging in preclinical Alzheimer disease: impact of APOE epsilon4 genotype. *Brain*, *141*(6), 1828-1839. https://doi.org/10.1093/brain/awy103

Mital, M., Wezynfeld, N. E., Fraczyk, T., Wiloch, M. Z., Wawrzyniak, U. E., Bonna, A., Tumpach, C., Barnham, K. J., Haigh, C. L., Bal, W., & Drew, S. C. (2015). A Functional Role for Abeta in Metal Homeostasis? N-Truncation and High-Affinity Copper Binding. *Angew Chem Int Ed Engl*, *54*(36), 10460-10464. https://doi.org/10.1002/anie.201502644

Mittal, M., Siddiqui, M. R., Tran, K., Reddy, S. P., & Malik, A. B. (2014). Reactive oxygen species in inflammation and tissue injury. *Antioxidants & Redox Signaling*, *20*(7), 1126-1167. https://doi.org/10.1089/ars.2012.5149

Mohandas, E., Rajmohan, V., & Raghunath, B. (2009). Neurobiology of Alzheimer's disease. *Indian J Psychiatry*, *51*(1), 55-61. https://doi.org/10.4103/0019-5545.44908

Montero-Odasso, M., Pieruccini-Faria, F., Bartha, R., Black, S. E., Finger, E., Freedman, M., Greenberg, B., Grimes, D. A., Hegele, R. A., Hudson, C., Kleinstiver, P. W., Lang, A. E., Masellis, M., McLaughlin, P. M., Munoz, D. P., Strother, S., Swartz, R. H., Symons, S., Tartaglia, M. C., . . . McIlroy, W. (2017). Motor Phenotype in Neurodegenerative Disorders: Gait and Balance Platform Study Design Protocol for the Ontario Neurodegenerative Research Initiative (ONDRI). *Journal of Alzheimer's disease : JAD*, *59*(2), 707-721. https://doi.org/10.3233/JAD-170149

Moreno-Grau, S., Hernandez, I., Heilmann-Heimbach, S., Ruiz, S., Rosende-Roca, M., Mauleon, A., Vargas, L., Rodriguez-Gomez, O., Alegret, M., Espinosa, A., Ortega, G., Aguilera, N., Abdelnour, C., Neuroimaging Initiative, A. D., Gil, S., Maier, W., Sotolongo-Grau, O., Tarraga, L., Ramirez, A., . . . Ruiz, A. (2018). Genome-wide significant risk factors on chromosome 19 and the APOE locus. *Oncotarget*, *9*(37), 24590-24600. https://doi.org/10.18632/oncotarget.25083

Mori, H., Takio, K., Ogawara, M., & Selkoe, D. J. (1992). Mass spectrometry of purified amyloid beta protein in Alzheimer's disease. *The Journal of Biological Chemistry*, *267*(24), 17082-17086. https://www.ncbi.nlm.nih.gov/pubmed/1512246

Morris, K. L., & Serpell, L. C. (2012). X-ray fibre diffraction studies of amyloid fibrils. *Methods Mol Biol*, *849*, 121-135. https://doi.org/10.1007/978-1-61779-551-0_9

Naslund, J., Schierhorn, A., Hellman, U., Lannfelt, L., Roses, A. D., Tjernberg, L. O., Silberring, J., Gandy, S. E., Winblad, B., Greengard, P., & et al. (1994). Relative abundance of Alzheimer A beta amyloid peptide variants in Alzheimer disease and normal aging. *Proceedings of the National Academy of Sciences of the United States of America*, *91*(18), 8378-8382. https://doi.org/10.1073/pnas.91.18.8378

Nathalie, P., & Jean-Noel, O. (2008). Processing of amyloid precursor protein and amyloid peptide neurotoxicity. *Curr Alzheimer Res*, *5*(2), 92-99. https://doi.org/10.2174/156720508783954721

Nhan, H. S., Chiang, K., & Koo, E. H. (2015). The multifaceted nature of amyloid precursor protein and its proteolytic fragments: friends and foes. *Acta Neuropathologica*, *129*(1), 1-19. https://doi.org/10.1007/s00401-014-1347-2

Noor, A., Zafar, S., & Zerr, I. (2021). Neurodegenerative Proteinopathies in the Proteoform Spectrum-Tools and Challenges. *International Journal of Molecular Sciences*, *22*(3). https://doi.org/10.3390/ijms22031085

Nordberg, A., & Svensson, A. L. (1998). Cholinesterase inhibitors in the treatment of Alzheimer's disease: a comparison of tolerability and pharmacology. *Drug Saf*, *19*(6), 465-480. https://doi.org/10.2165/00002018-199819060-00004

Nunan, J., & Small, D. H. (2000). Regulation of APP cleavage by alpha-, beta- and gamma-secretases. *FEBS Lett*, *483*(1), 6-10. https://doi.org/10.1016/s0014-5793(00)02076-7

O'Brien, R. J., & Wong, P. C. (2011). Amyloid precursor protein processing and Alzheimer's disease. *Annu Rev Neurosci*, *34*, 185-204. https://doi.org/10.1146/annurev-neuro-061010-113613

Ono, K., Condron, M. M., & Teplow, D. B. (2009). Structure-neurotoxicity relationships of amyloid beta-protein oligomers. *Proceedings of the National Academy of Sciences of the United States of America*, *106*(35), 14745-14750. https://doi.org/10.1073/pnas.0905127106

Opazo, C. M., Greenough, M. A., & Bush, A. I. (2014). Copper: from neurotransmission to neuroproteostasis. *Frontiers in Aging Neuroscience*, *6*, 143. https://doi.org/10.3389/fnagi.2014.00143

Paduraru, E., Iacob, D., Rarinca, V., Rusu, A., Jijie, R., Ilie, O. D., Ciobica, A., Nicoara, M., & Doroftei, B. (2022). Comprehensive Review Regarding Mercury Poisoning and Its Complex Involvement in Alzheimer's Disease. *International Journal of Molecular Sciences*, *23*(4). https://doi.org/10.3390/ijms23041992

Patterson, D., Gardiner, K., Kao, F. T., Tanzi, R., Watkins, P., & Gusella, J. F. (1988). Mapping of the gene encoding the beta-amyloid precursor protein and its relationship to the Down syndrome region of chromosome 21. *Proceedings of the National Academy of Sciences of the United States of America*, *85*(21), 8266-8270. https://doi.org/10.1073/pnas.85.21.8266

Pedersen, J. T., Ostergaard, J., Rozlosnik, N., Gammelgaard, B., & Heegaard, N. H. (2011). Cu(II) mediates kinetically distinct, non-amyloidogenic aggregation of amyloid-beta peptides. *The Journal of Biological Chemistry*, *286*(30), 26952-26963. https://doi.org/10.1074/jbc.M111.220863

Pettersen, E. F., Goddard, T. D., Huang, C. C., Couch, G. S., Greenblatt, D. M., Meng, E. C., & Ferrin, T. E. (2004). UCSF Chimera--a visualization system for exploratory research and analysis. *J Comput Chem*, *25*(13), 1605-1612. https://doi.org/10.1002/jcc.20084

Pike, C. J., Overman, M. J., & Cotman, C. W. (1995). Amino-terminal deletions enhance aggregation of beta-amyloid peptides in vitro. *The Journal of Biological Chemistry*, *270*(41), 23895-23898. https://doi.org/10.1074/jbc.270.41.23895

Plant, L. D., Boyle, J. P., Smith, I. F., Peers, C., & Pearson, H. A. (2003). The production of amyloid beta peptide is a critical requirement for the viability of central neurons. *J Neurosci*, *23*(13), 5531-5535. https://doi.org/10.1523/JNEUROSCI.23-13-05531.2003

Popugaeva, E., Chernyuk, D., & Bezprozvanny, I. (2020). Reversal of Calcium Dysregulation as Potential Approach for Treating Alzheimer's Disease. *Curr Alzheimer Res*, *17*(4), 344-354. https://doi.org/10.2174/1567205017666200528162046

Portelius, E., Bogdanovic, N., Gustavsson, M. K., Volkmann, I., Brinkmalm, G., Zetterberg, H., Winblad, B., & Blennow, K. (2010). Mass spectrometric characterization of brain amyloid beta isoform signatures in familial and sporadic Alzheimer's disease. *Acta Neuropathologica*, *120*(2), 185-193. https://doi.org/10.1007/s00401-010-0690-1

Price, J. L., & Morris, J. C. (1999). Tangles and plaques in nondemented aging and "preclinical" Alzheimer's disease. *Ann Neurol*, *45*(3), 358-368. https://doi.org/10.1002/1531-8249(199903)45:3<358::aid-ana12>3.0.co;2-x

Probst, A., Tolnay, M., Langui, D., Goedert, M., & Spillantini, M. G. (1996). Pick's disease: hyperphosphorylated tau protein segregates to the somatoaxonal compartment. *Acta Neuropathologica*, *92*(6), 588-596. https://doi.org/10.1007/s004010050565

Puzzo, D., Gulisano, W., Arancio, O., & Palmeri, A. (2015). The keystone of Alzheimer pathogenesis might be sought in Abeta physiology. *Neuroscience*, *307*, 26-36. https://doi.org/10.1016/j.neuroscience.2015.08.039

Qi, X. M., & Ma, J. F. (2017). The role of amyloid beta clearance in cerebral amyloid angiopathy: more potential therapeutic targets. *Translational Neurodegeneration*, *6*, 22. https://doi.org/10.1186/s40035-017-0091-7

Qin, Z., Sun, Y., Jia, B., Wang, D., Ma, Y., & Ma, G. (2017). Kinetic Mechanism of Thioflavin T Binding onto the Amyloid Fibril of Hen Egg White Lysozyme. *Langmuir*, *33*(22), 5398-5405. https://doi.org/10.1021/acs.langmuir.7b00221

Radomska, K., & Wolszczak, M. (2022). Spontaneous and Ionizing Radiation-Induced Aggregation of Human Serum Albumin: Dityrosine as a Fluorescent Probe. *International Journal of Molecular Sciences*, *23*(15). https://doi.org/10.3390/ijms23158090

Rambaran, R. N., & Serpell, L. C. (2008). Amyloid fibrils: abnormal protein assembly. *Prion*, *2*(3), 112-117. https://doi.org/10.4161/pri.2.3.7488

Raussens, V., Fisher, C. A., Goormaghtigh, E., Ryan, R. O., & Ruysschaert, J. M. (1998). The low density lipoprotein receptor active conformation of apolipoprotein E. Helix organization in n-terminal domain-phospholipid disc particles. *The Journal of Biological Chemistry*, *273*(40), 25825-25830. https://doi.org/10.1074/jbc.273.40.25825

Ray, P. D., Huang, B. W., & Tsuji, Y. (2012). Reactive oxygen species (ROS) homeostasis and redox regulation in cellular signaling. *Cell Signal*, *24*(5), 981-990. https://doi.org/10.1016/j.cellsig.2012.01.008

Rebeck, G. W., Reiter, J. S., Strickland, D. K., & Hyman, B. T. (1993). Apolipoprotein E in sporadic Alzheimer's disease: allelic variation and receptor interactions. *Neuron*, *11*(4), 575-580. https://doi.org/10.1016/0896-6273(93)90070-8

Reddy, P. H., Reddy, T. P., Manczak, M., Calkins, M. J., Shirendeb, U., & Mao, P. (2011). Dynamin-related protein 1 and mitochondrial fragmentation in neurodegenerative diseases. *Brain Res Rev*, *67*(1-2), 103-118. https://doi.org/10.1016/j.brainresrev.2010.11.004

Reitz, C., Brayne, C., & Mayeux, R. (2011). Epidemiology of Alzheimer disease. *Nat Rev Neurol*, *7*(3), 137-152. https://doi.org/10.1038/nrneurol.2011.2

Ricciarelli, R., & Fedele, E. (2017). The Amyloid Cascade Hypothesis in Alzheimer's Disease: It's Time to Change Our Mind. *Curr Neuropharmacol*, *15*(6), 926-935. https://doi.org/10.2174/1570159X15666170116143743

Rice, K. M., Walker, E. M., Jr., Wu, M., Gillette, C., & Blough, E. R. (2014). Environmental mercury and its toxic effects. *Journal of Preventive Medicine and Public Health*, *47*(2), 74-83. https://doi.org/10.3961/jpmph.2014.47.2.74

Roos, D., Seeger, R., Puntel, R., & Vargas Barbosa, N. (2012). Role of calcium and mitochondria in MeHg-mediated cytotoxicity. *Journal of Biomedicine and Biotechnology*, *2012*, 248764. https://doi.org/10.1155/2012/248764

Roses, A. D. (1996). Apolipoprotein E alleles as risk factors in Alzheimer's disease. *Annu Rev Med*, *47*, 387-400. https://doi.org/10.1146/annurev.med.47.1.387

Ruffo, P., Perrone, B., & Conforti, F. L. (2022). SOD-1 Variants in Amyotrophic Lateral Sclerosis: Systematic Re-Evaluation According to ACMG-AMP Guidelines. *Genes (Basel)*, *13*(3). https://doi.org/10.3390/genes13030537

Ryan, T. M., Kirby, N., Mertens, H. D., Roberts, B., Barnham, K. J., Cappai, R., Pham Cle, L., Masters, C. L., & Curtain, C. C. (2015). Small angle X-ray scattering analysis of Cu(2+)-induced oligomers of the Alzheimer's amyloid beta peptide. *Metallomics*, *7*(3), 536-543. https://doi.org/10.1039/c4mt00323c

Sabate, R., & Ventura, S. (2013). Cross-beta-sheet supersecondary structure in amyloid folds: techniques for detection and characterization. *Methods Mol Biol*, *932*, 237-257. https://doi.org/10.1007/978-1-62703-065-6_15

Sabia, S., Fayosse, A., Dumurgier, J., van Hees, V. T., Paquet, C., Sommerlad, A., Kivimaki, M., Dugravot, A., & Singh-Manoux, A. (2021). Association of sleep duration in middle and old age with incidence of dementia. *Nature Communications*, *12*(1), 2289. https://doi.org/10.1038/s41467-021-22354-2

Sack, G. H., Jr. (2020). Serum Amyloid A (SAA) Proteins. *Subcell Biochem*, *94*, 421-436. https://doi.org/10.1007/978-3-030-41769-7_17

Sakono, M., & Zako, T. (2010). Amyloid oligomers: formation and toxicity of Abeta oligomers. *FEBS J*, *277*(6), 1348-1358. https://doi.org/10.1111/j.1742-4658.2010.07568.x

Sankararamakrishnan, R., Verma, S., & Kumar, S. (2005). ATCUN-like metal-binding motifs in proteins: identification and characterization by crystal structure and sequence analysis. *Proteins*, *58*(1), 211-221. https://doi.org/10.1002/prot.20265

Scheff, S. W., & Price, D. A. (2001). Alzheimer's disease-related synapse loss in the cingulate cortex. *Journal of Alzheimer's disease : JAD*, *3*(5), 495-505. https://doi.org/10.3233/jad-2001-3509

Segrest, J. P., Jones, M. K., De Loof, H., Brouillette, C. G., Venkatachalapathi, Y. V., & Anantharamaiah, G. M. (1992). The amphipathic helix in the exchangeable apolipoproteins: a review of secondary structure and function. *J Lipid Res*, *33*(2), 141-166. https://www.ncbi.nlm.nih.gov/pubmed/1569369

Selkoe, D. J. (2001). Alzheimer's disease: genes, proteins, and therapy. *Physiol Rev*, *81*(2), 741-766. https://doi.org/10.1152/physrev.2001.81.2.741

Selkoe, D. J. (2008). Biochemistry and molecular biology of amyloid beta-protein and the mechanism of Alzheimer's disease. *Handb Clin Neurol*, *89*, 245-260. https://doi.org/10.1016/S0072-9752(07)01223-7

Senechal, Y., Kelly, P. H., & Dev, K. K. (2008). Amyloid precursor protein knockout mice show age-dependent deficits in passive avoidance learning. *Behav Brain Res*, *186*(1), 126-132. https://doi.org/10.1016/j.bbr.2007.08.003

Serra-Batiste, M., Ninot-Pedrosa, M., Bayoumi, M., Gairi, M., Maglia, G., & Carulla, N. (2016). Abeta42 assembles into specific beta-barrel pore-forming oligomers in membrane-mimicking environments. *Proceedings of the National Academy of Sciences of the United States of America*, *113*(39), 10866-10871. https://doi.org/10.1073/pnas.1605104113

Sgourakis, N. G., Yan, Y., McCallum, S. A., Wang, C., & Garcia, A. E. (2007). The Alzheimer's peptides Abeta40 and 42 adopt distinct conformations in water: a combined MD / NMR study. *J Mol Biol*, *368*(5), 1448-1457. https://doi.org/10.1016/j.jmb.2007.02.093

Shackleton, B., Ringland, C., Abdullah, L., Mullan, M., Crawford, F., & Bachmeier, C. (2019). Influence of Matrix Metallopeptidase 9 on Beta-Amyloid Elimination Across the Blood-Brain Barrier. *Mol Neurobiol*, *56*(12), 8296-8305. https://doi.org/10.1007/s12035-019-01672-z

Sharma, A., Pachauri, V., & Flora, S. J. S. (2018). Advances in Multi-Functional Ligands and the Need for Metal-Related Pharmacology for the Management of Alzheimer Disease. *Front Pharmacol*, *9*, 1247. https://doi.org/10.3389/fphar.2018.01247

Sheikh, M., Khan, S. J., Butt, H. A. T., Zaidi, S. A. T., & Na, V. (2023). From Symptomatic Treatment to Disease Modification: A Turning Point in Alzheimer's Disease Management. *Cureus*, *15*(10), e47251. https://doi.org/10.7759/cureus.47251

Shields, H. J., Traa, A., & Van Raamsdonk, J. M. (2021). Beneficial and Detrimental Effects of Reactive Oxygen Species on Lifespan: A Comprehensive Review of Comparative and Experimental Studies. *Front Cell Dev Biol*, *9*, 628157. https://doi.org/10.3389/fcell.2021.628157

Sipe, J. D., & Cohen, A. S. (2000). Review: history of the amyloid fibril. *J Struct Biol*, *130*(2-3), 88-98. https://doi.org/10.1006/jsbi.2000.4221

Sitammagari, K. K., & Masood, W. (2024). Creutzfeldt Jakob Disease. In *StatPearls*. https://www.ncbi.nlm.nih.gov/pubmed/29939637

Skovronsky, D. M., Doms, R. W., & Lee, V. M. (1998). Detection of a novel intraneuronal pool of insoluble amyloid beta protein that accumulates with time in culture. *J Cell Biol*, *141*(4), 1031-1039. https://doi.org/10.1083/jcb.141.4.1031

Smith, D. G., Cappai, R., & Barnham, K. J. (2007). The redox chemistry of the Alzheimer's disease amyloid beta peptide. *Biochimica et biophysica acta*, *1768*(8), 1976-1990. https://doi.org/10.1016/j.bbamem.2007.02.002

Smith, D. P., Ciccotosto, G. D., Tew, D. J., Fodero-Tavoletti, M. T., Johanssen, T., Masters, C. L., Barnham, K. J., & Cappai, R. (2007). Concentration dependent Cu2+ induced aggregation and dityrosine formation of the Alzheimer's disease amyloid-beta peptide. *Biochemistry*, *46*(10), 2881-2891. https://doi.org/10.1021/bi0620961

Soucek, T., Cumming, R., Dargusch, R., Maher, P., & Schubert, D. (2003). The regulation of glucose metabolism by HIF-1 mediates a neuroprotective response to amyloid beta peptide. *Neuron*, *39*(1), 43-56. https://doi.org/10.1016/s0896-6273(03)00367-2

Spuch, C., Ortolano, S., & Navarro, C. (2012). New insights in the amyloid-Beta interaction with mitochondria. *J Aging Res*, *2012*, 324968. https://doi.org/10.1155/2012/324968

Squitti, R., Simonelli, I., Ventriglia, M., Siotto, M., Pasqualetti, P., Rembach, A., Doecke, J., & Bush, A. I. (2014). Meta-analysis of serum non-ceruloplasmin copper in Alzheimer's disease. *Journal of Alzheimer's disease : JAD*, *38*(4), 809-822. https://doi.org/10.3233/JAD-131247

Stewart, K. L., & Radford, S. E. (2017). Amyloid plaques beyond Abeta: a survey of the diverse modulators of amyloid aggregation. *Biophys Rev*, *9*(4), 405-419. https://doi.org/10.1007/s12551-017-0271-9

Strittmatter, W. J., Saunders, A. M., Schmechel, D., Pericak-Vance, M., Enghild, J., Salvesen, G. S., & Roses, A. D. (1993). Apolipoprotein E: high-avidity binding to beta-amyloid and increased frequency of type 4 allele in late-onset familial Alzheimer disease. *Proceedings of the National Academy of Sciences of the United States of America*, *90*(5), 1977-1981. https://doi.org/10.1073/pnas.90.5.1977

Strydom, A., Coppus, A., Blesa, R., Danek, A., Fortea, J., Hardy, J., Levin, J., Nuebling, G., Rebillat, A. S., Ritchie, C., van Duijn, C., Zaman, S., & Zetterberg, H. (2018). Alzheimer's disease in Down syndrome: An overlooked population for prevention trials. *Alzheimers Dement (N Y)*, *4*, 703-713. https://doi.org/10.1016/j.trci.2018.10.006

Sunde, M., Serpell, L. C., Bartlam, M., Fraser, P. E., Pepys, M. B., & Blake, C. C. (1997). Common core structure of amyloid fibrils by synchrotron X-ray diffraction. *J Mol Biol*, *273*(3), 729-739. https://doi.org/10.1006/jmbi.1997.1348

Suryana, E., Rowlands, B. D., Bishop, D. P., Finkelstein, D. I., & Double, K. L. (2024). Empirically derived formulae for calculation of age- and region-related levels of iron, copper and zinc in the adult C57BL/6 mouse brain. *Neurobiol Aging*, *136*, 34-43. https://doi.org/10.1016/j.neurobiolaging.2024.01.003

Tamagno, E., Guglielmotto, M., Monteleone, D., Manassero, G., Vasciaveo, V., & Tabaton, M. (2018). The Unexpected Role of Abeta1-42 Monomers in the Pathogenesis of Alzheimer's Disease. *Journal of Alzheimer's disease : JAD*, *62*(3), 1241-1245. https://doi.org/10.3233/JAD-170581

Taniguchi, K., Yamamoto, F., Amano, A., Tamaoka, A., Sanjo, N., Yokota, T., Kametani, F., & Araki, W. (2022). Amyloid-beta oligomers interact with NMDA receptors containing GluN2B subunits and metabotropic glutamate receptor 1 in primary cortical neurons: Relevance to the synapse pathology of Alzheimer's disease. *Neurosci Res*, *180*, 90-98. https://doi.org/10.1016/j.neures.2022.03.001

Terry, R. D., Masliah, E., Salmon, D. P., Butters, N., DeTeresa, R., Hill, R., Hansen, L. A., & Katzman, R. (1991). Physical basis of cognitive alterations in Alzheimer's disease: synapse loss is the major correlate of cognitive impairment. *Ann Neurol*, *30*(4), 572-580. https://doi.org/10.1002/ana.410300410

Thacker, D., Barghouth, M., Bless, M., Zhang, E., & Linse, S. (2023). Direct observation of secondary nucleation along the fibril surface of the amyloid beta 42 peptide. *Proceedings of the National Academy of Sciences of the United States of America*, *120*(25), e2220664120. https://doi.org/10.1073/pnas.2220664120

Tharp, W. G., & Sarkar, I. N. (2013). Origins of amyloid-beta. *BMC Genomics*, *14*, 290. https://doi.org/10.1186/1471-2164-14-290

Tiiman, A., Jarvet, J., Gräslund, A., & Vukojevic, V. (2015). Heterogeneity and Turnover of Intermediates during Amyloid-beta (Abeta) Peptide Aggregation Studied by Fluorescence Correlation Spectroscopy. *Biochemistry*, *54*(49), 7203-7211. https://doi.org/10.1021/acs.biochem.5b00976

Tiiman, A., Luo, J., Wallin, C., Olsson, L., Lindgren, J., Jarvet, J., Roos, P., Sholts, S. B., Rahimipour, S., Abrahams, J. P., Karlström, A. E., Gräslund, A., & Wärmländer, S. K. (2016). Specific Binding of Cu(II) Ions to Amyloid-Beta Peptides Bound to Aggregation-Inhibiting Molecules or SDS Micelles Creates Complexes that Generate Radical Oxygen Species. *Journal of Alzheimer's disease : JAD*, *54*(3), 971-982. https://doi.org/10.3233/JAD-160427

Tosh, J. L., Rhymes, E. R., Mumford, P., Whittaker, H. T., Pulford, L. J., Noy, S. J., Cleverley, K., LonDown, S. C., Walker, M. C., Tybulewicz, V. L. J., Wykes, R. C., Fisher, E. M. C., & Wiseman, F. K. (2021). Genetic dissection of down syndrome-associated alterations in APP/amyloid-beta biology using mouse models. *Scientific Reports*, *11*(1), 5736. https://doi.org/10.1038/s41598-021-85062-3

Trojsi, F., Christidi, F., Migliaccio, R., Santamaria-Garcia, H., & Santangelo, G. (2018). Behavioural and Cognitive Changes in Neurodegenerative Diseases and Brain Injury. *Behav Neurol*, *2018*, 4935915. https://doi.org/10.1155/2018/4935915

Turner, R. S., Suzuki, N., Chyung, A. S., Younkin, S. G., & Lee, V. M. (1996). Amyloids beta40 and beta42 are generated intracellularly in cultured human neurons and their secretion increases with maturation. *The Journal of Biological Chemistry*, *271*(15), 8966-8970. https://doi.org/10.1074/jbc.271.15.8966

U.S Food and Drug Administration. (2021). *FDA Grants Accelerated Approval for Alzheimer's Drug*. Retrieved 08-16 from https://www.fda.gov/news-events/press-announcements/fda-grants-accelerated-approval-alzheimers-drug

U.S Food and Drug Administration. (2023). *FDA Converts Novel Alzheimer's Disease Treatment to Traditional Approval*. Retrieved 08-16 from https://www.fda.gov/news-events/press-announcements/fda-converts-novel-alzheimers-disease-treatment-traditional-approval

UNEP. (2019). *Global Mercury Assessment 2018*. Retrieved 08-12 from https://www.unep.org/resources/publication/global-mercury-assessment-2018

van der Flier, W. M., & Scheltens, P. (2005). Epidemiology and risk factors of dementia. *J Neurol Neurosurg Psychiatry*, *76 Suppl 5*(Suppl 5), v2-7. https://doi.org/10.1136/jnnp.2005.082867

Vaz, M., & Silvestre, S. (2020). Alzheimer's disease: Recent treatment strategies. *Eur J Pharmacol*, *887*, 173554. https://doi.org/10.1016/j.ejphar.2020.173554

Vellingiri, B. (2023). A deeper understanding about the role of uranium toxicity in neurodegeneration. *Environ Res*, *233*, 116430. https://doi.org/10.1016/j.envres.2023.116430

Viola, K. L., & Klein, W. L. (2015). Amyloid beta oligomers in Alzheimer's disease pathogenesis, treatment, and diagnosis. *Acta Neuropathologica*, *129*(2), 183-206. https://doi.org/10.1007/s00401-015-1386-3

Vitek, M. P., Brown, C. M., & Colton, C. A. (2009). APOE genotype-specific differences in the innate immune response. *Neurobiol Aging*, *30*(9), 1350-1360. https://doi.org/10.1016/j.neurobiolaging.2007.11.014

Vosough, F., & Barth, A. (2021). Characterization of Homogeneous and Heterogeneous Amyloid-beta42 Oligomer Preparations with Biochemical Methods and Infrared Spectroscopy Reveals a Correlation between Infrared Spectrum and Oligomer Size. *ACS Chem Neurosci*, *12*(3), 473-488. https://doi.org/10.1021/acschemneuro.0c00642

Walker, L. C., & Jucker, M. (2017). The Exceptional Vulnerability of Humans to Alzheimer's Disease. *Trends Mol Med*, *23*(6), 534-545. https://doi.org/10.1016/j.molmed.2017.04.001

Walker, L. C., Schelle, J., & Jucker, M. (2016). The Prion-Like Properties of Amyloid-beta Assemblies: Implications for Alzheimer's Disease. *Cold Spring Harb Perspect Med*, *6*(7). https://doi.org/10.1101/cshperspect.a024398

Wallin, C., Kulkarni, Y. S., Abelein, A., Jarvet, J., Liao, Q., Strodel, B., Olsson, L., Luo, J., Abrahams, J. P., Sholts, S. B., Roos, P. M., Kamerlin, S. C., Gräslund, A., & Wärmländer, S. K. (2016). Characterization of Mn(II) ion binding to the amyloid-beta peptide in Alzheimer's disease. *J Trace Elem Med Biol*, *38*, 183-193. https://doi.org/10.1016/j.jtemb.2016.03.009

Wallin, C., Sholts, S. B., Österlund, N., Luo, J., Jarvet, J., Roos, P. M., Ilag, L., Gräslund, A., & Wärmländer, S. (2017). Alzheimer's disease and cigarette smoke components: effects of nicotine, PAHs, and Cd(II), Cr(III), Pb(II), Pb(IV) ions on amyloid-beta peptide aggregation. *Scientific Reports*, *7*(1), 14423. https://doi.org/10.1038/s41598-017-13759-5

Walsh, D. M., & Selkoe, D. J. (2004). Oligomers on the brain: the emerging role of soluble protein aggregates in neurodegeneration. *Protein Pept Lett*, *11*(3), 213-228. https://doi.org/10.2174/0929866043407174

Wang, F., & Zhang, L. (2015). Intervention Strategies for Metal Deficiency and Overload. In J. O. Nriagu & E. P. Skaar (Eds.), *Trace Metals and Infectious Diseases*. https://www.ncbi.nlm.nih.gov/pubmed/33886191

Wang, L., Yin, Y. L., Liu, X. Z., Shen, P., Zheng, Y. G., Lan, X. R., Lu, C. B., & Wang, J. Z. (2020). Current understanding of metal ions in the pathogenesis of Alzheimer's disease. *Translational Neurodegeneration*, *9*, 10. https://doi.org/10.1186/s40035-020-00189-z

Wang, X., Su, B., Lee, H. G., Li, X., Perry, G., Smith, M. A., & Zhu, X. (2009). Impaired balance of mitochondrial fission and fusion in Alzheimer's disease. *J Neurosci*, *29*(28), 9090-9103. https://doi.org/10.1523/JNEUROSCI.1357-09.2009

Weisgraber, K. H. (1994). Apolipoprotein E: structure-function relationships. *Adv Protein Chem*, *45*, 249-302. https://doi.org/10.1016/s0065-3233(08)60642-7

Wiatrak, B., Piasny, J., Kuzniarski, A., & Gasiorowski, K. (2021). Interactions of Amyloid-beta with Membrane Proteins. *International Journal of Molecular Sciences*, *22*(11). https://doi.org/10.3390/ijms22116075

Wild, K., August, A., Pietrzik, C. U., & Kins, S. (2017). Structure and Synaptic Function of Metal Binding to the Amyloid Precursor Protein and its Proteolytic Fragments. *Front Mol Neurosci*, *10*, 21. https://doi.org/10.3389/fnmol.2017.00021

Wilker, E. H., Osman, M., & Weisskopf, M. G. (2023). Ambient air pollution and clinical dementia: systematic review and meta-analysis. *BMJ : British Medical Journal*, *381*, e071620. https://doi.org/10.1136/bmj-2022-071620

Willbold, D., Strodel, B., Schroder, G. F., Hoyer, W., & Heise, H. (2021). Amyloid-type Protein Aggregation and Prion-like Properties of Amyloids. *Chem Rev*, *121*(13), 8285-8307. https://doi.org/10.1021/acs.chemrev.1c00196

Williams, T. L., Serpell, L. C., & Urbanc, B. (2016). Stabilization of native amyloid beta-protein oligomers by Copper and Hydrogen peroxide Induced Cross-linking of Unmodified Proteins (CHICUP). *Biochimica et biophysica acta*, *1864*(3), 249-259. https://doi.org/10.1016/j.bbapap.2015.12.001

Wilson, C., Wardell, M. R., Weisgraber, K. H., Mahley, R. W., & Agard, D. A. (1991). Three-dimensional structure of the LDL receptor-binding domain of human apolipoprotein E. *Science*, *252*(5014), 1817-1822. https://doi.org/10.1126/science.2063194

Wimo, A., Seeher, K., Cataldi, R., Cyhlarova, E., Dielemann, J. L., Frisell, O., Guerchet, M., Jonsson, L., Malaha, A. K., Nichols, E., Pedroza, P., Prince, M., Knapp, M., & Dua, T. (2023). The worldwide costs of dementia in 2019. *Alzheimers Dement*, *19*(7), 2865-2873. https://doi.org/10.1002/alz.12901

Wirths, O., Zampar, S., & Weggen, S. (2019). N-Terminally Truncated Aβ Peptide Variants in Alzheimer's Disease. In T. Wisniewski (Ed.), *Alzheimer's disease* (pp. 107-122). Codon Publications. https://www.ncbi.nlm.nih.gov/books/NBK552142/

Wisniewski, T., Castano, E. M., Golabek, A., Vogel, T., & Frangione, B. (1994). Acceleration of Alzheimer's fibril formation by apolipoprotein E in vitro. *Am J Pathol*, *145*(5), 1030-1035. https://www.ncbi.nlm.nih.gov/pubmed/7977635

World Health Organization. (2021). *Compendium of WHO and other UN guidance on health and environment*. Retrieved 08-12 from https://www.who.int/tools/compendium-on-health-and-environment

World Health Organization. (2023). *Dementia*. Retrieved 2024-06-03 from https://www.who.int/news-room/fact-sheets/detail/dementia

World Health Organization. (2024). *World health statistics 2024: monitoring health for the SDGs, sustainable development goals*. https://www.who.int/publications/i/item/9789240094703

Wärmländer, S., Österlund, N., Wallin, C., Wu, J., Luo, J., Tiiman, A., Jarvet, J., & Gräslund, A. (2019). Metal binding to the amyloid-beta peptides in the presence of biomembranes: potential mechanisms of cell toxicity. *J Biol Inorg Chem*, *24*(8), 1189-1196. https://doi.org/10.1007/s00775-019-01723-9

Xiong, F., Ge, W., & Ma, C. (2019). Quantitative proteomics reveals distinct composition of amyloid plaques in Alzheimer's disease. *Alzheimers Dement*, *15*(3), 429-440. https://doi.org/10.1016/j.jalz.2018.10.006

Xu, G., Ran, Y., Fromholt, S. E., Fu, C., Yachnis, A. T., Golde, T. E., & Borchelt, D. R. (2015). Murine Abeta over-production produces diffuse and compact Alzheimer-type amyloid deposits. *Acta Neuropathol Commun*, *3*, 72. https://doi.org/10.1186/s40478-015-0252-9

Yamauchi, Y., Deguchi, N., Takagi, C., Tanaka, M., Dhanasekaran, P., Nakano, M., Handa, T., Phillips, M. C., Lund-Katz, S., & Saito, H. (2008). Role of the N- and C-terminal domains in binding of apolipoprotein E isoforms to heparan sulfate and dermatan sulfate: a surface plasmon resonance study. *Biochemistry*, *47*(25), 6702-6710. https://doi.org/10.1021/bi8003999

Yan, D., Zhang, Y., Liu, L., & Yan, H. (2016). Pesticide exposure and risk of Alzheimer's disease: a systematic review and meta-analysis. *Scientific Reports*, *6*, 32222. https://doi.org/10.1038/srep32222

Yang, L. G., March, Z. M., Stephenson, R. A., & Narayan, P. S. (2023). Apolipoprotein E in lipid metabolism and neurodegenerative disease. *Trends Endocrinol Metab*, *34*(8), 430-445. https://doi.org/10.1016/j.tem.2023.05.002

Ye, S., Huang, Y., Mullendorff, K., Dong, L., Giedt, G., Meng, E. C., Cohen, F. E., Kuntz, I. D., Weisgraber, K. H., & Mahley, R. W. (2005). Apolipoprotein (apo) E4 enhances amyloid beta peptide production in cultured neuronal cells: apoE structure as a potential therapeutic target. *Proceedings of the National Academy of Sciences of the United States of America*, *102*(51), 18700-18705. https://doi.org/10.1073/pnas.0508693102

Young, T. R., Kirchner, A., Wedd, A. G., & Xiao, Z. (2014). An integrated study of the affinities of the Abeta16 peptide for Cu(I) and Cu(II): implications for the catalytic production of reactive oxygen species. *Metallomics*, *6*(3), 505-517. https://doi.org/10.1039/c4mt00001c

Zempel, H., & Mandelkow, E. (2014). Lost after translation: missorting of Tau protein and consequences for Alzheimer disease. *Trends Neurosci*, *37*(12), 721-732. https://doi.org/10.1016/j.tins.2014.08.004

Zhang, W., Tarutani, A., Newell, K. L., Murzin, A. G., Matsubara, T., Falcon, B., Vidal, R., Garringer, H. J., Shi, Y., Ikeuchi, T., Murayama, S., Ghetti, B., Hasegawa, M., Goedert, M., & Scheres, S. H. W. (2020). Novel tau filament fold in corticobasal degeneration. *Nature*, *580*(7802), 283-287. https://doi.org/10.1038/s41586-020-2043-0

Zhang, W., Xiao, D., Mao, Q., & Xia, H. (2023). Role of neuroinflammation in neurodegeneration development. *Signal Transduct Target Ther*, *8*(1), 267. https://doi.org/10.1038/s41392-023-01486-5

Zhang, Y., Chen, H., Li, R., Sterling, K., & Song, W. (2023). Amyloid beta-based therapy for Alzheimer's disease: challenges, successes and future. *Signal Transduct Target Ther*, *8*(1), 248. https://doi.org/10.1038/s41392-023-01484-7

Zhang, Y. W., Thompson, R., Zhang, H., & Xu, H. (2011). APP processing in Alzheimer's disease. *Mol Brain*, *4*, 3. https://doi.org/10.1186/1756-6606-4-3

Zhao, W. Q., De Felice, F. G., Fernandez, S., Chen, H., Lambert, M. P., Quon, M. J., Krafft, G. A., & Klein, W. L. (2008). Amyloid beta oligomers induce impairment of neuronal insulin receptors. *FASEB J*, *22*(1), 246-260. https://doi.org/10.1096/fj.06-7703com

Zheng, H., Jiang, M., Trumbauer, M. E., Sirinathsinghji, D. J., Hopkins, R., Smith, D. W., Heavens, R. P., Dawson, G. R., Boyce, S., Conner, M. W., Stevens, K. A., Slunt, H. H., Sisoda, S. S., Chen, H. Y., & Van der Ploeg, L. H. (1995). beta-Amyloid precursor protein-deficient mice show reactive gliosis and decreased locomotor activity. *Cell*, *81*(4), 525-531. https://doi.org/10.1016/0092-8674(95)90073-x

Zheng, H., & Koo, E. H. (2011). Biology and pathophysiology of the amyloid precursor protein. *Molecular Neurodegeneration*, *6*(1), 27. https://doi.org/10.1186/1750-1326-6-27

Zheng, Z., & Diamond, M. I. (2012). Huntington disease and the huntingtin protein. *Prog Mol Biol Transl Sci*, *107*, 189-214. https://doi.org/10.1016/B978-0-12-385883-2.00010-2

Zhiwu Zhu, R. M., Christopher L. Chavez. (2000). Chapter 20 - Signaling in Copper Ion Homeostasi. *Cell and Molecular Response to Stress*, *1*, 293-300. https://doi.org/https://doi.org/10.1016/S1568-1254(00)80022-4

Zorko, M. (2010). Structural Organization of Proteins. In T. F. Group (Ed.), *Introduction to Peptides and Proteins* (Vol. 1, pp. 50-51). CRC Press.

Acknowledgements

First, I would like to express my sincere gratitude to my supervisor **Peep Palumaa** for all the guidance, help and patience. I am grateful that you believed in and supported me on this journey.

Thank you to my co-supervisor **Sebastian Wärmländer**, for always being available for discussion and helping me on every step of the way. Your constant encouragement and for pushing me has been invaluable. I could not have done this without your help and guidance.

To my other co-supervisor **Per Roos**, thank you for all the good discussions, feedback and great ideas.

I would also like to thank **Astrid Gräslund** for letting me into her lab with open arms. Thank you for all the great discussions and your enthusiasm. It has been an honor to be a part of your research.

To **Jüri Jarvet**, thank you for everything. Thank you for always being there to help, to discuss results and thank you for your honest opinions.

In the **Palumaa** Lab, special thank you to **Merlin Friedmann**, **Andra Normägi** and **Julia Smirnova** for welcoming me with open arms, letting me be a part of your projects and teaching me your methods. Also, thanks to **Vello Tõugu** for all great input on data and analysis.

During my years in the **Gräslund** Lab, I have had the opportunity to work with many amazing people. Thank you, **Amanda Lakela**, **Fanny Asplund**, **Nicklas Österlund**, **Xiaolin Dong** and many others for all collaborations.

In the **Andreas Barth group**, Thank you **Andreas, Faraz Vosough** and **Suman Paul** for many fruitful collaborations. I would also like to thank the **Ludmilla A Morozova-Roche** lab at Umeå University, for the great collaborations.

And to my family,

Mum, Mammut. Thank you for all the endless love and support. *Alltid oavsett*. To **Kennie** and **Linda,** thank you for all the insightful discussions and all the inspiration. **Louna**, you have brought me so much happiness, you are the best!

Pappa, thanks for never being more than a phone call away when I needed to disconnect and just think about something else.

Peter, my dear uncle. Thank you for always keeping me on my toes, asking questions and being interested.

To **Bengt** and **Lise**, thank you for your kindness, encouragement and support during this time. To the rest of the **Mattsson** and **Langseth** family, thank you for your warmth and generosity along the way.

To **Vilma**. Thank you for changing everything, for giving me new a perspective and purpose.

Finally, thank you **Christoffer**. Thank you for the all the peptalks when I was ready to give up, and for picking up the pieces when I already had. Thank you for always being there, for being my safe place and for supporting and encouraging me on every step of the way.

Abstract

Interaction of metal ions with peptides and proteins related to Alzheimer's disease

Alzheimer's disease (AD) is the most common cause of dementia with approximately 55 million patients worldwide. The disease has been studied for decades, and although significant progress has been made, there are still many gaps in our knowledge. So far, no effective disease-modifying treatments have been developed, despite ongoing efforts. The underlying molecular mechanisms remain debated, but it is widely accepted that aggregation of the amyloid-β (Aβ) peptide is involved in the disease pathology.

The Aβ peptide is known to self-assemble into aggregates, ranging from dimers to lots of peptides, with large amyloid plaques as the end-product. Many hypotheses have been proposed regarding the cause of the disease. One of them is the metal hypothesis, which argues that metal dysregulation plays a crucial role in AD pathology. Increased levels of Cu, Fe and Zn have been found in the amyloid plaques of AD brains; however, the mechanism of metal involvement remains to be elucidated. There are indications that some metals can affect the cleavage of the Aβ precursor protein, thereby increasing the Aβ production, particularly the more aggregation-prone Aβ variants. Additionally, it has been suggested that metal ions affect the aggregation pathway of the Aβ peptide, and to some extent stabilize toxic oligomeric species. A third possibility is that the metals are not actually involved in the aggregation. Instead, they might bind to already formed aggregates and contribute to the formation of harmful oxygen radicals.

In this thesis, some effects of metal ions on AD-related proteins have been investigated. Significant work has previously been published on the most biologically relevant metals, such as Cu, Zn and Fe, although with a lot of variations in the results. We were able to show that the truncated Aβ peptides containing an ATCUN-motif have similar binding affinities to Cu(II) as the well-known Cu(II) binding protein human serum albumin (HSA). It can be concluded that the truncated Aβ variants with an ATCUN-motif are not able to remove substantial amounts of Cu(II) ions from HSA in blood or CFS and do likely not have a dominant role in the regulation of Cu(II) ions in these environments.

We also wanted to contribute to the field by investigating metals that are available in our environment, but which are not required for any biological processes in the human body. These studies can provide insights into the general mechanism of metal-induced peptide aggregation and toxicity. The selected metals are nickel, mercury, and uranium.

We show that both nickel and uranium can slow down the fibrillization kinetics and direct the aggregates towards amorphous structures. The Ni(II) ions bind specifically to the N-terminal, particularly to the His residues and were also shown to induce the formation of dityrosine crosslinks, which generates aggregates that are more stable and more resistant to dissociation. The uranyl ions on the other hand did not show specific binding and are instead thought to interact with the peptide through electrostatic interactions. Interestingly, the uranyl ions showed strongest binding at pH 5.1, which could be explained by interference of the His sidechains at neutral pH and by the chemical properties of the uranyl ions that might become hydrolyzed at low pH. Therefore, the presence of monomeric and dimeric hydroxyl species mixed with the uranyl ions might affect the binding. Both Ni(II) and uranyl ions were able to induce β-sheet formation in aqueous solution and thereby stabilizing and promoting aggregation of the peptide.

Although the Aβ peptide is of great interest, there are many other peptides and proteins that are involved in AD. The apolipoprotein ApoE occurs in three isoforms, where the ApoE4 has been shown to be the main genetic risk factor for developing sporadic AD. Interestingly, ApoE4 carriers have also been shown to be more susceptible to mercury toxicity. Therefore, it has been suggested that the ApoE protein might be involved in the clearance of Hg and/or Aβ peptides, and that the ApoE4 isoform might be less effective at this task.

We showed that the binding affinity for Hg(II) ions is largely the same for all three ApoE isoforms, but that a larger structural change can be observed for the ApoE4 isoform upon addition of Hg(II) ions. This indicates that the amino acid variations between the different isoforms are not directly involved in the binding of Hg(II) ions, but that the differences in structure induction might be connected to the ApoE-ε4 gene being a risk factor for mercury intoxication.

In this thesis, the studied peptides/proteins are different variants of amyloid-β, ApoE, and human serum albumin. Numerous biophysical methods, mainly spectroscopic and imaging techniques, have been used to characterize different aspects of the interactions between the selected metal ions and the protein/peptide variants. The focus has been to determine binding affinities, identify specific binding residues, and to monitor metal-induced effects on secondary structure and aggregation of selected peptides/proteins. The obtained results widen our insights into the role of metal ions in AD pathology, highlighting specific interactions that may influence the progression of the disease.

Lühikokkuvõte

Metalliioonide interaktsioonid Alzheimeri tõvega seotud peptiidide ja valkudega

Alzheimeri tõbi (AD) on kõige levinum dementsuse põhjus, mõjutades umbes 55 miljonit inimest üle kogu maailma. Haigust on uuritud kümneid aastaid ja kuigi on tehtud märkimisväärseid edusamme, on meie teadmistes endiselt palju lünki. Vaatamata jätkuvatele pingutustele pole seni veel välja arendatud tõhusaid haigust muutvaid ravimeetodeid. Haiguse aluseks olevad molekulaarsed mehhanismid on endiselt vaieldavad, kuid on laialdaselt aktsepteeritud, et amüloidi-β (Aβ) peptiidi agregatsioon on seotud haiguse patoloogiaga.

Aβ peptiid on tuntud oma võime poolest ise kokku koonduda agregaatideks, mis hõlmavad nii oligomeere, kui ka paljudest peptiididest koosnevaid amüloidseid naastusid. On pakutud välja mitmeid hüpoteese, mis käsitlevad haiguse põhjust. Üks neist on metallide hüpotees, mis väidab, et metallide düsregulatsioon mängib AD patoloogias olulist rolli. Näiteks Cu, Fe ja Zn, kõrgenenud kontsentratsioone on leitud AD ajus amüloidsetes naastudes, kuid metallide osaluse mehhanism on veel uurimisjärgus. On viiteid sellele, et mõned metallid võivad mõjutada Aβ eellasvalgu lõhustumist, suurendades rohkem agregatsioonile kalduvate Aβ peptiidide tootmist. Lisaks võivad metalliioonid mõjutada Aβ peptiidi agregatsiooniteed ja osaliselt stabiliseerida toksilisi oligomeerseid vorme. Kolmanda võimaluse kohaselt ei osale metallid Aβ agregatsioonis, kuid selle asemel võivad nad seostuda juba moodustunud agregaatidega ja aidata kaasa kahjulike hapniku radikaalide tekkele.

Käesolevas töös on uuritud mõningate metalliioonide mõju AD-ga seotud valkudele. Varasemalt on teostatud mahukas töö bioloogiliselt kõige olulisemate metallide kohta, nagu Cu, Zn ja Fe, kuigi tulemused varieeruvad. Me suutsime näidata, et lühenenud Aβ peptiid, mis sisaldab ATCUN-motiivi, seondub Cu(II)-ioonidega sarnaselt tuntud Cu(II) siduva valgu - inimese seerumi albumiiniga (HSA). Võib järeldada, et lühenenud Aβ variandid, mis sisaldavad ATCUN-motiivi, ei suuda veres või tserebrospinaalvedelikus eemaldada Cu(II) ioone HSA-lt ja ei mängi tõenäoliselt domineerivat rolli Cu(II) ioonide regulatsioonis neis keskkondades.

Soovisime samuti panustada valdkonda, uurides metalle, mis esinevad meie keskkonnas, kuid mis ei ole inimorganismi funktsioneerimiseks vajalikud. Need uuringud võivad anda täiendavat informatsiooni metalliioonide poolt põhjustatud peptiidide agregatsiooni ja toksilisuse üldmehhanismide kohta. Valitud metallideks olid nikkel, elavhõbe ja uraan.

Me näitasime, et nii nikkel(II), kui ka uranüülioonid suudavad aeglustada Aβ fibrilliseerumise kineetikat ja suunata protsessi amorfsete agregaatide tekke suunas. Ni(II) ioonid seonduvad spetsiifiliselt Aβ N-terminaalses osas paiknevate His-jääkidega, ning suudavad samuti indutseerida ditürosiini-ristsidemete moodustumist, mis tekitab stabiilsemaid ja dissotsiatsioonile vastupidavamaid agregaate. Uranüülioonid seevastu ei näidanud spetsiifilist sidumist Aβ-ga, millest järeldub, et need ioonid mõjutavad peptiide elektrostaatiliste interaktsioonide kaudu. Uranüülioonid näitasid tugevaimat sidumist pH-l 5,1 juures, mida võiks selgitada His-külgahelate segava toimega neutraalses pH alas ja uranüülioonide keemiliste omadustega, mis võivad madalal pH-l hüdrolüüsuda. Seetõttu võib monomeersete ja dimeersete hüdroksüülühendite ja uranüülioonide segu mõjutada seostumist. Nii Ni(II) kui ka uranüülioonid suutsid

indutseerida β-lehtstruktuuride moodustumist vesilahuses ja seeläbi stabiliseerida ja soodustada Aβ peptiidi agregatsiooni.

Kuigi Aβ peptiid on oluline huviobjekt, on palju teisi peptiide ja valke, mis on seotud AD-ga. Apolipoproteiin ApoE esineb kolmes isovormis, kus ApoE4 on peamine geneetiline riskitegur sporaadilise AD tekkes. On huvitav märkida, et ApoE4 kandjate puhul on näidatud, et nad on ka tundlikumad elavhõbeda toksilisusele. Seetõttu on välja pakutud, et ApoE valk võib osaleda elavhõbeda ja/või Aβ peptiidide väljutamises organismist ning et ApoE4 isoform võib olla vähem efektiivne selle ülesande täitmisel. Näitasime, et elavhõbe (Hg(II)) ioonide sidumisafiinsus on kõigi kolme ApoE isoformi puhul küllalt sarnane, kuid Hg(II) ioonide lisamisel on ApoE4 isoformi puhul täheldatav suurem struktuuri muutus. See viitab sellele, et erinevate isoformide vahelised järjestuse variatsioonid ei osale otseselt Hg(II) ioonide sidumises, kuid struktuuri indutseerimise erinevused võivad olla seotud ApoE4 suurema elavhõbedamürgituse riskiteguriga.

Käesolevas töös uuritud peptiidid/valgud on erinevad Aβ variandid, ApoE ja HSA. Erinevate metalliioonide ja valgu/peptiidi variantide vaheliste interaktsioonide iseloomustamiseks on kasutatud mitmesuguseid biofüüsikalisi meetodeid. Fookus on olnud sidumisafiinsuste määramisel, spetsiifiliste sidumiskohtade tuvastamisel ning metallide poolt põhjustatud mõjude jälgimisel valkude/peptiidide sekundaarstruktuurile ja agregatsioonile. Saadud tulemused laiendavad meie arusaama metalliioonide rollist AD patogeneesis, tuues esile spetsiifilised interaktsioonid, mis võivad mõjutada haiguse progresseerumist.

Appendix

Publication I

Berntsson, E., Sardis, M., Noormagi, A., Jarvet, J., Roos, P. M., Tougu, V., Graslund, A., Palumaa, P., & Warmlander, S. (2022). Mercury Ion Binding to Apolipoprotein E Variants ApoE2, ApoE3, and ApoE4: Similar Binding Affinities but Different Structure Induction Effects. ACS Omega, 7(33), 28924-28931. https://doi.org/10.1021/acsomega.2c02254

Mercury Ion Binding to Apolipoprotein E Variants ApoE2, ApoE3, and ApoE4: Similar Binding Affinities but Different Structure Induction Effects

Elina Berntsson,* Merlin Sardis, Andra Noormägi, Jüri Jarvet, Per M. Roos, Vello Tõugu, Astrid Gräslund, Peep Palumaa, and Sebastian K. T. S. Wärmländer*

Read Online

ACCESS | Metrics & More | Article Recommendations

ABSTRACT: Mercury intoxication typically produces more severe outcomes in people with the *APOE-ε4* gene, which codes for the ApoE4 variant of apolipoprotein E, compared to individuals with the *APOE-ε2* and *APOE-ε3* genes. Why the *APOE-ε4* allele is a risk factor in mercury exposure remains unknown. One proposed possibility is that the ApoE protein could be involved in clearing of heavy metals, where the ApoE4 protein might perform this task worse than the ApoE2 and ApoE3 variants. Here, we used fluorescence and circular dichroism spectroscopies to characterize the *in vitro* interactions of the three different ApoE variants with Hg(I) and Hg(II) ions. Hg(I) ions displayed weak binding to all ApoE variants and induced virtually no structural changes. Thus, Hg(I) ions appear to have no biologically relevant interactions with the ApoE protein. Hg(II) ions displayed stronger and very similar binding affinities for all three ApoE isoforms, with K_D values of 4.6 μM for ApoE2, 4.9 μM for ApoE3, and 4.3 μM for ApoE4. Binding of Hg(II) ions also induced changes in ApoE superhelicity, that is, altered coil−coil interactions, which might modify the protein function. As these structural changes were most pronounced in the ApoE4 protein, they could be related to the *APOE-ε4* gene being a risk factor in mercury toxicity.
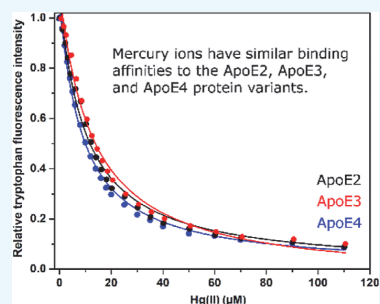
1. INTRODUCTION

Mercury (Hg) is a toxic metal that contributes to severe and permanent health problems and even death.[1−4] According to the Global Mercury Assessment 2018 report,[5] the estimated global anthropogenic emission of mercury to the atmosphere was approximately 20% higher in 2015 than in 2010. Most of these emissions originate from industrial activities related to mining and coal and oil combustion,[5] where Asia is responsible for 49% of the total emissions, followed by South America (18%) and Sub-Saharan Africa (16%). Hg is neurotoxic and genotoxic and induces damage to organs such as the brain and kidneys.[1,2,6] The different forms of Hg, that is, metallic, inorganic such as Hg(I), and Hg(II) ions, and organometallic complexes such as methyl-Hg and ethyl-Hg, have different properties and toxicity profiles.[1,2] Mercury vapor and organic Hg readily pass through membranes such as the blood−brain−barrier and the placental barrier, and thus become distributed throughout the entire human body including the fetus.[7−9] Developing neurites[10] and growing organs seem to be particularly susceptible to Hg damage, and Hg exposure is therefore especially harmful for children and fetuses.[11−15] The molecular mechanisms underlying Hg toxicity remain unclear,[16] but appear to include toxic molecular mimicry[8] and blocking of antioxidants[17] especially in the mitochondria.[18]

Interestingly, the susceptibility to Hg toxicity is influenced by genetic factors.[19,20] Notably, Hg exposure has been found to produce more severe outcomes in people with the *APOE-ε4* gene, which codes for the ApoE4 version of the apolipoprotein E protein, compared to individuals with the *APOE-ε2* and *APOE-ε3* genes.[6,12−14,19,21−23] *APOE-ε4* is also a genetic risk factor for Alzheimer's disease (AD)[21,24−29] and likely for other proteinopathies as well,[30,31] while Hg exposure might be an environmental risk factor for AD.[28,32−35] Why *APOE-ε4* carriers are more susceptible to both mercury intoxication and AD remains unclear. A number of possible explanations have been proposed,[28,36,37] including the possibility that the ApoE protein might be involved in the clearance of Hg and/or of amyloid-β (Aβ) peptides,[21,27,38] whose aggregation plays a central role in AD pathology.[39,40]

Figure 1. Primary structure of the apolipoprotein E3 protein. The ApoE2 (Cys112 and Cys158), ApoE3 (Cys112 and Arg158), and ApoE4 (Arg112 and Arg158) variants differ in positions 112 and 158, marked in red. The regions known to adopt α-helix conformations are shown in blue and green based on the information in Chen *et al.* 2011.[49]

Apolipoprotein E (ApoE) is a 299-residue-long (34 kDa) glycoprotein (Figure 1) involved in lipid metabolism: it transports lipid-soluble vitamins and lipids such as cholesterol in the central nervous system, into the lymph system, and then into the blood.[41−43] In the brain, ApoE is mainly produced by the astrocytes and microglial cells and interacts with ApoE receptors.[38,44] The three common variants of the ApoE protein differ at residues 112 and 158, that is, ApoE2 (Cys112 and Cys158), ApoE3 (Cys112 and Arg158), and ApoE4 (Arg112 and Arg158).[22,42] As the cysteine −SH groups are capable of binding metal ions including Hg ions,[35,45−47] it has been speculated that the ApoE residues Cys112 and Cys158 might bind Hg ions, which subsequently could be transported out from the tissue.[6,21,22,28,46,48] ApoE4 would then not be able to perform this task very well as it has Arg instead of Cys residues at positions 112 and 158 (Figure 1). Mercury would then accumulate in the tissues of *APOE-ε4* individuals, which would aggravate the toxic effects, which possibly could include Hg-induced neurodegeneration and AD.[6] To the best of our knowledge, no one has so far tested this hypothesis experimentally. Here, we use the biophysical techniques circular dichroism (CD) and fluorescence spectroscopy to study *in vitro* the binding interactions between inorganic Hg(I) and Hg(II) ions and the three different ApoE protein variants.

2. MATERIALS AND METHODS

2.1. Reagents and Sample Preparation. Lyophilized ApoE2, ApoE3, and ApoE4 protein variants were purchased from AlexoTech AB (Umeå, Sweden) and stored at −20 °C. All proteins were produced recombinantly with an additional methionine residue in position-1. The integrity of the proteins was confirmed by MALDI-TOF mass spectrometry. Before measurements, samples were dissolved in 10 mM NaOH (prepared in Milli-Q water) according to the manufacturer's instructions and then allowed to equilibrate at 4 °C for at least 1 h. The concentration was initially determined by weight and then confirmed by UV−vis spectroscopy. The samples were then diluted in either sodium phosphate buffer or MES [2-(*N*-morpholino)ethane sulfonic acid] buffer to a final buffer concentration of 20 mM at pH 7.3 or pH 5.5.

2.2. Fluorescence Spectroscopy. The binding affinities between Hg ions and ApoE variants were evaluated by fluorescence measurements using a LS-55 fluorescence spectrophotometer (PerkinElmer Inc., Waltham, MA, USA) equipped with a magnetic stirrer. In order to study both Hg(I) and Hg(II) ions, some measurements were carried out in the presence of 1 mM of the reducing agent TCEP [tris(2-carboxyethyl)phosphine], which reduces the Hg(II) ions from the HgCl₂ salt to the Hg(I) form. Small aliquots of HgCl₂

(stock concentrations of 1, 2, or 10 mM) were titrated to a sample containing either 0.2 or 1.0 μM ApoE protein in 20 mM MES buffer, pH 7.3 or 5.5, at 25 °C, in quartz cuvettes with a 5 mm path length. After each addition of HgCl₂, the solution was stirred for 30 s before recording fluorescence emission spectra at 350 nm (excitation 276 nm). All titrations were repeated 3 times. The measured tryptophan fluorescence intensities were plotted against the concentration of Hg ions, and dissociation constants (K_D) were evaluated by fitting the data curves to either eq 1 (the isotherm or hyperbolic equation together with a Hill coefficient)[50] or eq 2 (the Morrison equation)[51]

$$I = I_0 + \frac{(I_\infty - I_0) \cdot [\mathrm{Hg}]^n}{K_D^n + [\mathrm{Hg}]^n} \qquad (1)$$

$$I = I_0 + \frac{I_\infty - I_0}{2 \cdot [\mathrm{BS}]} \cdot \big((K_D + [\mathrm{Hg}] + [\mathrm{BS}]) \\ - \sqrt{(K_D + [\mathrm{Hg}] + [\mathrm{BS}])^2 - 4 \cdot [\mathrm{Hg}] \cdot [\mathrm{BS}]} \big) \qquad (2)$$

Here, I_0 is the initial fluorescence intensity with no added Hg ions, I_∞ is the steady-state intensity at the end of the titration, [Hg] is the concentration of the added Hg ions, K_D is the dissociation constant, n (in eq 1) is the Hill coefficient, and [BS] (in eq 2) is the concentration of the binding sites, which is equal to the protein concentration if the protein has a single binding site. Adding a term for the fluorescence quenching effect of free Hg ions appeared unnecessary.[52]

2.3. CD Spectroscopy. CD spectra were recorded between 190 and 260 nm with a step size of 0.5 nm and 5 s per data point at 20 °C using a Chirascan CD spectrometer from Applied Photophysics, UK. Samples of 5 μM ApoE protein in 20 mM sodium phosphate buffer, pH 7.3, were measured in a quartz cuvette with an optical path length of 2 mm. Sodium phosphate buffer was used to avoid the interference of MES buffer with the CD measurements. In order to study both Hg(I) and Hg(II) ions, some measurements were carried out in the presence of 1 mM of the reducing agent TCEP, which reduces the Hg(II) ions from the HgCl₂ salt to the Hg(I) form. After the initial measurement of ApoE alone, 1−2 μL HgCl₂ was added in steps from stock concentrations of 1, 2, or 10 mM to produce final HgCl₂ concentrations of 2, 5, 40, and 80 μM. All titrations were repeated two or three times.

3. RESULTS AND DISCUSSION

3.1. Fluorescence Spectroscopy. To determine the binding strength of Hg(I) and Hg(II) ions to the ApoE isoforms, the quenching effect of the ions on the intrinsic tryptophan fluorescence was monitored. ApoE contains seven
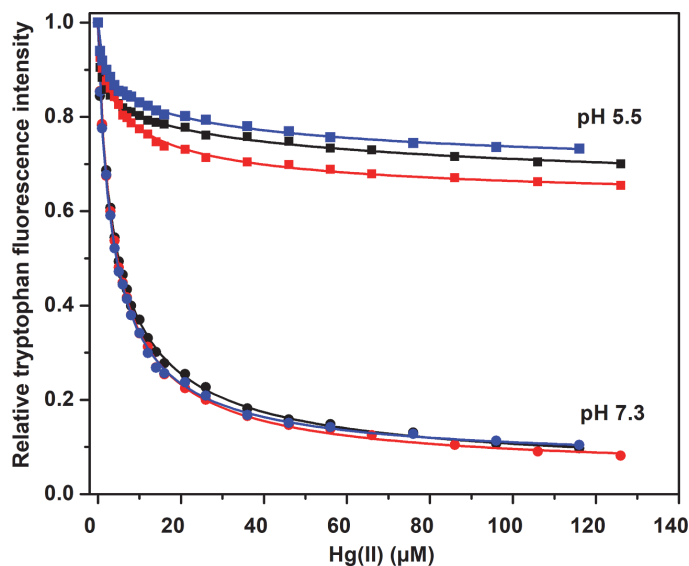
Figure 2. Intrinsic ApoE tryptophan fluorescence upon titration with HgCl$_2$ recorded at 350 nm (excitation 276 nm) for 0.2 μM ApoE protein at +25 °C in 20 mM MES buffer either at pH 7.3 or pH 5.5. Black—ApoE2; red—ApoE3; blue—ApoE4; circles—pH 7.3; and squares—pH 5.5. Fitting eq 1 to the titration data produces apparent dissociation constants (K_D^{app}).

tryptophan residues (Figure 1), which exhibit a strong fluorescence signal at 350 nm when excited around 276 nm.

Titrating HgCl$_2$ to 0.2 μM protein samples at either pH 7.3 or pH 5.5 produced the binding curves shown in Figure 2. Fitting eq 1 to the pH 7.3 curves yielded the dissociation constants (K_D) for Hg(II) binding shown in Table 1, that is,

Table 1. Apparent K_D Values (K_D^{app}) in μM for the ApoE·Hg(II) Complex Obtained by Fitting Eq 1 to the pH 7.3 Fluorescence Titration Curves Shown in Figure 2

	titration 1	titration 2	titration 3	average K_D
ApoE2	4.54 ± 0.29	4.33 ± 0.36	5.00 ± 0.44	4.62
ApoE3	4.65 ± 0.32	5.11 ± 0.27	4.90 ± 0.22	4.89
ApoE4	4.33 ± 0.35	4.33 ± 0.42	4.29 ± 0.23	4.32

on average 4.62 μM for ApoE2, 4.89 μM for ApoE3, and 4.32 μM for ApoE4. The Hill coefficients (n in eq 1) were all found to be around 1, indicating little or no binding cooperativity. The hyperbolic equation (i.e., eq 1) was used as the protein concentration clearly was lower than the binding affinity of the studied complex. Even though MES is a good buffer devised to have minimal interactions with metal ions and other cations,[53] no corrections were made for potential interactions between the buffer and the Hg(II) ions. Thus, the calculated K_D values in Table 1 should be considered as apparent, that is, K_D^{app}. The most important thing about these K_D^{app} values is that they (and the corresponding binding curves) are all very similar. We therefore conclude that the Hg(II) ions are bound by the same (or at least very similar) binding sites in all three ApoE variants and that these binding sites do not involve as binding ligands the residues 112 and 158, which vary between the protein isoforms (Figure 1).

These conclusions clearly contradict the previously suggested hypothesis that different binding affinities to

mercury ions could explain why the *APOE-ε4* gene is a risk factor in Hg intoxication but not the *APOE-ε2* and *APOE-ε3* genes.[6,21,22,28,46,48] However, it cannot be ruled out that other forms of mercury, such as organic methyl-Hg or ethyl-Hg, could display different binding properties to the different ApoE variants. Future studies might investigate the details of ApoE binding to other forms of Hg than the inorganic ions studied here.

The HgCl$_2$ titrations at pH 5.5 produced a much lower reduction in Trp fluorescence intensity than the titrations at pH 7.3 (Figure 2). This strongly indicates weaker binding of Hg(II) ions at acidic pH, even though no K_D values could be derived from these curves. The main difference in the proteins between pH 7.3 and pH 5.5 is protonation of His residues, which have pK_a values around 6.5.[54] As His residues are previously known to bind a range of metal ions, including Hg(II) ions,[32] and as protonation of His residues lowers their affinity for positively charged molecules, the different titration results at pH 7.3 and pH 5.5 shown in Figure 2 strongly suggest that His residues are involved in coordinating the Hg(II) ions. As shown in Figure 1, the ApoE proteins have two His residues, that is, His140 and His299.

Titrations with HgCl$_2$ at pH 7.3 were also carried out at a slightly higher protein concentration, that is, 1.0 μM (Figure 3). As the protein concentration is now close to the binding affinity, it is not appropriate to fit the binding curves with the hyperbolic/isotherm eq 1. The data was instead fitted with eq 2, where the binding site concentration is included as one of the fitted parameters. For the Hg(II) ion titrations, eq 2 produced average K_D values around 4.2 (ApoE2), 4.1 (ApoE3), and 4.8 (ApoE4). These K_D values are very close to those obtained at 0.2 μM ApoE concentration (Figure 2 and Table 1), thus confirming their accuracy. The fittings to eq 2 also produced binding site concentrations around 10 μM, for all three proteins. Although this should be regarded as an
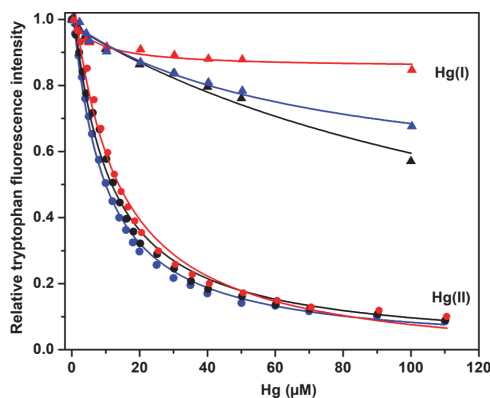
Figure 3. Intrinsic ApoE tryptophan fluorescence upon titration with HgCl$_2$ recorded at 350 nm (excitation 276 nm) for 1 μM ApoE protein in 20 mM MES buffer, pH 7.3 at +25 °C. Black—ApoE2; red—ApoE3; blue—ApoE4; circles—Hg(II) ions; and triangles—Hg(I) ions (1 mM TCEP added). Fitting eq 2 to the titration data produces apparent dissociation constants (K_D^{app}).

approximate number, it is clearly larger than the protein concentration of 1 μM. This indicates that there are multiple binding sites for Hg(II) ions on all three ApoE variants.

Adding 1 mM of the reducing agent TCEP reduces the Hg ions to their monovalent Hg(I) state. As shown in Figure 3, titrations with Hg(I) ions yield much lower Trp fluorescence reduction than titrations with Hg(II) ions for all three ApoE variants. It was not possible to fit a binding equation to the Hg(I) data, but the binding of Hg(I) ions appears to be weak—likely in the millimolar range. It is however possible that Hg(I) ions may not quench Trp fluorescence as efficiently as Hg(II) ions, and the Hg(I) titration results should therefore be interpreted with caution.

3.2. CD Spectroscopy. ApoE is previously known to be a mainly α-helical protein in aqueous solutions.[49,55] This was confirmed by our CD measurements, where all three ApoE variants exhibit CD spectra with characteristic minima around 208 and 222 nm (Figure 4), which are typical for α-helical secondary structures.[55] Upon titration with Hg(II) ions, the CD spectra gradually lost some intensity, although they generally maintained α-helical shapes. These changes cannot be explained by dilution of the sample, as the total increase in volume during the titrations did not exceed 2%.

When titrated with Hg(II) ions, the three ApoE variants showed different intensity losses for the 208 and 222 nm minima (Figure 4 and Table 2). The $[\theta_{222}]/[\theta_{208}]$ ratio in CD spectra has previously been shown to reflect hydrophobic coil—coil interactions of α-helical secondary structures, also known as α-helical supercoiling or simply superhelicity.[56−58] The largest increase in the $[\theta_{222}]/[\theta_{208}]$ ratio, indicative of increased helix supercoiling upon addition of Hg(II) ions, is observed for the ApoE4 variant, which changes from 0.96 to 1.16 (Table 2). ApoE2 displays the smallest change, from 0.93 to 0.98, while ApoE3 increases from 0.99 to 1.13 (Table 2). A careful investigation of the ApoE4 CD spectra furthermore shows that the minima display small but clear changes during the titration: in the presence of 80 μM Hg(II) ions, the minima have moved from, respectively, 208.5 to 209.5 nm and from 221 to 222.5 nm (Figure 4(C1)), which is a further indication

of secondary structure alterations. All three repetitions of this titration gave the same results. For the ApoE2 variant, no such shifts were observed (Figure 4(A1)). These changes are in line with our previous observations that metal ions can promote protein supercoiling,[59] and also with earlier reports that Hg(II) ions can generally affect protein folding, misfolding, and aggregation.[60−62] A previous study showed that the ApoE C-terminal domain, which contains lipoprotein binding and ApoE self-association sites, has an intrinsic propensity to form coil-coiled interactions stabilized by salt bridges.[63] Thus, it is possible that the observed Hg(II)-induced structural changes take place in the C-terminal domain. Future research should be able to identify the exact location(s) of the Hg(II) binding site(s), the nature of the structural changes, and if binding of Hg(II) ions affects the protein's function(s).

Titrations with monovalent Hg(I) ions, that is, with 1 mM TCEP reducing agent added to the samples, produced much smaller changes in the CD spectra (Figure 4), indicating weaker ApoE binding affinity for Hg(I) ions than for Hg(II) ions. These results are in line with those from the fluorescence measurements (Figure 4), where Hg(I) ions for all three ApoE variants produced much weaker Trp fluorescence reduction than Hg(II) ions. However, it cannot be ruled out that the monovalent Hg(I) ions might have different binding sites and/or different binding configurations than Hg(II) ions and may therefore not induce the same structural changes as Hg(II) ions. Overall though, it appears that the Hg(I) interactions with ApoE proteins are weak and of little biological relevance. As 1 mM TCEP roughly corresponds to the reducing environment inside human cells, our results suggest that biologically relevant interactions between inorganic Hg ions and ApoE proteins will not take place intracellularly, but rather in the oxidizing extracellular environment, where the Hg ions are in their divalent Hg(II) state.

It should be noted that already before addition of the HgCl$_2$ salt, there are slight differences in the CD spectra and in superhelicity between the three ApoE variants (Figure 4 and Table 2), indicating different secondary structures. It has previously been suggested that the ApoE variants could exhibit different secondary structures due to the mutations in positions 112 and 158. Specifically, it has been proposed that the N- and C-termini would be positioned closer to each other in ApoE4, than in ApoE2 and ApoE3, due to the interaction between Arg61 and Glu255 in ApoE4.[64,65] Such an interaction is considered unlikely in ApoE2 and ApoE3, where the Arg61 residue is believed to interact with Cys112 and therefore be unavailable for interactions with Glu255. Given the different initial structures, it is not surprising that addition of Hg(II) ions appears to induce somewhat different structural alterations in the three variants.

4. CONCLUSIONS

Hg(II) ions bind all three ApoE variants with approximately the same binding affinity, around 4−5 μM (Figure 2 and Table 1). This indicates similar binding sites with similar binding ligands in all protein variants. The residues that differ between the variants, that is, Cys112 residues in ApoE2 and ApoE3 and Cys158 in ApoE2, are therefore most likely not directly involved in Hg(II) coordination. Instead, the weaker binding to Hg(II) ions at acidic pH (Figure 2), where histidines are protonated, suggests that the His140 and His299 residues could be involved as Hg(II) binding ligands. Hg(II) binding was found to be non-cooperative, with Hill coefficients around
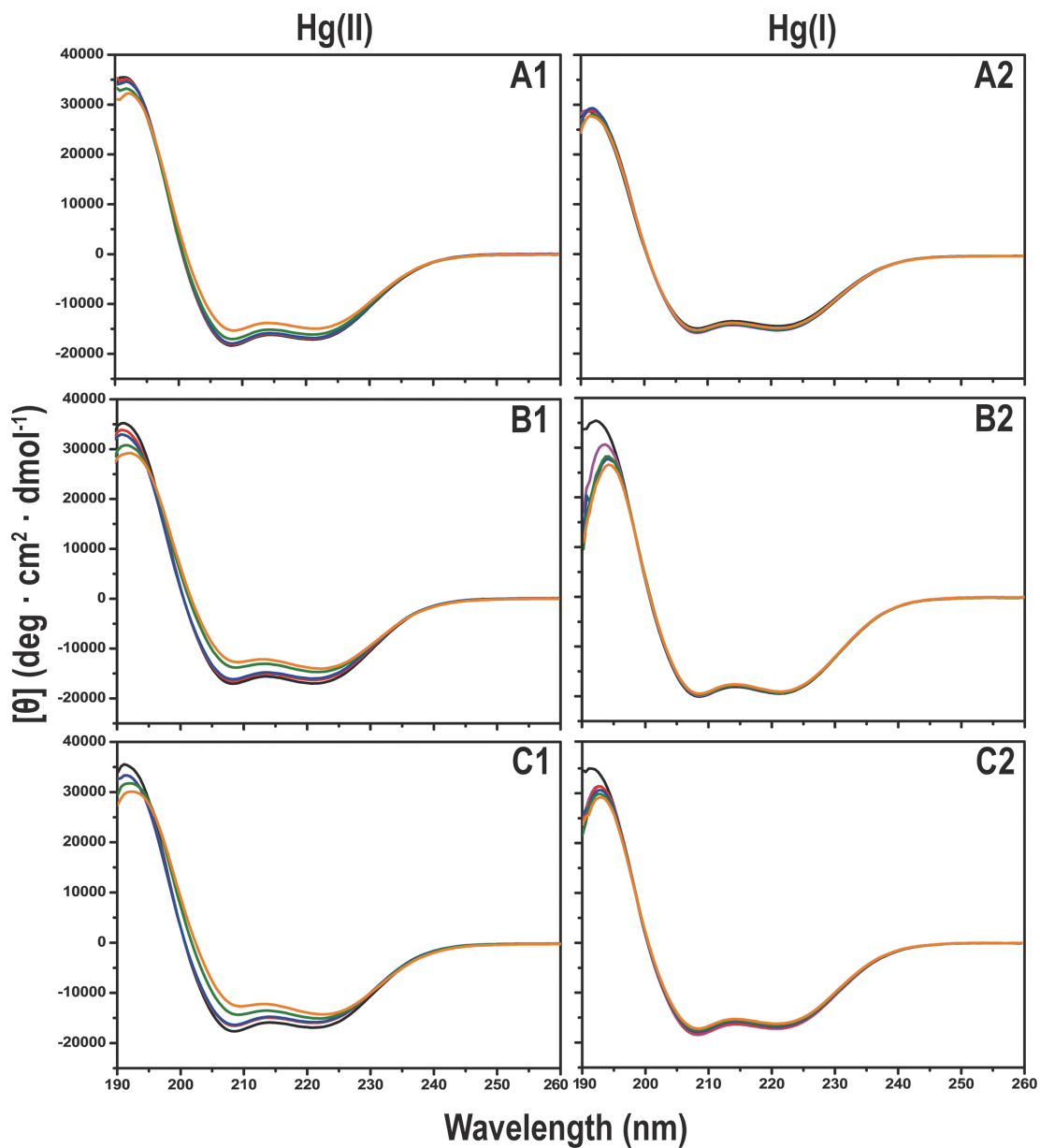
Figure 4. CD spectra showing titrations of 5 μM ApoE protein with HgCl$_2$ in 20 mM sodium phosphate buffer, pH 7.3 at 20 °C. Row A: ApoE2; row B: ApoE3; and row C: ApoE4; column 1: Hg(II) ions and column 2: Hg(I) ions (1 mM TCEP added, pink). HgCl$_2$ was added in steps of 0 μM (black), 2 μM (red), 5 μM (blue), 40 μM (green), and 80 μM (orange).

1, and multiple binding sites are likely present. Monovalent Hg(I) ions display much weaker binding affinities to all three ApoE variants, likely in the millimolar region (Figure 3), and induce virtually no change in the ApoE secondary structure (Figure 4). It therefore appears that the ApoE proteins do not have biologically relevant interactions with Hg(I) ions, which exist in reducing intracellular environments, but rather with Hg(II) ions, which exist in oxidizing extracellular environ-

ments. Bound Hg(II) ions induce minor but distinct structural alterations in all ApoE protein variants, interpreted as increased superhelicity and possibly located to the C-terminal domain, which contains lipoprotein binding and ApoE self-association sites and which has an intrinsic propensity to form coil-coiled interactions. The structural alterations are most pronounced in ApoE4 and least pronounced in ApoE2 (Figure 4). Thus, while the Hg(II) binding affinity is virtually the same for the three

Table 2. Negative CD Signal Intensities $[\theta \times 10^{-3}]$ at 208 and 222 nm together with the Calculated $[\theta_{222}]/[\theta_{208}]$ Ratios Derived from the CD Spectra Shown in Figure 3

Hg(II) (μM)	ApoE2					ApoE3					ApoE4				
	0	2	5	40	80	0	2	5	40	80	0	2	5	40	80
θ at 208 nm	18.4	18.1	17.9	17.0	15.2	17.3	16.6	16.2	13.7	12.6	17.6	16.5	16.3	14.2	12.3
θ at 222 nm	17.0	16.8	16.8	16.0	14.9	17.1	16.4	16.2	14.9	14.2	16.8	15.9	15.7	15.0	14.2
$[\theta_{222}]/[\theta_{208}]$	0.93	0.93	0.94	0.94	0.98	0.99	0.99	1.0	1.08	1.13	0.96	0.96	0.96	1.06	1.16

ApoE variants, the differences in structure induction between the three ApoE variants might conceivably be connected to the *APOE-ε4* gene being a risk factor in mercury intoxication but not the *APOE-ε2* and *APOE-ε3* genes. Future studies should clarify the binding sites for Hg(II) ions in the ApoE protein, the nature of the structural changes induced by the Hg(II) ions, and how these changes may affect the protein's function(s).

■ AUTHOR INFORMATION

Corresponding Authors

Elina Berntsson − *Department of Chemistry and Biotechnology, Tallinn University of Technology, 12618 Tallinn, Estonia; Department of Biochemistry and Biophysics, Stockholm University, 106 91 Stockholm, Sweden;* ● orcid.org/0000-0002-7544-092X; Email: elina.berntsson@dbb.su.se

Sebastian K. T. S. Wärmländer − *Department of Biochemistry and Biophysics, Stockholm University, 106 91 Stockholm, Sweden; CellPept Sweden AB, 118 47 Stockholm, Sweden;* Phone: +46 8 162444; Email: seb@student.su.se

Authors

Merlin Sardis − *Department of Chemistry and Biotechnology, Tallinn University of Technology, 12618 Tallinn, Estonia*

Andra Noormägi − *Department of Chemistry and Biotechnology, Tallinn University of Technology, 12618 Tallinn, Estonia*

Jüri Jarvet − *Department of Biochemistry and Biophysics, Stockholm University, 106 91 Stockholm, Sweden; The National Institute of Chemical Physics and Biophysics, 12618 Tallinn, Estonia; CellPept Sweden AB, 118 47 Stockholm, Sweden;* ● orcid.org/0000-0002-7863-1887

Per M. Roos − *Institute of Environmental Medicine, Karolinska Institutet, 171 77 Stockholm, Sweden; Department of Clinical Physiology, Capio Saint Göran Hospital, 112 19 Stockholm, Sweden*

Vello Tõugu − *Department of Chemistry and Biotechnology, Tallinn University of Technology, 12618 Tallinn, Estonia*

Astrid Gräslund − *Department of Biochemistry and Biophysics, Stockholm University, 106 91 Stockholm, Sweden; CellPept Sweden AB, 118 47 Stockholm, Sweden*

Peep Palumaa − *Department of Chemistry and Biotechnology, Tallinn University of Technology, 12618 Tallinn, Estonia;* ● orcid.org/0000-0002-3505-3466

Complete contact information is available at:
https://pubs.acs.org/10.1021/acsomega.2c02254

Notes

The authors declare no competing financial interest.

■ REFERENCES

(1) Rice, K. M.; Walker, E. M., Jr.; Wu, M.; Gillette, C.; Blough, E. R. Environmental mercury and its toxic effects. *J. Prev. Med. Public Health* **2014**, *47*, 74−83.

(2) Bernhoft, R. A. Mercury toxicity and treatment: a review of the literature. *J. Environ. Public Health* **2012**, *2012*, 460508.

(3) Nierenberg, D. W.; Nordgren, R. E.; Chang, M. B.; Siegler, R. W.; Blayney, M. B.; Hochberg, F.; Toribara, T. Y.; Cernichiari, E.; Clarkson, T. Delayed cerebellar disease and death after accidental exposure to dimethylmercury. *N. Engl. J. Med.* **1998**, *338*, 1672−1676.

(4) Nordberg, G. F.; Fowler, B. A.; Nordberg, M. *Handbook on the Toxicology of Metals*, 4th ed.; Academic Press: London, U.K., 2015.

(5) UNEP. Global Mercury Assessment 2018. 2019, https://www.unep.org/resources/publication/global-mercury-assessment-2018. Accessed 2020-12-08.

(6) Arrifano, G. P. F.; Martín-Doimeadios, R. C. R.; Jiménez-Moreno, M.; Fernández-Trujillo, S.; Augusto-Oliveira, M.; Souza-Monteiro, J. R.; Macchi, B. M.; Alvarez-Leite, J. I.; do Nascimento, J. L. M.; Amador, M. T.; Santos, S.; Ribeiro-dos-Santos, A.; Silva-Pereira, L. C.; Oriá, R. B.; Crespo-Lopez, M. E. Genetic Susceptibility to Neurodegeneration in Amazon: Apolipoprotein E Genotyping in Vulnerable Populations Exposed to Mercury. *Front. Genet.* **2018**, *9*, 285.

(7) Aschner, M.; Aschner, J. L. Mercury neurotoxicity: mechanisms of blood-brain barrier transport. *Neurosci. Biobehav. Rev.* **1990**, *14*, 169−176.

(8) Bridges, C. C.; Zalups, R. K. Molecular and ionic mimicry and the transport of toxic metals. *Toxicol. Appl. Pharmacol.* **2005**, *204*, 274−308.

(9) Kerper, L. E.; Ballatori, N.; Clarkson, T. W. Methylmercury transport across the blood-brain barrier by an amino acid carrier. *Am. J. Physiol.* **1992**, *262*, R761−R765.

(10) Leong, C. C.; Syed, N. I.; Lorscheider, F. L. Retrograde degeneration of neurite membrane structural integrity of nerve growth cones following in vitro exposure to mercury. *Neuroreport* **2001**, *12*, 733−737.

(11) Bose-O'Reilly, S.; McCarty, K. M.; Steckling, N.; Lettmeier, B. Mercury exposure and children's health. *Curr. Probl. Pediatr. Adolesc. Health Care* **2010**, *40*, 186−215.

(12) Ng, S.; Lin, C. C.; Jeng, S. F.; Hwang, Y. H.; Hsieh, W. S.; Chen, P. C. Mercury, APOE, and child behavior. *Chemosphere* **2015**, *120*, 123−130.

(13) Ng, S.; Lin, C.-C.; Hwang, Y.-H.; Hsieh, W.-S.; Liao, H.-F.; Chen, P.-C. Mercury, APOE, and children's neurodevelopment. *Neurotoxicology* **2013**, *37*, 85−92.

(14) Snoj Tratnik, J.; Falnoga, I.; Trdin, A.; Mazej, D.; Fajon, V.; Miklavčič, A.; Kobal, A. B.; Osredkar, J.; Sešek Briški, A.; Krsnik, M.; Neubauer, D.; Kodrič, J.; Stropnik, S.; Gosar, D.; Lešnik Musek, P.; Marc, J.; Jurkovič Mlakar, S.; Petrović, O.; Vlašić-Cicvarić, I.; Prpić, I.; Milardović, A.; Radić Nišević, J.; Vuković, D.; Fišić, E.; Špirić, Z.; Horvat, M. Prenatal mercury exposure, neurodevelopment and

apolipoprotein E genetic polymorphism. *Environ. Res.* **2017**, *152*, 375−385.

(15) Grandjean, P.; Pichery, C.; Bellanger, M.; Budtz-Jørgensen, E. Calculation of mercury's effects on neurodevelopment. *Environ. Health Perspect.* **2012**, *120*, A452 ; author reply A452.

(16) Clarkson, T. W. Mercury. *J. Am. Coll. Toxicol.* **1989**, *8*, 1291−1295.

(17) Suzuki, K. T.; Sasakura, C.; Yoneda, S. Binding sites for the (Hg-Se) complex on selenoprotein P. *Biochim. Biophys. Acta* **1998**, *1429*, 102−112.

(18) Carocci, A.; Rovito, N.; Sinicropi, M. S.; Genchi, G. Mercury toxicity and neurodegenerative effects. *Rev. Environ. Contam. Toxicol.* **2014**, *229*, 1−18.

(19) Andreoli, V.; Sprovieri, F. Genetic Aspects of Susceptibility to Mercury Toxicity: An Overview. *Int. J. Environ. Res. Public Health* **2017**, *14*, 93.

(20) Woods, J. S.; Heyer, N. J.; Russo, J. E.; Martin, M. D.; Farin, F. M. Genetic polymorphisms affecting susceptibility to mercury neurotoxicity in children: summary findings from the Casa Pia Children's Amalgam clinical trial. *Neurotoxicology* **2014**, *44*, 288−302.

(21) Godfrey, M. E.; Wojcik, D. P.; Krone, C. A. Apolipoprotein E genotyping as a potential biomarker for mercury neurotoxicity. *J. Alzheimer's Dis.* **2003**, *5*, 189−195.

(22) Arrifano, G. P. F.; de Oliveira, M. A.; Souza-Monteiro, J. R.; Paraense, R. O.; Ribeiro-Dos-Santos, A.; Vieira, J.; Silva, A.; Macchi, B. M.; do Nascimento, J. L. M.; Burbano, R. M. R.; Crespo-Lopez, M. E. Role for apolipoprotein E in neurodegeneration and mercury intoxication. *Front. Biosci., Elite Ed.* **2018**, *10*, 229−241.

(23) Wojcik, D. P.; Godfrey, M. E.; Christie, D.; Haley, B. E. Mercury toxicity presenting as chronic fatigue, memory impairment and depression: diagnosis, treatment, susceptibility, and outcomes in a New Zealand general practice setting (1994-2006). *Neuroendocrinol. Lett.* **2006**, *27*, 415−423.

(24) Farrer, L. A.; Cupples, L. A.; Haines, J. L.; Hyman, B.; Kukull, W. A.; Mayeux, R.; Myers, R. H.; Pericak-Vance, M. A.; Risch, N.; van Duijn, C. M. Effects of age, sex, and ethnicity on the association between apolipoprotein E genotype and Alzheimer disease. A meta-analysis. APOE and Alzheimer Disease Meta Analysis Consortium. *J. Am. Med. Assoc.* **1997**, *278*, 1349−1356.

(25) Manelli, A. M.; Bulfinch, L. C.; Sullivan, P. M.; LaDu, M. J. Aβ42 neurotoxicity in primary co-cultures: effect of apoE isoform and Abeta conformation. *Neurobiol. Aging* **2007**, *28*, 1139−1147.

(26) Corder, E. H.; Saunders, A. M.; Strittmatter, W. J.; Schmechel, D. E.; Gaskell, P. C.; Small, G. W.; Roses, A. D.; Haines, J. L.; Pericak-Vance, M. A. Gene dose of apolipoprotein E type 4 allele and the risk of Alzheimer's disease in late onset families. *Science* **1993**, *261*, 921−923.

(27) Miyata, M.; Smith, J. D. Apolipoprotein E allele-specific antioxidant activity and effects on cytotoxicity by oxidative insults and beta-amyloid peptides. *Nat. Genet.* **1996**, *14*, 55−61.

(28) Mutter, J.; Naumann, J.; Sadaghiani, C.; Schneider, R.; Walach, H. Alzheimer disease: mercury as pathogenetic factor and apolipoprotein E as a moderator. *Neuroendocrinol. Lett.* **2004**, *25*, 331−339.

(29) Kim, J.; Basak, J. M.; Holtzman, D. M. The role of apolipoprotein E in Alzheimer's disease. *Neuron* **2009**, *63*, 287−303.

(30) Rodriguez-Vieitez, E.; Nielsen, H. M. Associations Between APOE Variants, Tau and α-Synuclein. *Adv. Exp. Med. Biol.* **2019**, *1184*, 177−186.

(31) Shi, Y.; Yamada, K.; Liddelow, S. A.; Smith, S. T.; Zhao, L.; Luo, W.; Tsai, R. M.; Spina, S.; Grinberg, L. T.; Rojas, J. C.; Gallardo, G.; Wang, K.; Roh, J.; Robinson, G.; Finn, M. B.; Jiang, H.; Sullivan, P. M.; Baufeld, C.; Wood, M. W.; Sutphen, C.; McCue, L.; Xiong, C.; Del-Aguila, J. L.; Morris, J. C.; Cruchaga, C.; Fagan, A. M.; Miller, B. L.; Boxer, A. L.; Seeley, W. W.; Butovsky, O.; Barres, B. A.; Paul, S. M.; Holtzman, D. M. ApoE4 markedly exacerbates tau-mediated neurodegeneration in a mouse model of tauopathy. *Nature* **2017**, *549*, 523−527.

(32) Wallin, C.; Friedemann, M.; Sholts, S. B.; Noormägi, A.; Svantesson, T.; Jarvet, J.; Roos, P. M.; Palumaa, P.; Gräslund, A.; Wärmländer, S. K. T. S. Mercury and Alzheimer's Disease: Hg(II) Ions Display Specific Binding to the Amyloid-β Peptide and Hinder Its Fibrillization. *Biomolecules* **2019**, *10*, 44.

(33) Mutter, J.; Curth, A.; Naumann, J.; Deth, R.; Walach, H. Does inorganic mercury play a role in Alzheimer's disease? A systematic review and an integrated molecular mechanism. *J. Alzheimer's Dis.* **2010**, *22*, 357−374.

(34) Bjørklund, G.; Tinkov, A. A.; Dadar, M.; Rahman, M. M.; Chirumbolo, S.; Skalny, A. V.; Skalnaya, M. G.; Haley, B. E.; Ajsuvakova, O. P.; Aaseth, J. Insights into the Potential Role of Mercury in Alzheimer's Disease. *J. Mol. Neurosci.* **2019**, *67*, 511−533.

(35) Rooney, J. P. The role of thiols, dithiols, nutritional factors and interacting ligands in the toxicology of mercury. *Toxicology* **2007**, *234*, 145−156.

(36) Luo, J.; Maréchal, J. D.; Wärmländer, S.; Gräslund, A.; Perálvarez-Marín, A. In silico analysis of the apolipoprotein E and the amyloid beta peptide interaction: misfolding induced by frustration of the salt bridge network. *PLoS Comput. Biol.* **2010**, *6*, No. e1000663.

(37) Morris, M. C.; Brockman, J.; Schneider, J. A.; Wang, Y.; Bennett, D. A.; Tangney, C. C.; van de Rest, O. Association of Seafood Consumption, Brain Mercury Level, and APOE epsilon4 Status With Brain Neuropathology in Older Adults. *J. Am. Med. Assoc.* **2016**, *315*, 489−497.

(38) Lin, Y. T.; Seo, J.; Gao, F.; Feldman, H. M.; Wen, H. L.; Penney, J.; Cam, H. P.; Gjoneska, E.; Raja, W. K.; Cheng, J.; Rueda, R.; Kritskiy, O.; Abdurrob, F.; Peng, Z.; Milo, B.; Yu, C. J.; Elmsaouri, S.; Dey, D.; Ko, T.; Yankner, B. A.; Tsai, L. H. APOE4 Causes Widespread Molecular and Cellular Alterations Associated with Alzheimer's Disease Phenotypes in Human iPSC-Derived Brain Cell Types. *Neuron* **2018**, *98*, 1294.

(39) Lee, S. J.; Nam, E.; Lee, H. J.; Savelieff, M. G.; Lim, M. H. Towards an understanding of amyloid-β oligomers: characterization, toxicity mechanisms, and inhibitors. *Chem. Soc. Rev.* **2017**, *46*, 310−323.

(40) Selkoe, D. J.; Hardy, J. The amyloid hypothesis of Alzheimer's disease at 25 years. *EMBO Mol. Med.* **2016**, *8*, 595−608.

(41) Pitas, R. E.; Ji, Z. S.; Weisgraber, K. H.; Mahley, R. W. Role of apolipoprotein E in modulating neurite outgrowth: potential effect of intracellular apolipoprotein E. *Biochem. Soc. Trans.* **1998**, *26*, 257−261.

(42) Jeong, W.; Lee, H.; Cho, S.; Seo, J. ApoE4-Induced Cholesterol Dysregulation and Its Brain Cell Type-Specific Implications in the Pathogenesis of Alzheimer's Disease. *Mol. Cells* **2019**, *42*, 739−746.

(43) Bu, G. Apolipoprotein E and its receptors in Alzheimer's disease: pathways, pathogenesis and therapy. *Nat. Rev. Neurosci.* **2009**, *10*, 333−344.

(44) Pitas, R. E.; Boyles, J. K.; Lee, S. H.; Foss, D.; Mahley, R. W. Astrocytes synthesize apolipoprotein E and metabolize apolipoprotein E-containing lipoproteins. *Biochim. Biophys. Acta* **1987**, *917*, 148−161.

(45) Ajsuvakova, O. P.; Tinkov, A. A.; Aschner, M.; Rocha, J. B. T.; Michalke, B.; Skalnaya, M. G.; Skalny, A. V.; Butnariu, M.; Dadar, M.; Sarac, I.; Aaseth, J.; Bjørklund, G. Sulfhydryl groups as targets of mercury toxicity. *Coord. Chem. Rev.* **2020**, *417*, 213343.

(46) Giles, N. M.; Watts, A. B.; Giles, G. I.; Fry, F. H.; Littlechild, J. A.; Jacob, C. Metal and redox modulation of cysteine protein function. *Chem. Biol.* **2003**, *10*, 677−693.

(47) Mesterházy, E.; Lebrun, C.; Crouzy, S.; Jancsó, A.; Delangle, P. Short oligopeptides with three cysteine residues as models of sulphur-rich Cu(i)- and Hg(ii)-binding sites in proteins. *Metallomics* **2018**, *10*, 1232−1244.

(48) Mejáre, M.; Bülow, L. Metal-binding proteins and peptides in bioremediation and phytoremediation of heavy metals. *Trends Biotechnol.* **2001**, *19*, 67−73.

(49) Chen, J.; Li, Q.; Wang, J. Topology of human apolipoprotein E3 uniquely regulates its diverse biological functions. *Proc. Natl. Acad. Sci. U.S.A.* **2011**, *108*, 14813−14818.

(50) Prinz, H. Hill coefficients, dose-response curves and allosteric mechanisms. *J. Chem. Biol.* **2010**, *3*, 37−44.

(51) Kuzmic, P. *History, Variants and Usage of the "Morrison Equation" in Enzyme Inhibition Kinetics*; BioKin Technical Note TN-2015-01 [Online], 2015. www.biokin.com/TN/2015/01.

(52) Lindgren, J.; Segerfeldt, P.; Sholts, S. B.; Gräslund, A.; Karlström, A. E.; Wärmländer, S. K. Engineered non-fluorescent Affibody molecules facilitate studies of the amyloid-beta (Abeta) peptide in monomeric form: low pH was found to reduce Abeta/Cu(II) binding affinity. *J. Inorg. Biochem.* **2013**, *120*, 18−23.

(53) Good, N. E.; Winget, G. D.; Winter, W.; Connolly, T. N.; Izawa, S.; Singh, R. M. Hydrogen ion buffers for biological research. *Biochemistry* **1966**, *5*, 467−477.

(54) Pogostin, B. H.; Malmendal, A.; Londergan, C. H.; Åkerfeldt, K. S. pKa Determination of a Histidine Residue in a Short Peptide Using Raman Spectroscopy. *Molecules* **2019**, *24*, 405.

(55) Georgiadou, D.; Chroni, A.; Drosatos, K.; Kypreos, K. E.; Zannis, V. I.; Stratikos, E. Allele-dependent thermodynamic and structural perturbations in ApoE variants associated with the correction of dyslipidemia and formation of spherical ApoE-containing HDL particles. *Atherosclerosis* **2013**, *226*, 385−391.

(56) Lau, S. Y.; Taneja, A. K.; Hodges, R. S. Synthesis of a model protein of defined secondary and quaternary structure. Effect of chain length on the stabilization and formation of two-stranded alpha-helical coiled-coils. *J. Biol. Chem.* **1984**, *259*, 13253−13261.

(57) Zhou, N. E.; Kay, C. M.; Hodges, R. S. Synthetic model proteins: the relative contribution of leucine residues at the nonequivalent positions of the 3-4 hydrophobic repeat to the stability of the two-stranded alpha-helical coiled-coil. *Biochemistry* **1992**, *31*, 5739−5746.

(58) Zhou, N. E.; Kay, C. M.; Hodges, R. S. Synthetic model proteins. Positional effects of interchain hydrophobic interactions on stability of two-stranded alpha-helical coiled-coils. *J. Biol. Chem.* **1992**, *267*, 2664−2670.

(59) Tiiman, A.; Luo, J.; Wallin, C.; Olsson, L.; Lindgren, J.; Jarvet, J.; Per, P. M.; Sholts, S. B.; Rahimipour, S.; Abrahams, J. P.; Karlström, A. E.; Gräslund, A.; Wärmländer, S. K. T. S. Specific Binding of Cu(II) Ions to Amyloid-Beta Peptides Bound to Aggregation-Inhibiting Molecules or SDS Micelles Creates Complexes that Generate Radical Oxygen Species. *J. Alzheimer's Dis.* **2016**, *54*, 971−982.

(60) Arnhold, F.; Gührs, K. H.; von Mikecz, A. Amyloid domains in the cell nucleus controlled by nucleoskeletal protein lamin B1 reveal a new pathway of mercury neurotoxicity. *PeerJ* **2015**, *3*, No. e754.

(61) Sharma, S. K.; Goloubinoff, P.; Christen, P. Heavy metal ions are potent inhibitors of protein folding. *Biochem. Biophys. Res. Commun.* **2008**, *372*, 341−345.

(62) Tamás, M. J.; Sharma, S. K.; Ibstedt, S.; Jacobson, T.; Christen, P. Heavy metals and metalloids as a cause for protein misfolding and aggregation. *Biomolecules* **2014**, *4*, 252−267.

(63) Choy, N.; Raussens, V.; Narayanaswami, V. Inter-molecular coiled-coil formation in human apolipoprotein E C-terminal domain. *J. Mol. Biol.* **2003**, *334*, 527−539.

(64) Dong, L. M.; Weisgraber, K. H. Human apolipoprotein E4 domain interaction. Arginine 61 and glutamic acid 255 interact to direct the preference for very low density lipoproteins. *J. Biol. Chem.* **1996**, *271*, 19053−19057.

(65) Dong, L. M.; Wilson, C.; Wardell, M. R.; Simmons, T.; Mahley, R. W.; Weisgraber, K. H.; Agard, D. A. Human apolipoprotein E. Role of arginine 61 in mediating the lipoprotein preferences of the E3 and E4 isoforms. *J. Biol. Chem.* **1994**, *269*, 22358−22365.

Publication II

Berntsson, E., Vosough, F., Svantesson, T., Pansieri, J., Iashchishyn, I. A., Ostojic, L., Dong, X., Paul, S., Jarvet, J., Roos, P. M., Barth, A., Morozova-Roche, L. A., Graslund, A., & Warmlander, S. (2023). Residue-specific binding of Ni(II) ions influences the structure and aggregation of amyloid beta (Abeta) peptides. Scientific Reports, 13(1), 3341. https://doi.org/10.1038/s41598-023-29901-5

scientific reports

Check for updates

OPEN

Residue-specific binding of Ni(II) ions influences the structure and aggregation of amyloid beta (Aβ) peptides

Elina Berntsson[1,2✉], Faraz Vosough[1], Teodor Svantesson[1], Jonathan Pansieri[3], Igor A. Iashchishyn[3], Lucija Ostojić[3], Xiaolin Dong[1], Suman Paul[1], Jüri Jarvet[1,4], Per M. Roos[5,6], Andreas Barth[1], Ludmilla A. Morozova-Roche[3], Astrid Gräslund[1] & Sebastian K. T. S. Wärmländer[7✉]

Alzheimer's disease (AD) is the most common cause of dementia worldwide. AD brains display deposits of insoluble amyloid plaques consisting mainly of aggregated amyloid-β (Aβ) peptides, and Aβ oligomers are likely a toxic species in AD pathology. AD patients display altered metal homeostasis, and AD plaques show elevated concentrations of metals such as Cu, Fe, and Zn. Yet, the metal chemistry in AD pathology remains unclear. Ni(II) ions are known to interact with Aβ peptides, but the nature and effects of such interactions are unknown. Here, we use numerous biophysical methods—mainly spectroscopy and imaging techniques—to characterize Aβ/Ni(II) interactions in vitro, for different Aβ variants: Aβ(1–40), Aβ(1–40)(H6A, H13A, H14A), Aβ(4–40), and Aβ(1–42). We show for the first time that Ni(II) ions display specific binding to the N-terminal segment of full-length Aβ monomers. Equimolar amounts of Ni(II) ions retard Aβ aggregation and direct it towards non-structured aggregates. The His6, His13, and His14 residues are implicated as binding ligands, and the Ni(II)·Aβ binding affinity is in the low μM range. The redox-active Ni(II) ions induce formation of dityrosine cross-links via redox chemistry, thereby creating covalent Aβ dimers. In aqueous buffer Ni(II) ions promote formation of beta sheet structure in Aβ monomers, while in a membrane-mimicking environment (SDS micelles) coil–coil helix interactions appear to be induced. For SDS-stabilized Aβ oligomers, Ni(II) ions direct the oligomers towards larger sizes and more diverse (heterogeneous) populations. All of these structural rearrangements may be relevant for the Aβ aggregation processes that are involved in AD brain pathology.

Alzheimer's disease (AD), the leading cause of dementia worldwide, is a progressive, irreversible, and currently incurable chronic neurodegenerative disorder[1–3], primarily manifesting as short-term memory loss. Pathological hallmarks of AD include brain atrophy, with extensive brain deposits of amyloid plaques and neurofibrillary Tau tangles occurring years before symptom manifestation[3–5]. The plaques, which consist mainly of amyloid-β (Aβ) peptides aggregated into insoluble fibrils[6], display a characteristic cross-β structure at the core of their constituent fibrils[7,8]. The plaques are the end-product of an aggregation process involving formation of extra- and intracellular intermediates such as neurotoxic Aβ oligomers[9–14]. The oligomeric aggregates may spread from neuron to neuron via exosomes[15,16]. However, the relationship between Aβ aggregation, neurodegenerative mechanisms, cognitive decline, the proposed amyloid cascade hypothesis, and disease progression is not fully understood[2,13,14,17].

The 36–43 residues long Aβ peptides found in the plaques are produced by enzymatic cleavage of the membrane-binding amyloid-β precursor protein, APP[18]. In monomeric form, the Aβ peptides are intrinsically disordered and soluble in water. The central and C-terminal segments are hydrophobic and may interact with

[1]Department of Biochemistry and Biophysics, Arrhenius Laboratories, Stockholm University, 106 91 Stockholm, Sweden. [2]Department of Chemistry and Biotechnology, Tallinn University of Technology, Tallinn, Estonia. [3]Department of Medical Biochemistry and Biophysics, Umeå University, 901 87 Umeå, Sweden. [4]The National Institute of Chemical Physics and Biophysics, Tallinn, Estonia. [5]Institute of Environmental Medicine, Karolinska Institutet, Nobels Väg 13, 171 77 Stockholm, Sweden. [6]Department of Clinical Physiology, Capio St. Göran Hospital, St. Göransplan 1, 112 19 Stockholm, Sweden. [7]Chemistry Section, Arrhenius Laboratories, Stockholm University, 106 91, Stockholm, Sweden. ✉email: elina.berntsson@dbb.su.se; seb@student.su.se

membranes or fold into a hairpin conformation that likely is required for aggregation[19]. The negatively charged N-terminal segment is hydrophilic and readily interacts with metal ions and other cationic molecules[20–23].

AD brains typically display altered metal homeostasis[17,24,25], and AD plaques accumulate metals such as calcium (Ca), copper (Cu), iron (Fe), and zinc (Zn)[26–28]. Thus, dysregulated metal chemistry might be part of the AD pathology process[29–32]. The precursor protein APP is known to bind Cu and Zn ions[33], and a possible physiological role of APP (and perhaps its fragments) might be to regulate the Cu(II) and Zn(II) concentrations in the neuronal synaptic clefts, where these ions are released in their free form[34] and where $A\beta$ aggregation may be initiated[35]. Metal ions such as Cu(II), Fe(II), Mn(II), Pb(IV) and Zn(II) have previously been shown to bind to specific $A\beta$ residues and modulate the $A\beta$ aggregation pathways[20,29,36–40]. Binding of metal ions, and also of other cationic molecules such as polyamines, has furthermore been reported to modulate and sometimes inhibit $A\beta$ toxicity[21,22,41]. However, it is unclear which possible metal interactions may be relevant for AD pathology, and which exogenous or endogenous metal ions may participate in such interactions[30–32].

Nickel (Ni) is a common metal in the industrialized world, where it is used in e.g. stainless steel alloys, Ni–Cd batteries, coins, and jewelry. As a result of low-level exposure, between 10 and 20% of all people have developed some degree of contact allergy towards Ni[42,43]. It is therefore important to clarify the health effects of long-term Ni exposure, including potential effects on neurodegenerative diseases[44]. Some studies have demonstrated specific binding between Ni(II) ions and N-terminal $A\beta$ fragments, with possible effects on $A\beta$ structure and toxicity[41,45–47]. Yet, the interactions between pathologically relevant (i.e., full-length) $A\beta$ peptides and Ni ions are poorly explored.

In this study, we use a range of biophysical spectroscopy and imaging techniques to investigate in vitro interactions between Ni(II) ions and $A\beta$ peptides, with a focus on characterizing binding properties and effects on $A\beta$ structure and aggregation. The different $A\beta$ peptides studied include the pathologically relevant $A\beta(1–40)$, $A\beta(4–40)$, and $A\beta(1–42)$ variants, together with the $A\beta(1–40)$(H6A, H13A, H14A) mutant. Because the $A\beta$ peptides interact with membranes[48], and as membrane-disruption is a possible toxicity mechanism for $A\beta$ oligomers[30], the measurements have been carried out in aqueous solution as well as in a membrane-mimetic model consisting of micelles of the SDS (sodium dodecyl sulfate) detergent[49]. The results are compared to previous studies of the effects of both different chemical environments and metal ion interactions on $A\beta$ peptides[37,38,40,48–53].

Biological relevance of Ni and sources of exposure.
Even though Ni function is limited in human biology[54], it has been suggested as an essential element in humans[55], just as it is for many human-associated bacteria[56] and possibly all higher plants[57]. Elevated Ni concentrations are however toxic to plants[58]. In animals, inadequate Ni amounts have shown adverse effects on nutrient absorption and metabolism[59,60]. Due to the abundance of Ni in many plant-based foods[58,61], Ni deficiency is unlikely to occur in humans, even though only some 10% of ingested Ni is absorbed[62]. Ni concentrations in potable water vary between 2 and 13 mg/L with a WHO limit of 70 mg/L, which is exceeded in Ni mining regions, where Ni concentrations of 200 mg/L have been found[63]. Respiratory Ni exposure is related to Ni industries and fossil fuel combustion, which overall are the main global sources of Ni emissions[58,62], and to cigarette smoking including e-cigarettes[38,64]. In addition to Ni–Cd batteries, the main industrial uses of Ni is as a whitening agent in Cu alloys for e.g. coins and jewellery, which may cause allergic contact dermatitis[58], and as a provider of corrosion resistance in steel alloys for e.g. surgical tools, biomedical implants, and body piercings. One study of Ni-containing hip prosthetic devices found that Ni blood concentration rose about twofold after metal-on-metal hip arthroplasty[65]. Ni is also present in some formulations for dental amalgam fillings[66].

The human health risks of Ni exposure are well-known and widespread, as Ni use and exposure has gradually grown from human prehistory[67] to modern times[68]. Ni is known to be haematotoxic, immunotoxic, neurotoxic, genotoxic, reproductive toxic, pulmonary toxic, nephrotoxic, hepatotoxic and carcinogenic[58,69]. Other pathological effects of Ni exposure in the occupational settings are rhinitis, asthma, nasal septum perforation, nasal sinus cancer, and respiratory cancer[70]. Ni can pass the placental barriers and accumulate in the fetus[71]. It can also pass the blood–brain barrier, and brain accumulation can result from high levels of exposure[54]. Yet, most people experience low exposure levels[66], and the most common health effect is allergic reactions[42,43].

The neurotoxic properties of Ni are well documented, but data on Ni in neurodegenerative disorders are scarce[44]. A case report of skin tissue Ni concentrations in a patient recovering from ALS after metal chelation described a Ni concentration of 850 µg/kg[72]. A 44 year old ALS patient died after 9 years of heavy metal exposure in a nickel–cadmium battery factory[73]. Increased blood Ni concentrations have been detected in multiple sclerosis (MS) patients[74], and soil Ni was found to be elevated in a Canadian MS cluster[75]. Recent data also indicate a possible contribution from Ni in the causation of neurodevelopmental dysfunctional states such as autism[76].

As a component of tobacco, cigarette smoke, and air pollution, Ni may contribute to environmental risk factors for AD. Mice exposed to a Ni nanoparticle model of air pollution showed doubled brain levels of $A\beta_{40}$ and $A\beta_{42}$ within 24 h, even at a permissible limit of nickel hydroxide exposure according to occupational safety and health standards[77]. Another study reported higher yet not statistically significantly elevated Ni concentrations in post-mortem brain and ventricular fluid of AD patients (n = 14), compared to healthy controls (n = 15)[25]. A recent study reported that Ni(II) ions interfered with aggregation of the Tau protein[78].

Materials and methods
Samples and preparations.
Ni(II) acetate and 2-(N-Morpholino)ethanesulfonic acid hydrate (MES) buffer were purchased from Sigma (Sigma/Merck KGaA, Darmstadt, Germany). The SDS detergent was bought from ICN Biomedicals Inc (USA). Sodium chloride and sodium hydroxide were purchased from Sigma-Aldrich (St. Louis, MO, USA).

Wild-type (wt) Aβ(1–42) peptides, abbreviated as $Aβ_{42}$, with the primary sequence $DAEFR_5HDSGY_{10}EVHHQ_{15}KLVFF_{20}AEDVG_{25}SNKGA_{30}IIGLM_{35}VGGVV_{40}IA$, were purchased synthetically manufactured from JPT Peptide Technologies (Germany), while recombinantly produced $Aβ_{42}$ peptides were purchased from rPeptide LLC (USA). Recombinantly produced wild-type (wt) Aβ(1–40) peptides, abbreviated as $Aβ_{40}$, as well as N-terminal truncated Aβ(4–40) peptides, were purchased as lyophilized powder from AlexoTech AB (Umeå, Sweden). The $Aβ_{40}$ peptides were either unlabeled, uniformly ^{15}N-labeled, or uniformly $^{13}C,^{15}N$-labeled. A recombinantly produced mutant version of $Aβ_{40}$, where the three histidine residues H6, H13, and H14 have been replaced with alanines, i.e. Aβ(1–40)(H6A, H13A, H14A) was also purchased from Alexo-Tech AB. This mutant is here abbreviated as $Aβ_{40}$(NoHis). All Aβ variants were stored at − 80 °C until use, when they were dissolved to monomeric form before the measurements. The $Aβ_{40}$ and Aβ(4–40) peptides were then dissolved in 10 mM NaOH to 100 µM concentration, and sonicated for 5 min in an ice-bath to dissolve possible pre-formed aggregates. Finally, buffer was added to the peptide solutions. All preparation steps were performed on ice, and the peptide concentrations were determined by weighing the dry powder and/or by NanoDrop measurements of dissolved material.

Preparation of Aβ₄₂ oligomers.

Monomeric solutions of $Aβ_{42}$ peptides were prepared via size exclusion chromatography, according to the following procedure. First, lyophilized $Aβ_{42}$ powder (1 mg) was dissolved in pure dimethyl sulfoxide (DMSO; 250 µL). A solution of 5 mM NaOH (pH = 12.3) was used to equilibrate a Sephadex G-250 HiTrap desalting column (GE Healthcare, Uppsala), which was then washed with 10–15 mL of 5 mM NaOH (pD = 12.7)[79]. The $Aβ_{42}$ solution in DMSO was added to the column, followed by 5 mM NaOD (1.25 mL). Peptide fractions in 5 mM NaOD were then collected on ice at a flow rate of 1 mg/mL. Ten fractions of 1 mL were collected in 1.5 mL low-binding reaction tubes. The $Aβ_{42}$ concentration in each fraction was measured with a NanoDrop instrument (Eppendorf, Germany) at 280 nm, using a molar extinction coefficient of 1280 M^{-1} cm^{-1} for the single tyrosine residue in the peptide[80]. Liquid nitrogen was used to flash-freeze the fractions, which then were topped with argon gas, and stored at − 80 °C until use. Two well-defined sizes of SDS-stabilized $Aβ_{42}$ oligomers—named according to the SDS concentration used: $AβO_{0.05\%SDS}$ (approximately dodecamers) and $AβO_{0.2\%SDS}$ (approximately tetramers)—were prepared using an established protocol[81] with the following modifications: the preparations were carried out in D_2O without the original dilution step, and at a fourfold lower peptide concentration[82]. The reaction mixtures, consisting of 100 µM $Aβ_{42}$ peptide in phosphate buffered saline (PBS) buffer containing either 0.05% SDS or 0.2% SDS, which corresponds to 1.7 mM and 6.9 mM SDS, respectively, were incubated at 37 °C for 24 h together with 0–500 µM of Ni(II) acetate. Liquid nitrogen was used to flash-freeze the prepared oligomer solutions, which then were stored at − 20 °C until further use. When thawed at room temperature for experimental analyses, the oligomers were stable for several days.

NMR spectroscopy measurements of Aβ₄₀ binding to Ni(II) ions.

1D and 2D nuclear magnetic resonance (NMR) spectra were recorded on Bruker Avance 500 and 700 MHz spectrometers equipped with cryoprobes. First 42 µM and then 84 µM of Ni(II) acetate was added to 84 µM of monomeric $Aβ_{40}$ peptides, either $^{13}C,^{15}N$-double-labelled or ^{15}N-mono-labelled, in 20 mM sodium phosphate buffer at pH 7.3 or pH 5.6 (90/10 H_2O/D_2O). During the titrations, 2D $^1H,^{15}N$-HSQC and 2D $^1H,^{13}C$-HSQC spectra were recorded at 5 °C. Measurements were also conducted in the presence of 50 mM SDS detergent, at 25 °C. As the critical micelle concentration for SDS is 8.2 mM in water at 25 °C[83], micelles have clearly formed under these conditions. SDS micelles are simple membrane models suitable for NMR spectroscopy due to their small size, i.e. on average 62 molecules per micelle[49]. Thus, there is approximately 0.8 mM of SDS micelles in the sample, i.e., around 10× more micelles than $Aβ_{40}$ peptides, which means that no micelle should harbour multiple Aβ peptides. All NMR data were processed and evaluated using the Topspin software (v. 3.2), employing already published HSQC crosspeak assignments for $Aβ_{40}$ in buffer[84–86] and in the presence of SDS micelles[51].

CD spectroscopy measurements of Ni(II)-induced changes in Aβ secondary structure.

Circular dichroism (CD) was carried out in a Chirascan CD spectrometer (Applied Photophysics Ltd., U.K.) using a 2 mm quartz cuvette containing 600 µl of Aβ peptide in 20 mM phosphate buffer, pH 7.3. The studied Aβ variants were $Aβ_{40}$ (10 µM), $Aβ_{40}$(NoHis) (10 µM), and Aβ(4–40) (5 µM).

Measurements were conducted either in buffer only or with added SDS micelles. CD spectra were recorded at 25 °C between 190 and 260 nm, using steps of 0.5 nm. After the first recorded spectrum, 50 mM SDS detergent was added to some of the samples. Then, small volumes of Ni(II) acetate (2 mM and 10 mM stock solutions) were titrated to each sample, in steps of 2 µM, 4 µM, 16 µM, 56 µM, 156 µM, 256 µM, and finally 512 µM. All data was processed with an eight points smoothing filter (Savitsky-Golay) using the Chirascan Pro-Data v.4.4.1 software (Applied Photophysics Ltd., U.K.).

Binding affinity of Ni(II)·Aβ complexes.

Binding affinities for Ni(II)·Aβ complexes were estimated by fitting NMR and CD titration data, respectively, to Eq. (1) (the Morrison equation[87]):

$$I = I_0 + \frac{I_\infty - I_0}{2 * [Aβ]} * \left((K_D + [Ni] + [Aβ]) - \sqrt{(K_D + [Ni] + [Aβ])^2 - 4 * [Ni] * [Aβ]} \right) \quad (1)$$

This equation assumes a single metal binding site, where [Aβ] is the peptide concentration, [Ni] is the concentration of the titrated Ni(II) ions, I_0 is the initial signal intensity, I_∞ is the steady-state (saturated) signal intensity at the end of the titration series, and K_D is the dissociation constant for the Ni(II)·Aβ complex. As no corrections for buffer conditions are done, the computed dissociation constants should be considered as apparent (K_D^{App}).

For the CD data, a binding curve was generated by plotting the CD intensity at 208 nm vs the Ni(II) concentration. For the NMR data, binding curves were generated by plotting HSQC crosspeak intensities versus Ni(II) concentration. The measured crosspeak intensities were normalized to the intensity of the V40 crosspeak for each step of added Ni(II) ions.

$A\beta_{40}$ aggregation kinetics monitored via ThT fluorescence measurements. The kinetics of amyloid aggregation over time for $A\beta_{40}$ peptides together with Ni(II) ions was monitored via measurements with a 96-well plate reader (FLUOstar Omega) of the fluorescence signal of the dye Thioflavin T (ThT), a molecular probe that displays strong fluorescence intensity when bound to amyloid material[88,89]. The samples contained 10 μM $A\beta_{40}$ peptide, 10 mM sodium phosphate buffer, pH 7.4, 40 μM ThT dye, and 0, 1, 2.5, 5, 7.5, 10, 20, or 50 μM of Ni(II) acetate. The peptide concentration was determined using a NanoDrop microvolume spectrophotometer. Measurements were recorded at three-minute intervals for 24 h at 37 °C, with five replicate samples per condition and excitation and emission wavelengths of 440 and 480 nm, respectively. The samples were continuously shaken (orbital mode) between the measurements. To determine the maximum growth rate and the half-time of $A\beta$ aggregation, the resulting ThT fluorescence data were fitted to a sigmoidal curve using Eq. (2)[90]:

$$F(t) = F_0 + \frac{A}{1 + \exp\left[-r_{max}\left(t - t_{1/2}\right)\right]} \qquad (2)$$

where F_0 is the baseline fluorescence intensity, A is the total increase in fluorescence intensity, r_{max} is the maximum growth rate, and $t_{1/2}$ is the time when half of the $A\beta$ monomers have aggregated.

Atomic force microscopy images of $A\beta_{40}$ aggregates. Images of $A\beta_{40}$ aggregates were recorded with a BioScope Catalyst (Bruker Corp., USA) atomic force microscope (AFM), operating in peak force mode in air and using MSLN and SLN cantilevers (Bruker Corp., USA). The scan rate was 0.51 Hz, with a resolution of 512 Å ~ 512 pixels. Samples of 10 μM $A\beta_{40}$ peptide were incubated for 24 h with either 0, 1, 10, or 50 μM Ni(II) acetate, using the same conditions as in the ThT experiments described above. At the end of the procedure, 30 μL samples were diluted in 30 μL Milli-Q water and then applied on freshly prepared mica substrates. After 20 min, the mica substrates were washed three times with Milli-Q water and left to air-dry.

Blue native polyacrylamide gel electrophoresis of $A\beta_{42}$ oligomers. The $A\beta_{42}$ oligomer samples prepared with 0–500 μM Ni(II) acetate, as described in the materials section, were analyzed with blue native polyacrylamide gel electrophoresis (BN-PAGE) using the Invitrogen electrophoresis system. First, 4–16% Bis–Tris Novex gels (ThermoFisher Scientific, USA) were loaded with $A\beta_{42}$ oligomer samples (10 μL) in addition to the Amersham High Molecular Weight Calibration Kit for native electrophoresis (GE Healthcare, USA). The gels were run at 4 °C according to the Invitrogen instructions (ThermoFisher Scientific, USA). Staining was done with the Pierce Silver Staining Kit (ThermoFisher Scientific, USA).

Infrared spectroscopy. Fourier-transformed infrared (FTIR) spectra of the $A\beta_{42}$ oligomers prepared with 0–500 μM Ni(II) acetate, as described in the materials section, were recorded on a Tensor 37 FTIR spectrometer (Bruker Optics, Germany) operating in transmission mode at room temperature and equipped with a liquid nitrogen-cooled MeCdTe detector and a sample shutter. During the measurements, the instrument was continuously purged with dry air. 8–10 μL of the 80 μM $A\beta_{42}$ oligomer samples were placed between two flat CaF_2 discs, which were separated by a 50 μm plastic spacer that had been covered with vacuum grease at the periphery. The mounted IR cuvette was put in a holder inside the sample chamber, and was then allowed to sit for at least 20 min after the chamber lid was closed, to remove H_2O vapor. FTIR spectra were recorded between 1900 and 800 cm^{-1}, at a resolution of 2 cm^{-1} and with 6 mm aperture. The IR intensity above 2200 cm^{-1} was blocked with a germanium filter, and that below 1500 cm^{-1} with a cellulose membrane, to increase the light intensity in the relevant spectral range[91]. The OPUS 5.5 software was used for analysis and plotting of the spectra. Second derivatives were computed with a smoothing factor of 17.

Fluorescence measurements of Ni(II)-induced formation of dityrosine in $A\beta_{40}$. A Jobin Yvon Horiba Fluorolog 3 fluorescence spectrometer (Longjumeau, France) was used to record fluorescence emission spectra between 330 and 500 nm (excitation at 315 nm) at room temperature of 10 μM $A\beta_{40}$ peptide dissolved in 20 mM MES buffer, pH 7.3. The samples were put in a quartz cuvette with 4 mm path length (volume 1 mL). To investigate the effect of Ni(II) ions on dityrosine formation, one sample contained 100 μM Ni(II) acetate. The control sample contained 50 μM of the chelator EDTA, to remove possible free metal ions. Spectra were recorded after 0 and 6 h of incubation, where the sample was kept at room temperature without agitation or other treatment. All experiments were conducted in triplicate, and before the final measurement, 300 μM of EDTA was added to the sample to remove metal ions.

Results
NMR spectroscopy: molecular details of Ni(II) binding to the $A\beta_{40}$ monomer. High-resolution NMR experiments were conducted to investigate possible residue-specific molecular interactions between Ni(II) ions and monomeric $A\beta_{40}$ peptides. Figures 1 and 2 show 2D ^{1}H,^{15}N-HSQC spectra for the amide crosspeak region for 84 μM ^{13}C,^{15}N-labeled $A\beta_{40}$ peptides at either pH 7.3 or pH 5.6, recorded before and after addition of first 42 μM and then 84 μM Ni(II) acetate, i.e. Ni(II):$A\beta_{40}$ ratios of respectively 1:2 and 1:1. Similar measure-
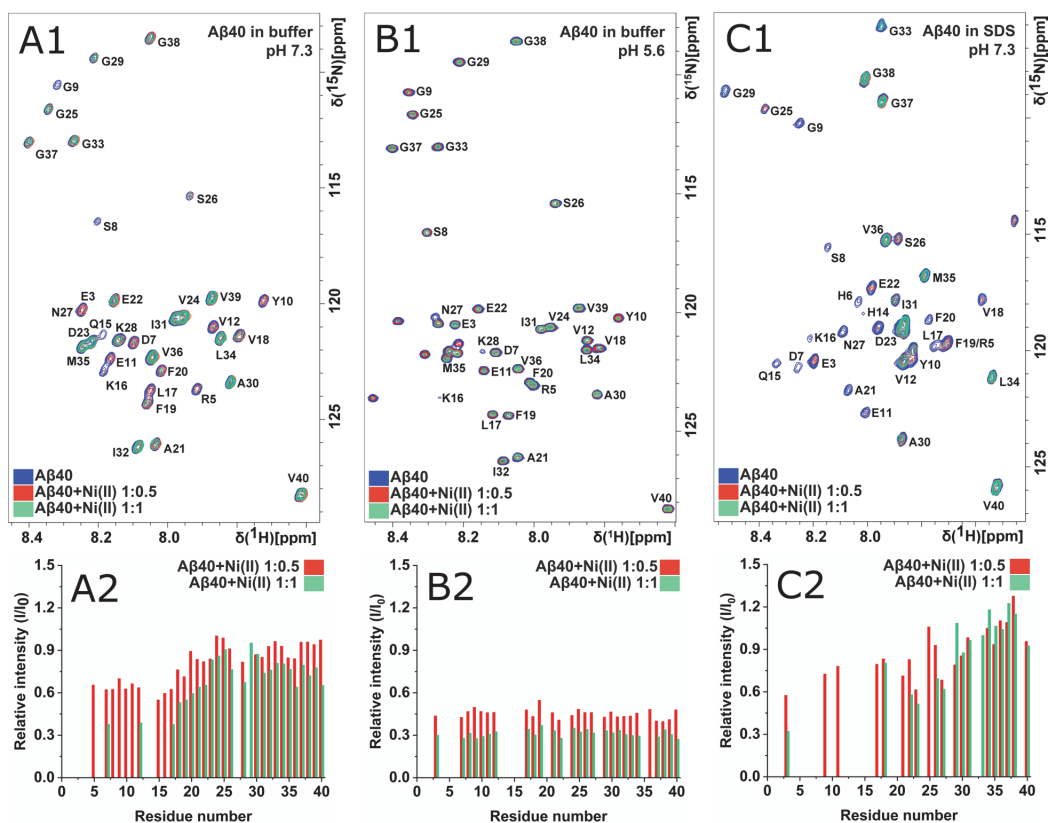
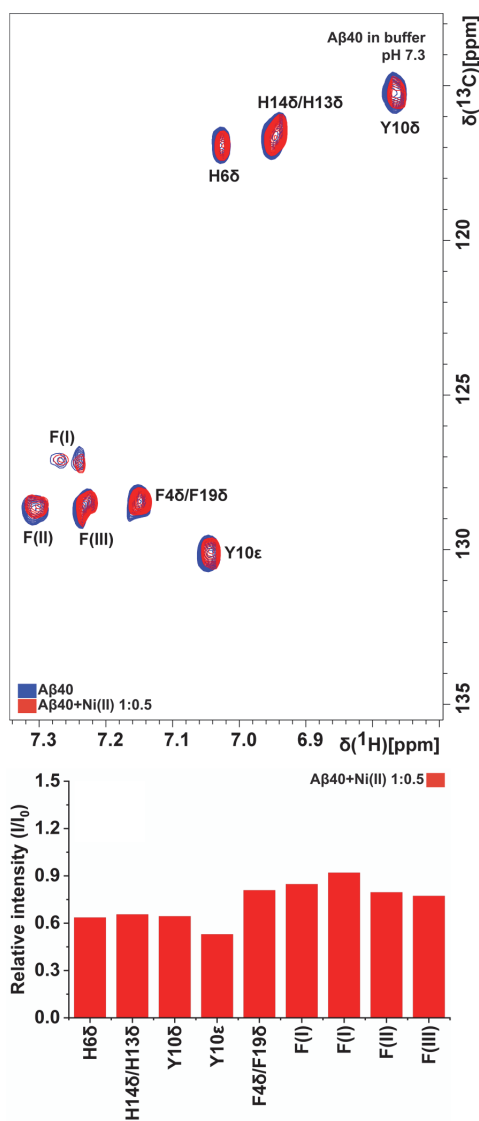**Figure 1.** NMR 2D ^{1}H,^{15}N-HSQC-spectra of 84 μM ^{15}N-labeled Aβ$_{40}$ peptides before (blue peaks) and after addition of first 42 μM (red peaks) and then 84 μM (teal peaks) Ni(II) acetate. Spectra were recorded at 5 °C in 20 mM sodium phosphate buffer at pH 7.3 (**A**), at pH 5.6 (**B**), and at pH 7.3 together with 50 mM SDS detergent (**C**). The peak intensity in the bar charts is given as the ratio between the crosspeak intensity with added Ni(II) ions relative to the intensity before addition of Ni(II) ions, i.e. I/I$_0$.

ments were conducted also for Aβ$_{40}$ peptides together with SDS micelles (50 mM SDS detergent concentration) at pH 7.3 (Fig. 1C).

For Aβ$_{40}$ in aqueous pH 7.3 buffer, addition of Ni(II) ions induces a concentration-dependent loss of amide crosspeak intensity, especially in the N-terminal region (Fig. 1A). This indicates specific binding of Ni(II) ions to N-terminal Aβ$_{40}$ residues. The specific loss of N-terminal crosspeak intensity is likely caused by intermediate or even slow (on the NMR time-scale) chemical exchange between a free and a bound state of the Aβ$_{40}$ peptides, similar to the effect induced by Cu(II) and Zn(II) ions[40,92], probably together with paramagnetic quenching effects of the Ni(II) ions[93]. When the Ni(II) ions are added to the sample, no new crosspeaks corresponding to Ni(II)-bound Aβ$_{40}$ peptides are observed (Fig. 1A). This suggests that no single well-defined Ni(II)·Aβ$_{40}$ complex exists. Instead, a range of Ni(II)-bound states of the Aβ$_{40}$ peptides are likely present, probably at different stages of aggregation and oligomerization. Each state is then too weakly populated to create distinct NMR crosspeaks. This is in line with earlier NMR studies reporting that Aβ$_{40}$ peptides are in a dynamic exchange between NMR-observable monomers and heterogeneous NMR-invisible oligomers (a "dark state")[92,94].

There is also a general loss of crosspeak intensity for all Aβ$_{40}$ residues, including the central and C-terminal amino acids, upon addition of Ni(II) acetate. This effect is likely caused by a combination of non-specific Ni(II) binding interactions, on an intermediate or slow NMR time-scale, and by the Ni(II) ions promoting aggregation of the Aβ$_{40}$ peptides into complexes that are too large to be observed with HSQC NMR, or they may simply precipitate out of the solution.

At pH 5.6, the loss of crosspeak intensity after added Ni(II) ions is very uniform, i.e., there is no residue-specific binding (Fig. 1B). The main difference at this lower pH is that histidine residues are protonated, as they have pKa values around 6.8 in short peptides[95]. Naturally, protonated His residues are less prone to bind cationic metal ions. The loss of residue-specific Ni(II) ion binding at pH 5.6 therefore strongly indicates that histidines are involved in the observed residue-specific Ni(II) ion binding at neutral pH. This is supported by the NMR results at pH 7.3 for the Aβ$_{40}$ aromatic side chains, where the aromatic rings of the N-terminal residues His6, His13,

Figure 2. NMR 2D ^{1}H,^{13}C-HSQC spectra of 84 μM ^{13}C,^{15}N-labeled Aβ$_{40}$ peptides in 20 mM phosphate buffer, pH 7.3, before (blue) and after (red) addition of 42 μM Ni(II) acetate. Some Phe crosspeaks could not be assigned to individual residues, and are instead listed as F(I), F(II), and F(III).

and His14, together with Tyr10, display a somewhat larger loss of crosspeak signal intensity than the aromatic rings of the Phe4, Phe19, and Phe20 residues (Fig. 2).

Specific loss of crosspeak intensity for N-terminal residues, upon addition of Ni(II) acetate, is observed also for Aβ$_{40}$ peptides positioned in SDS micelles (Fig. 1C), which constitute a simple model for bio-membranes[48,49]. The central and C-terminal Aβ regions are known to insert themselves as α-helices into SDS micelles[48,51], and thus, the ^{1}H,^{15}N-HSQC spectrum for Aβ$_{40}$ in SDS micelles corresponds to an α-helical conformation of the Aβ peptide. The N-terminal segment is known to remain unstructured outside the micelle surface, where it is available for interactions with e.g. metal ions[96]. The C-terminal residues are unaffected by the added Ni(II) ions (Fig. 1C), which shows that they are neither affected by direct Ni(II)-binding, nor by Ni(II)-induced aggregation—most likely Aβ peptides cannot aggregate when bound to SDS micelles, at least when there is on average
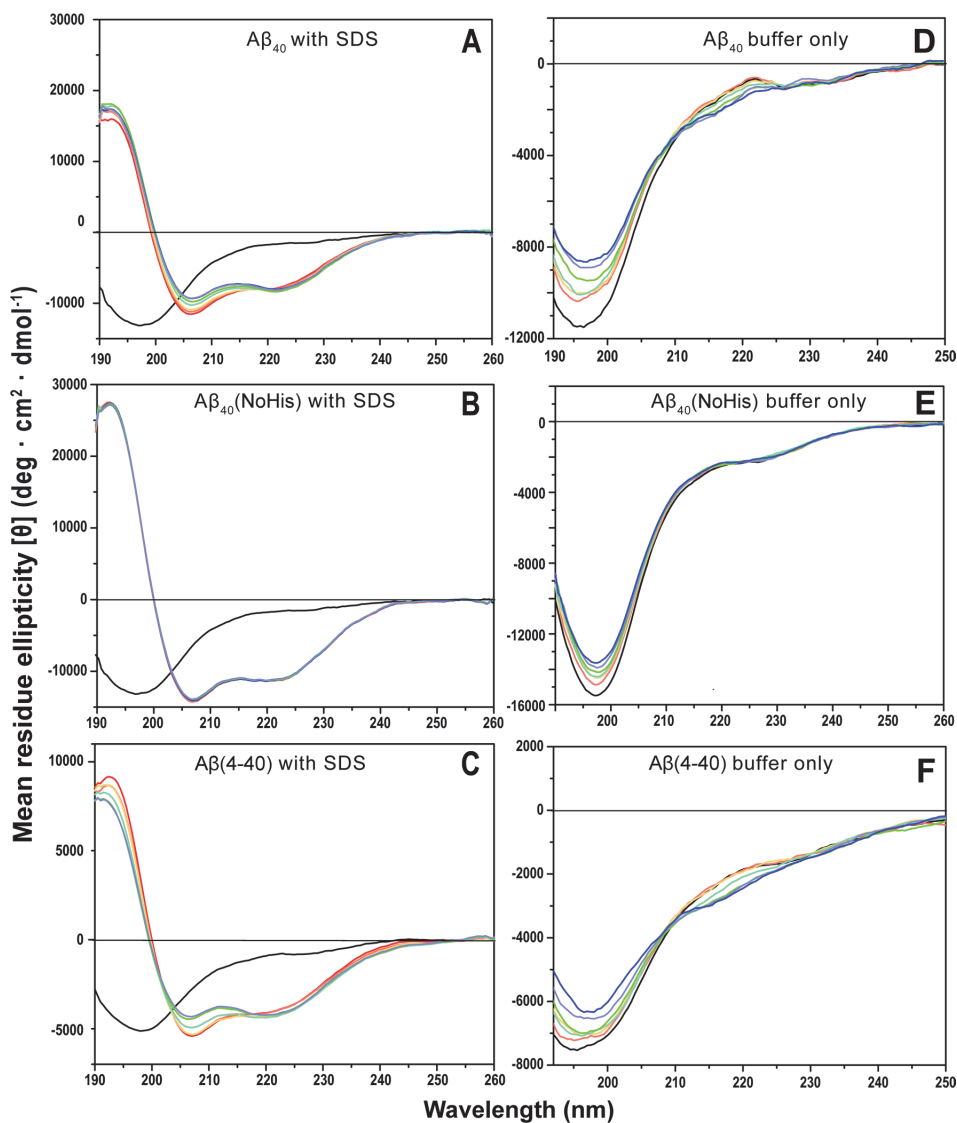
Figure 3. CD spectra of Ni(II) acetate titrated to Aβ peptides in 20 mM phosphate buffer, pH 7.3, at 25 °C. The titrations were conducted either in the presence of SDS micelles (**A–C**) or in aqueous buffer only (**D–F**), for three different peptide variants, i.e. 10 μM Aβ$_{40}$ (**A,D**), 10 μM Aβ$_{40}$(NoHis) (**B,E**), and 5 μM Aβ(4–40) (**C,F**). The black spectra show Aβ peptides in buffer only. For samples A–C, 50 mM SDS was then added (red spectra). Next, for all samples, Ni(II) acetate was titrated in steps of 2 μM (orange), 4 μM (yellow), 16 μM (turquoise), 56 μM (green), 156 μM (purple), and finally 256 μM (blue spectra).

less than one peptide per micelle. Thus, also in the presence of SDS micelles (Fig. 1C), the NMR spectrum reflects Ni(II) ion binding to monomeric Aβ$_{40}$ peptides.

CD spectroscopy measurements of Aβ secondary structure.
CD spectroscopy was used to investigate possible changes in Aβ secondary structure upon addition of Ni(II) ions, both in aqueous buffer and in a membrane-mimetic environment (i.e., SDS micelles). The three peptide variants Aβ$_{40}$, Aβ$_{40}$(NoHis) mutant, and Aβ(4–40) were investigated. In aqueous buffer, the CD spectra for monomers of all three variants display typical random coil signals with minima around 196–198 nm (Fig. 3).

Addition of Ni(II) ions to Aβ peptides in aqueous buffer induces concentration-dependent changes in the CD spectra for the monomers of all three peptide variants (Fig. 3D–F). For the Aβ$_{40}$(NoHis) peptide, these changes

	Wavelength (nm)	0 μM Ni(II)	2 μM Ni(II)	4 μM Ni(II)	16 μM Ni(II)	56 μM Ni(II)	156 μM Ni(II)	256 μM Ni(II)
$A\beta_{40}$	208	− 11,131	− 10,808	− 10,557	− 9928	− 9515	− 9064	− 9025
	222	− 7793	− 7925	− 8074	− 8241	− 8339	− 8012	− 8114
	222/208	0.700	0.733	0.765	0.830	0.8764	0.884	0.899
$A\beta_{40}$(NoHis)	208	− 14,062.7	− 13,979	− 14,112.3	− 13,919.9	− 13,962.9	19,802.9	13,725.2
	222	− 11,184.4	− 11,100.6	− 11,249.3	− 11,138.9	− 11,172.6	− 11,149.8	− 11,039.3
	222/208	0.7953	0.7941	0.7971	0.8002	0.8002	0.8078	0.8043
$A\beta(4–40)$	208	− 5335.7	− 5265.9	− 5258.7	− 4876.8	− 4338.2	− 4235.2	− 4150.7
	222	− 3978.0	− 3989.9	− 4193.3	− 4302.0	− 4205.2	− 4176.1	4268.9
	222/208	0.746	0.758	0.797	0.882	0.969	0.986	1.028

Table 1. CD signal intensities at 208 nm and 222 nm for the three Aβ variants $A\beta_{40}$, $A\beta_{40}$(NoHis), and $A\beta(4–40)$, as a function of added Ni(II) acetate.

correspond to a decrease in intensity, without changing the shape of the spectrum (Fig. 3). This likely means that the Ni(II) ions induce peptide aggregation and precipitation, thereby reducing the effective Aβ concentration in the solution.

For the $A\beta_{40}$ and $A\beta(4–40)$ variants, addition of Ni(II) ions induces structural transitions between two distinct conformations, as evidenced by the isodichroic points around 210 nm (Fig. 3D,F). Aβ peptides in solution are known to contain some polyproline II (PPII) helix structure, especially at low temperatures[50]. The loss of signal intensity around 196–198 nm, and the isodichroic points around 210 nm, might be compatible with a conversion of PPII helix into random coil structure[50,97,98]. However, the difference spectra created by subtracting the CD spectra with no added Ni(II) acetate from those with 256 μM Ni(II) acetate, shown in Supp. Fig. S1, clearly correspond to β-sheet secondary structure[99]. Formation of β-sheets upon addition of Ni(II) ions is supported also by the IR spectra shown in Supp. Fig. S2. We therefore conclude that Ni(II) ions induce β-sheet structure in $A\beta_{40}$ and $A\beta(4–40)$ peptides, in aqueous solution at neutral pH.

When SDS micelles were added to the three peptide variants, all of them adopted α-helical secondary structures, producing CD signals with characteristic minima around 208 and 222 nm (Fig. 3A–C). This is consistent with previous studies reporting that Aβ peptides adopt α-helical conformations in membrane-like environments, at least when there is on average less than one peptide per micelle[48,49,51,96,100]. The $A\beta_{40}$(NoHis) variant, where the three His residues have been replaced with alanines, displays the strongest α-helical CD signal after addition of SDS, compared to the intensity of the $A\beta_{40}$(NoHis) random coil signal before adding SDS (Fig. 3). This is reasonable given the strong propensity of alanines to form α-helices[101]. The $A\beta(4–40)$ peptide also shows a relatively strong α-helical CD signal, compared to the $A\beta(4–40)$ random coil intensity before added SDS. This might be related to a lack of α-helical structure[51] in the first three residues of $A\beta_{40}$, which are missing in the $A\beta(4–40)$ variant.

Addition of Ni(II) ions induces a concentration-dependent loss of CD signal around 208 nm, but not around 222 nm, for the $A\beta_{40}$ and the $A\beta(4–40)$ peptides, although not for the $A\beta_{40}$(NoHis) mutant (Fig. 3). As the 222 nm signal intensity remains approximately constant, the observed spectral changes do not correspond to a general loss of α-helicity but may rather be due to a change in helix supercoiling, i.e. when two or more α-helices form coiled coils via hydrophobic interactions[102–104]. The degree of helix supercoiling is known to be reflected by the $[\theta_{222}]/[\theta_{208}]$ ratio, where ratios close to 1 reflect large amounts of superhelicity[105]. During the titrations with Ni(II) acetate the $[\theta_{222}]/[\theta_{208}]$ ratio increases from 0.70 to 0.89 for $A\beta_{40}$, and from 0.75 to 1.03 for the $A\beta(4–40)$ variant (Table 1). In both cases this would correspond to a significant increase in superhelicity. Such metal-induced changes of Aβ superhelicity, in a membrane environment, has previously been reported to be induced by Cu(II) ions[96]. The lack of any Ni(II)-induced structural effects in the $A\beta_{40}$(NoHis) mutant (Fig. 3; Table 1) appears to support Ni(II) binding to Aβ via the His residues. But it is also possible that the His residues are necessary for forming a coiled-coil Aβ structure.

Estimates of Aβ·Ni(II) binding affinity. Ni(II)·Aβ binding curves were generated by plotting crosspeak intensities from the NMR titrations (Fig. 1A) and 208 nm intensities from the CD titrations (Table 1) versus Ni(II) concentration (Fig. 4). Fitting Eq. (1) to these curves yields apparent dissociation constants (K_D) for the Ni(II)·Aβ complexes.

For the CD data (Fig. 4D,E), the signal intensities have been normalized to the first value in each titration series, i.e. the signal intensity without added Ni(II) ions. The derived K_D values are 7.8 μM for binding to $A\beta_{40}$, and 17.2 μM for binding to the $A\beta(4–40)$ variant. These K_D values should however only be considered as approximations, as there may not be a direct correlation between Ni(II) binding and the structural changes observed in the CD spectra (Fig. 3). Our NMR measurements (Fig. 1C) confirm earlier studies showing that the N-terminal Aβ segment is free to interact with metal ions also when the central and C-terminal Aβ segments are inserted into SDS micelles[48,51,96]. Yet, earlier studies with Cu(II) ions have shown that the binding affinity for metal ions is reduced when the central Aβ segment is bound to some other entity[106], although this effect appears to be minor for SDS micelles[96].

For the NMR data, each crosspeak in Fig. 1A generates one binding curve. However, the Ni(II)-induced loss of crosspeak intensity is not only related to concentration-dependent chemical exchange, on an intermediate NMR
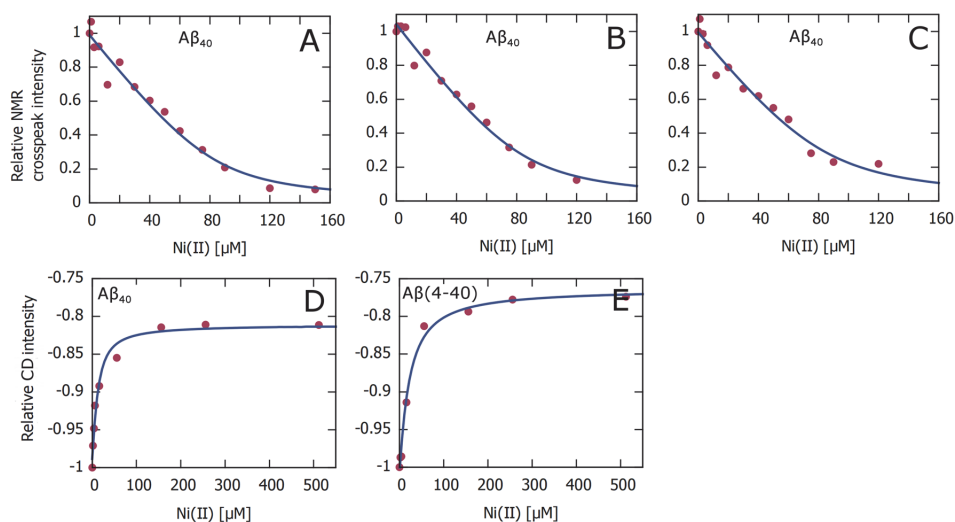
Figure 4. Binding curves for Ni(II)·Aβ complexes, derived from the NMR data in Fig. 1A and the CD data in Fig. 3A,C, respectively. The NMR and CD signal intensities are given as the ratio between the intensity with added Ni(II) ions relative to the intensity before addition of Ni(II) ions, i.e. I/I0. Apparent binding affinities were obtained by fitting Eq. (1) to the curves. (**A–C**) NMR crosspeak intensity vs Ni(II) concentration for three of the crosspeaks/residues in Fig. 1A, i.e. for 84 μM $A\beta_{40}$ in 20 mM sodium phosphate buffer, pH 7.3 at 5 °C. (**D,E**) CD intensity at 208 nm vs Ni(II) concentration for the CD data in Fig. 3A,C, i.e. for 10 μM $A\beta_{40}$ (**D**) and 5 μM Aβ(4–40) (**E**) in 20 mM phosphate buffer, pH 7.3 at 25 °C.
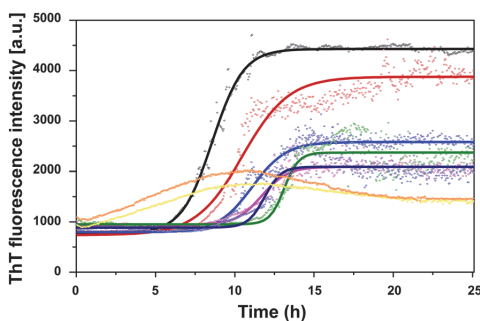
Figure 5. ThT kinetic time curves for aggregation of 10 μM $A\beta_{40}$, in 10 mM sodium phosphate buffer, pH 7.4, together with different concentrations of Ni(II) acetate: 0 μM (black), 1 μM (red), 2.5 μM (azure blue), 5 μM (magenta), 7.5 μM (green), 10 μM (navy blue), 20 μM (yellow), and 50 μM (orange). The solid lines show curves fitted with Eq. (2) to the ThT data sets.

time-scale, but also to Ni(II)-induced peptide aggregation and paramagnetic quenching of the NMR signal. Even though these effects are somewhat mitigated by normalizing the crosspeak intensity values to the V40 crosspeak intensity, for each titration step (thereby obtaining the relative intensity scale used in Fig. 4A–C), the derived K_D values should only be considered as rough approximations. The binding curves shown in Fig. 4A–C correspond to the three $A\beta_{40}$ crosspeaks that display the strongest apparent binding, with K_D values of respectively 5.3 μM, 6.7 μM, and 7.0 μM. These values are very similar to the apparent K_D value of 7.8 μM derived for $A\beta_{40}$ from the CD measurements (Fig. 4D), but they should still only be regarded as lower limits for the true K_D value. Thus, we conclude that the binding affinity for the $A\beta_{40}$·Ni(II) complex is in the low μM range.

Effects of Ni(II) ions on $A\beta_{40}$ aggregation kinetics. To investigate the influence of Ni(II) ions on $A\beta_{40}$ aggregation, samples of 10 μM $A\beta_{40}$ were incubated for 24 h in the absence or presence of increasing concentrations of Ni(II) acetate. The resulting ThT curves are shown in Fig. 5, and the r_{max}, $t_{1/2}$, and A parameters obtained from fitting the curves to Eq. (2) are shown in Table 2. For sub-stoichiometric Ni(II):$A\beta_{40}$ ratios, the Ni(II) ions

Ni(II)	0 µM	1 µM	2.5 µM	5 µM	7.5 µM	10 µM	20 µM	50 µM
r_{max} [h^{-1}]	0.96 ± 0.22	1.08 ± 0.36	0.88 ± 0.34	1.0 ± 0.45	1.02 ± 0.85	0.96 ± 0.58	n/a	n/a
$t_{1/2}$ [h]	8.3 ± 1.5	10.2 ± 0.3	11.8 ± 1.2	11.2 ± 0.7	12.5 ± 0.5	13.5 ± 1.4	n/a	n/a
A	4115 ± 436	2967 ± 238	2085 ± 575	1449 ± 480	1511 ± 132	1803 ± 442	n/a	n/a

Table 2. Parameters r_{max}, $t_{1/2}$, and A for aggregation of 10 µM Aβ$_{40}$ in the presence of different concentrations of Ni(II) acetate. The parameters were obtained from sigmoidal curve-fitting (Eq. 2) to the ThT curves shown in Fig. 5.

slow down the Aβ$_{40}$ aggregation kinetics in a concentration-dependent manner. The aggregation half-time ($t_{1/2}$) increases with increasing Ni(II) concentrations, i.e. from around 8 h without Ni(II) ions to over 13 h with 10 µM Ni(II) ions. The maximum aggregation rate r_{max} shows no systematic change with increasing Ni(II) concentration, instead it fluctuates around 0.9 h^{-1} to 1 h^{-1} (Table 2). The end-point ThT fluorescence intensities (parameter "A" in Eq. 2) generally decrease with increasing Ni(II) concentrations (Fig. 5), suggesting that less amyloid material (ThT-binding aggregates) is formed when Ni(II) ions are present. Other explanations are however possible, such as binding competition between ThT molecules and Ni(II) ions, or formation of very large Aβ aggregates that may block the transmitted light, or simply precipitate out of the solution. For the samples with high Ni(II) concentrations, i.e. 20 µM and 50 µM, above the stoichiometric Ni(II):Aβ$_{40}$ ratio, the ThT curves first increase but then decrease back towards the starting value (Fig. 5). Our best explanation for this unusual behaviour is formation of large samples that precipitate, thereby effectively reducing the Aβ$_{40}$ concentration in the sample. It was not possible to fit Eq. (2) to these data curves.

AFM imaging: effects of Ni(II) ions on the morphology of Aβ$_{40}$ aggregates.

To further characterize the influence of Ni(II) ions on Aβ$_{40}$ fibril morphology, AFM images were recorded on Aβ$_{40}$ aggregates formed after 24 h incubation in the presence and the absence of Ni(II) (Fig. 6). Without Ni(II) acetate, 10 µM Aβ$_{40}$ formed typical amyloid fibrils with an apparent height around 4–5 nm (Fig. 2A), which is in line with previously published work on Aβ fibrils formed in vitro[107–109]. A similar apparent height was observed in the presence of 1 µM Ni(II) ions (Fig. 6B). The presence of 10 µM Ni(II) ions, i.e. a 1:1 Ni(II):Aβ$_{40}$ ratio, significantly reduces fibril formation: only occasional very short Aβ$_{40}$ fibril fragments were observed, which display the same height as the fibrils formed by Aβ$_{40}$ alone (Fig. 6C). In the presence of 50 µM Ni(II) ions no fibrils were present, but instead amorphous clumps of Aβ$_{40}$ aggregates with variable heights around 13 nm (Fig. 6D). These results are consistent with the concentration-dependent effects of Ni(II) acetate on the Aβ$_{40}$ aggregation process observed with the ThT measurements (Fig. 5).

Influence of Ni(II) ions on Aβ$_{42}$ oligomer formation.

PAGE analysis was used to investigate the effect of Ni(II) ions on the formation of Aβ$_{42}$ oligomers, using a previously published protocol for formation of stable and homogeneous Aβ$_{42}$ oligomers together with SDS detergent[81,82]. While most of the current study investigates variants of the Aβ$_{40}$ peptide, oligomers of Aβ$_{40}$ are not stable and therefore not suitable model systems. Thus, SEC-purified monomeric solutions of synthetic Aβ$_{42}$ peptides were mixed with low concentrations of SDS, i.e., below the critical micelle concentration. Incubation of Aβ$_{42}$ with 0.2% SDS (6.9 mM) leads to formation of mostly tetrameric oligomers (AβO$_{0.2\%SDS}$), while incubation with 0.05% SDS (1.7 mM) produces larger oligomers—predominantly dodecamers (AβO$_{0.05\%SDS}$)[81] (Fig. 7, lanes 2 and 6). Figure 7 also shows the effect of different Ni(II) concentrations on oligomer formation. In the absence of Ni(II) ions, the AβO$_{0.05\%SDS}$ (Lane 2) and AβO$_{0.2\%SDS}$ (Lane 6) oligomers are the dominating species in their respective lanes. With increasing Ni(II) concentration, the band intensity for the major oligomeric structure declines in both cases, while smears towards higher molecular weights appear (Fig. 7, Lanes 3–5 and 7–9). Formation of AβO$_{0.05\%SDS}$ is largely disrupted when Ni(II) ions are present at 500 µM concentration (Aβ$_{42}$:Ni(II) molar ratio of 1:5), while the smear extends over almost the entire length of the lane (Fig. 7, Lane 5). A similar, but less drastic effect is observed for the smaller AβO$_{0.05\%SDS}$ (Fig. 7, Lane 9). For both types of SDS-stabilized oligomers, Ni(II) ion concentrations above ~ 100 µM disrupt oligomer formation and more heterogeneous Aβ$_{42}$ oligomeric solutions containing larger oligomers are produced. A similar smearing effect of Ni(II) ions on the formation of SDS-stabilized Aβ$_{42}$ oligomers was observed also by SDS-PAGE experiments. These results are shown and discussed in the supplementary information (Fig. S3).

FTIR spectroscopy of Aβ$_{42}$ oligomers formed in the presence of Ni(II) ions.

FTIR spectroscopy is a powerful technique for studying the secondary structure of proteins[110–116], and can be used to characterize the backbone conformation for different aggregation states of amyloid proteins, including Aβ peptides[117–119]. Here, the effects of Ni(II) ions on the secondary structures of both AβO$_{0.05\%SDS}$ and AβO$_{0.2\%SDS}$ oligomers were studied with transmission mode FTIR spectroscopy, using a D$_2$O-based buffer. The results are presented in Fig. 8 as second derivatives of IR absorption spectra, where negative bands indicate the component bands of the absorption spectra. The respective absorbance spectra are shown in Fig. S4 of the Supplementary Information.

For both types of Aβ$_{42}$ oligomers, two bands are resolved in the amide I region (i.e., 1700–1600 cm^{-1}): a high intensity, low wavenumber band around 1630 cm^{-1} (the main band for β-sheet structure), and a low intensity, high wavenumber band at 1685 cm^{-1}. This pattern with a split double-band in the amide I region is routinely
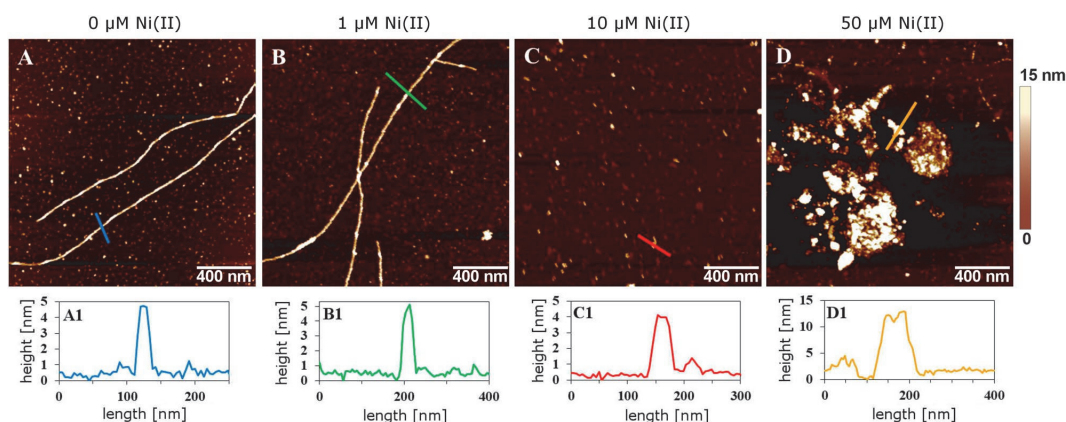
Figure 6. Top row: AFM images of the aggregation products obtained after incubation of 10 μM Aβ$_{40}$ peptides for 24 h together with either 0, 1, 10, or 50 μM Ni(II) acetate. Bottom row: Representative AFM cross-sections of respectively Aβ$_{40}$ amyloid fibrils (**A,B**) and Aβ$_{40}$ unstructured aggregates (**C,D**), corresponding to the colored lines shown in the AFM images.
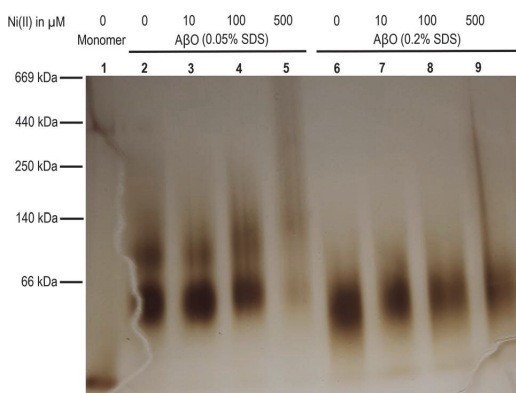

Figure 7. Effects of Ni(II) ions on formation of SDS-stabilized Aβ$_{42}$ oligomers (AβO$_{0.05\%SDS}$ and AβO$_{0.2\%SDS}$) studied by BN-PAGE. Lane 1: Monomers; Lanes 2–5: AβO$_{0.05\%SDS}$ oligomers with respectively 0, 10, 100, and 500 μM Ni(II) ions; Lanes 6–9: AβO$_{0.2\%SDS}$ oligomers with respectively 0, 10, 100, and 500 μM Ni(II) ions.

considered as indicative of the anti-parallel β-sheet structure[117,118,120]. When Ni(II) acetate is introduced during the Aβ$_{42}$ oligomer formation reactions, the main band is slightly down-shifted: for AβO$_{0.05\%SDS}$ (Fig. 8, upper row) from 1629.2 cm^{-1} in the absence of Ni(II) acetate to 1628.0 cm^{-1} at 500 μM of Ni(II) acetate (the highest concentration), and for AβO$_{0.2\%SDS}$ (Fig. 8, lower row) from 1630.1 to 1629.6 cm^{-1} upon addition of Ni(II) acetate up to 500 μM. The downshift is smaller for the oligomers prepared at the higher SDS concentration, indicating that they are less sensitive to Ni(II)-induced effects on the oligomer conformation. The spectral changes observed with Ni(II) are in interesting contrast to the absence of spectral effects upon addition of Li(I) ions[121]. The downshift is mainly observed in the presence of Ni(II) concentrations between 10 and 100 μM, which agrees with the binding affinities estimated from the CD and NMR results. Detailed analysis of the spectra in Fig. 8 shows that the shifts in band position are associated with a widening of the main β-sheet band on its low wavenumber side, indicating a higher abundance of larger oligomers[82]. Most of this widening occurs between 10 and 100 μM Ni(II). It further increases between 100 and 500 μM Ni(II), which correlates with the appearance of a high molecular weight smear on the BN-PAGE gel (Fig. 7).

Our previous study on the IR characterization of Aβ$_{42}$ oligomers has revealed a relationship between oligomer size and position of the main band in the amide I region[82]. According to these findings, the downshift of the main IR band is associated with an increase in average oligomer size and a concomitant extension of their β-sheet structure. However, the Ni(II)-induced size change is rather modest. The band position of AβO$_{0.2\%SDS}$ at the highest Ni(II) ion concentration is still higher than the AβO$_{0.05\%SDS}$ band position in the absence of Ni(II) ions, indicating that the oligomers contain less than twelve peptides. Also, the band position of AβO$_{0.05\%SDS}$ at 500 μM Ni(II) concentration is considerably higher than that of oligomers formed in the absence of SDS (1623.1 cm^{-1}),
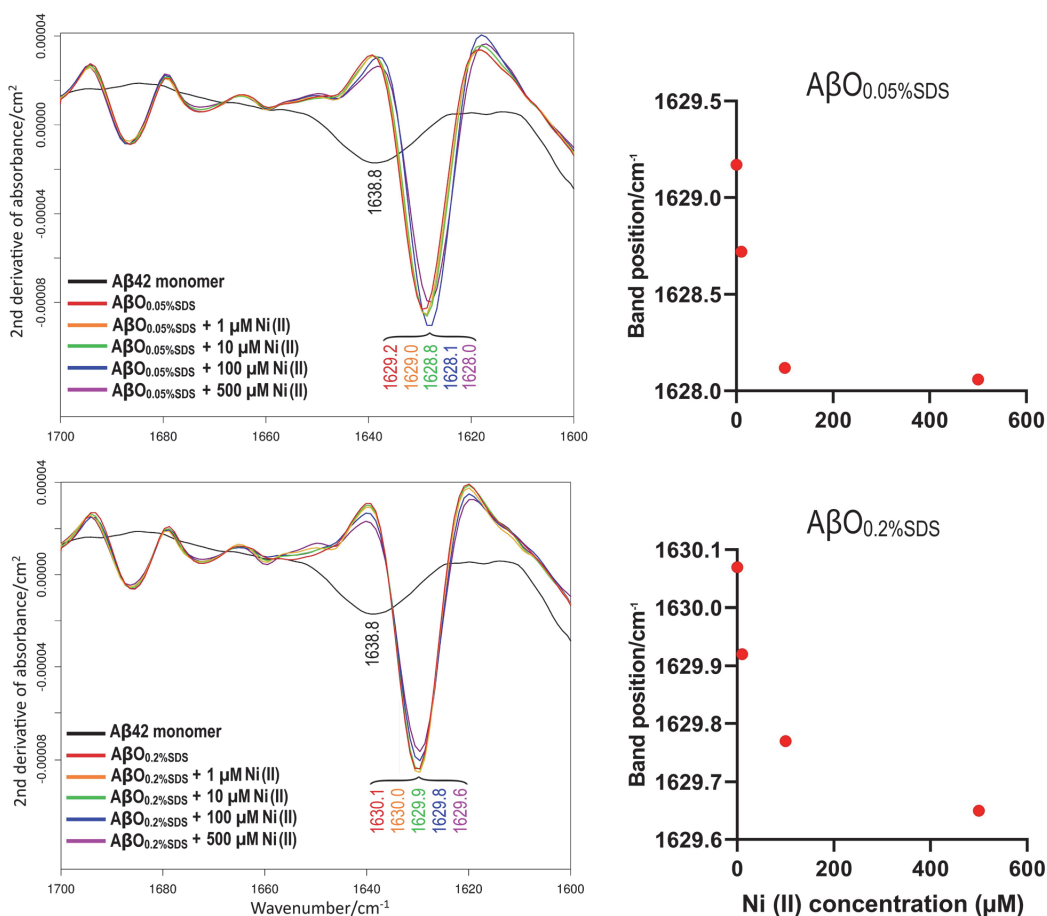
Figure 8. Transmission FTIR data for synthetic AβO$_{0.05\%SDS}$ (upper row) and synthetic AβO$_{0.2\%SDS}$ (lower row) formed in the presence of different concentrations of Ni(II) ions. The spectra show raw data without normalization. Left: Second derivatives of IR absorbance spectra in the amide I range (1700–1600 cm^{-1}) at zero Ni(II) (red); 1 μM Ni(II) (orange); 10 μM Ni(II)—(green); 100 μM Ni(II) (blue); 500 μM Ni(II) (violet). The black spectrum is for Aβ$_{42}$ monomers. Right: Dependence on Ni(II) ion concentration for the position (in cm^{-1}) of the main amide I band. For a more clear presentation, the data point at 1 μM was omitted.

which had an average molecular weight of ~ 100 kDa according to Western blotting[82]. Thus, the dominant β-sheet containing oligomer species of AβO$_{0.05\%SDS}$ seem to be smaller than ~ 100 kDa.

The interpretation of the current IR results is in good agreement with the results from the gel electrophoresis experiments, particularly with the BN-PAGE data (Fig. 7). Both IR and PAGE results indicate that addition of Ni(II) ions appears to interfere with the SDS-induced conversion of Aβ$_{42}$ monomers into homogeneous and stable oligomeric structures, instead favoring formation of larger and more diverse (heterogeneous) oligomer populations.

Ni(II)-induced dityrosine formation. Fluorescence measurements were carried out to investigate if binding of Ni(II) ions could induce formation of covalent dityrosine crosslinks in Aβ peptides, similar to what has been observed for Cu(II) ions[122–125]. Fluorescence emission spectra for Aβ$_{40}$ peptides incubated over time with or without Ni(II) acetate are shown in Fig. 9.

The control sample without added Ni(II) ions, which contained 50 μM EDTA to ensure no free metal ions were present, displayed virtually identical spectra before and after 6 h of incubation (Fig. 9A). This is in stark contrast to the sample with 100 μM Ni(II) ions added, where two large new peaks around 410 nm and 435 nm formed during the incubation time (Fig. 9B). The peak around 410 nm is from dityrosine[126], while the peak around 435 nm likely is from a different but related system, such as excimers[127]. These results are not surprising, as nickel is known to be very redox-active. Both the Ni(I)/Ni(II) and Ni(II)/Ni(III) redox pairs could be
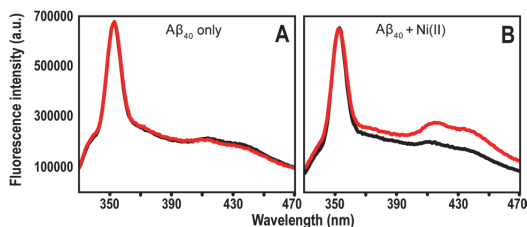
Figure 9. Fluorescence spectra of 10 μM Aβ$_{40}$ in 20 mM MES buffer, pH 7.3, incubated together with 50 μM EDTA (**A**) or with 100 μM Ni(II) acetate (**B**). Black line—0 h; red line—6 h.

involved in generating the oxygen radicals required for dityrosine formation[128]. It should be noted that weak peaks around 410 nm and 435 nm are present in both samples already at time zero (Fig. 9). This shows that some dityrosine cross-links have been generated even before the experiment was initiated, which is consistent with previous reports stating that Aβ peptides can induce oxidative stress on their own, especially in somewhat aggregated states[129,130].

Discussion

Nickel is a well-known neurotoxicant, but its role in neurodegenerative diseases remains unclear[44]. Several studies have investigated the possible effects of transition metals such as Cu and Zn in AD neuropathology, with an emphasis on interactions with the amyloid-forming Aβ peptides[29–32]. We therefore interpret our current results on Aβ interactions with Ni(II) ions mainly in the light of earlier work on Aβ binding to Cu(II) and Zn(II) ions.

Residue-specific binding of Ni(II) ions to Aβ peptides.   Our NMR results show that equimolar amounts of Ni(II) ions display residue-specific binding to the N-terminal segment of the Aβ$_{40}$ peptide (Fig. 1). This is in line with earlier studies showing that Ni(II) ions can bind N-terminal Aβ fragments[45–47]. The 2D ^{1}H-^{13}C-HSQC NMR data (Fig. 2) suggest that the three histidine residues His6, His13, and His14 are involved as binding ligands, possibly together with the Tyr10 residue. Previous work has established the metal-binding capacity of the Tyr phenol ring[131], and in Aβ peptides the Tyr10 residue seems to be involved in binding to Pb(IV) ions[38]. The weaker Ni(II)/Aβ$_{40}$ interactions observed at low pH (Fig. 1) further support the histidines being binding ligands, as these residues become protonated at low pH and therefore less prone to interact with cations[92,106,132]. The CD spectroscopy measurements also support the histidines being involved as binding ligands: addition of Ni(II) ions induces structural changes in Aβ$_{40}$ peptides, but not in Aβ$_{40}$(NoHis) mutant peptides (Fig. 3). This indicates that Ni(II) ions do not bind Aβ peptides when the His residues are absent, which is not surprising, given that Ni(II) ions are known to bind His residues such as those in protein His-tags[133]. Thus, Ni(II) ions seem to belong to a family of metal ions that coordinate to the Aβ N-terminal segment mainly by the His residues, just like Ag(I), Cu(II), Fe(II), Hg(II), Mn(II), Zn(II), and possibly Pb(IV) ions[20,37,38,40,47,52,53,92,134,135]. The exact binding coordination could not be determined from our measurements, and it is possible that multiple alternating binding conformations exist, as has been shown for Cu(II) ions[136].

According to the Irving-Williams series[137], the binding affinities of certain divalent metal ions to peptides and proteins should follow the order Mn(II) < Fe(II) < Co(II) < Ni(II) < Cu(II) > Zn(II). Metal binding affinities are however notoriously difficult to quantify, as they tend to vary both with the experimental conditions (buffer, temperature) and the employed measurement technique[138]. For example, binding affinities varying by several orders of magnitude have previously been reported for the Aβ·Cu(II) complex, with a consensus value in the low nM region for buffer-corrected affinity[138]. In our earlier studies, we have reported apparent (not buffer-corrected) K$_D$ values around 50–100 μM for Mn(II) ions in phosphate buffer, pH 7.35[37], around 1–10 μM for Zn(II) ions in phosphate or Hepes buffer, pH 7.2[40], and around 0.5 – 2.5 μM for Cu(II) ions in phosphate or Hepes buffer, pH 7.2–pH 7.35[40,96,106].

Both the CD and the NMR measurements suggest an affinity in the low μM range for Ni(II) binding to Aβ peptides (Fig. 4), i.e. weaker than Cu(II) ions, stronger than Mn(II) ions, and perhaps somewhat similar to Zn(II) binding affinity, which would be consistent with the Irving-Williams series. As the Ni(II) ions bind to the N-terminal Aβ segment, the binding affinity should be rather the same for Aβ$_{40}$ and Aβ$_{42}$ peptides, and also for shorter Aβ versions such as Aβ(1–28) and Aβ(1–16). The CD measurements indicate that the Ni(II) binding affinity to the truncated Aβ(4–40) peptide is similar to, or even somewhat weaker than, the affinity to the full-length Aβ$_{40}$ peptide (Figs. 3 and 4). This is unexpected, as the Aβ(4–40) peptide has been reported to contain an N-terminal binding motif that supposedly provides very strong binding to Cu(II) and Ni(II) ions[139], i.e. possibly fM affinity for Cu(II) ions[140]. Binding of metal ions to truncated Aβ variants is biologically relevant as such variants, and especially Aβ(4–42), are abundant in amyloid plaques from both healthy and AD brain tissues[141–144].

Effects of Ni(II) ions on Aβ structure and aggregation.   Similar to e.g. Ag(I), Cu(II), Hg(II), and Zn(II) ions[39,40,52,53], Ni(II) ions retard Aβ$_{40}$ amyloid formation in a concentration-dependent manner by directing the aggregation pathways towards non-fibrillar amorphous aggregates as demonstrated both by ThT fluorescence and AFM imaging (Figs. 5 and 6). Already at a 1:1 Ni(II)/Aβ ratio, Aβ$_{40}$ fibrillation appears to be com-

pletely inhibited. This supports earlier studies reporting that Ni(II) ions can influence protein aggregation[145]. We have previously shown that low Zn(II) concentrations induce a Zn(II)-bound structure that prevents the Aβ peptides from forming the β-hairpin required for fibrillation[19,40]. At higher Zn(II) concentrations β-sheet structure was induced[92], similar to our current observations with CD spectroscopy that Ni(II) ions induce β-sheet structure in Aβ$_{40}$ and Aβ(4–40) peptides (Fig. 3D,F). Aβ aggregation is promoted by the direct electrostatic effect of binding cations to the anionic Aβ peptides, thereby reducing repulsion between the Aβ peptides[40]. Given that Ni(II) and Zn(II) ions have similar charge and binding ligands, they likely affect Aβ aggregation and fibrillation via similar mechanisms.

Although Aβ fibrils, such as those shown in Fig. 6A,B, are the end products of Aβ aggregation, intermediate aggregates known as soluble oligomers are now generally considered to be the main toxic species in AD pathology[146,147]. The toxic mechanisms are unclear, but may involve membrane disruption[30], as some studies have reported that Aβ oligomers can form membrane-spanning "pores" that can induce leakage of e.g. Ca(II) ions[148]. Interestingly, other studies have reported that this harmful Ca(II) leakage can be inhibited by histidine-associating compounds, such as imidazole, Zn(II), and Ni(II) ions[41,149]. Because Cu(II), Zn(II), and other divalent ions have been shown to affect the structure, stability, and/or toxicity of Aβ oligomers[149–152], it is worth noting that both our FTIR (Figs. 8 and S2) and CD results (Figs. 3 and S1) show that Ni(II) ions induce structural changes in both Aβ oligomers and Aβ monomers. This is in line with earlier studies showing that both SDS-stabilized Aβ$_{42}$ oligomers[81,153,154], and SDS micelle-bound Aβ monomers[51,96] contain surface-exposed N-termini which makes it possible for the N-terminal H6, H13, and H14 residues to interact with metal ions. We speculate that Ni(II) ions affect Aβ oligomer structure in similar ways as Cu(II) and Zn(II) ions do, even though the exact mechanisms are not fully understood[30]. Addition of Ni(II) ions reduces the intensity of the NMR crosspeaks for monomeric Aβ$_{40}$ peptides in random coil structure (Fig. 1), showing that this conformation becomes less populated. But no new NMR crosspeaks appear (Fig. 1), which shows that the Ni(II) ions do not bind to form a single well-defined Ni(II)·Aβ complex. Instead, a range of heterogeneous β-sheet-containing structures are induced, which most likely exist in different stages of aggregation. They can be observed in CD and FTIR spectra, but not in NMR spectra[92,94].

Effects of Ni(II) ions on Aβ dityrosine formation.

Ni(II) ions may affect the Aβ aggregation processes also via formation of reactive oxygen species (ROS). Nickel is well known as a redox-active metal that can adopt a wide range of oxidation states, i.e., from − 1 to + 4[155]. While this can be usefully employed in engineering contexts such as in Ni–Cd batteries, in biological systems it means that Ni can induce oxidative stress, and this may be one of the main mechanisms of Ni toxicity[69]. Our experiments show that addition of Ni(II) ions initiates formation of Aβ$_{40}$ dityrosine cross-links (Fig. 9), which is a common ROS effect. Earlier studies have shown that bound redox-active Cu ions can initiate dityrosine formation, both in Aβ and other peptides and proteins[96,122–125,152,156,157]. It is therefore not surprising that a similar effect is observed for Ni(II) ions, especially as the NMR results indicate that Tyr10 is one of the Ni(II) binding ligands (Fig. 2). As wt Aβ peptides only contain one Tyr residue, i.e. Tyr10, dityrosine formation must involve two Aβ peptides, which then combine into a covalently linked dimer. Such dityrosine-linked Aβ dimers are of biological significance, as they have been found in amyloid plaques in AD brains[158]. As these plaques contain elevated levels of bound redox-active Cu and Fe ions[26,27], it is likely that the Aβ dityrosine links observed in AD patients are generated by metal-induced ROS. Because dimerization is the first step towards peptide aggregation, dityrosine formation in Aβ peptides is clearly a process that influences aggregation. In vitro studies have shown that dityrosine-linked Aβ dimers undergo rapid aggregation into oligomers that are stable, soluble, and neurotoxic[159].

Conclusions

We here show for the first time that Ni(II) ions bind to the N-terminal segment of biologically relevant (i.e., full-length) Aβ peptides. The Ni(II) binding affinity is in the low μM range, with the three N-terminal His residues and possibly Tyr10 involved as binding ligands. At equimolar amounts, Ni(II) ions impede Aβ fibrillation by directing the aggregation towards amorphous aggregates. The redox-active Ni(II) ions induce dityrosine cross-links via redox chemistry, thereby creating covalent Aβ dimers. Ni(II) ions induce structural alterations in Aβ monomers, both in aqueous buffer (formation of beta sheets) and in membrane-mimicking SDS micelles (likely formation of coil-coil helix), and affect also Aβ oligomerization. Although Ni(II) binding to Aβ is somewhat weaker than Cu(II) binding, the two metal ions induce similar effects on Aβ structure and aggregation. Exposure to stochiometric amounts of Ni(II) ions induces formation of heterogeneous Aβ oligomers, which can be observed with CD and IR but not NMR spectroscopy. These oligomers, which are in a dynamic equilibrium with Aβ monomers, may be important contributors to AD brain pathology.

Data availability

All data generated or analysed during this study are included in this published article (and its supplementary information files). The raw data for the spectroscopy measurements are available from the corresponding author on reasonable request.

References

1. Prince, M. *et al.* World Alzheimer Report 2015—The Global Impact of Dementia (Alzheimer's Disease International (ADI), London, UK, 2015).

2. Alzheimer's-Association. 2017 Alzheimer's disease facts and figures. *Alzheimer's Dementia* **13**, 325–373 (2017).
3. Fan, L. *et al.* New insights into the pathogenesis of Alzheimer's disease. *Front. Neurol* **10**, 1312. https://doi.org/10.3389/fneur.2019.01312 (2019).
4. Masters, C. L. *et al.* Alzheimer's disease. *Nat. Rev. Dis. Primers* **1**, 15056. https://doi.org/10.1038/nrdp.2015.56 (2015).
5. Irvine, G. B., El-Agnaf, O. M., Shankar, G. M. & Walsh, D. M. Protein aggregation in the brain: The molecular basis for Alzheimer's and Parkinson's diseases. *Mol. Med.* **14**, 451–464. https://doi.org/10.2119/2007-00100.Irvine (2008).
6. Glenner, G. G. & Wong, C. W. Alzheimer's disease: Initial report of the purification and characterization of a novel cerebrovascular amyloid protein. *Biochem. Biophys. Res. Commun.* **120**, 885–890 (1984).
7. Sunde, M. & Blake, C. C. From the globular to the fibrous state: Protein structure and structural conversion in amyloid formation. *Q. Rev. Biophys.* **31**, 1–39 (1998).
8. Eisenberg, D. & Jucker, M. The amyloid state of proteins in human diseases. *Cell* **148**, 1188–1203. https://doi.org/10.1016/j.cell.2012.02.022 (2012).
9. Haass, C. & Selkoe, D. J. Soluble protein oligomers in neurodegeneration: Lessons from the Alzheimer's amyloid β-peptide. *Nat. Rev. Mol. Cell Biol.* **8**, 101–112. https://doi.org/10.1038/nrm2101 (2007).
10. Walsh, D. M. & Selkoe, D. J. Aβ oligomers—A decade of discovery. *J. Neurochem.* **101**, 1172–1184. https://doi.org/10.1111/j.1471-4159.2006.04426.x (2007).
11. Glabe, C. G. Structural classification of toxic amyloid oligomers. *J. Biol. Chem.* **283**, 29639–29643. https://doi.org/10.1074/jbc.R800016200 (2008).
12. Sandberg, A. *et al.* Stabilization of neurotoxic Alzheimer amyloid-β oligomers by protein engineering. *Proc. Natl. Acad. Sci. USA* **107**, 15595–15600. https://doi.org/10.1073/pnas.1001740107 (2010).
13. Luo, J., Wärmländer, S. K., Gräslund, A. & Abrahams, J. P. Cross-interactions between the Alzheimer disease amyloid-β peptide and other amyloid proteins: A further aspect of the amyloid cascade hypothesis. *J. Biol. Chem.* **291**, 16485–16493. https://doi.org/10.1074/jbc.R116.714576 (2016).
14. Selkoe, D. J. & Hardy, J. The amyloid hypothesis of Alzheimer's disease at 25 years. *EMBO Mol. Med.* **8**, 595–608. https://doi.org/10.15252/emmm.201606210 (2016).
15. Nath, S. *et al.* Spreading of neurodegenerative pathology via neuron-to-neuron transmission of β-amyloid. *J. Neurosci.* **32**, 8767–8777. https://doi.org/10.1523/JNEUROSCI.0615-12.2012 (2012).
16. Sardar Sinha, M. *et al.* Alzheimer's disease pathology propagation by exosomes containing toxic amyloid-β oligomers. *Acta Neuropathol.* **136**, 41–56. https://doi.org/10.1007/s00401-018-1868-1 (2018).
17. Aaseth, J. *et al.* Copper, iron, selenium and lipo-glycemic dysmetabolism in Alzheimer's disease. *Int. J. Mol. Sci.* https://doi.org/10.3390/ijms22179461 (2021).
18. Owen, M. C. *et al.* Effects of in vivo conditions on amyloid aggregation. *Chem. Soc. Rev.* https://doi.org/10.1039/c8cs00034d (2019).
19. Abelein, A. *et al.* The hairpin conformation of the amyloid β peptide is an important structural motif along the aggregation pathway. *J. Biol. Inorg. Chem.* **19**, 623–634. https://doi.org/10.1007/s00775-014-1131-8 (2014).
20. Wärmländer, S. *et al.* Biophysical studies of the amyloid β-peptide: Interactions with metal ions and small molecules. *ChemBioChem* **14**, 1692–1704. https://doi.org/10.1002/cbic.201300262 (2013).
21. Luo, J. *et al.* Endogenous polyamines reduce the toxicity of soluble Aβ peptide aggregates associated with Alzheimer's disease. *Biomacromol* **15**, 1985–1991. https://doi.org/10.1021/bm401874j (2014).
22. Luo, J. *et al.* Cellular polyamines promote amyloid-beta (Aβ) peptide fibrillation and modulate the aggregation pathways. *ACS Chem. Neurosci.* **4**, 454–462. https://doi.org/10.1021/cn300170x (2013).
23. Wallin, C., Luo, J., Jarvet, J., Wärmländer, S. & Gräslund, A. The Amyloid-β peptide in amyloid formation processes: Interactions with blood proteins and naturally occurring metal ions. *Isr. J. Chem.* **57**, 674–685. https://doi.org/10.1002/ijch.201600105 (2017).
24. Duce, J. A., Bush, A. I. & Adlard, P. A. Role of amyloid-β–metal interactions in Alzheimer's disease. *Future Neurol.* **6**, 641–659 (2011).
25. Szabo, S. T., Harry, G. J., Hayden, K. M., Szabo, D. T. & Birnbaum, L. Comparison of metal levels between postmortem brain and ventricular fluid in Alzheimer's disease and nondemented elderly controls. *Toxicol. Sci.* **150**, 292–300. https://doi.org/10.1093/toxsci/kfv325 (2016).
26. Lovell, M. A., Robertson, J. D., Teesdale, W. J., Campbell, J. L. & Markesbery, W. R. Copper, iron and zinc in Alzheimer's disease senile plaques. *J. Neurol. Sci.* **158**, 47–52 (1998).
27. Miller, L. M. *et al.* Synchrotron-based infrared and X-ray imaging shows focalized accumulation of Cu and Zn co-localized with β-amyloid deposits in Alzheimer's disease. *J. Struct. Biol.* **155**, 30–37. https://doi.org/10.1016/j.jsb.2005.09.004 (2006).
28. Beauchemin, D. & Kisilevsky, R. A method based on ICP-MS for the analysis of Alzheimer's amyloid plaques. *Anal. Chem.* **70**, 1026–1029 (1998).
29. Tiiman, A., Palumaa, P. & Tougu, V. The missing link in the amyloid cascade of Alzheimer's disease-metal ions. *Neurochem. Int.* **62**, 367–378. https://doi.org/10.1016/j.neuint.2013.01.023 (2013).
30. Wärmländer, S. K. T. S. *et al.* Metal binding to the amyloid-β peptides in the presence of biomembranes: Potential mechanisms of cell toxicity. *J. Biol. Inorganic Chem.* **24**, 1189–1196. https://doi.org/10.1007/s00775-019-01723-9 (2019).
31. Huat, T. J. *et al.* Metal toxicity links to Alzheimer's disease and neuroinflammation. *J. Mol. Biol.* **431**, 1843–1868. https://doi.org/10.1016/j.jmb.2019.01.018 (2019).
32. Kim, A. C., Lim, S. & Kim, Y. K. Metal ion effects on Aβ and Tau aggregation. *Int. J. Mol. Sci.* https://doi.org/10.3390/ijms19010128 (2018).
33. Wild, K., August, A., Pietrzik, C. U. & Kins, S. Structure and synaptic function of metal binding to the amyloid precursor protein and its proteolytic fragments. *Front. Mol. Neurosci.* **10**, 21. https://doi.org/10.3389/fnmol.2017.00021 (2017).
34. Ayton, S., Lei, P. & Bush, A. I. Metallostasis in Alzheimer's disease. *Free Radic. Biol. Med.* **62**, 76–89. https://doi.org/10.1016/j.freeradbiomed.2012.10.558 (2013).
35. Branch, T., Barahona, M., Dodson, C. A. & Ying, L. Kinetic analysis reveals the identity of Aβ-metal complex responsible for the initial aggregation of Aβ in the synapse. *ACS Chem. Neurosci.* **8**, 1970–1979. https://doi.org/10.1021/acschemneuro.7b00121 (2017).
36. Miller, Y., Ma, B. & Nussinov, R. Metal binding sites in amyloid oligomers: Complexes and mechanisms. *Coord. Chem. Rev.* **256**, 2245–2252 (2012).
37. Wallin, C. *et al.* Characterization of Mn(II) ion binding to the amyloid-β peptide in Alzheimer's disease. *J. Trace Elem. Med. Biol.* **38**, 183–193. https://doi.org/10.1016/j.jtemb.2016.03.009 (2016).
38. Wallin, C. *et al.* Alzheimer's disease and cigarette smoke components: Effects of nicotine, PAHs, and Cd(II), Cr(III), Pb(II), Pb(IV) ions on amyloid-β peptide aggregation. *Sci. Rep.* **7**, 14423. https://doi.org/10.1038/s41598-017-13759-5 (2017).
39. Faller, P., Hureau, C. & Berthoumieu, O. Role of metal ions in the self-assembly of the Alzheimer's amyloid-β peptide. *Inorg. Chem.* **52**, 12193–12206. https://doi.org/10.1021/ic4003059 (2013).
40. Danielsson, J., Pierattelli, R., Banci, L. & Gräslund, A. High-resolution NMR studies of the zinc-binding site of the Alzheimer's amyloid β-peptide. *FEBS J.* **274**, 46–59. https://doi.org/10.1111/j.1742-4658.2006.05563.x (2007).
41. Arispe, N., Diaz, J. C. & Flora, M. Efficiency of histidine-associating compounds for blocking the Alzheimer's Aβ channel activity and cytotoxicity. *Biophys. J.* **95**, 4879–4889. https://doi.org/10.1529/biophysj.108.135517 (2008).

42. ATSDR. *Agency for Toxic Substances and Disease Registry: Toxicological Profile for Nickel* (2005).
43. Uter, W., Pfahlberg, A., Gefeller, O., Geier, J. & Schnuch, A. Risk factors for contact allergy to nickel—Results of a multifactorial analysis. *Contact Dermatitis* **48**, 33–38. https://doi.org/10.1034/j.1600-0536.46.s4.29_102.x (2003).
44. Ijomone, O. M. *Advances in Neurotoxicology* (ed Ashner, M.) 263–284 (Academic Press, 2021).
45. Józsa, E. *et al.* Nickel(II) and mixed metal complexes of amyloid-β N-terminus. *Dalton Trans.* **39**, 7046–7053. https://doi.org/10.1039/c0dt00189a (2010).
46. Grenács, A. & Sóvágó, I. Copper(II), nickel(II) and zinc(II) complexes of the N-terminal nonapeptide fragment of amyloid-β and its derivatives. *J. Inorg. Biochem.* **139**, 49–56. https://doi.org/10.1016/j.jinorgbio.2014.06.001 (2014).
47. Lermyte, F. *et al.* Metal ion binding to the amyloid β peptide studied by native top-down FTICR mass spectrometry. *J. Am. Soc. Mass Spectrom.* https://doi.org/10.1007/s13361-019-02283-7 (2019).
48. Österlund, N. *et al.* Amyloid-β peptide interactions with amphiphilic surfactants: Electrostatic and hydrophobic effects. *ACS Chem. Neurosci.* **9**, 1680–1692. https://doi.org/10.1021/acschemneuro.8b00065 (2018).
49. Österlund, N., Luo, J., Wärmländer, S. K. T. S. & Gräslund, A. Membrane-mimetic systems for biophysical studies of the amyloid-β peptide. *Biochim. Biophys. Acta Proteins Proteom.* **492–501**, 2019. https://doi.org/10.1016/j.bbapap.2018.11.005 (1867).
50. Danielsson, J., Jarvet, J., Damberg, P. & Gräslund, A. The Alzheimer β-peptide shows temperature-dependent transitions between left-handed 3-helix, β-strand and random coil secondary structures. *FEBS J.* **272**, 3938–3949. https://doi.org/10.1111/j.1742-4658.2005.04812.x (2005).
51. Jarvet, J., Danielsson, J., Damberg, P., Oleszczuk, M. & Gräslund, A. Positioning of the Alzheimer Aβ(1–40) peptide in SDS micelles using NMR and paramagnetic probes. *J. Biomol. NMR* **39**, 63–72. https://doi.org/10.1007/s10858-007-9176-4 (2007).
52. Wallin, C. *et al.* Mercury and Alzheimer's disease: Hg(II) ions display specific binding to the amyloid-β peptide and hinder its fibrillization. *Biomolecules* https://doi.org/10.3390/biom10010044 (2019).
53. Wallin, C. *et al.* Metal ion coordination delays amyloid-β peptide self-assembly by forming an aggregation-inert complex. *J. Biol. Chem.* **295**, 7224–7234. https://doi.org/10.1074/jbc.RA120.012738 (2020).
54. Klein, C. & Costa, M. *Handbook on the Toxicology of Metals, 4th ed. Volume II: Specific Metals* (eds Nordberg, G. F. *et al.*) (Elsevier, 2015).
55. Anke, M., Groppel, B., Kronemann, H. & Grun, M. *Nickel—An essential element* 339–365 (IARC Sci Publ, 1984).
56. Fischer, F. *et al.* Characterization in *Helicobacter pylori* of a nickel transporter essential for colonization that was acquired during evolution by gastric *Helicobacter* species. *PLoS Pathog.* **12**, e1006018. https://doi.org/10.1371/journal.ppat.1006018 (2016).
57. Eskew, D. L., Welch, R. M. & Cary, E. E. Nickel: An essential micronutrient for legumes and possibly all higher plants. *Science* **222**, 621–623. https://doi.org/10.1126/science.222.4624.621 (1983).
58. Genchi, G., Carocci, A., Lauria, G., Sinicropi, M. S. & Catalano, A. Nickel: Human health and environmental toxicology. *Int. J. Environ. Res. Public Health* https://doi.org/10.3390/ijerph17030679 (2020).
59. Nielsen, F. H., Ollerich, D. A., Fosmire, G. J. & Sandstead, H. H. Nickel deficiency in chicks and rats: Effects on liver morphology, function and polysomal integrity. *Adv. Exp. Med. Biol.* **48**, 389–403. https://doi.org/10.1007/978-1-4684-0943-7_18 (1974).
60. Stangl, G. I. & Kirchgessner, M. Nickel deficiency alters liver lipid metabolism in rats. *J. Nutr.* **126**, 2466–2473. https://doi.org/10.1093/jn/126.10.2466 (1996).
61. Mania, M., Rebeniak, M. & Postupolski, J. Exposure assessment of the population in Poland to the toxic effects of nickel from vegetable and their products. *Rocz. Panstw. Zakl. Hig.* **70**, 401–406. https://doi.org/10.32394/rpzh.2019.0095 (2019).
62. World Health, O. Air quality guidelines for Europe. *WHO Reg Publ Eur Ser*, V-X, 1–273 (2000).
63. Chain, E. P. o. c. i. t. F. *et al.* Update of the risk assessment of nickel in food and drinking water. *EFSA J.* **18**, e06268. https://doi.org/10.2903/j.efsa.2020.6268 (2020).
64. Bernhard, D., Rossmann, A. & Wick, G. Metals in cigarette smoke. *IUBMB Life* **57**, 805–809. https://doi.org/10.1080/15216540500459667 (2005).
65. Dahlstrand, H., Stark, A., Anissian, L. & Hailer, N. P. Elevated serum concentrations of cobalt, chromium, nickel, and manganese after metal-on-metal alloarthroplasty of the hip: A prospective randomized study. *J. Arthroplasty* **24**, 837–845. https://doi.org/10.1016/j.arth.2008.07.019 (2009).
66. Setcos, J. C., Babaei-Mahani, A., Silvio, L. D., Mjor, I. A. & Wilson, N. H. The safety of nickel containing dental alloys. *Dent. Mater.* **22**, 1163–1168. https://doi.org/10.1016/j.dental.2005.11.033 (2006).
67. Cheng, C. F. & Schwitter, C. M. Nickel in ancient bronzes. *Am. J. Archaeol.* **61**, 351–365 (1957).
68. Rauch, J. N. & Pacyna, J. M. Earth's global Ag, Al, Cr, Cu, Fe, Ni, Pb, and Zn cycles. *Glob. Biogeochem. Cycles* **23**, GB2001. https://doi.org/10.1029/2008GB003376 (2009).
69. Das, K. K., Das, S. N. & Dhundasi, S. A. Nickel, its adverse health effects & oxidative stress. *Indian J. Med. Res.* **128**, 412–425 (2008).
70. Nordberg, G. & Costa, M. *Handbook on the Toxicology of Metals* 5th edn. (Academic Press, 2022).
71. Hou, Y. P. *et al.* The characteristics of placental transfer and tissue concentrations of nickel in late gestational rats and fetuses. *Placenta* **32**, 277–282. https://doi.org/10.1016/j.placenta.2010.12.021 (2011).
72. Mangelsdorf, I., Walach, H. & Mutter, J. Healing of amyotrophic lateral sclerosis: A case report. *Complement. Med. Res.* **24**, 175–181. https://doi.org/10.1159/000477397 (2017).
73. Bar-Sela, S., Reingold, S. & Richter, E. D. Amyotrophic lateral sclerosis in a battery-factory worker exposed to cadmium. *Int. J. Occup. Environ. Health* **7**, 109–112. https://doi.org/10.1179/107735201800339470 (2001).
74. Forte, G. *et al.* Quantification of chemical elements in blood of patients affected by multiple sclerosis. *Ann. Ist. Super Sanita* **41**, 213–216 (2005).
75. Irvine, D. G., Schiefer, H. B. & Hader, W. J. Geotoxicology of multiple sclerosis: The Henribourg, Saskatchewan, cluster focus. II. The soil. *Sci. Total Environ.* **77**, 175–188. https://doi.org/10.1016/0048-9697(88)90054-x (1988).
76. Frye, R. E. *et al.* Early life metal exposure dysregulates cellular bioenergetics in children with regressive autism spectrum disorder. *Transl. Psychiatry* **10**, 223. https://doi.org/10.1038/s41398-020-00905-3 (2020).
77. Kim, S. H. *et al.* Rapid doubling of Alzheimer's amyloid-β40 and 42 levels in brains of mice exposed to a nickel nanoparticle model of air pollution. *F1000Res* **1**, 70. https://doi.org/10.12688/f1000research.1-70.v1 (2012).
78. Gorantla, N. V., Das, R., Balaraman, E. & Chinnathambi, S. Transition metal nickel prevents Tau aggregation in Alzheimer's disease. *Int. J. Biol. Macromol.* **156**, 1359–1365. https://doi.org/10.1016/j.ijbiomac.2019.11.176 (2020).
79. Glasoe, P. K. & Long, F. A. Use of glass electrodes to measure acidities in deuterium oxide. *J. Phys. Chem.* **64**, 88–90 (1960).
80. Edelhoch, H. Spectroscopic determination of tryptophan and tyrosine in proteins. *Biochemistry* **6**, 1948–1954 (1967).
81. Barghorn, S. *et al.* Globular amyloid β-peptide1-42 oligomer—A homogenous and stable neuropathological protein in Alzheimer's disease. *J. Neurochem.* **95**, 834–847 (2005).
82. Vosough, F. & Barth, A. Characterization of homogeneous and heterogeneous amyloid-β42 oligomer preparations with biochemical methods and infrared spectroscopy reveals a correlation between infrared spectrum and oligomer size. *ACS Chem. Neurosci.* **12**, 473–488. https://doi.org/10.1021/acschemneuro.0c00642 (2021).
83. Dominguez, A., Fernandez, A., Gonzalez, N., Iglesias, E. & Motenegro, E. Determination of critical micelle concentration of some surfactants by three techniques. *J. Chem. Educ.* **74**, 1227–1231 (1997).
84. Danielsson, J., Andersson, A., Jarvet, J. & Gräslund, A. 15N relaxation study of the amyloid β-peptide: Structural propensities and persistence length. *Magn. Reason. Chem.* **44**, S114–S121. https://doi.org/10.1002/mrc.1814 (2006).

85. Roche, J., Shen, Y., Lee, J. H., Ying, J. & Bax, A. Monomeric Aβ(1–40) and Aβ (1–42) peptides in solution adopt very similar Ramachandran map distributions that closely resemble random coil. *Biochemistry* **55**, 762–775. https://doi.org/10.1021/acs.biochem.5b01259 (2016).

86. Yamaguchi, T., Matsuzaki, K. & Hoshino, M. Transient formation of intermediate conformational states of amyloid-β peptide revealed by heteronuclear magnetic resonance spectroscopy. *FEBS Lett.* **585**, 1097–1102. https://doi.org/10.1016/j.febslet.2011.03.014 (2011).

87. Kuzmic, P. *History, variants and usage of the "Morrison equation" in enzyme inhibition kinetics, BioKin Technical Note TN-2015-01* http://www.biokin.com/TN/2015/01 *(2015).*

88. Biancalana, M. & Koide, S. Molecular mechanism of Thioflavin-T binding to amyloid fibrils. *Biochem. Biophys. Acta.* **1405–1412**, 2010. https://doi.org/10.1016/j.bbapap.2010.04.001 (1804).

89. Gade Malmos, K. *et al.* ThT 101: A primer on the use of thioflavin T to investigate amyloid formation. *Amyloid* **24**, 1–16. https://doi.org/10.1080/13506129.2017.1304905 (2017).

90. Hellstrand, E., Boland, B., Walsh, D. M. & Linse, S. Amyloid β-protein aggregation produces highly reproducible kinetic data and occurs by a two-phase process. *ACS Chem Neurosci* **1**, 13–18. https://doi.org/10.1021/cn900015v (2010).

91. Baldassarre, M. & Barth, A. Pushing the detection limit of infrared spectroscopy for structural analysis of dilute protein samples. *Analyst* **139**, 5393–5399. https://doi.org/10.1039/c4an00918e (2014).

92. Ghalebani, L., Wahlström, A., Danielsson, J., Wärmländer, S. K. & Gräslund, A. pH-dependence of the specific binding of Cu(II) and Zn(II) ions to the amyloid-β peptide. *Biochem. Biophys. Res. Commun.* **421**, 554–560. https://doi.org/10.1016/j.bbrc.2012.04.043 (2012).

93. Barnhart, J. L. & Berk, R. N. Influence of paramagnetic ions and pH on proton NMR relaxation of biologic fluids. *Investig. Radiol.* **21**, 132–136. https://doi.org/10.1097/00004424-198602000-00009 (1986).

94. Fawzi, N. L., Ying, J., Torchia, D. A. & Clore, G. M. Kinetics of amyloid β monomer-to-oligomer exchange by NMR relaxation. *J. Am. Chem. Soc.* **132**, 9948–9951. https://doi.org/10.1021/ja1048253 (2010).

95. Pogostin, B. H., Malmendal, A., Londergan, C. H. & Akerfeldt, K. S. pKa determination of a histidine residue in a short peptide using Raman spectroscopy. *Molecules* https://doi.org/10.3390/molecules24030405 (2019).

96. Tiiman, A. *et al.* Specific binding of Cu(II) ions to amyloid-β peptides bound to aggregation-inhibiting molecules or SDS micelles creates complexes that generate radical oxygen species. *J. Alzheimers Dis.* **54**, 971–982. https://doi.org/10.3233/JAD-160427 (2016).

97. Gielnik, M. *et al.* The prion protein octarepeat domain forms transient β-sheet structures upon residue-specific Cu(II) and Zn(II) binding. *bioRxiv* https://doi.org/10.1101/2021.12.12.472308 (2021).

98. Kjaergaard, M. *et al.* Temperature-dependent structural changes in intrinsically disordered proteins: Formation of alpha-helices or loss of polyproline II?. *Protein Sci.* **19**, 1555–1564. https://doi.org/10.1002/pro.435 (2010).

99. Greenfield, N. & Fasman, G. D. Computed circular dichroism spectra for the evaluation of protein conformation. *Biochemistry* **8**, 4108–4116. https://doi.org/10.1021/bi00838a031 (1969).

100. Usachev, K. S., Filippov, A. V., Khairutdinov, B. I., Antzutkin, O. N. & Klochkov, V. V. NMR structure of the Arctic mutation of the Alzheimer's Aβ(1–40) peptide docked to SDS micelles. *J. Mol. Struct.* **1076**, 518–523 (2014).

101. Lopez-Llano, J., Campos, L. A. & Sancho, J. Alpha-helix stabilization by alanine relative to glycine: Roles of polar and apolar solvent exposures and of backbone entropy. *Proteins* **64**, 769–778. https://doi.org/10.1002/prot.21041 (2006).

102. Lau, S. Y., Taneja, A. K. & Hodges, R. S. Synthesis of a model protein of defined secondary and quaternary structure. Effect of chain length on the stabilization and formation of two-stranded alpha-helical coiled-coils. *J. Biol. Chem.* **259**, 13253–13261 (1984).

103. Zhou, N. E., Kay, C. M. & Hodges, R. S. Synthetic model proteins: The relative contribution of leucine residues at the non-equivalent positions of the 3–4 hydrophobic repeat to the stability of the two-stranded alpha-helical coiled-coil. *Biochemistry* **31**, 5739–5746. https://doi.org/10.1021/bi00140a008 (1992).

104. Zhou, N. E., Kay, C. M. & Hodges, R. S. Synthetic model proteins. Positional effects of interchain hydrophobic interactions on stability of two-stranded alpha-helical coiled-coils. *J. Biol. Chem.* **267**, 2664–2670 (1992).

105. Barbar, E. & Nyarko, A. NMR characterization of self-association domains promoted by interactions with LC8 hub protein. *Comput. Struct. Biotechnol. J.* **9**, e201402003. https://doi.org/10.5936/csbj.201402003 (2014).

106. Lindgren, J. *et al.* Engineered non-fluorescent Affibody molecules facilitate studies of the amyloid-beta (Aβ) peptide in mono-meric form: Low pH was found to reduce Aβ/Cu(II) binding affinity. *J. Inorg. Biochem.* **120**, 18–23. https://doi.org/10.1016/j.jinorgbio.2012.11.005 (2013).

107. Luo, J. *et al.* Inhibiting and reversing amyloid-β peptide (1–40) fibril formation with gramicidin S and engineered analogues. *Chemistry* **19**, 17338–17348. https://doi.org/10.1002/chem.201301535 (2013).

108. Luo, J., Wärmländer, S. K., Gräslund, A. & Abrahams, J. P. Human lysozyme inhibits the in vitro aggregation of Aβ peptides, which in vivo are associated with Alzheimer's disease. *Chem. Commun.* **49**, 6507–6509. https://doi.org/10.1039/c3cc42325e (2013).

109. Luo, J., Wärmländer, S. K., Gräslund, A. & Abrahams, J. P. Reciprocal molecular interactions between the Aβ peptide linked to Alzheimer's disease and insulin linked to diabetes mellitus type II. *ACS Chem. Neurosci.* **7**, 269–274. https://doi.org/10.1021/acschemneuro.5b00325 (2016).

110. Barth, A. Infrared spectroscopy of proteins. *Biochem. Biophys. Acta.* **1767**, 1073–1101. https://doi.org/10.1016/j.bbabio.2007.06.004 (2007).

111. Barth, A. & Zscherp, C. What vibrations tell us about proteins. *Q. Rev. Biophys.* **35**, 369–430. https://doi.org/10.1017/s003358350 2003815 (2002).

112. Yang, H., Yang, S., Kong, J., Dong, A. & Yu, S. Obtaining information about protein secondary structures in aqueous solution using Fourier transform IR spectroscopy. *Nat. Protoc.* **10**, 382–396. https://doi.org/10.1038/nprot.2015.024 (2015).

113. Goormaghtigh, E., Cabiaux, V. & Ruysschaert, J. M. Determination of soluble and membrane protein structure by Fourier transform infrared spectroscopy. III. Secondary structures. *Subcell Biochem.* **23**, 405–450. https://doi.org/10.1007/978-1-4615-1863-1_10 (1994).

114. Jackson, M. & Mantsch, H. H. The use and misuse of FTIR spectroscopy in the determination of protein structure. *Crit. Rev. Biochem. Mol. Biol.* **30**, 95–120. https://doi.org/10.3109/10409239509085140 (1995).

115. Arrondo, J. L., Muga, A., Castresana, J. & Goni, F. M. Quantitative studies of the structure of proteins in solution by Fourier-transform infrared spectroscopy. *Prog. Biophys. Mol. Biol.* **59**, 23–56. https://doi.org/10.1016/0079-6107(93)90006-6 (1993).

116. Fabian, H. & Mäntele, W. *Handbook of Vibrational Spectroscopy* (eds Chalmers, J. M. & Griffiths, P.) 3399–3426 (Wiley, 2002).

117. Sarroukh, R., Goormaghtigh, E., Ruysschaert, J. M. & Raussens, V. ATR-FTIR: A "rejuvenated" tool to investigate amyloid proteins. *Biochem. Biophys. Acta.* **2328–2338**, 2013. https://doi.org/10.1016/j.bbamem.2013.04.012 (1828).

118. Li, H., Lantz, R. & Du, D. Vibrational approach to the dynamics and structure of protein amyloids. *Molecules* https://doi.org/10.3390/molecules24010186 (2019).

119. Moran, S. D. & Zanni, M. T. How to get insight into amyloid structure and formation from infrared spectroscopy. *J. Phys. Chem. Lett.* **5**, 1984–1993. https://doi.org/10.1021/jz500794d (2014).

120. Cerf, E. *et al.* Antiparallel β-sheet: A signature structure of the oligomeric amyloid β-peptide. *Biochem. J.* **421**, 415–423. https://doi.org/10.1042/BJ20090379 (2009).

121. Berntsson, E. *et al.* Lithium ions display weak interaction with amyloid-beta (Aβ) peptides and have minor effects on their aggregation. *Acta Biochim. Pol.* **68**, 169–179. https://doi.org/10.18388/abp.2020_5493 (2021).

122. Atwood, C. S. *et al.* Copper mediates dityrosine cross-linking of Alzheimer's amyloid-β. *Biochemistry* **43**, 560–568. https://doi.org/10.1021/bi0358824 (2004).

123. Dong, X. *et al.* Copper ions induce dityrosine-linked dimers in human but not in murine islet amyloid polypeptide (IAPP/amylin). *Biochem. Biophys. Res. Commun.* **510**, 520–524. https://doi.org/10.1016/j.bbrc.2019.01.120 (2019).

124. Gu, M., Bode, D. C. & Viles, J. H. Copper redox cycling inhibits Aβ fibre formation and promotes fibre fragmentation, while generating a dityrosine Aβ dimer. *Sci. Rep.* **8**, 16190. https://doi.org/10.1038/s41598-018-33935-5 (2018).

125. Vazquez, G. *et al.* Copper, dityrosine cross-links and amylod-β aggregation. *J. Biol. Inorg. Chem.* **24**, 1217–1229. https://doi.org/10.1007/s00775-019-01734-6 (2019).

126. Huggins, T. G., Wells-Knecht, M. C., Detorie, N. A., Baynes, J. W. & Thorpe, S. R. Formation of o-tyrosine and dityrosine in proteins during radiolytic and metal-catalyzed oxidation. *J. Biol. Chem.* **268**, 12341–12347 (1993).

127. Keleti, T. The excimer fluorescence of tryptophan, tyrosine and D-glyceraldehyde-3-phosphate dehydrogenase. *FEBS Lett.* **7**, 280–282. https://doi.org/10.1016/0014-5793(70)80181-8 (1970).

128. Zilbermann, I., Maimon, E., Cohen, H. & Meyerstein, D. Redox chemistry of nickel complexes in aqueous solutions. *Chem. Rev.* **105**, 2609–2625. https://doi.org/10.1021/cr030717f (2005).

129. Harris, M. E., Hensley, K., Butterfield, D. A., Leedle, R. A. & Carney, J. M. Direct evidence of oxidative injury produced by the Alzheimer's β-amyloid peptide (1–40) in cultured hippocampal neurons. *Exp. Neurol.* **131**, 193–202. https://doi.org/10.1016/0014-4886(95)90041-1 (1995).

130. Cenini, G. *et al.* Generation of reactive oxygen species by β amyloid fibrils and oligomers involves different intra/extracellular pathways. *Amino Acids* **38**, 1101–1106. https://doi.org/10.1007/s00726-009-0319-7 (2010).

131. Shimazaki, Y., Yajima, T. & Yamauchi, O. Properties of the indole ring in metal complexes. A comparison with the phenol ring. *J. Inorg. Biochem.* **148**, 105–115. https://doi.org/10.1016/j.jinorgbio.2015.03.001 (2015).

132. Zhang, S., Casey, N. & Lee, J. P. Residual structure in the Alzheimer's disease peptide: Probing the origin of a central hydrophobic cluster. *Fold. Des.* **3**, 413–422. https://doi.org/10.1016/S1359-0278(98)00054-6 (1998).

133. Knecht, S., Ricklin, D., Eberle, A. N. & Ernst, B. Oligohis-tags: Mechanisms of binding to Ni^{2+}-NTA surfaces. *J. Mol. Recognit.* **22**, 270–279. https://doi.org/10.1002/jmr.941 (2009).

134. Bousejra-ElGarah, F., Bijani, C., Coppel, Y., Faller, P. & Hureau, C. Iron(II) binding to amyloid-β, the Alzheimer's peptide. *Inorg. Chem.* **50**, 9024–9030. https://doi.org/10.1021/ic201233b (2011).

135. Faller, P. & Hureau, C. Bioinorganic chemistry of copper and zinc ions coordinated to amyloid-β peptide. *Dalton Trans.* https://doi.org/10.1039/b813398k (2009).

136. Faller, P. Copper and zinc binding to amyloid-β: Coordination, dynamics, aggregation, reactivity and metal-ion transfer. *ChemBioChem* **10**, 2837–2845. https://doi.org/10.1002/cbic.200900321 (2009).

137. Irving, H. M. N. H. & Williams, R. J. P. The stability of transition-metal complexes. *J. Chem. Soc.* 3192–3210 (1953).

138. Alies, B. *et al.* Cu(II) affinity for the Alzheimer's peptide: Tyrosine fluorescence studies revisited. *Anal. Chem.* **85**, 1501–1508. https://doi.org/10.1021/ac302629u (2013).

139. Bar-Or, D., Curtis, G., Rao, N., Bampos, N. & Lau, E. Characterization of the Co(2+) and Ni(2+) binding amino-acid residues of the N-terminus of human albumin. An insight into the mechanism of a new assay for myocardial ischemia. *Eur. J. Biochem.* **268**, 42–47. https://doi.org/10.1046/j.1432-1327.2001.01846.x (2001).

140. Mital, M. *et al.* A functional role for Aβ in metal homeostasis? N-truncation and high-affinity copper binding. *Angew. Chem. Int. Ed. Engl.* **54**, 10460–10464. https://doi.org/10.1002/anie.201502644 (2015).

141. Masters, C. L. *et al.* Amyloid plaque core protein in Alzheimer disease and Down syndrome. *Proc. Natl. Acad. Sci. USA* **82**, 4245–4249. https://doi.org/10.1073/pnas.82.12.4245 (1985).

142. Masters, C. L. *et al.* Neuronal origin of a cerebral amyloid: Neurofibrillary tangles of Alzheimer's disease contain the same protein as the amyloid of plaque cores and blood vessels. *EMBO J.* **4**, 2757–2763. https://doi.org/10.1002/j.1460-2075.1985.tb04000.x (1985).

143. Lewis, H. *et al.* Quantification of Alzheimer pathology in ageing and dementia: Age-related accumulation of amyloid-β(42) peptide in vascular dementia. *Neuropathol. Appl. Neurobiol.* **32**, 103–118. https://doi.org/10.1111/j.1365-2990.2006.00696.x (2006).

144. Portelius, E. *et al.* Mass spectrometric characterization of brain amyloid β isoform signatures in familial and sporadic Alzheimer's disease. *Acta Neuropathol.* **120**, 185–193. https://doi.org/10.1007/s00401-010-0690-1 (2010).

145. Hedberg, Y. S. *et al.* Synergistic effects of metal-induced aggregation of human serum albumin. *Colloids Surf. B Biointerfaces* **173**, 751–758. https://doi.org/10.1016/j.colsurfb.2018.10.061 (2019).

146. Lee, S. J., Nam, E., Lee, H. J., Savelieff, M. G. & Lim, M. H. Towards an understanding of amyloid-β oligomers: Characterization, toxicity mechanisms, and inhibitors. *Chem. Soc. Rev.* **46**, 310–323. https://doi.org/10.1039/c6cs00731g (2017).

147. Sengupta, U., Nilson, A. N. & Kayed, R. The role of amyloid-β oligomers in toxicity, propagation, and immunotherapy. *EBioMedicine* **6**, 42–49. https://doi.org/10.1016/j.ebiom.2016.03.035 (2016).

148. Bode, D. C., Baker, M. D. & Viles, J. H. Ion channel formation by amyloid-β42 oligomers but not amyloid-β40 in cellular membranes. *J. Biol. Chem.* **292**, 1404–1413. https://doi.org/10.1074/jbc.M116.762526 (2017).

149. Kim, M., Son, J. & Kim, Y. NMR studies of the ion channel-forming human amyloid-β with zinc ion concentrations. *Membranes* https://doi.org/10.3390/membranes11110799 (2021).

150. Lee, M. C. *et al.* Zinc ion rapidly induces toxic, off-pathway amyloid-β oligomers distinct from amyloid-β derived diffusible ligands in Alzheimer's disease. *Sci. Rep.* **8**, 4772. https://doi.org/10.1038/s41598-018-23122-x (2018).

151. Garai, K., Sengupta, P., Sahoo, B. & Maiti, S. Selective destabilization of soluble amyloid β oligomers by divalent metal ions. *Biochem. Biophys. Res. Commun.* **345**, 210–215. https://doi.org/10.1016/j.bbrc.2006.04.056 (2006).

152. Williams, T. L., Serpell, L. C. & Urbanc, B. Stabilization of native amyloid β-protein oligomers by copper and hydrogen peroxide induced cross-linking of unmodified proteins (CHICUP). *Biochem. Biophys. Acta.* **249–259**, 2016. https://doi.org/10.1016/j.bbapap.2015.12.001 (1864).

153. Yu, L. *et al.* Structural characterization of a soluble amyloid β-peptide oligomer. *Biochemistry* **48**, 1870–1877. https://doi.org/10.1021/bi802046n (2009).

154. Gu, L., Liu, C. & Guo, Z. Structural insights into Aβ42 oligomers using site-directed spin labeling. *J. Biol. Chem.* **288**, 18673–18683. https://doi.org/10.1074/jbc.M113.457739 (2013).

155. Nag, K. & Chakravorty, A. Monovalent, trivalent and tetravalent nickel. *Coord. Chem. Rev.* **33**, 87–147 (1980).

156. Smith, D. P. *et al.* Concentration dependent Cu^{2+} induced aggregation and dityrosine formation of the Alzheimer's disease amyloid-β peptide. *Biochemistry* **46**, 2881–2891. https://doi.org/10.1021/bi0620961 (2007).

157. Wang, J. *et al.* Peptide backbone-copper ring structure: A molecular insight into copper-induced amyloid toxicity. *Chin. Phys. B.* **31**(10), 108702. https://doi.org/10.1088/1674-1056/ac8920 (2022).

158. Al-Hilaly, Y. K. *et al.* A central role for dityrosine crosslinking of Amyloid-β in Alzheimer's disease. *Acta Neuropathol. Commun.* **1**, 83. https://doi.org/10.1186/2051-5960-1-83 (2013).

159. Kok, W. M. *et al.* Synthetic dityrosine-linked β-amyloid dimers form stable, soluble, neurotoxic oligomers. *Chem. Sci.* **4**, 4449–4454 (2013).

Author contributions

A.G., E.B., P.R., S.W., and T.S. designed the study. F.V. and A.B carried out and evaluated the IR and PAGE studies. E.B., S.P., and S.W. carried out and evaluated the NMR studies. I.I., J.P., L.A.M.-R., and L.O. carried out and evaluated the AFM studies. E.B., J.J., S.W., T.S., and X.D. carried out and evaluated the CD and fluorescence studies. All authors helped with preparing the manuscript.

Competing interests

The authors declare no competing interests.

Additional information

Supplementary Information The online version contains supplementary material available at https://doi.org/10.1038/s41598-023-29901-5.

Correspondence and requests for materials should be addressed to E.B. or S.K.T.S.W.

Reprints and permissions information is available at www.nature.com/reprints.

Publisher's note Springer Nature remains neutral with regard to jurisdictional claims in published maps and institutional affiliations.

Publication III

Noormagi, A., Golubeva, T., **Berntsson, E**., Warmlander, S., Tougu, V., & Palumaa, P. (2023). Direct Competition of ATCUN Peptides with Human Serum Albumin for Copper(II) Ions Determined by LC-ICP MS. ACS Omega, 8(37), 33912-33919. https://doi.org/10.1021/acsomega.3c04649

Article

Direct Competition of ATCUN Peptides with Human Serum Albumin for Copper(II) Ions Determined by LC-ICP MS

Andra Noormägi, Tatjana Golubeva, Elina Berntsson, Sebastian K.T.S. Wärmländer, Vello Tõugu, and Peep Palumaa*
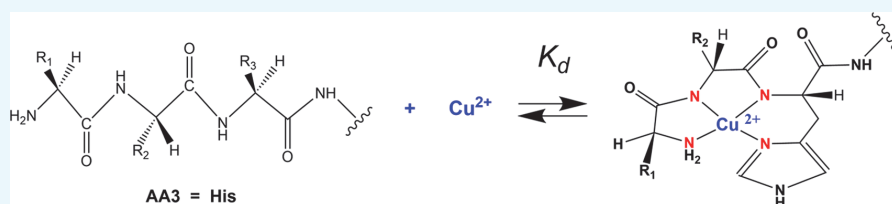
Read Online

ACCESS | Metrics & More | Article Recommendations | Supporting Information

ABSTRACT: Copper is an indispensable biometal, primarily serving as a redox-competent cofactor in numerous proteins. Apart from preformed copper-binding sites within the protein structures, small peptide motifs exist called ATCUN, which are composed of an N-terminal tripeptide XZH, able to bind Cu(II) ions in exchangeable form. These motifs are common for serum albumin, but they are also present in a wide range of proteins and peptides. These proteins and peptides can be involved in copper metabolism, and copper ions can affect their biological role. The distribution of copper between the ATCUN peptides, including truncated amyloid-β (Aβ) peptides Aβ4−42 and Aβ11−42, which may be involved in Alzheimer's disease pathogenesis, is mainly determined by their concentrations and relative Cu(II)-binding affinities. The Cu(II)-binding affinity (log K_d) of several ATCUN peptides, determined by different methods and authors, varies by more than three orders of magnitude. This variation may be attributed to the chemical properties of peptides but can also be influenced by the differences in methods and experimental conditions used for the determination of K_d. In the current study, we performed direct competition experiments between selected ATCUN peptides and HSA by using an LC-ICP MS-based approach. We demonstrated that ATCUN and truncated Aβ peptides Aβ4−16 and Aβ11−15 bind Cu(II) ions with an affinity similar to that for HSA. Our results demonstrate that ATCUN motifs cannot compete with excess HSA for the binding of Cu(II) ions in the blood and cerebrospinal fluid.

■ INTRODUCTION

Copper is an essential microelement for all forms of life, but its chemical properties make it potentially toxic, which is why its metabolism is always tightly regulated in living organisms. The biological functions of copper are almost exclusively carried out in the protein-bound form. Bioinformatic analysis revealed that Cu proteome constitutes approximately 0.05−1.3% of the total proteome of an organism, considering both eukaryotes and prokaryotes.[1] It is estimated that there are 54 Cu-binding proteins in the human proteome.[2]

In addition to 3D copper-binding pockets within protein structures, Cu(II) ions can also strongly bind to an N-terminal motif called ATCUN (amino terminal Cu- and Ni-binding motif). The ATCUN motif contains a His residue in the third position (XZH) and is present in more than 400 human proteins, including human serum albumin (HSA).[3] Approximately 10% of the total copper present in human serum is bound to the ATCUN motif of HSA. This copper binding is exchangeable, and it is possible that all other extracellular ATCUN proteins can also play a role in copper metabolism or that their biological functions may depend on copper binding.

To participate in copper metabolism or perform their biological functions, other extracellular ATCUN proteins must compete with HSA for copper binding. The amount of copper that these proteins can bind depends on their relative concentration and affinity for metal binding. The metal-binding affinities of peptides with an ATCUN motif have been intensively studied by different methods, and the range of log K_a values determined for ATCUN sites ranges from 11.0 to 14.6.[4] Selected values of dissociation constants for ATCUN motif-containing peptides and proteins from the literature are listed in Table 1.

ATCUN complexes have a characteristic four-nitrogen (4N) square-planar coordination mode, where the metal ion is

A

Table 1. Dissociation Constants for Cu(II) Complexes with ATCUN Motif-Containing Peptides and Proteins

peptide/protein	method	K_d	refs
MDH-NH$_2$	potentiometric titration, pH 7.4	7.94×10^{-14}	5
MDHSHHMGMSYMDS-NH$_2$	potentiometric titration, pH 7.4	1.0×10^{-13}	6
GGH	potentiometric titration, pH 7.4	6.10×10^{-13}	7
HSA	potentiometric titration, pH 7.4	9.55×10^{-14}	7
DAH − NH$_2$	potentiometric titration, pH 7.4	2.00×10^{-14}	8,5
MEHFPGP (Semax)	potentiometric titration, pH 7.4	1.3×10^{-15}	9
DTHFPI-NH$_2$ (Hepcidin N-terminus)	potentiometric titration, pH 7.4	$2{,}19 \times 10^{-15}$	10
Aβ4−16-NH$_2$	potentiometric titration, pH 7.4	3×10^{-14}	4
Aβ11−15-NH$_2$	competition with Gly and His	2.5×10^{-14} (Gly) 4.2×10^{-14} (His)	11

located in the center of a square whose edges are occupied by four nitrogen atoms, provided by the N-terminal amine, two subsequent nitrogen atoms in peptide backbone, and the N-1 nitrogen of the His imidazole ring (Figure 1).
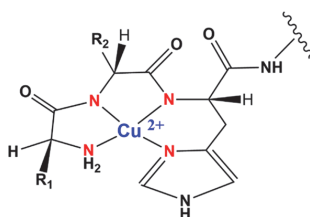
Figure 1. Schematic presentation of the Cu(II)−ATCUN complex.

Numerous explanations have been proposed to account for the differences in reported K_d values for ATCUN motifs, such as differences in the pK_a values of individual peptide nitrogens,[12,13] variances in the hydrophobicity of the first two amino acid residues,[13] and variances in the secondary coordination sphere effects. Although all of these factors may influence Cu(II)-binding affinities to some extent, differences might also be caused by using many different methods for calculating metal-binding affinities. It is well known that such measurements are strongly affected by the experimental conditions, which typically vary between different studies.[14] An example depicting this is the data showing that two residues at the N-terminal side of His3 do not significantly contribute to the binding of Cu(II) ions.[12] This uncertain situation complicates the possibility of studying copper trafficking in the organisms and modeling the availability of copper ions to different peptides and proteins.

The binding of Cu(II) to an ATCUN motif substantially alters the electrochemical properties of the Cu(II)/Cu(I) redox couple. The Cu−ATCUN complex has antioxidant properties, as it shows a redox-silent component in the presence of the biological reductant ascorbate due to its high redox potential and inherent geometry problem between Cu(II) and Cu(I) complexes.[15]

Having a clear understanding of copper trafficking is crucial for understanding the possible involvement of copper ions in Alzheimer's disease (AD) pathogenesis. AD is characterized by the initial formation of amyloid plaques in the brain, followed by formation of neurofibrillary tangles inside the neurons.[16] Amyloid plaques are composed of amyloid-β peptides (Aβ) of various lengths, mainly Aβ1−40 and Aβ1−42.[16,17] However, an initial study by Masters et al. demonstrated that the plaques contained a significant amount of the truncated Aβ4−42

peptide.[18] In later mass spectrometric studies, substantial amounts of truncated Aβ4−42[19] and Aβ11−42 peptides[20,21] were found in plaques as well as in the cerebrospinal fluid (CSF).[22] Since both truncated peptides carry the ATCUN motifs, it raises the question of whether Aβ peptides can bind Cu(II) ions in vivo in the presence of HSA.

The interactions of Aβ peptides with Cu(II) ions have been extensively studied. It has been demonstrated that full-length Aβ peptides can bind Cu(II) ions with relatively strong affinity, with a K_d value up to 0.1−1 nM,[14,23,24] which is still several orders of magnitude lower than that of HSA. Truncated Aβ peptides Aβ4-X and Aβ11-X contain the FRH- and EVH-ATCUN motifs, respectively. By using potentiometric titration, it was demonstrated that Aβ4−16 binds Cu(II) with a conditional K_d value of 3×10^{-14} M at pH 7.4,[4] which characterized at that time 30 times higher affinity than that for HSA ($K_d = 1 \times 10^{-12}$ M was determined from the competition with NTA[25]). Based on these results, it was suggested that Aβ4−40 could have a physiological role in copper homeostasis,[4] which might be linked to the scavenging of Cu(II) ions in the synaptic cleft.[26] The Cu(II)-binding affinity of Aβ11−40 determined from the results of CD spectroscopic titration of the Cu(II)−Aβ11−40 complex with His and Gly is similar to that for Aβ4−16, i.e., $K_d = 3.4 \times 10^{-14}$ M.[11] At that time, this pointed toward efficient competition with HSA. Recently, the K_d value for HSA was corrected to 0.955×10^{-13} M by using potentiometric titration,[7] which reflects only three times lower affinity than those for Aβ4−16 and Aβ11−40. HSA is present in CSF at 3 μM concentration,[27] which is much higher than the nM concentration of Aβ peptides.[28] These data suggest that Aβ peptides should not be able to compete with HSA for Cu(II) binding.[11] However, direct competition experiments have not yet been conducted.

In this study, we attempted to answer the following two related questions: "Do different ATCUN motifs show different Cu(II)-binding affinities under the conditions of direct competition?" "Can truncated Aβ peptides with ATCUN motifs compete in CSF with HSA for the binding of Cu(II) ions?" To address the raised questions, we employed an innovative LC-ICP MS technique, enabling the use of size exclusion chromatography (SEC) to separate and quantify the substances with high molecular weight (HSA) and low molecular weight (ATCUN peptides) involved in metal binding within the reaction mixture.[29]

We determined the relative Cu(II)-binding affinities for several model peptides and two truncated Aβ peptides in comparison with HSA. Results demonstrate that different ATCUN-containing peptides and HSA have very similar Cu(II)-binding affinities, and truncated Aβ peptides cannot

compete with HSA for the binding of Cu(II) ions in blood or even in CSF.

RESULTS

First, Cu(II) competition experiments were performed with the aim of determining the incubation time required to achieve the equilibrium of Cu(II) distribution between HSA- and ATCUN-containing peptides. Figure 2 demonstrates that equilibrium is reached within 30 min.

Kinetic experiments were also conducted in conditions where Aβ(11−15) was added to the metalated HSA (Figures S1 and S2) and when HSA was added to the metalated Aβ(11−15) (data not shown). In the first case, equilibrium was reached in 30 min (Figure S3) both in the equimolar mixture and in the presence of a 2-fold excess of the competing (apo) ligand. In the second case, the equilibrium was reached very quickly within 2 min. Based on this kinetic information for subsequent experiments, Cu(II) ions were added to the mixture of HSA and ATCUN peptides, and an incubation time of 30 min was selected.

The next series of experiments involved determining the competition between HSA and ATCUN peptides for Cu(II) binding. Figure 3 shows an example of the results obtained with the Aβ(11−15) peptide. When this peptide and HSA are present in equimolar concentrations, Cu(II) ions are distributed 60% in HSA and 40% in the Aβ(11−15) peptide (Figure 3c). This suggests that both HSA and the Aβ(11−15) peptide are able to compete almost equally for Cu(II) binding. As the Aβ(11−15) concentration is increased, the distribution of Cu(II) ions shifts toward the peptide, and at an Aβ(11−15) concentration of 40 μM, the metal distribution reaches a ratio of 13:87 in favor of the Aβ(11−15) peptide (Figure 3g).

The obtained results were analyzed according to eq 2, which predicts a linear relationship between X = [Cu(Pept)]([HSA]$_T$ − [Cu(HSA)]) and Y = [Cu(HSA)]([Pept]$_T$ − [Cu(Pept)]), where [Cu(HSA)] and [Cu(Pept)] are determined from the chromatograms as the copper content of high- and low-molecular-weight fractions and [HSA]$_T$ and [Pept]$_T$ are the total added concentrations of each ligand (see eqs 1−4 from the Materials and Methods). The relationship observed from three independent experiments is shown in Figure 4B, and it is linear with a slope of K_d (Aβ11−15)/K_d(HSA) equal to 1.56 ± 0.09. Using the known value of K_d for HSA, which is equal to 0.955 × 10^{-13} M,[7] we can calculate the K_d value for Aβ11−15 to be 1.49 ± 0.09 × 10^{-13} M.

The representative examples of primary data for other ATCUN peptides are provided in the Supporting Information. Relationships between X and Y, based on eq 2, for these peptides are shown in Figures 5 and S8.

The obtained K_d values are presented in Table 2.

DISCUSSION

The distribution of copper ions between competing ligands, such as peptides and proteins with ATCUN motifs, is determined by thermodynamic and kinetic factors. The distribution in equilibrium can be calculated from the K_d values of the ATCUN−Cu(II) complexes. However, the K_d values can be affected by several factors; for instance, they can be affected by experimental conditions and intermolecular interactions at higher concentrations of the reagents. In this paper, we have determined the relative binding affinities for different Cu(II)-binding ligands in direct competition experi-
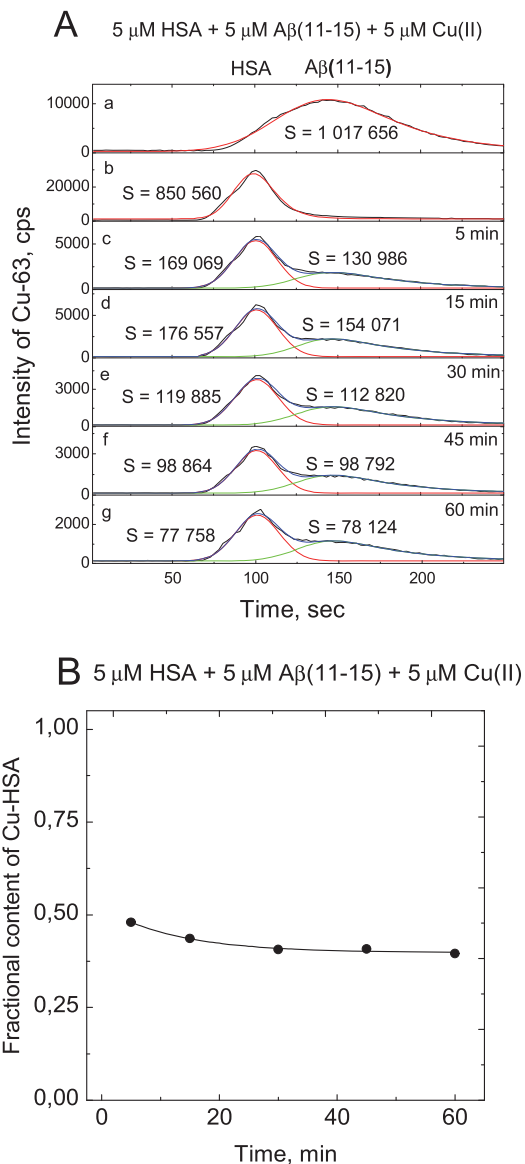
Figure 2. Competition between HSA and Aβ(11−15) peptide for Cu(II) ions. (A) SEC chromatograms of copper distribution (incubation time and integrated peak area values are shown in labels). (B) Decrease of the relative content of copper in the HSA fraction with time. Conditions: 5 μM HSA, 5 μM Aβ(11−15), and 5 μM Cu(II); incubation buffer 50 mM HEPES, 50 mM NaCl, pH 7.4; LC-ICP MS: column, 1 mL Sephadex G25 Superfine; elution buffer 200 mM NH$_4$NO$_3$, pH 7.4; flow rate 0.4 mL/min; injection volume 10 μL; Cu-63 was monitored by ICP MS.
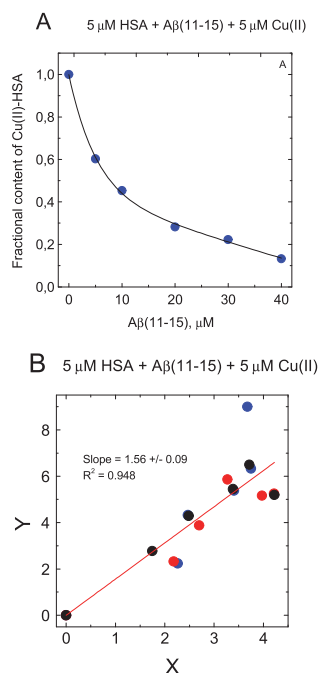
ments with binary mixtures. We have conducted such experiments with different Cu(II)-binding peptides and HSA as standard by using LC-ICP MS technology, which is suitable for this purpose. In these experiments, the different ATCUN-containing peptides display rather similar abilities to compete
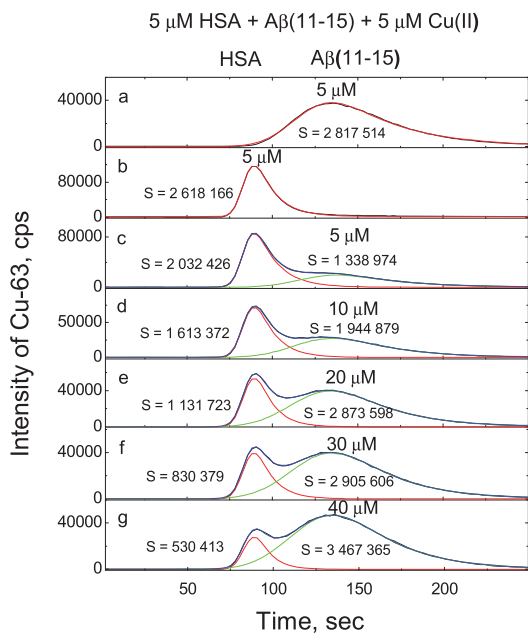
Figure 3. Competition between HSA and the Aβ(11−15) peptide for Cu(II) ions. SEC chromatograms of (a) 5 μM Cu(II)● Aβ(11−15), (b) 5 μM Cu(II)●HSA, and (c−g) 5 μM HSA and Cu(II) in the presence of increasing concentration of Aβ(11−15). The peptide concentrations and peak areas are shown in labels. Conditions; incubation buffer 50 mM HEPES, 50 mM NaCl, pH 7.4; incubation time 30 min; LC-ICP MS: column, 1 mL Sephadex G25 Superfine; elution buffer 200 mM NH4NO3, pH 7.4; flow rate 0.4 mL/min; injection volume 10 μL; Cu-63 was monitored by ICP MS.

Figure 4. Calculation of the relative Cu(II)-binding affinity of Aβ(11−15) from LC-ICP MS results. (A) Decrease of the fractional content of the Cu●HSA complex, caused by the increase of Aβ(11−15) concentration. (B) Application of eq 2. Results of three separate experiments are presented with different colors—red, blue, and black.

with HSA for Cu(II) ions. Correspondingly, their binding affinities toward Cu(II) ions are also similar. These results are different from the results of potentiometric titration measurements. A comparison between DAH-NH2 and DAH-COOH indicates that C-terminal amidated peptides have slightly higher binding affinities than peptides with a free C-terminal carboxyl group, which is in agreement with the literature.[8] At the same time, the K_d value for DAH-NH2, a tripeptide originating from HSA, was almost similar to the K_d value for HSA, demonstrating that amidated tripeptides can be good and sufficient Cu(II)-binding models for ATCUN-containing proteins.

In the literature, the amidated hexa- and heptapeptides (DTHFPI-NH2 and MEHFPGP) have shown binding affinities that exceed that of HSA by 44 and 73 times, respectively (Table 1). However, in the direct competition experiments, these peptides displayed rather similar K_d values to HSA and also to the simplest model peptide GGH. This result suggests that the primary coordination sphere of the ATCUN motif, composed of four nitrogen atoms provided by the N-terminal amine, two subsequent peptide nitrogen atoms, and the N-1 nitrogen of the His imidazole ring, plays a crucial role in the binding of Cu(II) ions and determines the binding affinity. It also suggests that the chemical properties of the first two amino acid side chains and the post-His amino acid residues do not contribute significantly to the metal binding.

Direct competition experiments showed that truncated Aβ peptides, i.e., Aβ4−16 and Aβ11−15, have K_d values similar to HSA for Cu(II) binding (Table 2). Aβ11−15 has a 1.3 times higher affinity toward Cu(II) ions than Aβ4−16. This small difference might be explained by the His14 residue contributing to ATCUN motif Cu(II) binding in the Aβ11−15 peptide. HSA is present in blood at 650 μM[30] and in CSF at 3 μM concentration,[27] which are much higher than the nM concentrations of Aβ peptides in CSF and blood.[28,31] Based on these numbers, we conclude that Aβ peptides cannot compete with HSA for Cu(II) binding[11] in blood or CSF.

Overall, we argue that the direct competition experiments with HSA and the K_d values determined from these experiments describe the properties of ACTUN-motif-containing peptides in biological conditions more correctly than the K_d values determined from separate potentiometric titration experiments. In the latter case, the interactions between the peptides in the solution may also affect the titration results in a way that does not occur in biological conditions where the peptide concentration is very low.

■ CONCLUSIONS

Peptides with His in the third position are known as ATCUN peptides, which are able to bind Cu(II) ions with a high affinity. In the literature, the reported dissociation constants for different ATCUN peptides vary widely. We performed direct competition experiments with selected ATCUN motifs, including truncated Aβ peptides, in relation to HSA using an LC-ICP MS-based approach. We demonstrated that Cu(II)-
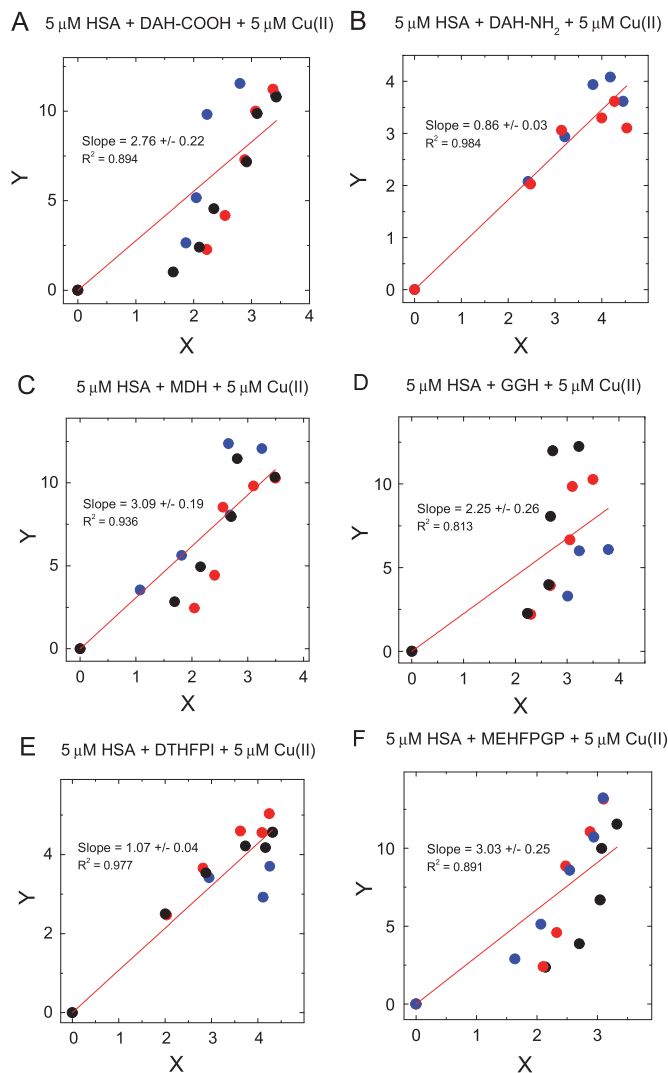
Figure 5. Calculation of the relative Cu(II)-binding affinity of ATCUN peptides from LC-ICP MS results according to eq 2. (A) DAH-COOH, (B) DAH-NH$_2$, (C) MDH-NH$_2$, (D) GGH-NH$_2$, (E) DTHFPI-NH$_2$, and (F) MEHFPGP-NH$_2$. Results of three separate experiments are presented with different colors: red, blue, and black.

binding affinities of ATCUN and truncated Aβ peptides are similar to those for HSA and vary in a narrow range. Our results demonstrate that ATCUN motifs cannot remove substantial amounts of Cu(II) ions from excess HSA in blood and CSF environments.

■ MATERIALS AND METHODS

Materials. The following lyophilized protein and peptides were used: human serum albumin (HSA) from Sigma/Merck (Darmstadt, Germany), Aβ(4−16) and Aβ(11−15) peptides from rPeptide (Watkinsville, GA), and DAH-COOH, DAH-NH$_2$, MDH-NH$_2$, GGH-NH$_2$, DTHFPI-NH$_2$, and MEHFPGP-NH$_2$ were synthesized at the Institute of Technology of the University of Tartu. The peptides were

synthesized on an automated peptide synthesizer (Biotage Initiator+ Alstra, Sweden) using a fluorenylmethyloxycarbonyl (Fmoc) solid-phase peptide synthesis strategy and purified by reverse-phase liquid chromatography on a C4 column (Phenomenex Jupiter C4, 5 μm, 300 A, 250 × 10 mm) using a gradient of acetonitrile/water containing 0.1% TFA. The molecular weight of the peptides was determined by a MALDI-TOF mass spectrometer (Bruker Microflex LT/SH). 1,1,1,3,3,3-Hexafluoro-2-propanol (HFIP), sodium chloride, sodium hydroxide, and 4-(2-hydroxyethyl)-1-piperazineetha-nesulfonic acid (Hepes) were purchased from Sigma-Aldrich (St. Louis, MO). Cu(II)acetate was purchased from Sigma (Sigma/Merck KGaA, Darmstadt, Germany). Nitric acid (HNO$_3$, trace metal grade) was purchased from Fisher

Table 2. Dissociation Constants for Cu(II) Complexes of ATCUN Motif-Containing Peptides and HSA

peptide	K_d, M
GGH-NH$_2$	$(2.15 \pm 0.25) \times 10^{-13}$
MDH-NH$_2$	$(2.95 \pm 0.18) \times 10^{-13}$
DAH-COOH	$(2.64 \pm 0.21) \times 10^{-13}$
DAH-NH$_2$	$(8.21 \pm 0.29) \times 10^{-14}$
DTHFPI-NH$_2$	$(1.02 \pm 0.04) \times 10^{-13}$
MEHFPGP-NH$_2$	$(2.89 \pm 0.24) \times 10^{-13}$
Aβ(11−15)	$(1.49 \pm 0.09) \times 10^{-13}$
Aβ(4−16)	$(2.00 \pm 0.11) \times 10^{-13}$
HSA*	9.55×10^{-14}

*From ref 4.

Scientific (UK Limited Leicestershire, UK), and ammonium hydroxide 25% solution was from Honeywell Fluka (Seelze, Germany). Ultrapure Milli-Q water with a resistivity of 18.2 MΩ/cm, produced by a Merck Millipore Direct-Q & Direct−Q UV water purification system (Merck KGaA, Darmstadt, Germany), was used for all applications.

Competition for Cu(II) Ions Determined by LC-ICP MS Analysis. *Sample Preparation.* All lyophilized peptides were dissolved in HFIP at a concentration of 100 μM to disassemble the preformed aggregates. The solution was divided into aliquots; HFIP was evaporated in vacuum, and the tubes containing the peptide film were stored at −80 °C until used.

A stock solution of HSA was prepared in Milli-Q water and further diluted into a reaction buffer solution composed of 50 mM Hepes and 50 mM NaCl, pH 7.4. HFIP-treated peptide aliquots were dissolved in 50 mM HEPES and 50 mM NaCl, pH 7.4, at a concentration of 50 μM and further diluted to the final concentration with reaction buffer. Cu(II)acetate was used as a Cu(II) source for proteins and peptides. For a competition experiment, an appropriate concentration of competing peptides (Aβ(11−15), Aβ(4−16), DAH-COOH, DAH-NH$_2$, MDH-NH$_2$, GGH-NH$_2$, DTHFPI-NH$_2$, or MEHFPGP-NH$_2$) and a 5 μM solution of HSA were mixed with 5 μM Cu(II), and the sample was incubated 30 min at room temperature. All reagent solutions were prepared daily before experiments.

LC-ICP MS Measurements. For LC-ICP MS analyses, an Agilent Technologies (Santa Clara) Infinity HPLC system, which consisted of a 1260 series μ-degasser, a 1200 series capillary pump, a Micro WPS autosampler, and a 1200 series MWD VL detector, was connected to an Agilent 7800 series ICP MS instrument. For instrument control and data acquisition, ICP MS MassHunter 4.4 software, version C 01.04, from Agilent was used. ICP MS was operated under the following conditions: RF power: 1550 W, nebulizer gas flow: 1.03 L/min, auxiliary gas flow: 0.90 L/min, plasma gas flow: 15 L/min, nebulizer type: MicroMist, and isotope monitored: Cu-63. To perform the separation of HMW and LMW pools, a 1 mL gel filtration column, self-packed with HiTrap Desalting resin Sephadex G25 Superfine (Amersham/GE Healthcare, Buckinghamshire, UK), was used. An injection volume of 10 μL for each sample was used. The mobile phase for gel filtration was 200 mM NH$_4$NO$_3$ at pH 7.5, prepared from TraceMetal grade nitric acid and ammonium hydroxide 25% solution, which is compatible with ICP MS. An ICP MS compatible flow rate of 0.4 mL/min was used in all separations. To get rid of contaminating metal ions in the buffer, the mobile phase was eluted through the Chelex 100 Chelating Ion

Exchange resin (Sigma, Merck KGaA, Darmstadt, Germany) prior to liquid chromatographic separation. The demetalation of the SEC columns before each experiment was conducted by injecting 1 mM EDTA into the columns (injection volumes were the same for all experiments).

Separation of the HMW and LMW peak areas was conducted with Origin Pro 8.5 software. An exponentially modified Gaussian peak function (GaussMod) was used to obtain peak areas that were further used to calculate a decrease in the fractional content of the metalated protein. All experiments were repeated three times.

Determination of Relative Dissociation Constants. Experimental results for competition for Cu(II) ions between HSA- and ATCUN-containing peptides were used for the determination of the relative dissociation constant for the ATCUN-containing peptide and HSA copper complexes. The ratio of the dissociation constants for the peptide and HSA can be expressed as follows[7]

$$\frac{K_{d(Pept)}^{Cu}}{K_{d(HSA)}^{Cu}} = \frac{[Cu(HSA)]([Pept]_T - [Cu(Pept)])}{[Cu(Pept)]([HSA]_T - [Cu(HSA)])} \quad (1)$$

or

$$[Cu(HSA)]([Pept]_T - [Cu(Pept)])$$
$$= \frac{K_{d(Peptide)}^{Cu}}{K_{d(HSA)}^{Cu}}[Cu(Pept)]([HSA]_T - [Cu(HSA)]) \quad (2)$$

$$X = [Cu(Pept)]([HSA]_T - [Cu(HSA)]) \quad (3)$$

$$Y = [Cu(HSA)]([Pept]_T - [Cu(Pept)]) \quad (4)$$

where [Cu(HSA)] and [Cu(Pept)] are determined from the chromatograms as the copper content of high- and low-molecular-weight fractions, and [HSA]$_T$ and [Pept]$_T$ are the total added concentrations of each ligand.

■ ASSOCIATED CONTENT

ⓢ Supporting Information

The Supporting Information is available free of charge at https://pubs.acs.org/doi/10.1021/acsomega.3c04649.

Kinetics of Cu(II) exchange between HSA and ATCUN peptides (Figures S1−S3); competitions between HSA and ATCUN peptides for Cu(II) ions (Figures S4−S10); and calculation of relative Cu(II)-binding affinity of Aβ(4−16) (Figure S11) (PDF)

■ AUTHOR INFORMATION

Corresponding Author

Peep Palumaa − *Department of Chemistry and Biotechnology, Tallinn University of Technology, 12618 Tallinn, Estonia;* ◉ orcid.org/0000-0002-3505-3466; Phone: +372 6204410; Email: peep.palumaa@taltech.ee

Authors

Andra Noormägi − *Department of Chemistry and Biotechnology, Tallinn University of Technology, 12618 Tallinn, Estonia*

Tatjana Golubeva − *Department of Chemistry and Biotechnology, Tallinn University of Technology, 12618 Tallinn, Estonia*

Elina Berntsson − *Department of Chemistry and Biotechnology, Tallinn University of Technology, 12618*

Tallinn, Estonia; Chemistry Section, Stockholm University, 10691 Stockholm, Sweden; ● orcid.org/0000-0002-7544-092X

Sebastian K.T.S. Wärmländer − Chemistry Section, Stockholm University, 10691 Stockholm, Sweden

Vello Tõugu − Department of Chemistry and Biotechnology, Tallinn University of Technology, 12618 Tallinn, Estonia

Complete contact information is available at:
https://pubs.acs.org/10.1021/acsomega.3c04649

Author Contributions

P.P., V.T., and A.N. conceived and designed the experiments. A.N., T.G., and E.B. carried out the experiments. All authors contributed to the analysis and interpretation of the results. P.P. and V.T. wrote the manuscript with support from S.W. and A.N. Review and editing were carried out by P.P., V.T., and S.W. All authors discussed the results and contributed to the final manuscript. P.P. supervised the project.

Notes

The authors declare no competing financial interest.

■ REFERENCES

(1) Andreini, C.; Banci, L.; Bertini, I.; Rosato, A. Occurrence of copper proteins through the three domains of life: A bioinformatic approach. *J. Proteome Res.* **2008**, *7* (1), 209−216.

(2) Blockhuys, S.; Celauro, E.; Hildesjo, C.; Feizi, A.; Stal, O.; Fierro-Gonzalez, J. C.; Wittung-Stafshede, P. Defining the human copper proteome and analysis of its expression variation in cancers. *Metallomics* **2017**, *9* (2), 112−123.

(3) Frączyk, T. Cu(II)-Binding N-Terminal Sequences of Human Proteins. *Chem. Biodiversity* **2021**, *18* (4), No. e2100043.

(4) Mital, M.; Wezynfeld, N. E.; Fraczyk, T.; Wiloch, M. Z.; Wawrzyniak, U. E.; Bonna, A.; Tumpach, C.; Barnham, K. J.; Haigh, C. L.; Bal, W.; et al. A Functional Role for Abeta in Metal Homeostasis? N-Truncation and High-Affinity Copper Binding. *Angew. Chem., Int. Ed. Engl.* **2015**, *54* (36), 10460−10464. Research Support, Non-U.S. Gov't

(5) Bossak, K.; Drew, S. C.; Stefaniak, E.; Plonka, D.; Bonna, A.; Bal, W. The Cu(II) affinity of the N-terminus of human copper transporter CTR1: Comparison of human and mouse sequences. *J. Inorg. Biochem.* **2018**, *182*, 230−237.

(6) Stefaniak, E.; Plonka, D.; Drew, S. C.; Bossak-Ahmad, K.; Haas, K. L.; Pushie, M. J.; Faller, P.; Wezynfeld, N. E.; Bal, W. The N-terminal 14-mer model peptide of human Ctr1 can collect Cu(ii) from albumin. Implications for copper uptake by Ctr1. *Metallomics* **2018**, *10* (12), 1723−1727.

(7) Bossak-Ahmad, K.; Fraczyk, T.; Bal, W.; Drew, S. C. The Sub-picomolar Cu(2+) Dissociation Constant of Human Serum Albumin. *Chembiochem* **2020**, *21* (3), 331−334. From NLM Medline.

(8) Mlynarz, P.; Valensin, D.; Kociolek, K.; Zabrocki, J.; Olejnik, J.; Kozlowski, H. Impact of the peptide sequence on the coordination abilities of albumin-like tripeptides towards Cu2+, Ni2+ and Zn2+ ions. Potential albumin-like peptide chelators. *New J. Chem.* **2002**, *26* (2), 264−268.

(9) Tabbì, G.; Magri, A.; Giuffrida, A.; Lanza, V.; Pappalardo, G.; Naletova, I.; Nicoletti, V. G.; Attanasio, F.; Rizzarelli, E. Semax, an ACTH4−10 peptide analog with high affinity for copper(II) ion and protective ability against metal induced cell toxicity. *J. Inorg. Biochem.* **2015**, *142*, 39−46. From NLM Medline.

(10) Płonka, D.; Bal, W. The N-terminus of hepcidin is a strong and potentially biologically relevant Cu(II) chelator. *Inorg. Chim. Acta* **2018**, *472*, 76−81.

(11) Barritt, J. D.; Viles, J. H. Truncated Amyloid-beta(11−40/42) from Alzheimer Disease Binds Cu2+ with a Femtomolar Affinity and Influences Fiber Assembly. *J. Biol. Chem.* **2015**, *290* (46), 27791−27802. Research Support, Non-U.S. Gov't

(12) Mlynarz, P.; Bal, W.; Kowalik-Jankowska, T.; Stasiak, M.; Leplawy, M. T.; Kozlowski, H. Introduction of alpha-hydroxyme-thylserine residues in a peptide sequence results in the strongest peptidic, albumin-like, copper(II) chelator known to date. *J. Chem. Soc. Dalton Trans.* **1999**, No. 2, 109−110.

(13) Miyamoto, T.; Fukino, Y.; Kamino, S.; Ueda, M.; Enomoto, S. Enhanced stability of Cu2+-ATCUN complexes under physiologically relevant conditions by insertion of structurally bulky and hydrophobic amino acid residues into the ATCUN motif. *Dalton Trans.* **2016**, *45* (23), 9436−9445.

(14) Alies, B.; Renaglia, E.; Rozga, M.; Bal, W.; Faller, P.; Hureau, C. Cu(II) affinity for the Alzheimer's peptide: tyrosine fluorescence studies revisited. *Anal. Chem.* **2013**, *85* (3), 1501−1508.

(15) Gonzalez, P.; Bossak, K.; Stefaniak, E.; Hureau, C.; Raibaut, L.; Bal, W.; Faller, P. N-Terminal Cu-Binding Motifs (Xxx-Zzz-His, Xxx-His) and Their Derivatives: Chemistry, Biology and Medicinal Applications. *Chem. − Eur. J.* **2018**, *24* (32), 8029−8041.

(16) Selkoe, D. J.; Hardy, J. The amyloid hypothesis of Alzheimer's disease at 25 years. *EMBO Mol. Med.* **2016**, *8* (6), 595−608.

(17) Glenner, G. G.; Wong, C. W. Alzheimer's disease: initial report of the purification and characterization of a novel cerebrovascular amyloid protein. *Biochem. Biophys. Res. Commun.* **1984**, *120* (3), 885−890.

(18) Masters, C. L.; Simms, G.; Weinman, N. A.; Multhaup, G.; McDonald, B. L.; Beyreuther, K. Amyloid plaque core protein in Alzheimer disease and Down syndrome. *Proc. Natl. Acad. Sci. U.S.A.* **1985**, *82* (12), 4245−4249. Research Support, Non-U.S. Gov't

(19) Portelius, E.; Bogdanovic, N.; Gustavsson, M. K.; Volkmann, I.; Brinkmalm, G.; Zetterberg, H.; Winblad, B.; Blennow, K. Mass spectrometric characterization of brain amyloid beta isoform signatures in familial and sporadic Alzheimer's disease. *Acta Neuropathol.* **2010**, *120* (2), 185−193. Research Support, N.I.H., Extramural Research Support, Non-U.S. Gov't

(20) Näslund, J.; Schierhorn, A.; Hellman, U.; Lannfelt, L.; Roses, A. D.; Tjernberg, L. O.; Silberring, J.; Gandy, S. E.; Winblad, B.; Greengard, P.; et al. Relative abundance of Alzheimer A beta amyloid peptide variants in Alzheimer disease and normal aging. *Proc. Natl. Acad. Sci. U.S.A.* **1994**, *91* (18), 8378−8382. Research Support, Non-U.S. Gov't Research Support, U.S. Gov't, P.H.S

(21) Liu, K.; Solano, I.; Mann, D.; Lemere, C.; Mercken, M.; Trojanowski, J. Q.; Lee, V. M. Characterization of Abeta11−40/42 peptide deposition in Alzheimer's disease and young Down's syndrome brains: implication of N-terminally truncated Abeta species in the pathogenesis of Alzheimer's disease. *Acta Neuropathol.* **2006**, *112* (2), 163−174. Research Support, N.I.H., Extramural

(22) Seubert, P.; Vigo-Pelfrey, C.; Esch, F.; Lee, M.; Dovey, H.; Davis, D.; Sinha, S.; Schlossmacher, M.; Whaley, J.; Swindlehurst, C.; et al. Isolation and quantification of soluble Alzheimer's beta-peptide from biological fluids. *Nature* **1992**, *359* (6393), 325−327. From NLM Medline.

(23) Young, T. R.; Kirchner, A.; Wedd, A. G.; Xiao, Z. An integrated study of the affinities of the Abeta16 peptide for Cu(I) and Cu(II): implications for the catalytic production of reactive oxygen species. *Metallomics* **2014**, *6* (3), 505−517. Research Support, Non-U.S. Gov't

(24) Conte-Daban, A.; Borghesani, V.; Sayen, S.; Guillon, E.; Journaux, Y.; Gontard, G.; Lisnard, L.; Hureau, C. Link between Affinity and Cu(II) Binding Sites to Amyloid-beta Peptides Evaluated by a New Water-Soluble UV-Visible Ratiometric Dye with a Moderate Cu(II) Affinity. *Anal. Chem.* **2017**, *89* (3), 2155−2162.

(25) Rózga, M.; Sokolowska, M.; Protas, A. M.; Bal, W. Human serum albumin coordinates Cu(II) at its N-terminal binding site with 1 pM affinity. *J. Biol. Inorg. Chem.* **2007**, *12* (6), 913−918.

(26) Wezynfeld, N. E.; Stefaniak, E.; Stachucy, K.; Drozd, A.; Plonka, D.; Drew, S. C.; Krezel, A.; Bal, W. Resistance of Cu(Abeta4− 16) to Copper Capture by Metallothionein-3 Supports a Function for the Abeta4−42 Peptide as a Synaptic Cu(II) Scavenger. *Angew. Chem., Int. Ed.* **2016**, *55* (29), 8235−8238. Research Support, Non-U.S. Gov't

(27) Stevens, R. W.; Elmendorf, D.; Gourlay, M.; Stroebel, E.; Gaafar, H. A. Application of fluoroimmunoassay to cerebrospinal fluid immunoglobulin G and albumin. *J. Clin. Microbiol.* **1979**, *10* (3), 346−350. From NLM Medline.

(28) van Steenoven, I.; van der Flier, W. M.; Scheltens, P.; Teunissen, C. E.; Lemstra, A. W. Amyloid-beta peptides in cerebrospinal fluid of patients with dementia with Lewy bodies. *Alzheimers Res. Ther.* **2019**, *11* (1), 83. From NLM Medline.

(29) Kirsipuu, T.; Zadorožnaja, A.; Smirnova, J.; Friedemann, M.; Plitz, T.; Tõugu, V.; Palumaa, P. Copper(II)-binding equilibria in human blood. *Sci. Rep.* **2020**, *10*, No. 5686.

(30) Jun, J. E.; Lee, S. E.; Lee, Y. B.; Jee, J. H.; Bae, J. C.; Jin, S. M.; Hur, K. Y.; Lee, M. K.; Kim, J. H. Increase in serum albumin concentration is associated with prediabetes development and progression to overt diabetes independently of metabolic syndrome. *PLoS One* **2017**, *12* (4), No. e0176209.

(31) Wallin, C.; Luo, J.; Jarvet, J.; Wärmländer, S. K. T. S.; Gräslund, G. The Amyloid-b Peptide in Amyloid Formation Processes: Interactions with Blood Proteins and Naturally Occurring Metal Ions. *Isr. J. Chem.* **2017**, *57*, 674−685.

Publication IV

Berntsson, E., Vosough, F., Noormagi, A., Padari, K., Asplund, F., Gielnik, M., Paul, S., Jarvet, J., Tougu, V., Roos, P. M., Kozak, M., Graslund, A., Barth, A., Pooga, M., Palumaa, P., & Warmlander, S. (2023). Characterization of Uranyl (UO_2^{2+}) Ion Binding to Amyloid Beta (Abeta) Peptides: Effects on Abeta Structure and Aggregation. ACS Chem Neurosci, 14(15), 2618-2633. https://doi.org/10.1021/acschemneuro.3c00130

Characterization of Uranyl (UO$_2^{2+}$) Ion Binding to Amyloid Beta (Aβ) Peptides: Effects on Aβ Structure and Aggregation

Elina Berntsson,* Faraz Vosough, Andra Noormägi, Kärt Padari, Fanny Asplund, Maciej Gielnik, Suman Paul, Jüri Jarvet, Vello Tõugu, Per M. Roos, Maciej Kozak, Astrid Gräslund, Andreas Barth, Margus Pooga, Peep Palumaa, and Sebastian K. T. S. Wärmländer*

Cite This: ACS Chem. Neurosci. 2023, 14, 2618–2633

Read Online

ACCESS | Metrics & More | Article Recommendations

ABSTRACT: Uranium (U) is naturally present in ambient air, water, and soil, and depleted uranium (DU) is released into the environment via industrial and military activities. While the radiological damage from U is rather well understood, less is known about the chemical damage mechanisms, which dominate in DU. Heavy metal exposure is associated with numerous health conditions, including Alzheimer's disease (AD), the most prevalent age-related cause of dementia. The pathological hallmark of AD is the deposition of amyloid plaques, consisting mainly of amyloid-β (Aβ) peptides aggregated into amyloid fibrils in the brain. However, the toxic species in AD are likely oligomeric Aβ aggregates. Exposure to heavy metals such as Cd, Hg, Mn, and Pb is known to increase Aβ production, and these metals bind to Aβ peptides and modulate their aggregation. The possible effects of U in AD pathology have been sparsely studied. Here, we use biophysical techniques to study in vitro interactions between Aβ peptides and uranyl ions, UO$_2^{2+}$, of DU. We show for the first time that uranyl ions bind to Aβ peptides with affinities in the micromolar range, induce structural changes in Aβ monomers and oligomers, and inhibit Aβ fibrillization. This suggests a possible link between AD and U exposure, which could be further explored by cell, animal, and epidemiological studies. General toxic mechanisms of uranyl ions could be modulation of protein folding, misfolding, and aggregation.

KEYWORDS: Alzheimer's disease, amyloid aggregation, metal–protein binding, neurodegeneration, heavy metal toxicity
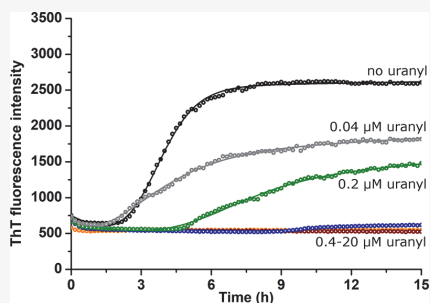
1. INTRODUCTION

Alzheimer's disease (AD) is the most common neurodegenerative disease among elderly people.[1,2] The main AD risk factors are old age and genetic factors such as unfavorable alleles of the ApoE gene and sometimes Down's syndrome[1,2] and also environmental risk factors such as smoking, diabetes, and traumatic brain injury.[2–4] Identifying molecular targets to diagnose and treat the disease is imperative,[5,6] and a number of drug candidates have been proposed with varying success.[7–10]

The main molecular events underlying AD pathology appear to be the aggregation of intrinsically disordered amyloid-β (Aβ) peptides and tau proteins into toxic soluble oligomers[11–13] and then into insoluble amyloid fibrils or tangles[14] that deposit as plaques in the brains of AD patients.[2,15] The Aβ peptides are cleaved by β- and γ-secretase enzymes from the Aβ precursor protein (APP) into peptides of different lengths,[16] where Aβ (1–40), i.e., Aβ$_{40}$, and Aβ (1–42), i.e., Aβ$_{42}$, are the most common.[17] Both variants are unstructured monomers in an aqueous solution but can adopt β-sheet[18] or α-helix[19] secondary structures in other environments.[20] The β-sheet structure is of particular interest as Aβ

peptides in β-sheet hairpin conformations appear to be the building blocks of the aggregated fibrils.[18]

The accumulation and aggregation of Aβ peptides can be influenced by a number of interacting factors,[3,21] such as other proteins and peptides,[10,22,23] including other amyloid peptides/proteins,[24–27] cationic molecules and metal ions,[28–30] and various small molecules.[8] Redox-active metal ions such as Cu(II) and Fe(II) are of special interest[29,31,32] as they are present in the plaques of AD brains.[33,34] For example, they can generate harmful oxygen radicals (reactive oxygen species, ROS) that may contribute to the AD pathology.[35–38] Heavy metals are generally known to be toxic, but their toxic mechanisms are not fully understood.[39] Known molecular mechanisms for metal toxicity include molecular and ionic

mimicry,[40] but other mechanisms are also possible, such as modulation of protein misfolding or aggregation.[41−43] Thus, lead (Pb) ions not only compete with ions of essential metals such as zinc and calcium,[44] but they also increase the expression of APP and β-secretase,[45] and Pb(IV) ions bind to Aβ peptides and modulate their aggregation.[3] Similar effects on Aβ production and aggregation have been observed for the heavy metals mercury and cadmium.[3,31,45−48]

Uranium (U) is a heavy metal with known neurotoxic effects,[39] but these effects are sparsely studied, and a relation between U exposure and AD has not been established.[49] However, the blood−brain barrier does not prevent the transfer of U into the central nervous system (CNS),[50] and U has been shown to accumulate in the brain.[51] Uranium has no biological function in the human body,[52,53] and the adverse health effects of U exposure involve combined chemical and radiological mechanisms.[54,55] Although the chemical toxicity is more severe,[56] the radiological damage mechanisms are currently better understood.[39,55] The chemical toxicity obviously dominates in depleted uranium (DU), where the amount of the ^{235}U isotope has been significantly reduced in favor of the less radioactive (i.e., longer half-life) ^{238}U isotope.[52] As DU is used in military equipment, including certain ammunitions,[57] DU contamination has emerged as a potential environmental problem in regions of war such as Iraq and the Balkans,[58−64] with unclear health consequences for soldiers and civilians.[52,54,65−67] To what extent DU contributes to leukemia or lung cancer remains debated.[68−71]

Here, we use biophysical spectroscopic and imaging techniques to investigate the binding interactions between uranyl ions and the three Aβ peptide variants Aβ$_{40}$, Aβ$_{42}$, and Aβ$_{40}$ (H6A, H13A, and H14A) mutant. Of particular interest is the effect of uranyl on the Aβ structure and aggregation.

1.1. Chemical, Environmental, and Toxicological Aspects of Uranium and Uranyl Ions.

Uranium is present in ambient air, water, and soil. The highest human exposures result from drinking well water in geological regions rich in U.[39,53,72−75] Regulatory agencies have limited the highest allowed concentration of U in drinking water to 30 μg/L,[76] replacing a previous WHO limit of 15 μg/L. Absorption of U is low regardless of exposure route and highly dependent on its solubility.[39] Inhaled U-dust particles of low solubility can be retained in tissues for many years.[77] Occupational exposure to U has historically involved workers in the production of phosphate fertilizers, workers producing glazed pottery, and miners handling uranium oxide, so-called "yellowcake".[39,78] Sleep disturbances and possibly encephalitis have been linked to U exposure in former U mining districts in Kazakhstan.[79]

The main target for U toxicity is the kidney where atrophy and necrosis of glomerular walls have been noted.[39,80−82] Uranium also accumulates in bone.[39,60,83−85] Uranium crosses the blood−brain barrier to accumulate in the CNS.[50] Here, inhalation and ingestion of U yields heterogeneous but specific accumulations, most prominent in the hippocampus region,[86] responsible for memory recall. Rats surgically implanted with U pellets for 6 months have shown the presence of U in the cortex, midbrain, and cerebellum.[87] A study on mice showed toxic effects of DU in the mouse fetus,[88] indicating that U can also cross the placental barrier.

There are currently no known correlations between uranium exposure and diseases such as leukemia,[73] stomach cancer,[89] liver or bladder cancer,[90] or, as mentioned above, AD.[49] One study, however, found cerebrospinal fluid U concentrations, albeit at low overall concentrations, to be significantly elevated in 17 patients with amyotrophic lateral sclerosis (ALS) when compared to 10 controls.[91] Studies in rodents have related U exposure to distorted social behavior[92] and weakened sensorimotor behavior.[93] Laboratory experiments using organisms such as rats and *Caenorhabditis elegans* have concluded with a low acute neurotoxic potential of U following exposure and a protective potential from the small metal-regulating protein metallothionein.[87,94] Protective effects have also been observed for the ghrelin hormone[95] and for antioxidant agents, including glutathione.[96,97]

The most predominant, most stable, and most relevant form of uranium in aerobic environments is the uranyl oxycation, UO$_2^{2+}$. This ion is common in uranium-containing minerals, but it is also water-soluble and is present in the ocean at a concentration of 13.7 nM.[98] The uranyl ion is paramagnetic,[99,100] and in aqueous solution, it acts as a weak acid with a pK_a of around 4.2.[101] It behaves as a hard acceptor and prefers to form complexes with fluoride and oxygen donor atoms, preferably in planar geometry involving four, five, or even six binding ligands.[102] The capacity to accommodate five or six equatorial ligands in pentagonal or hexagonal bipyramidal coordination separates the uranyl ion from most other metal ions.[98] Thus, these uncommon binding geometries have been employed in attempts to design uranyl-specific binding proteins, e.g., to extract uranium from seawater.[98] As the most common form of uranium, most experimental studies of uranium toxicity have actually been conducted with uranyl ions rather than with metallic uranium, which is extremely rare in nature.

Interestingly, U intoxication and AD appear to have a common risk factor in the gene coding for apolipoprotein E (ApoE). U exposure in mice was found to induce cognitive impairment in ApoE-deficient (ApoE−/−) males, together with some changes in cholesterol levels and metabolism.[103,104] This is consistent with the ApoEε4 allele of the ApoE gene being a risk factor for mercury toxicity[105,106] and with ApoE-deficient mice showing increased iron accumulation in tissue over time.[107] It therefore appears likely that the ApoE protein is involved in regulating metal homeostasis. The ApoEε4 allele is further linked to an increased probability of developing AD.[108−112] Why the ApoE gene is a risk factor for both heavy metal toxicity and AD is currently unclear, and various explanations have been proposed.[108,113,114] The previously suggested hypothesis that ApoE might bind and transport metal ions via Cys residues,[105,106] which are present in ApoE2 and ApoE3 but not in ApoE4, has recently been called into question.[115]

2. RESULTS

2.1. ThT Fluorescence Measurements of Aβ$_{40}$ Aggregation Kinetics.

The fluorescence intensity of ThT, a common marker for amyloid material,[116] was monitored when samples of 20 μM Aβ$_{40}$ peptides in 20 mM MES buffer, pH 7.3, were incubated with shaking for 15 h at 37 °C, together with different concentrations (0; 0.04; 0.2; 0.4; 2; and 20 μM) of uranyl acetate (Figure 1).

Fitting eq 1 to the ThT fluorescence curves in Figure 1 produced the kinetic parameters T_{lag} and $t_{1/2}$ (Table 1). For the three highest concentrations of uranyl acetate, i.e., 0.4, 2, and 20 μM, the ThT kinetic curves are mostly flat, and fitting eq 1 to these curves was not possible. The flat shape of the three curves indicates that no or very little amyloid material has
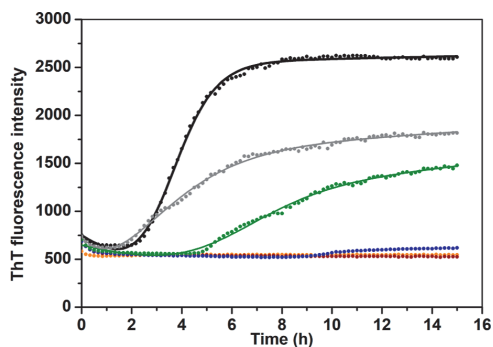
Figure 1. Monitoring the fibril formation of $A\beta_{40}$ peptides via thioflavin T fluorescence. 20 μM $A\beta_{40}$ was incubated at 37 °C in 20 mM MES buffer, pH 7.3, together with different concentrations of uranyl acetate: 0 μM (black); 0.04 μM (gray); 0.2 μM (green); 0.4 μM (blue); 2 μM (red); and 20 μM (orange).

Figure 2. TEM images for aggregates of 20 μM $A\beta_{40}$ in 20 mM MES buffer, pH 7.3, incubated for 20 h on a thermo shaker at 37 °C and 300 rpm, together with different concentrations of uranyl acetate: (A) 0; (B) 0.2; (C) 2; and (D) 20 μM. White scale bars are either 2 (A,C) or 1 μm (B,D).

formed, although for the 0.4 μM uranyl sample, small amounts of the ThT-binding material have begun to form after approximately 9 h. It is obvious that the amount of the amyloid material formed at the end of the measurements, i.e., ΔThT, strictly decreases with the amount of added uranyl acetate (Figure 1 and Table 1). The two samples with 0 and 0.04 μM uranyl both have aggregation half-times of around 3 h and lag times of around 2 h under the experimental conditions (Table 1). The aggregation of the 0.2 μM uranyl sample is clearly slower, with a half-time of almost 7 h and a lag time of around 5 h. Given the visually estimated lag time of around 9 h for the 0.4 μM uranyl sample and that the 2 and 20 μM uranyl samples show no obvious signs of aggregation after 15 h, uranyl ions clearly increase the lag time for $A\beta_{40}$ aggregation.

2.2. TEM Imaging of Aggregated $A\beta_{40}$ Peptides. Negative staining transmission electron microscopy (TEM) images were recorded for 20 μM $A\beta_{40}$ peptide, incubated for 20 h with different concentrations of uranyl acetate, i.e., 0, 0.2, 2, and 20 μM (Figure 2). The uranyl additions correspond to uranyl/$A\beta_{40}$ ratios of 1:100, 1:10, and 1:1. The control sample without UO_2^{2+} ions displays numerous amyloid fibrils that are several microns long, together with occasional larger clumps and smaller aggregates, which may be proto-fibrils (Figure 2A). This is in line with previous in vitro studies of $A\beta_{40}$ aggregates.[8,25,116] The $A\beta_{40}$ samples incubated together with 0.2 μM of uranyl acetate display amyloid fibrils of similar size and shape (Figure 2B). In the presence of 2 μM uranyl acetate, there are fewer fibrils and they are shorter, i.e., only a few microns long (Figure 2C). At the highest concentration of uranyl acetate, i.e., 20 μM, no fibrils have formed at all (Figure 2D). Instead, the $A\beta_{40}$ peptides have aggregated into large amorphous clumps, which coexist with smaller particles
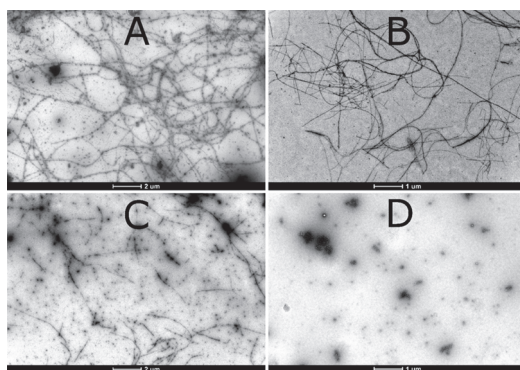
(Figure 2D). These results show that UO_2^{2+} ions inhibit the formation of $A\beta$ amyloid fibrils in a concentration-dependent manner, with complete inhibition at stoichiometric uranyl/$A\beta_{40}$ ratios.

2.3. NMR Spectroscopy on Uranyl Binding to $A\beta_{40}$ Monomers. High-resolution nuclear magnetic resonance (NMR) experiments were conducted to investigate if there were residue-specific molecular interactions between uranyl ions and monomeric $A\beta_{40}$ peptides. Figure 3 shows 2D ^{1}H, ^{15}N-HSQC spectra for the amide cross-peak region for 92 μM ^{15}N-labeled $A\beta_{40}$ peptides, at either pH 7.3 or pH 5.1, recorded before and after the addition of uranyl acetate.

At pH 7.3, addition of first 46 μM and then 92 μM uranyl ions (1:2 and 1:1 uranyl/$A\beta_{40}$ ratio, respectively) induces a concentration-dependent loss of amide cross-peak intensity (Figure 3A). The intensity loss is uniformly distributed across the peptide sequence, which shows that the uranyl ions do not bind to specific residues of the $A\beta_{40}$ monomer. Instead, the observed binding is likely driven by general electrostatic interactions between the cationic uranyl ions and the anionic $A\beta$ peptides. The loss of cross-peak intensity is probably caused by several factors, such as paramagnetic quenching effects[99,100] and intermediate (on the NMR time-scale) chemical exchange between free $A\beta_{40}$ peptides and the $A\beta_{40}$ uranyl complex, similar to the effects observed when Cu(II), Ni(II), and Zn(II) ions bind to $A\beta$ peptides.[117−120] In addition, the uranyl ions likely promote the formation of $A\beta$ aggregates that either precipitate out of the solution or are too large and heterogeneous to produce distinct NMR signals.[119,120] As no NMR signals are observed for the $A\beta_{40}$

Table 1. Kinetic Parameters for $A\beta_{40}$ Aggregation in the Presence of Different Concentrations of Uranyl Acetate, Derived from the ThT Fluorescence Curves Shown in Figure 1[a]

uranyl ions	0 μM	0.04 μM	0.2 μM	0.4 μM	2 μM	20 μM
$t_{1/2}$ (h)	3.5 ± 0.3	3.1. ± 1.5	6.7 ± 1.4	n/a	n/a	n/a
T_{lag} (h)	2.4 ± 0.2	2.0 ± 1.1	5.2 ± 0.9	n/a	n/a	n/a
ΔThT (a.u.)	2067	1286	958	101	0	0

[a]Aggregation halftime ($t_{1/2}$) and lag time (T_{lag}) were obtained from fitting the ThT curves to eq 1. The increase in ThT fluorescence (ΔThT) is presented in arbitrary fluorescence units (a.u.).
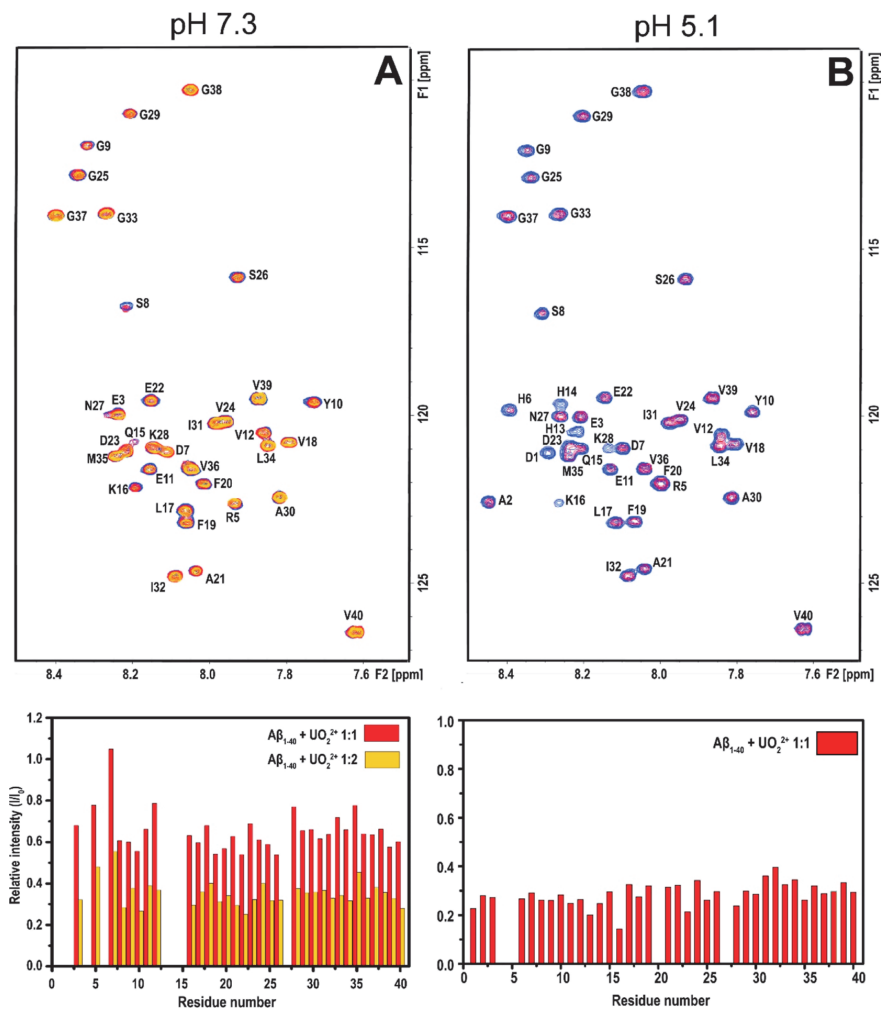
Figure 3. 2D NMR ^{1}H, ^{15}N-HSQC-spectra at 5 °C showing titrations of uranyl acetate to 92 μM monomeric ^{15}N-labeled Aβ_{40} peptides in 20 mM MES buffer at either pH 7.3 (A) or pH 5.1 (B). Blue cross-peaks: 84 μM Aβ_{40} only. Red cross-peaks: 1:2 uranyl/Aβ_{40}. Yellow cross-peaks (pH 7.3 only): 1:1 uranyl/Aβ_{40}. The peak intensities in the bar charts show ratios between the cross-peak intensities with added uranyl ions relative to the intensities before the addition of uranyl ions, i.e., I/I_0.

aggregates, nothing can be concluded about the binding configurations for uranyl ions in complex with such aggregates.

At pH 5.1, addition of uranyl ions again induces a uniform loss of amide cross-peak intensity (Figure 3B). Unexpectedly, the effect is stronger at pH 5.1 than at pH 7.3: addition of 46 μM uranyl acetate (1:2 uranyl/Aβ_{40} ratio) at pH 5.1 decreases the cross-peak intensity approximately as much as the addition of 92 μM uranyl acetate (1:1 ratio) at pH 7.3 (Figure 3). This suggests stronger binding of the uranyl ions at an acidic pH. When comparing the NMR spectra without added uranyl ions at neutral (Figure 3A) and acidic (Figure 3B) pH, NMR cross-peaks for a few additional residues (e.g., D1, A2, H6, H13, and H14) became visible at acidic pH (Figure 3B), probably due to slower proton exchange at this pH.[119]

2.4. Fluorescence Measurements of Uranyl Aβ Binding Affinity. Uranyl ions were found to quench the intrinsic

fluorescence of the Tyr10 residue in the Aβ peptide, similar to, e.g., Cu(II) ions.[121−123] Measurements of the Tyr10 fluorescence during titrations with uranyl acetate were therefore used to quantify binding affinities for Aβ·UO$_2^{2+}$ complexes under different conditions. The resulting titration/binding curves are shown in Figure 4. Fitting eq 2 to these curves produced the apparent dissociation constants (K_D^{App}) shown in Table 2.

For Aβ_{40} at pH 7.3, the titration data clearly deviate from the binding model, both for the measurements in buffer only (Figure 4A1) and in the presence of sodium dodecyl sulfate (SDS) micelles (Figure 4B1). Because of these deviations, the derived dissociation constants should not be trusted. As eq 2 is based on a model that assumes a single binding site, a possible explanation for this deviation is the binding of uranyl ions to multiple locations on the Aβ_{40} peptide under these conditions.
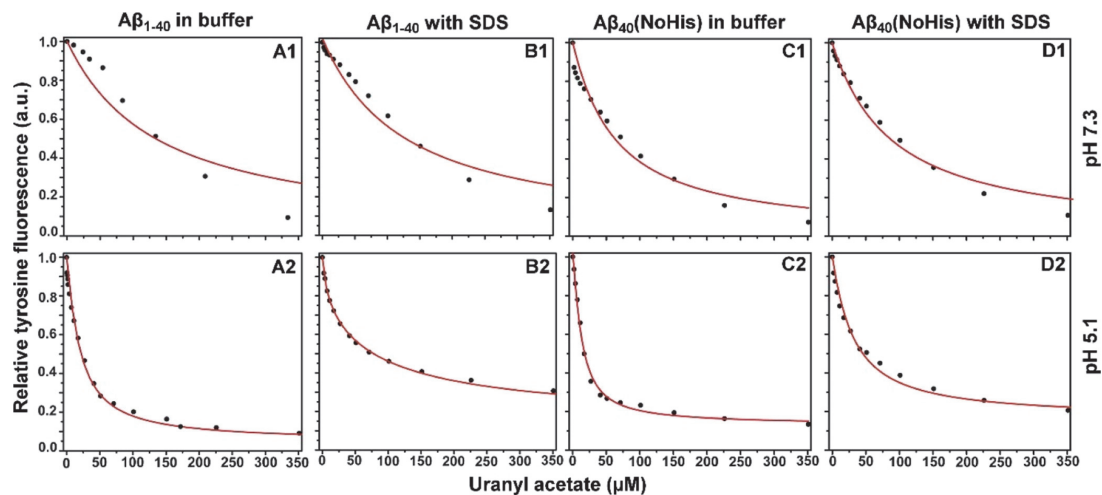
Figure 4. Fluorescence intensity curves for Aβ residue Tyr10, showing titrations of 20 μM Aβ_{40} peptide (A,B) or 20 μM Aβ_{40} (NoHis) mutant (C,D) with uranyl acetate in 20 mM MES buffer, either at pH 7.3 (1st row) or at pH 5.1 (2nd row). For (B,D), micelles of 50 mM SDS were added to the samples.

Table 2. Apparent Dissociation Constants (K_D^{App}) in μM for Uranyl·Aβ Complexes, Obtained by Fitting Fluorescence Titration Curves to eq 2 (Figure 4; Three Replicates per Condition)

	Aβ_{40}				Aβ_{40} (NoHis)			
	1	2	3	average	1	2	3	average
pH 7.3	130	141	148	140 ± 8	62	86	79	76 ± 11 μM
pH 7.3 + 50 mM SDS	206	252	251	236 ± 22	119	124	116	120 ± 4 μM
pH 5.1	14.0	13.7	21.3	16.3 ± 4	2.3	2.8	4.0	3.0 ± 1 μM
pH 5.1 + 50 mM SDS	21.8	21.7	27.4	23.6 ± 3	22.3	30.7	27.9	27.0 ± 4 μM

At pH 5.1, the binding curves follow the model very well (Figure 4A2,B2), yielding reliable K_D^{App} values of 16.3 μM for Aβ_{40} in buffer and 23.6 μM for Aβ_{40} bound to SDS micelles (Table 2). The main difference from the measurements at neutral pH is that the three His residues in the Aβ peptide become protonated at lower pH as their pK_a values are around 6.8.[124] Because protonated His residues are unlikely to interact with positive ions such as UO_2^{2+}, it is possible that binding interactions between uranyl ions and uncharged His residues are responsible for the deviations from the single-site binding scheme observed at pH 7.3 (Figure 4A1,B1).

The binding curves for the Aβ_{40} (NoHis) mutant at pH 7.3 follow the model rather well (Figure 4C1,D1), producing K_D^{App} values of 76 μM in buffer and 120 μM in the presence of SDS micelles (Table 2). At pH 5.1, the overlap with the fitted curve is even better (Figure 4C2,D2), and here, the K_D^{App} values are 3.0 μM in buffer and 27 μM in the presence of SDS micelles (Table 2). With these results, some comparisons can be made.

For both peptide versions, the uranyl ions display stronger binding at low pH. Even though reliable binding constants could not be obtained for Aβ_{40} at pH 7.3, it is clear from the measurement data that binding is overall stronger at pH 5.1 (Figure 4A,B). Addition of SDS micelles generally makes the binding weaker (Table 2). This effect is likely related to the SDS molecules being negatively charged, thereby competing for binding to the cationic uranyl ions. The strongest uranyl binding is observed for the Aβ_{40} (NoHis) mutant at pH 5.1 (3.0 μM), while the weakest binding is observed for Aβ_{40} at pH

7.3. It therefore appears that neutral (i.e., non-protonated) His residues might interfere with uranyl binding under the experimental conditions used.

2.5. CD Spectroscopy on the Aβ Secondary Structure. Circular dichroism (CD) spectroscopy was used to investigate the possible effects of uranyl ions on the secondary structure of Aβ_{40} peptides, both in aqueous buffer and in the presence of SDS micelles that mimic a membrane environment. The CD spectra for Aβ_{40} monomers in aqueous buffer display spectra with minima around 196–198 nm (Figure 5B,E), which is typical for a random coil conformation. At pH 5.1, addition of uranyl ions to Aβ_{40} induces a two-step structural transition as the CD signal changes in a concentration-dependent manner around an isodichroic point at approximately 214 nm (Figure 5E). The difference spectrum (Figure 5F) shows that the structural transition is a conversion from random coil to β-sheet. At pH 7.3, the structural effect induced by the uranyl ions is weaker, and it is unclear if an isodichroic point is present (Figure 5B). The difference spectrum is not conclusive but might represent β-sheet conformation (Figure 5C).

In the presence of SDS micelles, the CD signals for Aβ_{40} peptides display minima around 208 and 222 nm (Figure 5A,D), which is characteristic for the α-helical secondary structure. This is in line with previous reports that the central and C-terminal Aβ regions adopt α-helical conformations in membrane-like environments.[19,122,125,126] At pH 7.3, addition of uranyl ions induces no changes at all in the Aβ_{40} CD spectrum with SDS (Figure 5A). At pH 5.1, however, the
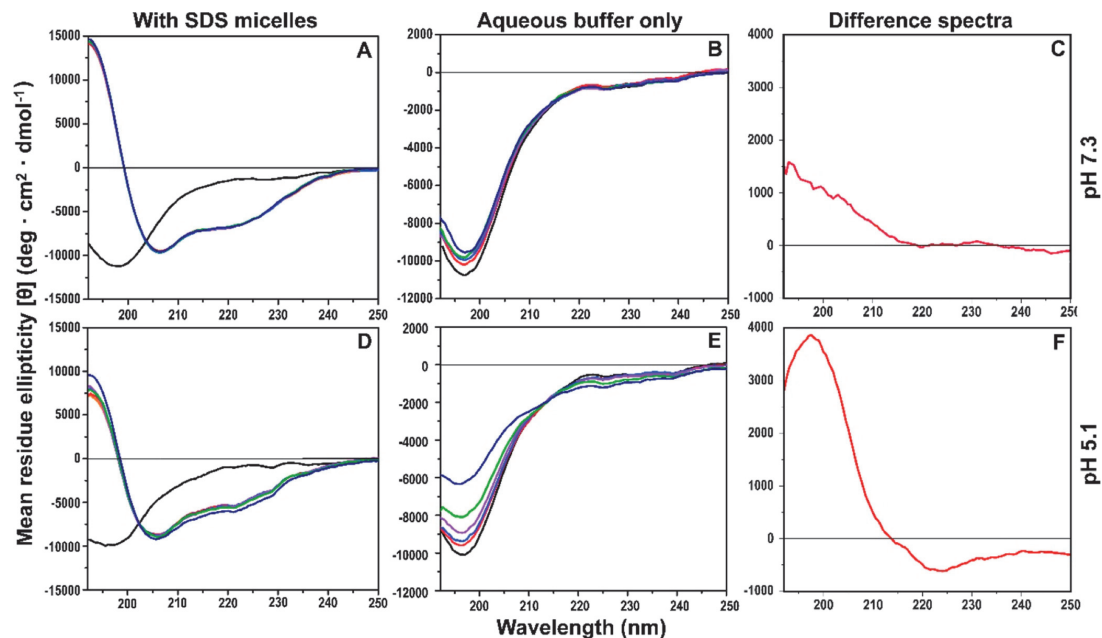
Figure 5. CD spectroscopic titrations of 10 μM Aβ_{40} with uranyl acetate in 20 mM sodium phosphate buffer at 20 °C, carried out in the presence of 50 mM SDS at pH 7.3 (A) or pH 5.1 (D), or in aqueous buffer only at pH 7.3 (B) or pH 5.1 (E). First, spectra were recorded for Aβ_{40} in buffer for all samples (black lines). Then, 50 mM SDS detergent was added to the samples in (A,D) (orange lines). To all samples, uranyl acetate was added in steps of 2, 6, 16, 56, and 256 μM (ruby red, ultramarine blue, plum purple, lime green, and navy blue lines, respectively). For the titrations in aqueous buffer, shown in (B,E), the difference spectra shown in (C,F) were created by subtracting the measurements with 256 μM added uranyl from the measurements without uranyl, at pH 7.3 (C) and pH 5.1 (F).
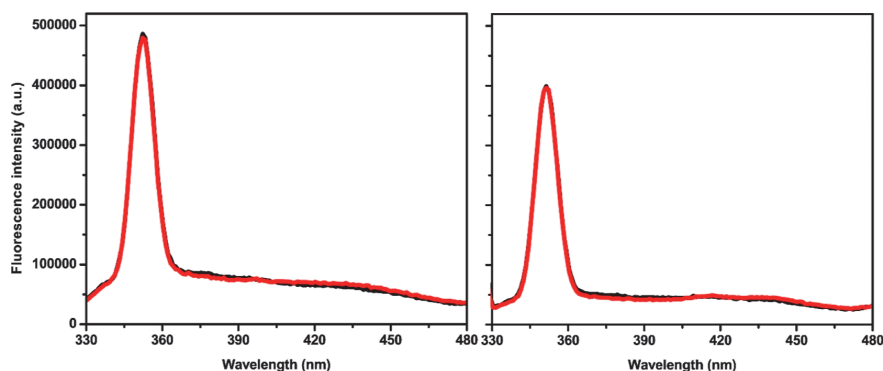
Figure 6. Fluorescence emission spectra of 10 μM Aβ_{40} peptides in 20 mM MES buffer, pH 7.3, incubated with 100 μM EDTA (A) or with 100 μM uranyl acetate (B). Black line—0 h and red line—24 h.

uranyl ions induce systematic changes in the CD spectra around an isodichroic point at approximately 203 nm (Figure 5D). This is the same wavelength as where the CD spectrum for Aβ_{40} peptides in aqueous solution (i.e., random coil structure) crosses the CD spectrum for Aβ_{40} peptides in SDS micelles (i.e., α-helical structure), when no uranyl ions are present (Figure 5D). Taken together, these observations indicate that uranyl ions at pH 5.1 induce a structural conversion from α-helix to a random coil in Aβ_{40} peptides in SDS micelles. Also, the changes in CD intensity at other wavelengths are consistent with the formation of a random coil

structure, even though the overall changes are small and difficult to interpret conclusively (Figure 5D). The overall larger structural effects induced by uranyl ions at acidic pH, compared to neutral pH, both in aqueous solution (Figure 5B,E) and in SDS micelles (Figure 5A,D), support the NMR (Figure 3) and fluorescence (Figure 4) spectroscopy results that the uranyl ions bind stronger to Aβ_{40} peptides at acidic pH.

2.6. Dityrosine Cross-Link Formation. Fluorescence measurements were carried out to investigate if uranyl ions could induce the formation of covalent dityrosine cross-links in

Aβ peptides via the generation of ROS, similar to what has been observed for redox-active Cu(II) ions[35,127−129] and Ni(II) ions.[118] Two samples of Aβ_{40} peptides were studied. The control sample contained 100 μM EDTA to remove possible contaminating metal ions that could promote dityrosine formation. The other sample contained 100 μM uranyl acetate. For both samples, the fluorescence spectra are virtually identical before and after 24 h of incubation (Figure 6). Specifically, no peak around 410 nm, indicative of dityrosine,[129,130] has emerged. The signal around 350 nm is a water Raman peak, which is useful for reference purposes as it does not change with the sample composition. These results clearly show that uranyl ions do not induce the formation of dityrosine cross-links under the experimental conditions employed here.

2.7. BN-PAGE Analysis of Aβ_{42} Oligomer Formation and Stability. Blue native polyacrylamide gel electrophoresis (BN-PAGE) analysis and Fourier-transform infrared (FTIR) analysis (below) were used to investigate possible effects of uranyl ions on Aβ oligomer formation. Because Aβ_{40} peptides do not form stable oligomers, Aβ_{42} peptides together with SDS detergent were used to create oligomers that remained stable for over a week. The Aβ_{42} oligomers were created with two different concentrations of stabilizing SDS molecules, 80−100 μM of Aβ_{42} peptides and 0−1000 μM of uranyl acetate, as described in Section 5.2.

The BN-PAGE analysis shows that in 0.05% SDS (1.7 mM) without uranyl acetate, larger oligomers with a molecular weight (MW) around 55−60 kD are formed (Figure 7, lane 3).
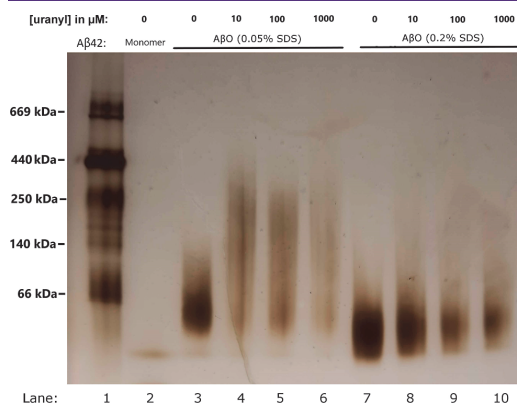
Figure 7. BN-PAGE gel showing the effects of different concentrations of uranyl acetate on the formation of SDS-stabilized Aβ_{42} oligomers (formed with 80−100 μM peptide). Lane 1: reference ladder. Lane 2: Aβ_{42} monomers. Lanes 3−6: AβO$_{0.05\%SDS}$ oligomers (likely dodecamers) prepared with 0, 10, 100, and 1000 μM uranyl ions, respectively. Lanes 7−10: AβO$_{0.2\%SDS}$ oligomers (likely tetramers) prepared with 0, 10, 100, and 1000 μM uranyl ions, respectively.

These larger oligomers, abbreviated AβO$_{0.05\%SDS}$, most likely contain twelve Aβ_{42} peptides and display a globular morphology, which is why they are sometimes called globulomers.[131] In the presence of different concentrations of uranyl acetate, no well-defined uniform oligomers were observed. Instead, the bands on the BN-PAGE gel appear smeared, indicating a heterogeneous size distribution of the

formed oligomers (Figure 7, lanes 4−6). This disruptive effect is already very strong at the lowest concentration (10 μM) of added uranyl ions.

In 0.2% SDS (6.9 mM), small Aβ_{42} oligomers with a MW around 16−20 kDa are formed (Figure 7, lane 7). These oligomers, abbreviated AβO$_{0.2\%SDS}$, likely contain a large fraction of tetramers.[131,132] Preparation of these oligomers in the presence of increasing uranyl concentrations (10, 100, and 1000 μM) yields oligomer bands that are weaker at the intermediate uranyl concentrations and weakest at the highest concentration, indicating gradually lower amounts of stable AβO$_{0.2\%SDS}$ oligomers (Figure 7, lanes 8−10). Thus, for the formation of the smaller AβO$_{0.2\%SDS}$ oligomers at the higher SDS concentration, the effect of uranyl ions is less disruptive and clearly concentration-dependent compared to the effect on the larger AβO$_{0.05\%SDS}$ oligomers (Figure 7).

2.8. FTIR Spectroscopy Reflecting the Aβ_{42} Oligomer Structure. The secondary structures of Aβ_{42} oligomers formed with different SDS and uranyl concentrations were studied with FTIR spectroscopy, where the amide I region (1700−1600 cm^{-1}) is very sensitive to changes in the protein backbone conformation, including differences in β-sheet structures.[133−135] When prepared in the absence of uranyl acetate, both types of Aβ_{42} oligomers (i.e., AβO$_{0.05\%SDS}$ and AβO$_{0.2\%SDS}$) produce two major bands in the amide I region: a high-intensity band near 1630 cm^{-1} and a smaller one near 1686 cm^{-1}.[132] This split pattern of IR bands in the amide I region is typical for anti-parallel β-sheet structures.[136−138]

For AβO$_{0.05\%SDS}$ oligomers in PBS buffer, the β-sheet main band shows a band shift due to uranyl acetate: the main band is observed at 1628.3 cm^{-1} without uranyl acetate, but shifts down to 1627.8 cm^{-1} in the presence of 1 mM (1000 μM) uranyl acetate (Figure 8A). In contrast to the AβO$_{0.05\%SDS}$ oligomers, the spectrum of the AβO$_{0.2\%SDS}$ oligomers (resolved at 1629.9 cm^{-1}, Figure 8B) is not significantly affected by the uranyl acetate concentration (1629.8 cm^{-1} at 0.01, 0.1, and 1 mM uranyl acetate) (Figure 8B). This result also indicates that band positions can be determined with an accuracy of 0.1 cm^{-1}, which is supported by our study of Li(I) ion effects,[139] where at both SDS concentrations, the standard deviation of the band positions for four Li(I) ion concentrations (0, 0.1, 1, and 10 mM) was 0.12 cm^{-1} and the band positions at zero and 10 mM Li(I) differed by less than 0.1 cm^{-1}.

These observations agree with the BN-PAGE results, which showed clear small oligomer bands for all uranyl concentrations at the higher SDS concentration, but extended smears instead in the presence of uranyl acetate for the lower SDS concentration. The results indicate again that the Aβ_{42} globulomers produced at the lower SDS concentration are more sensitive to uranyl-induced effects.

3. DISCUSSION

Uranium is a well-known neurotoxicant,[39] but the underlying molecular mechanisms and a possible role of U in neurodegenerative diseases remain unclear.[49,91] For AD, several studies have investigated how Aβ peptides interact with various metal ions[30,47,118,139−142] and with small cationic molecules.[28,143] We here interpret the current results on Aβ−uranyl interactions in the light of this earlier work.

3.1. Effects of Uranyl Ions on Aβ_{40} Aggregation. The ThT fluorescence curves (Figure 1) and TEM images (Figure 2) show that uranyl ions have a concentration-dependent inhibitory effect on the fibrillization of Aβ_{40} peptides at
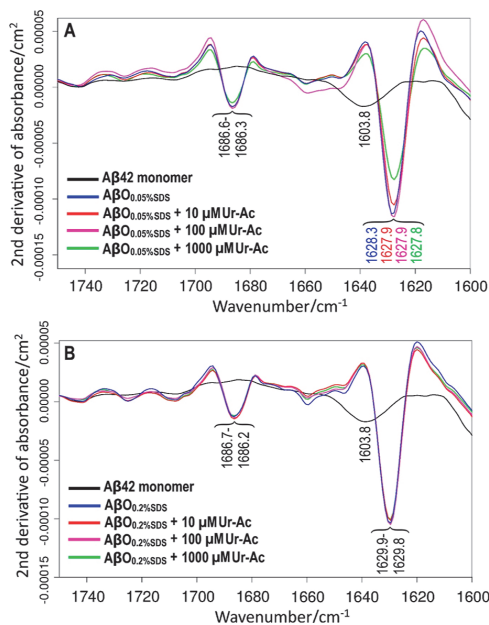
Figure 8. Second derivatives of infrared absorbance spectra for 80–100 μM SDS-stabilized Aβ_{42} oligomers formed in the absence (blue) and presence of 0.01 mM (red), 0.1 mM (purple), and 1 mM (green) uranyl acetate. The results are shown for larger Aβ_{42} oligomers formed with 0.05% SDS (A) and for smaller Aβ_{42} globulomers formed with 0.2% SDS (B).

physiological pH. Instead of forming proper amyloid fibrils, the Aβ_{40} peptides form non-fibrillar amorphous aggregates (clumps) already at a 1:1 uranyl/Aβ_{40} ratio (Figure 2). This effect is seen both in the TEM images and the ThT fluorescence experiments, even though the sample conditions are somewhat different (i.e., the TEM samples did not contain ThT dye and were incubated in Eppendorf tubes on a thermo shaker). Thus, the uranyl ions do not prevent the Aβ_{40} peptides from aggregating but rather direct the aggregation process toward non-fibrillar end-products. Similar effects on the Aβ aggregation pathways have previously been observed for other small cationic molecules and heavy metal ions such as Hg(II), Ni(II), Pb(II), and Pb(IV).[47,118,143] As small oligomeric aggregates of Aβ peptides are considered to be the main toxic species in AD pathology,[2,11] the finding that uranyl ions can modulate Aβ aggregation might be relevant for understanding AD progression and pathogenesis.

3.2. Binding of Uranyl Ions to Aβ_{40} Peptides. The NMR results show that uranyl ions have no obvious residue-specific binding to Aβ_{40} peptides (Figure 3). Because of the strong covalent O=U=O bonds in the uranyl ion, it is mainly the central U(VI) atom that interacts with other molecules.[144] Thus, the uranyl−Aβ binding is probably mediated via non-specific electrostatic interactions between the positive U(VI) atom and negative Aβ residues, such as Asp1, Asp7, Asp23, Glu3, Glu11, and Glu22. This is similar to Aβ binding to Mn(II) and Pb(II) ions,[3,140] but different from numerous small cationic species that display residue-specific interactions with Aβ peptides, such as polyamines[28] and Cu(II), Ni(II), Pb(IV), and Zn(II) ions.[3,117−119]

The results of the NMR measurements indicate that the Aβ binding of uranyl ions is stronger at acidic pH (Figure 3), which is confirmed by the fluorescence measurements of uranyl−Aβ binding affinity (Figure 4) and also by the CD spectroscopy results (Figure 5). At pH 5.1, the apparent binding affinity of uranyl ions is 16.3 ± 4 μM to Aβ_{40} peptides and 3.0 ± 1 μM to the Aβ_{40} (NoHis) mutant (Table 2). At neutral pH, the binding is about a magnitude weaker (Table 2) and also less well-defined (Figure 4). This is counter-intuitive. The main chemical difference at lower pH is that the Aβ His residues become protonated as they have pK_a values around 6.8 in short peptides.[124] It stands to reason that Aβ peptides with positively charged His residues should be less prone to interact with positive metal ions, as has been shown for, e.g., Cu(II) and Zn(II) ions.[119] On the other hand, the uranyl ion is a weak acid that undergoes hydrolysis, and the first pK_a is around 4−5.[145,146] Thus, at pH 5.1, the uranyl ions may be mixed with monomeric and dimeric hydroxide species. At pH 7.3, additional species might be present, such as the single-charged trimer $[(UO_2)_3(OH)_5]^+$. It is possible that such heterogeneity, which is likely more pronounced at neutral pH, could help explain the somewhat unexpected uranyl titration results.

The Tyr10 fluorescence measurements (Figure 4) show that the uranyl Aβ binding affinity increases at lower pH values and also when the three His residues are replaced by Ala residues (Table 2). In fact, the weakest binding is observed for Aβ_{40} at pH 7.3, and the strongest binding is observed for the Aβ_{40} (NoHis) mutant at pH 5.1 (Table 2). This trend is observed for Aβ samples both in aqueous buffer and in SDS micelles. It strongly suggests that the presence of uncharged His sidechains interferes with uranyl binding to Aβ peptides (Table 2). This tentative conclusion is supported by the shape of the fluorescence data curves, which are more uniform and better fit the single-binding-site model (eq 2), when the uncharged His residues H6, H13, and H14 are replaced with Ala residues in the Aβ_{40} (NoHis) mutant (Figure 4). In addition, at acidic pH, the uranyl binding is stronger both to the wild-type (wt) Aβ_{40} peptide and to the Aβ_{40} (NoHis) mutant. In the latter case, the effect is clearly not caused by His protonation as these residues are missing in the mutant peptide. Thus, the His residues are not the only factor responsible for the unusual properties of uranyl-Aβ binding. As discussed above, formation of uranyl hydroxide species is likely another confounding factor. The molecular details of uranyl-Aβ binding should therefore be further explored in future studies.

Because toxic Aβ aggregates appear to form in membrane environments,[147] and as membrane disruption might be one of the toxic mechanisms of Aβ aggregates,[148] it is important to clarify how Aβ interacts with uranyl ions also in a membrane environment. Here, we used SDS micelles as a simple membrane model. Even though such micelles are different from the phospholipid bilayers present in cell membranes, they do share some properties with real membranes, while being much more suitable for various spectroscopy measurements, including NMR.[125,126] Our fluorescence spectroscopy measurements showed that the uranyl binding affinities decrease slightly when SDS micelles are present in the sample for all Aβ variants and conditions (Figure 4 and Table 2). This effect is probably caused by the anionic SDS micelles competing for binding to the cationic uranyl ions. Similar results have earlier been obtained for Aβ binding to other metal ions, such as

Cu(II), Hg(II), and Ni(II), in the presence of SDS micelles.[47,118,122] Aβ peptides are known to insert only their central and C-terminal regions into an SDS micelle, while the negatively charged N-terminal region is positioned outside the micelle where it is free to interact with, e.g., cations.[118,122] Thus, it appears that Aβ peptides can (sometimes) bind uranyl ions mainly via their N-terminal part in a membrane environment. We may speculate that when multiple Aβ peptides are present in the membrane, a single uranyl ion might bind to the N-termini from two or more Aβ peptides, thereby bringing the peptides together and promoting aggregation.

3.3. Effects of Uranyl Ions on the Aβ₄₀ Peptide Structure.

In an aqueous buffer at pH 5.1, the CD spectroscopy measurements show that uranyl ions induce a two-state structural transition in the $A\beta_{40}$ peptides, from random coil to β-sheet structure (Figure 5E,F). At pH 7.3, a weaker structural transition is observed, which might be a similar conversion into a β-sheet structure (Figure 5B,C). Earlier studies have shown that such structural changes can be induced also by metal ions such as Cu(II), Ni(II), and Zn(II).[118,119] Because Aβ aggregates typically consist of peptides in β-sheet conformation,[18] this type of β-sheet structure formation likely promotes Aβ aggregation.

SDS micelles constitute a simple membrane model,[125,126] and the central and C-terminal regions of Aβ peptides are known to insert themselves into such micelles and adopt α-helical conformations.[19,126] In the presence of SDS micelles, uranyl ions have no effect on the $A\beta_{40}$ peptide conformation at pH 7.3 (Figure 5A). However, a weak structural transition is observed at pH 5.1, possibly involving the formation of random coils (Figure 5D). Previous studies have found that metal ions that bind to Aβ peptides mainly via the His residues, such as Cu(II), Ni(II), and Zn(II) ions, can induce altered coil−coil interactions in Aβ peptides positioned in SDS micelles.[118,122] No such alterations in the α-helical structure were observed upon the addition of uranyl ions (Figure 5A,D).

No dityrosine cross-links were observed after $A\beta_{40}$ peptides had been incubated together with uranyl acetate (Figure 4). Earlier studies have shown that redox-active metal ions such as Cu(II) and Ni(II) can induce the formation of dityrosine cross-links in amyloid peptides via redox-cycling of, e.g., the Cu(I)/Cu(II) redox pair, which generates harmful oxygen radicals via Fenton-like chemistry.[35,37,38,118,129] For short peptides with only one Tyr residue in the amino acid sequence, such as Aβ and amylin, dityrosine formation must involve two peptides, which then become linked to form a dimer.[129] As Cu(II) and Ni(II) bind Aβ peptides mainly via the His6, His13, and His14 residues, it is likely that these metal ions can promote Aβ aggregation by coordinating multiple His residues from more than one Aβ peptide.[141,149] Cu(II) and Ni(II) ions may therefore promote dityrosine formation not only by creating oxygen radicals but also by connecting two Aβ molecules and positioning their Tyr10 residues close to each other. It is known that the U(VI) ion in uranyl can be reduced to lower valency states such as U(IV) under appropriate reducing conditions.[144,150] Thus, as uranyl acetate has been found to induce oxidative stress in isolated cells,[97] the uranyl ions are likely redox-active under physiological conditions. We therefore speculate that the reason why uranyl ions do not promote dityrosine formation in $A\beta_{40}$ peptides (Figure 4) is the weak and non-specific binding under the experimental conditions used (Figures 7, 8, and Table 2).

3.4. Effects of Uranyl Ions on Aβ₄₂ Oligomers.

Although most of the measurements carried out in this study were performed on $A\beta_{40}$ monomers, it is also of interest to investigate the possible effects of uranyl ions on Aβ oligomers. Because $A\beta_{40}$ peptides do not form stable oligomers, BN-PAGE and FTIR studies were carried out on $A\beta_{42}$ oligomers stabilized by SDS detergent. The BN-PAGE experiments clearly show that uranyl ions interfere with the formation of homogeneous $A\beta_{42}$ oligomers (Figure 7). This is further supported by the FTIR measurements, where the position of the β-sheet main band is downshifted when increasing concentrations of uranyl ions are present during oligomer formation (Figure 8). The uranyl effect is more pronounced on the larger and mainly dodecameric $A\beta_{42}$ oligomers, which are formed in the presence of 0.05% SDS. The spectral changes observed with uranyl ions are consistent with the previously observed effects of Ni(II) ions.[118] However, only 10 μM of divalent uranyl ions (Figure 7, Lane 4) but 500 mM of divalent Ni(II) ions[118] are required for full disruption of homogeneous $A\beta O_{0.05\%SDS}$ oligomers, even though Ni(II) ions display a stronger binding affinity for Aβ peptides than uranyl ions at neutral pH (Figures 7, 8 and Table 2). In general, the effects of uranyl ions on Aβ oligomerization qualitatively resemble those of other transition metal ions, including Ni,[118] more than those of monovalent alkali ions, such as Li.[139] Such conclusions are consistent with the theoretical findings regarding the relative propensities of different metal ions for interactions with polypeptides.[151]

3.5. Medical Implications.

Our current results show that uranyl ions induce structural changes in Aβ monomers and Aβ oligomers and inhibit Aβ fibrillization and homogeneous oligomer formation already at sub-stoichiometric concentrations. It is unclear how these uranyl interactions may influence (or not) the toxicity of Aβ oligomers or the Aβ-induced pathology in AD patients. Furthermore, no link has been established between uranium/uranyl exposure and AD incidence. On the other hand, very few people have investigated such possible links. The current results show that uranyl ions affect Aβ peptide aggregation in similar ways as Pb and Hg ions, and Pb and Hg exposure might be linked to the development of AD and other neurodegenerative diseases.[3,47] Given these similar molecular interactions, it could be worthwhile to conduct cell studies, animal studies, and epidemiological studies on AD patients to find out if exposure to uranium/uranyl might induce AD. However, even if such an effect does exist, U is a well-known toxic metal, and it is possible that people exposed to U will suffer more immediate harmful health effects that will mask a slowly progressing dementia. The molecular mechanisms for the chemical toxicity of U are not fully understood. Our current results show that even low concentrations of uranyl can induce unstructured protein aggregation in Aβ peptides and, most likely, also in other peptides and proteins. Thus, a general toxic mechanism of uranyl ions could be to modulate protein folding, misfolding, and aggregation.

4. CONCLUSIONS

Uranyl ions, UO_2^{2+}, bind to $A\beta_{40}$ peptides via non-specific electrostatic interactions, with an apparent binding affinity of 16.3 ± 4 μM at pH 5.1. Uranyl binding is weaker and less uniform at neutral pH, possibly because of interference from His sidechains and from other uranyl species such as hydroxides. The uranyl ions inhibit Aβ fibrillization and

oligomer formation in a concentration-dependent manner, with clear effects already at sub-stoichiometric concentrations, and also induce structural changes in Aβ monomers and Aβ oligomers. A general toxic mechanism of uranyl ions could be to modulate protein folding, misfolding, and aggregation.

5. MATERIALS AND METHODS

5.1. Materials. SDS detergent, 2-(N-morpholino)ethanesulfonic acid (MES) hydrate, sodium phosphate, depleted uranyl acetate, and dimethyl sulfoxide (DMSO) were all purchased from Sigma-Aldrich (USA).

Synthetic lyophilized wt Aβ (1−42) peptides, abbreviated as Aβ$_{42}$, with the primary sequence DAEFR$_5$HDSGY$_{10}$EVHHQ$_{15}$KLVFF$_{20}$-AEDVG$_{25}$SNKGA$_{30}$IIGLM$_{35}$VGGVV$_{40}$IA, were purchased from JPT Peptide Technologies (Germany). Two recombinant Aβ variants were purchased as lyophilized powder from AlexoTech AB (Umeå, Sweden), namely, the Aβ$_{40}$ peptide and the Aβ$_{40}$ (H6A, H13A, and H14A) triple-mutant, which in the following is referred to as the Aβ$_{40}$ (NoHis) mutant. The Aβ$_{40}$ peptide was also purchased uniformly single-labeled with ^{15}N isotopes. All Aβ$_{40}$ peptide variants were stored at −80 °C until use. Before measurements, they were dissolved in 10 mM NaOH and then sonicated in an ice bath for 5 min to avoid pre-formed aggregates. The samples were then diluted in either sodium phosphate buffer at pH 7.3 or in MES buffer at pH 7.3 and 5.1. The peptide concentrations were initially estimated from the weight of the dry powder and then more accurately determined with a NanoDrop spectrophotometer.

5.2. Preparation of Aβ$_{42}$ Oligomers. Treatment of Aβ$_{42}$ peptides with low concentrations (≤7 mM) of SDS, i.e., below the critical micelle concentration for SDS, which is 8.2 mM in water at 25 °C,[152] leads to the formation of stable and homogeneous Aβ$_{42}$ oligomers of certain sizes and conformations.[131,132,153] To prepare such oligomers, size exclusion chromatography (SEC) was initially used to purify synthetic Aβ$_{42}$ peptides into monomeric form. First, 1 mg of lyophilized Aβ$_{42}$ powder was dissolved in 250 mL of DMSO. Next, a Sephadex G-250 HiTrap desalting column (GE Healthcare, Uppsala) was equilibrated with a 5 mM NaOH solution (pH = 12.3) and washed with a solution of 10−15 mL of 5 mM NaOD, pD = 12.7.[154] The peptide solution in DMSO was applied to the column, followed by an injection of 1.25 mL of 5 mM NaOD. The collection of peptide fractions in 5 mM NaOD on ice was started at a 1 mg/ mL flow rate. Ten fractions of 1 mL volumes were collected in 1.5 mL Eppendorf tubes. The absorbance for each fraction at 280 nm was measured with a NanoDrop instrument (Eppendorf, Germany), and peptide concentrations were determined using a molar extinction coefficient of 1280 M^{-1} cm^{-1} for the single Tyr in Aβ$_{42}$.[155] The peptide fractions were flash-frozen in liquid nitrogen, covered with argon gas on top in 1.5 mL Eppendorf tubes, and stored at −80 °C until used. SDS-stabilized Aβ$_{42}$ oligomers of two well-defined sizes (approximately tetramers and dodecamers) were prepared according to a previously published protocol,[131] but in D$_2$O, at a 4-fold lower peptide concentration and without the original dilution step.[132] The reaction mixtures [100−120 μM Aβ$_{42}$ in PBS, containing either 0.05% (1.7 mM) SDS or 0.2% (6.9 mM) SDS] were incubated together with 0−1000 μM uranyl acetate at 37 °C for 24 h and then flash-frozen in liquid nitrogen and stored at −20 °C for later analysis.

5.3. Thioflavin T Aggregation Kinetics. To monitor the effect of uranyl ions on Aβ$_{40}$ aggregation kinetics, a FLUOstar Omega microplate reader (BMG LABTECH, Germany) was used. Samples containing 20 μM Aβ$_{40}$wt, 20 mM MES buffer pH 7.3, 50 μM thioflavin T, and different concentrations of uranyl acetate (i.e., 0, 0.04, 0.2, 0.4, 2, and 20 μM) were added to a 384-well plate, with 35 μL of sample in each well. Thioflavin T is a benzothiazole dye that increases in fluorescence upon binding to amyloid aggregates[116] and is therefore used to monitor the formation of amyloid aggregates. The ThT dye was excited at 440 nm, and ThT fluorescence emission at 480 nm was measured every 5 min. Before each measurement, the plate was shaken in orbital mode for 140 s at 200 rpm. The samples were incubated for a total of 15 h, and the assay was repeated three

times with four replicates of each condition. To determine kinetic aggregation parameters, the data was fitted to eq 1:

$$F(t) = F_0 + m_0 \cdot t + \frac{F_\infty + m_\infty \cdot t}{1 + \exp[-(t - t_{1/2})/\tau]} \tag{1}$$

Here, F_0 and F_∞ are the intercepts of the initial and final fluorescence intensity baselines, m_0 and m_∞ are the slopes of the initial and final baselines, $t_{1/2}$ is the time needed to reach halfway through the elongation phase (i.e., aggregation half-time), and τ is the elongation time constant.[116]

5.4. Transmission Electron Microscopy Imaging. Negative staining TEM images were recorded for Aβ$_{40}$ peptides that had aggregated under the same conditions as in the ThT fluorescence studies (above). Thus, 20 μM of Aβ$_{40}$ in 20 mM MES buffer, pH 7.3, was incubated for 20 h on a thermo shaker at 37 °C and 300 rpm, together with 0, 0.2, 2, and 20 μM of uranyl acetate. Then, samples of 5 μL were put on copper grids of 200 μm mesh size, which were covered with a Pioloform film upon which a carbon layer had been deposited and then glow-discharged with a Leica EM ACE600 carbon coater (Leica Microsystems, Germany). The Aβ$_{40}$ samples were absorbed onto the grids for 5 min, rinsed with Milli-Q water two times, and then stained for 2 min with a 2% aqueous solution of uranyl acetate. Next, the excess stain was removed with filter paper, and the samples were left to air-dry. A digital Orius SC1000 camera was used to record TEM images in a FEI Tecnai G2 Spirit electron microscope (FEI, The Netherlands) operating at 120 kV accelerating voltage.

5.5. Circular Dichroism Spectroscopy Measurements of the Secondary Structure. CD measurements were carried out on a Chirascan CD spectrometer from Applied Photophysics Ltd. (U.K.). Samples containing 600 μL of 10 μM Aβ$_{40}$ peptide in 20 mM phosphate buffer, at either pH 7.3 or pH 5.1, were placed in a quartz cuvette with a 2 mm pathlength. CD spectra were recorded at 20 °C between 192 and 250 nm using steps of 0.5 nm and a sampling time of 5 s per data point. Then, small volumes of uranyl acetate were titrated to the samples in steps of 2, 6, 16, 56, and finally 256 μM. The total increase of volume upon the addition of the uranyl acetate was less than 3%. All data was processed with the Chirascan Pro-Data v.4.4.1 software (Applied Photophysics Ltd., U.K.), including smoothing with a ten-point smoothing filter. 50 mM SDS detergent was added to some of the samples as SDS micelles constitute a simple model for bio-membranes.[125,126] Aβ peptides are known to insert their central and C-terminal segments as α-helices into SDS micelles, while the N-terminal Aβ segment remains unstructured outside the micelle surface.[19,125] Because the critical micelle concentration for SDS is 8.2 mM in water at 25 °C,[152] micelles clearly formed under the experimental conditions. With approximately 62−65 SDS molecules per micelle,[156] 50 mM SDS yields a micelle concentration slightly below 1 mM, i.e., much higher than the concentration of Aβ peptides. This means that each micelle will generally contain no more than one Aβ peptide, which effectively prevents Aβ aggregation and ensures that uranyl interactions are with monomeric Aβ peptides. The high SDS concentration used to obtain this condition, i.e., 50 mM, does not pose a problem in the current experiments. Even though 50 mM SDS would efficiently denature most folded proteins, such denaturing effects are not relevant for small intrinsically disordered peptides such as Aβ (in monomeric form).

5.6. Fluorescence Measurements of Dityrosine Formation. Fluorescence emission spectra between 330 and 480 nm (excitation at 315 nm) were recorded at room temperature with a Jobin Yvon Horiba Fluorolog 3 fluorescence spectrometer (Longjumeau, France) for two samples of 10 μM Aβ$_{40}$ peptide in 20 mM MES buffer, pH 7.3. One sample contained 100 μM uranyl acetate to investigate the possible effects of uranyl ions on dityrosine formation. The control sample contained 100 μM of the chelator EDTA to remove any free metal ions. All measurements were conducted in triplicate using a quartz cuvette with a 4 mm path length and containing a 0.7 mL liquid sample. Spectra were recorded after 0 and 24 h of incubation,

during which the samples were kept at room temperature without agitation or other treatment.

5.7. Nuclear Magnetic Resonance Spectroscopy. NMR spectroscopy experiments were conducted on a Bruker Avance spectrometer operating at 500 MHz and being equipped with a cryoprobe for increased sensitivity. Uranyl acetate was titrated to 92 μM monomeric ^{15}N-labeled Aβ_{40} peptides in 20 mM MES buffer (90/10H$_2$O/D$_2$O) at either pH 7.3 or pH 5.1 at 5 °C. Two-dimensional ^{1}H, ^{15}N-HSQC (heteronuclear single quantum coherence) NMR spectra were recorded during the titrations using settings with 128 t1 increments, 24 scans, and a 1 s recycle delay. The spectra were then processed and evaluated in the Topspin software (v. 3.2) using already published assignments for HSQC cross-peaks of Aβ_{40} in buffer at neutral pH[157−159] or at acidic pH.[119]

5.8. Binding Affinity Measurements via Tyrosine Fluorescence Quenching. The binding affinities between uranyl ions and Aβ_{40} peptides were evaluated via the quenching effect of uranyl on the intrinsic fluorescence of Tyr10, the only natural fluorophore in the wt Aβ peptide. Fluorescence measurements were conducted on a Jobin Yvon Horiba Fluorolog 3 fluorescence spectrophotometer (Longjumeau, France) using a quartz cuvette with a 4 mm path length. The fluorescence emission intensity of samples containing 20 μM Aβ peptides in 20 mM MES buffer, at either pH 7.3 or pH 5.5 and without or with 50 mM SDS detergent present, was measured at 305 nm (excitation wavelength 276 nm) at 20 °C. Aliquots of uranyl acetate (stock concentrations of 1, 2, and 10 mM) were titrated to the samples, and the Tyr10 fluorescence intensity was plotted against the concentration of UO$_2^{2+}$ ions. Apparent dissociation constants (K_D^{App}) were determined by fitting the plots to eq 2

$$I = I_0 + \frac{I_\infty - I_0}{2\cdot[Ab]}\cdot\{(K_D + [U] + [Ab]) - \sqrt{(K_D + [U] + [Ab])^2 - 4\cdot[U]\cdot[Ab]}\,\} \quad (2)$$

where I_0 is the initial fluorescence intensity with no added UO$_2^{2+}$ ions, I_∞ is the steady-state intensity at the end of the titration, [Ab] is the protein concentration, and [U] is the concentration of added UO$_2^{2+}$ ions.[121,160]

5.9. Blue Native Polyacrylamide Gel Electrophoresis. Homogeneous solutions of oligomers of 80−100 μM Aβ_{42} peptides[132] prepared (as described in Section 5.2) in the presence of different concentrations of uranyl acetate (0−1000 μM) were analyzed by BN-PAGE using the Invitrogen system (Thermo Fisher Scientific, USA). Thus, 4−16% Bis−Tris Novex gels (Thermo Fisher Scientific, USA) were loaded with 10 μL samples containing Aβ_{42} oligomer solutions alongside alongside the Amersham high MW calibration kit for native electrophoresis (GE Healthcare, USA). The gels were run at 4 °C using the electrophoresis system according to the Invitrogen instructions (Thermo Fisher Scientific, USA) and then stained with the Pierce Silver Staining Kit according to the manufacturer's instructions (Thermo Fisher Scientific, USA). BN-PAGE was chosen for analysis instead of SDS−PAGE to avoid disruption of the SDS-stabilized and non-cross-linked Aβ_{42} oligomers by the high (>1%) SDS concentrations used in SDS−PAGE sample buffers.[161]

5.10. Infrared Spectroscopy. FTIR spectra of the SDS-stabilized Aβ_{42} oligomers (prepared as described in Section 5.2) were recorded in transmission mode on a Tensor 37 FTIR spectrometer (Bruker Optics, Germany) equipped with a sample shutter and a liquid nitrogen-cooled MCT detector. The unit was continuously purged with dry air during the measurements. 8−10 μL of the 80−100 μM Aβ_{42} oligomer samples, prepared (as described in Section 5.2) with different concentrations of uranyl acetate (0−1000 μM), was put between two flat CaF$_2$ disks separated by a 50 μm plastic spacer covered with vacuum grease at the periphery. The assembled IR cuvette was mounted into the sample position of a sample shuttle inside the instrument's sample chamber, while a metal grid (used as the background) was positioned in the reference holder. The sample shuttle was used to measure the sample and reference spectra without opening the chamber. The samples were allowed to sit for at least 15 min after closing the chamber lid to avoid interference from water

vapor. FTIR spectra were recorded at room temperature in the 1900−800 cm^{-1} range, with 300 scans for both background and sample spectra, using a 6 mm aperture and at a resolution of 2 cm^{-1}. The light intensities above 2200 cm^{-1} and below 1500 cm^{-1} were blocked with a germanium filter and a cellulose membrane, respectively.[162] The spectra were analyzed and plotted with the OPUS 5.5 software, and second derivatives were calculated with a 17 cm^{-1} smoothing range.

■ **AUTHOR INFORMATION**

Corresponding Authors

    Elina Berntsson − Chemistry Section, Arrhenius Laboratories, Stockholm University, 106 91 Stockholm, Sweden; Department of Chemistry and Biotechnology, Tallinn University of Technology, 19086 Tallinn, Estonia; ⊙ orcid.org/0000-0002-7544-092X; Email: elina.berntsson@dbb.su.se

    Sebastian K. T. S. Wärmländer − Chemistry Section, Arrhenius Laboratories, Stockholm University, 106 91 Stockholm, Sweden; CellPept Sweden AB, 118 47 Stockholm, Sweden; ⊙ orcid.org/0000-0003-3917-1838; Email: seb@student.su.se

Authors

    Faraz Vosough − Chemistry Section, Arrhenius Laboratories, Stockholm University, 106 91 Stockholm, Sweden

    Andra Noormägi − Department of Chemistry and Biotechnology, Tallinn University of Technology, 19086 Tallinn, Estonia

    Kärt Padari − Institute of Molecular and Cell Biology, University of Tartu, 50090 Tartu, Estonia

    Fanny Asplund − Chemistry Section, Arrhenius Laboratories, Stockholm University, 106 91 Stockholm, Sweden

    Maciej Gielnik − Department of Molecular Biology and Genetics, Aarhus University, 8000 Aarhus, Denmark; ⊙ orcid.org/0000-0002-1990-2800

    Suman Paul − Chemistry Section, Arrhenius Laboratories, Stockholm University, 106 91 Stockholm, Sweden

    Jüri Jarvet − Chemistry Section, Arrhenius Laboratories, Stockholm University, 106 91 Stockholm, Sweden; CellPept Sweden AB, 118 47 Stockholm, Sweden; ⊙ orcid.org/0000-0002-7863-1887

    Vello Tõugu − Department of Chemistry and Biotechnology, Tallinn University of Technology, 19086 Tallinn, Estonia

    Per M. Roos − Institute of Environmental Medicine, Karolinska Institutet, 171 77 Stockholm, Sweden; University Healthcare Unit of Capio St. Göran Hospital, 112 81 Stockholm, Sweden

    Maciej Kozak − Department of Biomedical Physics, Institute of Physics, Faculty of Physics, Adam Mickiewicz University, 61-712 Poznań, Poland; SOLARIS National Synchrotron Radiation Centre, Jagiellonian University, 31-007 Kraków, Poland; ⊙ orcid.org/0000-0003-3312-6518

    Astrid Gräslund − Chemistry Section, Arrhenius Laboratories, Stockholm University, 106 91 Stockholm, Sweden; CellPept Sweden AB, 118 47 Stockholm, Sweden

    Andreas Barth − Chemistry Section, Arrhenius Laboratories, Stockholm University, 106 91 Stockholm, Sweden; ⊙ orcid.org/0000-0001-5784-7673

    Margus Pooga − Institute of Technology, University of Tartu, 50090 Tartu, Estonia

    Peep Palumaa − Department of Chemistry and Biotechnology, Tallinn University of Technology, 19086 Tallinn, Estonia; ⊙ orcid.org/0000-0002-3505-3466

Author Contributions

A.G., P.P., P.R., and S.W. designed and funded the study, A.B. and F.V. conducted the IR and PAGE experiments, E.B., J.J., S.P., and S.W. conducted the NMR experiments, A.N., K.P., M.G., M.K., M.P., P.P., and V.T. conducted the TEM and peptide aggregation experiments, E.B., F.A., J.J., and S.W. conducted the CD and fluorescence experiments, and all authors helped with writing the manuscript.

Notes

The authors declare the following competing financial interest(s): A.G., J.J., and S.W. are shareholders in CellPept Sweden AB. Neither this company, nor the funding organizations, had any role in the design of the study; in the collection, analyses, or interpretation of data; in the writing of the manuscript; or in the decision to publish the results.

■ REFERENCES

(1) Scheltens, P.; De Strooper, B.; Kivipelto, M.; Holstege, H.; Chetelat, G.; Teunissen, C. E.; Cummings, J.; van der Flier, W. M. Alzheimer's disease. *Lancet* **2021**, *397*, 1577–1590.

(2) Alzheimer's-Association 2021. Alzheimer's disease facts and figures. *Alzheimers Dement.* **2021**, *17*, 327–406.

(3) Wallin, C.; Sholts, S. B.; Österlund, N.; Luo, J.; Jarvet, J.; Roos, P. M.; Ilag, L.; Gräslund, A.; Wärmländer, S. K. T. S. Alzheimer's disease and cigarette smoke components: effects of nicotine, PAHs, and Cd(II), Cr(III), Pb(II), Pb(IV) ions on amyloid-beta peptide aggregation. *Sci. Rep.* **2017**, *7*, 14423.

(4) Andrews, S. J.; Fulton-Howard, B.; O'Reilly, P.; Marcora, E.; Goate, A. M.; Farrer, L. A.; Haines, J. L.; Mayeux, R.; Naj, A. C.; Pericak-Vance, M. A.; et al. Causal Associations Between Modifiable Risk Factors and the Alzheimer's Phenome. *Ann. Neurol.* **2021**, *89*, 54–65.

(5) Bjørklund, G.; Aaseth, J.; Dadar, M.; Chirumbolo, S. Molecular Targets in Alzheimer's Disease. *Mol. Neurobiol.* **2019**, *56*, 7032–7044.

(6) Tiiman, A.; Jelic, V.; Jarvet, J.; Jaremo, P.; Bogdanovic, N.; Rigler, R.; Terenius, L.; Gräslund, A.; Vukojevic, V. Amyloidogenic Nanoplaques in Blood Serum of Patients with Alzheimer's Disease Revealed by Time-Resolved Thioflavin T Fluorescence Intensity Fluctuation Analysis. *J. Alzheimer's Dis.* **2019**, *68*, 571–582.

(7) Parums, D. V. Editorial: Targets for Disease-Modifying Therapies in Alzheimer's Disease, Including Amyloid beta and Tau Protein. *Med. Sci. Monit.* **2021**, *27*, No. e934077.

(8) Luo, J.; Otero, J. M.; Yu, C. H.; Wärmländer, S. K.; Gräslund, A.; Overhand, M.; Abrahams, J. P. Inhibiting and reversing amyloid-beta peptide (1-40) fibril formation with gramicidin S and engineered analogues. *Chemistry* **2013**, *19*, 17338–17348.

(9) Richman, M.; Wilk, S.; Chemerovski, M.; Wärmländer, S. K.; Wahlström, A.; Gräslund, A.; Rahimipour, S. In vitro and mechanistic studies of an antiamyloidogenic self-assembled cyclic D,L-alpha-peptide architecture. *J. Am. Chem. Soc.* **2013**, *135*, 3474–3484.

(10) Shi, M.; Chu, F.; Zhu, F.; Zhu, J. Impact of Anti-amyloid-beta Monoclonal Antibodies on the Pathology and Clinical Profile of Alzheimer's Disease: A Focus on Aducanumab and Lecanemab. *Front. Aging Neurosci.* **2022**, *14*, 870517.

(11) Lee, S. J.; Nam, E.; Lee, H. J.; Savelieff, M. G.; Lim, M. H. Towards an understanding of amyloid-beta oligomers: character-ization, toxicity mechanisms, and inhibitors. *Chem. Soc. Rev.* **2017**, *46*, 310–323.

(12) Niewiadomska, G.; Niewiadomski, W.; Steczkowska, M.; Gasiorowska, A. Tau Oligomers Neurotoxicity. *Life (Basel)* **2021**, *11*, 28.

(13) Nguyen, P. H.; Ramamoorthy, A.; Sahoo, B. R.; Zheng, J.; Faller, P.; Straub, J. E.; Dominguez, L.; Shea, J. E.; Dokholyan, N. V.; De Simone, A.; Ma, B.; Nussinov, R.; Najafi, S.; Ngo, S. T.; Loquet, A.; Chiricotto, M.; Ganguly, P.; McCarty, J.; Li, M. S.; Hall, C.; Wang, Y.; Miller, Y.; Melchionna, S.; Habenstein, B.; Timr, S.; Chen, J.; Hnath, B.; Strodel, B.; Kayed, R.; Lesne, S.; Wei, G.; Sterpone, F.; Doig, A. J.; Derreumaux, P. Amyloid Oligomers: A Joint Experimental/Computational Perspective on Alzheimer's Disease, Parkinson's Disease, Type II Diabetes, and Amyotrophic Lateral Sclerosis. *Chem. Rev.* **2021**, *121*, 2545–2647.

(14) Morgan, G. J. Transient disorder along pathways to amyloid. *Biophys. Chem.* **2022**, *281*, 106711.

(15) Glenner, G. G.; Wong, C. W. Alzheimer's disease: initial report of the purification and characterization of a novel cerebrovascular amyloid protein. *Biochem. Biophys. Res. Commun.* **1984**, *120*, 885–890.

(16) Zheng, H.; Koo, E. H. The amyloid precursor protein: beyond amyloid. *Mol. Neurodegener.* **2006**, *1*, 5.

(17) Funamoto, S.; Tagami, S.; Okochi, M.; Morishima-Kawashima, M. Successive cleavage of beta-amyloid precursor protein by gamma-secretase. *Semin. Cell Dev. Biol.* **2020**, *105*, 64–74.

(18) Abelein, A.; Abrahams, J. P.; Danielsson, J.; Gräslund, A.; Jarvet, J.; Luo, J.; Tiiman, A.; Wärmländer, S. K. The hairpin conformation of the amyloid beta peptide is an important structural motif along the aggregation pathway. *J. Biol. Inorg. Chem.* **2014**, *19*, 623–634.

(19) Jarvet, J.; Danielsson, J.; Damberg, P.; Oleszczuk, M.; Gräslund, A. Positioning of the Alzheimer Aβ(1−40) peptide in SDS micelles using NMR and paramagnetic probes. *J. Biomol. NMR* **2007**, *39*, 63–72.

(20) Wahlström, A.; Hugonin, L.; Perálvarez-Marin, A.; Jarvet, J.; Gräslund, A. Secondary structure conversions of Alzheimer's Aβ(1-40) peptide induced by membrane-mimicking detergents: Detergent-induced Aβ(1-40) secondary structures. *FEBS J.* **2008**, *275*, 5117–5128.

(21) Owen, M. C.; Gnutt, D.; Gao, M.; Wärmländer, S. K. T. S.; Jarvet, J.; Gräslund, A.; Winter, R.; Ebbinghaus, S.; Strodel, B. Effects of in vivo conditions on amyloid aggregation. *Chem. Soc. Rev.* **2019**, *48*, 3946–3996.

(22) Luo, J.; Wärmländer, S. K.; Gräslund, A.; Abrahams, J. P. Non-chaperone proteins can inhibit aggregation and cytotoxicity of Alzheimer amyloid beta peptide. *J. Biol. Chem.* **2014**, *289*, 27766–27775.

(23) Gallego-Villarejo, L.; Wallin, C.; Krol, S.; Enrich-Bengoa, J.; Suades, A.; Aguilella-Arzo, M.; Gomara, M. J.; Haro, I.; Wärmländer, S.; Munoz, F. J.; Gräslund, A.; Peralvarez-Marin, A. Big dynorphin is a neuroprotector scaffold against amyloid beta-peptide aggregation and cell toxicity. *Comput. Struct. Biotechnol. J.* **2022**, *20*, 5672–5679.

(24) Luo, J.; Wärmländer, S. K.; Gräslund, A.; Abrahams, J. P. Cross-interactions between the Alzheimer Disease Amyloid-beta Peptide and Other Amyloid Proteins: A Further Aspect of the Amyloid Cascade Hypothesis. *J. Biol. Chem.* **2016**, *291*, 16485–16493.

(25) Luo, J.; Wärmländer, S. K.; Gräslund, A.; Abrahams, J. P. Reciprocal Molecular Interactions between the Aβ Peptide Linked to Alzheimer's Disease and Insulin Linked to Diabetes Mellitus Type II. *ACS Chem. Neurosci.* **2016**, *7*, 269–274.

(26) Wallin, C.; Hiruma, Y.; Wärmländer, S. K. T. S.; Huvent, I.; Jarvet, J.; Abrahams, J. P.; Gräslund, A.; Lippens, G.; Luo, J. The

Neuronal Tau Protein Blocks in Vitro Fibrillation of the Amyloid-β (Aβ) Peptide at the Oligomeric Stage. *J. Am. Chem. Soc.* **2018**, *140*, 8138−8146.

(27) Henning-Knechtel, A.; Kumar, S.; Wallin, C.; Król, S.; Wärmländer, S.; Jarvet, J.; Esposito, G.; Kirmizialtin, S.; Gräslund, A.; Hamilton, A. D.; Magzoub, M. Designed cell-penetrating peptide inhibitors of amyloid-beta aggregation and cytotoxicity. *Cell Rep. Phys. Sci.* **2020**, *1*, 100014.

(28) Luo, J.; Yu, C. H.; Yu, H.; Borstnar, R.; Kamerlin, S. C.; Gräslund, A.; Abrahams, J. P.; Wärmländer, S. K. Cellular Polyamines Promote Amyloid-Beta (Aβ) Peptide Fibrillation and Modulate the Aggregation Pathways. *ACS Chem. Neurosci.* **2013**, *4*, 454−462.

(29) Chen, L. L.; Fan, Y. G.; Zhao, L. X.; Zhang, Q.; Wang, Z. Y. The metal ion hypothesis of Alzheimer's disease and the anti-neuroinflammatory effect of metal chelators. *Bioorg. Chem.* **2023**, *131*, 106301.

(30) Wallin, C.; Jarvet, J.; Biverstål, H.; Wärmländer, S.; Danielsson, J.; Gräslund, A.; Abelein, A. Metal ion coordination delays amyloid-beta peptide self-assembly by forming an aggregation-inert complex. *J. Biol. Chem.* **2020**, *295*, 7224−7234.

(31) Huat, T. J.; Camats-Perna, J.; Newcombe, E. A.; Valmas, N.; Kitazawa, M.; Medeiros, R. Metal Toxicity Links to Alzheimer's Disease and Neuroinflammation. *J. Mol. Biol.* **2019**, *431*, 1843−1868.

(32) Stefaniak, E.; Atrian-Blasco, E.; Goch, W.; Sabater, L.; Hureau, C.; Bal, W. The Aggregation Pattern of Aβ_{1-40} is Altered by the Presence of *N*-Truncated Aβ_{4-40} and/or Cu^{II} in a Similar Way through Ionic Interactions. *Chemistry* **2021**, *27*, 2798−2809.

(33) Lovell, M. A.; Robertson, J. D.; Teesdale, W. J.; Campbell, J. L.; Markesbery, W. R. Copper, iron and zinc in Alzheimer's disease senile plaques. *J. Neurol. Sci.* **1998**, *158*, 47−52.

(34) Miller, L. M.; Wang, Q.; Telivala, T. P.; Smith, R. J.; Lanzirotti, A.; Miklossy, J. Synchrotron-based infrared and X-ray imaging shows focalized accumulation of Cu and Zn co-localized with beta-amyloid deposits in Alzheimer's disease. *J. Struct. Biol.* **2006**, *155*, 30−37.

(35) Atwood, C. S.; Perry, G.; Zeng, H.; Kato, Y.; Jones, W. D.; Ling, K. Q.; Huang, X.; Moir, R. D.; Wang, D.; Sayre, L. M.; Smith, M. A.; Chen, S. G.; Bush, A. I. Copper Mediates Dityrosine Cross-Linking of Alzheimer's Amyloid-β. *Biochemistry* **2004**, *43*, 560−568.

(36) Wärmländer, S. K. T. S.; Österlund, N.; Wallin, C.; Wu, J.; Luo, J.; Tiiman, A.; Jarvet, J.; Gräslund, A. Metal binding to the Amyloid-β peptides in the presence of biomembranes: potential mechanisms of cell toxicity. *J. Biol. Inorg. Chem.* **2019**, *24*, 1189−1196.

(37) Jones, M. R.; Service, E. L.; Thompson, J. R.; Wang, M. C.; Kimsey, I. J.; DeToma, A. S.; Ramamoorthy, A.; Lim, M. H.; Storr, T. Dual-function triazole-pyridine derivatives as inhibitors of metal-induced amyloid-beta aggregation. *Metallomics* **2012**, *4*, 910−920.

(38) Savelieff, M. G.; Liu, Y.; Senthamarai, R. R.; Korshavn, K. J.; Lee, H. J.; Ramamoorthy, A.; Lim, M. H. A small molecule that displays marked reactivity toward copper- versus zinc-amyloid-beta implicated in Alzheimer's disease. *Chem. Commun. (Cambridge, U. K.)* **2014**, *50*, 5301−5303.

(39) Nordberg, G.; Costa, M. *Handbook on the Toxicology of Metals*, 5th ed.; Academic Press: London, U.K., 2021.

(40) Bridges, C. C.; Zalups, R. K. Molecular and ionic mimicry and the transport of toxic metals. *Toxicol. Appl. Pharmacol.* **2005**, *204*, 274−308.

(41) Sharma, S. K.; Goloubinoff, P.; Christen, P. Heavy metal ions are potent inhibitors of protein folding. *Biochem. Biophys. Res. Commun.* **2008**, *372*, 341−345.

(42) Tamas, M. J.; Sharma, S. K.; Ibstedt, S.; Jacobson, T.; Christen, P. Heavy metals and metalloids as a cause for protein misfolding and aggregation. *Biomolecules* **2014**, *4*, 252−267.

(43) Tamas, M. J.; Fauvet, B.; Christen, P.; Goloubinoff, P. Misfolding and aggregation of nascent proteins: a novel mode of toxic cadmium action in vivo. *Curr. Genet.* **2018**, *64*, 177−181.

(44) Li, S.; Liu, X. L.; Zhou, X. L.; Jiang, S. J.; Yuan, H. Expression of calmodulin-related genes in lead-exposed mice. *Interdiscip. Toxicol.* **2015**, *8*, 155−158.

(45) Ashok, A.; Rai, N. K.; Tripathi, S.; Bandyopadhyay, S. Exposure to As-Cd-and Pb-Mixture Induces Aβ, Amyloidogenic APP Processing and Cognitive Impairments via Oxidative Stress-Dependent Neuro-inflammation in Young Rats. *Toxicol. Sci.* **2015**, *143*, 64−80.

(46) Song, J. W.; Choi, B. S. Mercury induced the Accumulation of Amyloid Beta (Aβ) in PC12 Cells: The Role of Production and Degradation of Aβ. *Toxicol. Res.* **2013**, *29*, 235−240.

(47) Wallin, C.; Friedemann, M.; Sholts, S. B.; Noormagi, A.; Svantesson, T.; Jarvet, J.; Roos, P. M.; Palumaa, P.; Gräslund, A.; Wärmländer, S. K. T. S. Mercury and Alzheimer's Disease: Hg(II) Ions Display Specific Binding to the Amyloid-beta Peptide and Hinder Its Fibrillization. *Biomolecules* **2019**, *10*, 44.

(48) Notarachille, G.; Arnesano, F.; Calo, V.; Meleleo, D. Heavy metals toxicity: effect of cadmium ions on amyloid beta protein 1-42. Possible implications for Alzheimer's disease. *Biometals* **2014**, *27*, 371−388.

(49) Emard, J. F.; Andre, P.; Thouez, J.-P.; Mathieu, J.; Boily, C.; Beaudry, M.; Cholette, A.; Robitaille, Y.; Bouchard, R.; Daoud, N.; Veilleux, F.; Gauvreau, D. Geographical distribution of Alzheimer's disease cases at birth and the geochemical profile of Saguenay-Lac-Saint-Jean/Qu-bec, Canada (image project). *Water, Air, Soil Pollut.* **1994**, *72*, 251−264.

(50) Lemercier, V.; Millot, X.; Ansoborlo, E.; Menetrier, F.; Flury-Herard, V.; Rousselle, C.; Scherrmann, J. M. Study of uranium transfer across the blood-brain barrier. *Radiat. Prot. Dosim.* **2003**, *105*, 243−245.

(51) Dinocourt, C.; Legrand, M.; Dublineau, I.; Lestaevel, P. The neurotoxicology of uranium. *Toxicology* **2015**, *337*, 58−71.

(52) Bjørklund, G.; Pivina, L.; Dadar, M.; Semenova, Y.; Rahman, M. M.; Chirumbolo, S.; Aaseth, J. Depleted uranium and Gulf War Illness: Updates and comments on possible mechanisms behind the syndrome. *Environ. Res.* **2020**, *181*, 108927.

(53) Bjørklund, G.; Semenova, Y.; Pivina, L.; Dadar, M.; Rahman, M. M.; Aaseth, J.; Chirumbolo, S. Uranium in drinking water: a public health threat. *Arch. Toxicol.* **2020**, *94*, 1551−1560.

(54) Faa, A.; Gerosa, C.; Fanni, D.; Floris, G.; Eyken, P. V.; Lachowicz, J. I.; Nurchi, V. M. Depleted Uranium and Human Health. *Curr. Med. Chem.* **2018**, *25*, 49−64.

(55) Brugge, D.; de Lemos, J. L.; Oldmixon, B. Exposure pathways and health effects associated with chemical and radiological toxicity of natural uranium: a review. *Rev. Environ. Health* **2005**, *20*, 177−193.

(56) Agency for Toxic Substances and Disease Registry. *Toxicological Profile for Uranium*; Agency for Toxic Substances and Disease Registry, 2013.

(57) Marshall, A. C. Gulf war depleted uranium risks. *J. Exposure Sci. Environ. Epidemiol.* **2008**, *18*, 95−108.

(58) Besic, L.; Muhovic, I.; Asic, A.; Kurtovic-Kozaric, A. Meta-analysis of depleted uranium levels in the Balkan region. *J. Environ. Radioact.* **2017**, *172*, 207−217.

(59) Besic, L.; Muhovic, I.; Mrkulic, F.; Spahic, L.; Omanovic, A.; Kurtovic-Kozaric, A. Meta-analysis of depleted uranium levels in the Middle East region. *J. Environ. Radioact.* **2018**, *192*, 67−74.

(60) Abu-Qare, A. W.; Abou-Donia, M. B. Depleted uranium−the growing concern. *J. Appl. Toxicol.* **2002**, *22*, 149−152.

(61) Albertini, R. J.; Nicklas, J. A.; Vacek, P. M.; Carter, E. W.; McDiarmid, M. Longitudinal study of t-cell somatic mutations conferring glycosylphosphatidylinositol-anchor deficiency in gulf war I veterans exposed to depleted uranium. *Environ. Mol. Mutagen.* **2019**, *60*, 494−504.

(62) Nicklas, J. A.; Vacek, P. M.; Carter, E. W.; McDiarmid, M.; Albertini, R. J. Molecular analysis of glycosylphosphatidylinositol anchor deficient aerolysin resistant isolates in gulf war i veterans exposed to depleted uranium. *Environ. Mol. Mutagen.* **2019**, *60*, 470−493.

(63) Venus, M.; Puntaric, D.; Gvozdic, V.; Vidosavljevic, D.; Bijelic, L.; Puntaric, A.; Puntaric, E.; Vidosavljevic, M.; Matijana, J.; Jasenka, S. Determinations of uranium concentrations in soil, water, vegetables and biological samples from inhabitants of war affected areas in

eastern Croatia (ICP-MS method). *J. Environ. Radioact.* **2019**, *203*, 147−153.

(64) Savabieasfahani, M.; Basher Ahamadani, F.; Mahdavi Damghani, A. Living near an active U.S. military base in Iraq is associated with significantly higher hair thorium and increased likelihood of congenital anomalies in infants and children. *Environ. Pollut.* **2020**, *256*, 113070.

(65) Surdyk, S.; Itani, M.; Al-Lobaidy, M.; Kahale, L. A.; Farha, A.; Dewachi, O.; Akl, E. A.; Habib, R. R. Weaponised uranium and adverse health outcomes in Iraq: a systematic review. *BMJ Glob. Health* **2021**, *6*, No. e004166.

(66) McDiarmid, M. A.; Gaitens, J. M.; Hines, S.; Condon, M.; Roth, T.; Oliver, M.; Gucer, P.; Brown, L.; Centeno, J. A.; Dux, M.; Squibb, K. S. The U.S. Department of Veterans' Affairs depleted uranium exposed cohort at 25 Years: Longitudinal surveillance results. *Environ. Res.* **2017**, *152*, 175−184.

(67) McDiarmid, M. A.; Gucer, P.; Centeno, J. A.; Todorov, T.; Squibb, K. S. Semen Uranium Concentrations in Depleted Uranium Exposed Gulf War Veterans: Correlations with Other Body Fluid Matrices. *Biol. Trace Elem. Res.* **2019**, *190*, 45−51.

(68) Mould, R. F. Depleted uranium and radiation-induced lung cancer and leukaemia. *Br. J. Radiol.* **2001**, *74*, 677−683.

(69) Fathi, R. A.; Matti, L. Y.; Al-Salih, H. S.; Godbold, D. Environmental pollution by depleted uranium in Iraq with special reference to Mosul and possible effects on cancer and birth defect rates. *Med. Confl. Surviv.* **2013**, *29*, 7−25.

(70) Kathren, R. L. Invited editorial: Recent studies of the mortality and cancer morbidity experience of uranium workers and a fresh look at depleted uranium. *J. Radiol. Prot.* **2001**, *21*, 105−107.

(71) Yue, Y. C.; Li, M. H.; Wang, H. B.; Zhang, B. L.; He, W. The toxicological mechanisms and detoxification of depleted uranium exposure. *Environ. Health Prev. Med.* **2018**, *23*, 18.

(72) Nolan, J.; Weber, K. A. Natural uranium contamination in major US aquifers linked to nitrate. *Environ. Sci. Technol. Lett.* **2015**, *2*, 215−220.

(73) Seller, R. L. Temporal changes in water quality at a childhood leukemia cluster. *Ground Water* **2004**, *42*, 446−455.

(74) Karpas, Z.; Paz-Tal, O.; Lorber, A.; Salonen, L.; Komulainen, H.; Auvinen, A.; Saha, H.; Kurttio, P. Urine, hair, and nails as indicators for ingestion of uranium in drinking water. *Health Phys.* **2005**, *88*, 229−242.

(75) Wu, Y.; Wang, Y.; Xie, X. Occurrence, behavior and distribution of high levels of uranium in shallow groundwater at Datong basin, northern China. *Sci. Total Environ.* **2014**, *472*, 809−817.

(76) World Health Organization. *Uranium in Drinking-Water*; World Health Organization: Geneva, 2012. WHO/SDE/WSH/03.04/118/Rev/1.

(77) World Health Organization. *Health Effects of Depleted Uranium*, 2001.

(78) Bjørklund, G.; Christophersen, O. A.; Chirumbolo, S.; Selinus, O.; Aaseth, J. Recent aspects of uranium toxicology in medical geology. *Environ. Res.* **2017**, *156*, 526−533.

(79) Bersimbaev, R. I.; Bulgakova, O. The health effects of radon and uranium on the population of Kazakhstan. *Genes Environ.* **2015**, *37*, 18.

(80) de Rey, B. M.; Lanfranchi, H. E.; Cabrini, R. L. Percutaneous absorption of uranium compounds. *Environ. Res.* **1983**, *30*, 480−491.

(81) Opie, E. L.; Alford, L. B. The Influence of Diet Upon Necrosis Caused by Hepatic and Renal Poisons : Part Ii. Diet and the Nephritis Caused by Potassium Chromate, Uranium Nitrate, or Chloroform. *J. Exp. Med.* **1915**, *21*, 21−37.

(82) Konietzka, R. Gastrointestinal absorption of uranium compounds–a review. *Regul. Toxicol. Pharmacol.* **2015**, *71*, 125−133.

(83) Kurttio, P.; Komulainen, H.; Leino, A.; Salonen, L.; Auvinen, A.; Saha, H. Bone as a possible target of chemical toxicity of natural uranium in drinking water. *Environ. Health Perspect.* **2005**, *113*, 68−72.

(84) Bourgeois, D.; Burt-Pichat, B.; Le Goff, X.; Garrevoet, J.; Tack, P.; Falkenberg, G.; Van Hoorebeke, L.; Vincze, L.; Denecke, M. A.; Meyer, D.; Vidaud, C.; Boivin, G. Micro-distribution of uranium in bone after contamination: new insight into its mechanism of accumulation into bone tissue. *Anal. Bioanal. Chem.* **2015**, *407*, 6619−6625.

(85) Arzuaga, X.; Gehlhaus, M.; Strong, J. Modes of action associated with uranium induced adverse effects in bone function and development. *Toxicol. Lett.* **2015**, *236*, 123−130.

(86) Houpert, P.; Frelon, S.; Monleau, M.; Bussy, C.; Chazel, V.; Paquet, F. Heterogeneous accumulation of uranium in the brain of rats. *Radiat. Prot. Dosim.* **2007**, *127*, 86−89.

(87) Aschner, M.; Jiang, G. C. Toxicity studies on depleted uranium in primary rat cortical neurons and in Caenorhabditis elegans: what have we learned? *J. Toxicol. Environ. Health, Part B* **2009**, *12*, 525−539.

(88) Mirderikvand, N.; Mohammadzadeh Asl, B.; Naserzadeh, P.; Shaki, F.; Shokrzadeh, M.; Pourahmad, J. Embryo toxic effects of depleted uranium on the morphology of the mouse fetus. *Iran. J. Pharm. Res.* **2014**, *13*, 199−206.

(89) Auvinen, A.; Salonen, L.; Pekkanen, J.; Pukkala, E.; Ilus, T.; Kurttio, P. Radon and other natural radionuclides in drinking water and risk of stomach cancer: a case-cohort study in Finland. *Int. J. Cancer* **2005**, *114*, 109−113.

(90) Kurttio, P.; Salonen, L.; Ilus, T.; Pekkanen, J.; Pukkala, E.; Auvinen, A. Well water radioactivity and risk of cancers of the urinary organs. *Environ. Res.* **2006**, *102*, 333−338.

(91) Roos, P. M.; Vesterberg, O.; Syversen, T.; Flaten, T. P.; Nordberg, M. Metal concentrations in cerebrospinal fluid and blood plasma from patients with amyotrophic lateral sclerosis. *Biol. Trace Elem. Res.* **2013**, *151*, 159−170.

(92) Arfsten, D. P.; Wilfong, E. R.; Bekkedal, M. Y.; Johnson, E. W.; McInturf, S. M.; Eggers, J. S.; Schaeffer, D. J.; Still, K. R. Evaluation of the effect of implanted depleted uranium (DU) on adult rat behavior and toxicological endpoints. *J. Toxicol. Environ. Health, Part A* **2007**, *70*, 1995−2010.

(93) Abou-Donia, M. B.; Dechkovskaia, A. M.; Goldstein, L. B.; Shah, D. U.; Bullman, S. L.; Khan, W. A. Uranyl acetate-induced sensorimotor deficit and increased nitric oxide generation in the central nervous system in rats. *Pharmacol., Biochem. Behav.* **2002**, *72*, 881−890.

(94) Hao, Y.; Huang, J.; Gu, Y.; Liu, C.; Li, H.; Liu, J.; Ren, J.; Yang, Z.; Peng, S.; Wang, W.; Li, R. Metallothionein deficiency aggravates depleted uranium-induced nephrotoxicity. *Toxicol. Appl. Pharmacol.* **2015**, *287*, 306−315.

(95) Hao, Y.; Liu, C.; Huang, J.; Gu, Y.; Li, H.; Yang, Z.; Liu, J.; Wang, W.; Li, R. Ghrelin protects against depleted uranium-induced apoptosis of MC3T3-E1 cells through oxidative stress-mediated p38-mitogen-activated protein kinase pathway. *Toxicol. Appl. Pharmacol.* **2016**, *290*, 116−125.

(96) Obeid, M. H.; Oertel, J.; Solioz, M.; Fahmy, K. Mechanism of Attenuation of Uranyl Toxicity by Glutathione in Lactococcus lactis. *Appl. Environ. Microbiol.* **2016**, *82*, 3563−3571.

(97) Soltani, M.; Zarei, M. H.; Salimi, A.; Pourahmad, J. Mitochondrial protective and antioxidant agents protect toxicity induced by depleted uranium in isolated human lymphocytes. *J. Environ. Radioact.* **2019**, *203*, 112−116.

(98) Zhou, L.; Bosscher, M.; Zhang, C.; Ozcubukcu, S.; Zhang, L.; Zhang, W.; Li, C. J.; Liu, J.; Jensen, M. P.; Lai, L.; He, C. A protein engineered to bind uranyl selectively and with femtomolar affinity. *Nat. Chem.* **2014**, *6*, 236−241.

(99) Belford, R. L. Paramagnetism of Uranyl Ion. Effect of 6d Orbitals and Pi Bonding. *J. Chem. Phys.* **1961**, *34*, 318−321.

(100) Eisenstein, J. C.; Pryce, M. H. L. The electronic structure and magnetic properties of uranyl-like ions I. Uranyl and neptunyl. *Proc. R. Soc. London* **1955**, *229*, 20−38.

(101) Academic_Software IUPAC SC-Database: A comprehensive database of published data on equilibrium constants of metal complexes and ligands, http://www.acadsoft.co.uk/scdbase/scdbase.htm (accessed Aug, 2021).

(102) Evans, H. T., Jr. Uranyl Ion Coordination. *Science* **1963**, *141*, 154−158.

(103) Lestaevel, P.; Airault, F.; Racine, R.; Bensoussan, H.; Dhieux, B.; Delissen, O.; Manens, L.; Aigueperse, J.; Voisin, P.; Souidi, M. Influence of environmental enrichment and depleted uranium on behaviour, cholesterol and acetylcholine in apolipoprotein E-deficient mice. *J. Mol. Neurosci.* **2014**, *53*, 469−479.

(104) Souidi, M.; Racine, R.; Grandcolas, L.; Grison, S.; Stefani, J.; Gourmelon, P.; Lestaevel, P. Influence of depleted uranium on hepatic cholesterol metabolism in apolipoprotein E-deficient mice. *J. Steroid Biochem. Mol. Biol.* **2012**, *129*, 201−205.

(105) Mutter, J.; Curth, A.; Naumann, J.; Deth, R.; Walach, H. Does inorganic mercury play a role in Alzheimer's disease? A systematic review and an integrated molecular mechanism. *J. Alzheimer's Dis.* **2010**, *22*, 357−374.

(106) Crespo-Lopez, M. E.; de Oliveira, M. A.; Souza-Monteiro, J. R.; Paraense, R. O.; Ribeiro-Dos-Santos, A.; Vieira, J.; Silva, A.; Macchi, B. M.; do Nascimento, J. L. M.; Burbano, R. M. R.; Crespo-Lopez, M. E. Role for apolipoprotein E in neurodegeneration and mercury intoxication. *Front. Biosci., Elite Ed.* **2018**, *10*, 229−241.

(107) Ma, J.; Qian, C.; Bao, Y.; Liu, M. Y.; Ma, H. M.; Shen, M. Q.; Li, W.; Wang, J. J.; Bao, Y. X.; Liu, Y.; Ke, Y.; Qian, Z. M. Apolipoprotein E deficiency induces a progressive increase in tissue iron contents with age in mice. *Redox Biol.* **2021**, *40*, 101865.

(108) Corder, E. H.; Saunders, A. M.; Strittmatter, W. J.; Schmechel, D. E.; Gaskell, P. C.; Small, G. W.; Roses, A. D.; Haines, J. L.; Pericak-Vance, M. A. Gene dose of apolipoprotein E type 4 allele and the risk of Alzheimer's disease in late onset families. *Science* **1993**, *261*, 921−923.

(109) Miyata, M.; Smith, J. D. Apolipoprotein E allele-specific antioxidant activity and effects on cytotoxicity by oxidative insults and beta-amyloid peptides. *Nat. Genet.* **1996**, *14*, 55−61.

(110) Mutter, J.; Naumann, J.; Sadaghiani, C.; Schneider, R.; Walach, H. Alzheimer disease: mercury as pathogenetic factor and apolipoprotein E as a moderator. *Neuroendocrinol. Lett.* **2004**, *25*, 331−339.

(111) Godfrey, M. E.; Wojcik, D. P.; Krone, C. A. Apolipoprotein E genotyping as a potential biomarker for mercury neurotoxicity. *J. Alzheimer's Dis.* **2003**, *5*, 189−195.

(112) Kim, J.; Basak, J. M.; Holtzman, D. M. The role of apolipoprotein E in Alzheimer's disease. *Neuron* **2009**, *63*, 287−303.

(113) Luo, J.; Marechal, J. D.; Wärmländer, S.; Gräslund, A.; Peralvarez-Marin, A. In silico analysis of the apolipoprotein E and the amyloid beta peptide interaction: misfolding induced by frustration of the salt bridge network. *PLoS Comput. Biol.* **2010**, *6*, No. e1000663.

(114) Zhang, Y.; Gao, H.; Zheng, W.; Xu, H. Current understanding of the interactions between metal ions and Apolipoprotein E in Alzheimer's disease. *Neurobiol. Dis.* **2022**, *172*, 105824.

(115) Berntsson, E.; Sardis, M.; Noormägi, A.; Jarvet, J.; Roos, P. M.; Tõugu, V.; Gräslund, A.; Palumaa, P.; Wärmländer, S. K. T. S. Mercury Ion Binding to Apolipoprotein E Variants ApoE2, ApoE3, and ApoE4: Similar Binding Affinities but Different Structure Induction Effects. *ACS Omega* **2022**, *7*, 28924−28931.

(116) Gade Malmos, K.; Blancas-Mejia, L. M.; Weber, B.; Buchner, J.; Ramirez-Alvarado, M.; Naiki, H.; Otzen, D. ThT 101: a primer on the use of thioflavin T to investigate amyloid formation. *Amyloid* **2017**, *24*, 1−16.

(117) Danielsson, J.; Pierattelli, R.; Banci, L.; Gräslund, A. High-resolution NMR studies of the zinc-binding site of the Alzheimer's amyloid beta-peptide. *FEBS J.* **2007**, *274*, 46−59.

(118) Berntsson, E.; Vosough, F.; Svantesson, T.; Pansieri, J.; Iashchishyn, I. A.; Ostojic, L.; Dong, X.; Suman, P.; Jarvet, J.; Roos, P. M.; Barth, A.; Morozova-Roche, L. A.; Gräslund, A.; Wärmländer, S. K. T. S. Residue-specific binding of Ni(II) ions influences the structure and aggregation of amyloid-beta (Aβ) peptides. *Sci. Rep.* **2023**, *13*, 3341.

(119) Ghalebani, L.; Wahlström, A.; Danielsson, J.; Wärmländer, S. K.; Gräslund, A. pH-dependence of the specific binding of Cu(II) and

Zn(II) ions to the amyloid-beta peptide. *Biochem. Biophys. Res. Commun.* **2012**, *421*, 554−560.

(120) Fawzi, N. L.; Ying, J.; Torchia, D. A.; Clore, G. M. Kinetics of amyloid beta monomer-to-oligomer exchange by NMR relaxation. *J. Am. Chem. Soc.* **2010**, *132*, 9948−9951.

(121) Lindgren, J.; Segerfeldt, P.; Sholts, S. B.; Gräslund, A.; Karlström, A. E.; Wärmländer, S. K. Engineered non-fluorescent Affibody molecules facilitate studies of the amyloid-beta (Aβ) peptide in monomeric form: Low pH was found to reduce Aβ/Cu(II) binding affinity. *J. Inorg. Biochem.* **2013**, *120*, 18−23.

(122) Tiiman, A.; Luo, J.; Wallin, C.; Olsson, L.; Lindgren, J.; Jarvet, J.; Per, R.; Sholts, S. B.; Rahimipour, S.; Abrahams, J. P.; Karlström, A. E.; Gräslund, A.; Wärmländer, S. K. T. S. Specific Binding of Cu(II) Ions to Amyloid-Beta Peptides Bound to Aggregation-Inhibiting Molecules or SDS Micelles Creates Complexes that Generate Radical Oxygen Species. *J. Alzheimer's Dis.* **2016**, *54*, 971−982.

(123) Alies, B.; Renaglia, E.; Rozga, M.; Bal, W.; Faller, P.; Hureau, C. Cu(II) affinity for the Alzheimer's peptide: tyrosine fluorescence studies revisited. *Anal. Chem.* **2013**, *85*, 1501−1508.

(124) Pogostin, B. H.; Malmendal, A.; Londergan, C. H.; Akerfeldt, K. S. pKa Determination of a Histidine Residue in a Short Peptide Using Raman Spectroscopy. *Molecules* **2019**, *24*, 405.

(125) Österlund, N.; Kulkarni, Y. S.; Misiaszek, A. D.; Wallin, C.; Krüger, D. M.; Liao, Q.; Mashayekhy Rad, F.; Jarvet, J.; Strodel, B.; Wärmländer, S. K. T. S.; Ilag, L. L.; Kamerlin, S. C. L.; Gräslund, A. Amyloid-beta Peptide Interactions with Amphiphilic Surfactants: Electrostatic and Hydrophobic Effects. *ACS Chem. Neurosci.* **2018**, *9*, 1680−1692.

(126) Österlund, N.; Luo, J.; Wärmländer, S. K. T. S.; Gräslund, A. Membrane-mimetic systems for biophysical studies of the amyloid-beta peptide. *Biochim. Biophys. Acta, Proteins Proteomics* **2019**, *1867*, 492−501.

(127) Gu, M.; Bode, D. C.; Viles, J. H. Copper Redox Cycling Inhibits Aβ Fibre Formation and Promotes Fibre Fragmentation, while Generating a Dityrosine Aβ Dimer. *Sci. Rep.* **2018**, *8*, 16190.

(128) Vazquez, G.; Caballero, A. B.; Kokinda, J.; Hijano, A.; Sabate, R.; Gamez, P. Copper, dityrosine cross-links and amyloid-beta aggregation. *J. Biol. Inorg. Chem.* **2019**, *24*, 1217−1229.

(129) Dong, X.; Svantesson, T.; Sholts, S. B.; Wallin, C.; Jarvet, J.; Gräslund, A.; Wärmländer, S. K. T. S. Copper ions induce dityrosine-linked dimers in human but not in murine islet amyloid polypeptide (IAPP/amylin). *Biochem. Biophys. Res. Commun.* **2019**, *510*, 520−524.

(130) Huggins, T. G.; Wells-Knecht, M. C.; Detorie, N. A.; Baynes, J. W.; Thorpe, S. R. Formation of o-tyrosine and dityrosine in proteins during radiolytic and metal-catalyzed oxidation. *J. Biol. Chem.* **1993**, *268*, 12341−12347.

(131) Barghorn, S.; Nimmrich, V.; Striebinger, A.; Krantz, C.; Keller, P.; Janson, B.; Bahr, M.; Schmidt, M.; Bitner, R. S.; Harlan, J.; Barlow, E.; Ebert, U.; Hillen, H. Globular amyloid β-peptide1-42 oligomer − a homogenous and stable neuropathological protein in Alzheimer's disease. *J. Neurochem.* **2005**, *95*, 834−847.

(132) Vosough, F.; Barth, A. Characterization of Homogeneous and Heterogeneous Amyloid-β42 Oligomer Preparations with Biochemical Methods and Infrared Spectroscopy Reveals a Correlation between Infrared Spectrum and Oligomer Size. *ACS Chem. Neurosci.* **2021**, *12*, 473−488.

(133) Barth, A. Infrared spectroscopy of proteins. *Biochim. Biophys. Acta* **2007**, *1767*, 1073−1101.

(134) Goormaghtigh, E.; Cabiaux, V.; Ruysschaert, J. M. Determination of soluble and membrane protein structure by Fourier transform infrared spectroscopy. III. Secondary structures. *Subcell. Biochem.* **1994**, *23*, 405−450.

(135) Barth, A.; Zscherp, C. What vibrations tell about proteins. *Q. Rev. Biophys.* **2002**, *35*, 369−430.

(136) Cerf, E.; Sarroukh, R.; Tamamizu-Kato, S.; Breydo, L.; Derclaye, S.; Dufrene, Y. F.; Narayanaswami, V.; Goormaghtigh, E.; Ruysschaert, J. M.; Raussens, V. Antiparallel beta-sheet: a signature structure of the oligomeric amyloid beta-peptide. *Biochem. J.* **2009**, *421*, 415−423.

(137) Sarroukh, R.; Goormaghtigh, E.; Ruysschaert, J. M.; Raussens, V. ATR-FTIR: a "rejuvenated" tool to investigate amyloid proteins. *Biochim. Biophys. Acta* **2013**, *1828*, 2328−2338.

(138) Li, H.; Lantz, R.; Du, D. Vibrational Approach to the Dynamics and Structure of Protein Amyloids. *Molecules* **2019**, *24*, 186.

(139) Berntsson, E.; Paul, S.; Vosough, F.; Sholts, S. B.; Jarvet, J.; Roos, P. M.; Barth, A.; Gräslund, A.; Wärmländer, S. K. T. S. Lithium ions display weak interaction with amyloid-beta (Aβ) peptides and have minor effects on their aggregation. *Acta Biochim. Pol.* **2021**, *68*, 169−179.

(140) Wallin, C.; Kulkarni, Y. S.; Abelein, A.; Jarvet, J.; Liao, Q.; Strodel, B.; Olsson, L.; Luo, J.; Abrahams, J. P.; Sholts, S. B.; Roos, P. M.; Kamerlin, S. C.; Gräslund, A.; Wärmländer, S. K. T. S. Characterization of Mn(II) ion binding to the amyloid-beta peptide in Alzheimer's disease. *J. Trace Elem. Med. Biol.* **2016**, *38*, 183−193.

(141) Faller, P.; Hureau, C. Bioinorganic chemistry of copper and zinc ions coordinated to amyloid-beta peptide. *Dalton Trans.* **2009**, 1080−1094.

(142) Faller, P.; Hureau, C.; Berthoumieu, O. Role of metal ions in the self-assembly of the Alzheimer's amyloid-beta peptide. *Inorg. Chem.* **2013**, *52*, 12193−12206.

(143) Król, S.; Österlund, N.; Vosough, F.; Jarvet, J.; Wärmländer, S.; Barth, A.; Ilag, L. L.; Magzoub, M.; Gräslund, A.; Mörman, C. The amyloid-inhibiting NCAM-PrP peptide targets Aβ peptide aggregation in membrane-mimetic environments. *iScience* **2021**, *24*, 102852.

(144) Arnold, P. L.; Patel, D.; Wilson, C.; Love, J. B. Reduction and selective oxo group silylation of the uranyl dication. *Nature* **2008**, *451*, 315−317.

(145) Boulet, B.; Joubert, L.; Cote, G.; Bouvier-Capely, C.; Cossonnet, C.; Adamo, C. Theoretical study of the uranyl complexation by hydroxamic and carboxylic acid groups. *Inorg. Chem.* **2008**, *47*, 7983−7991.

(146) Liu, X.; Cheng, J.; He, M.; Lu, X.; Wang, R. Acidity constants and redox potentials of uranyl ions in hydrothermal solutions. *Phys. Chem. Chem. Phys.* **2016**, *18*, 26040−26048.

(147) Kotler, S. A.; Walsh, P.; Brender, J. R.; Ramamoorthy, A. Differences between amyloid-beta aggregation in solution and on the membrane: insights into elucidation of the mechanistic details of Alzheimer's disease. *Chem. Soc. Rev.* **2014**, *43*, 6692−6700.

(148) Fatafta, H.; Kav, B.; Bundschuh, B. F.; Loschwitz, J.; Strodel, B. Disorder-to-order transition of the amyloid-beta peptide upon lipid binding. *Biophys. Chem.* **2022**, *280*, 106700.

(149) Faller, P. Copper and Zinc Binding to Amyloid-β: Coordination, Dynamics, Aggregation, Reactivity and Metal-Ion Transfer. *Chembiochem* **2009**, *10*, 2837−2845.

(150) Fu, H.; Zhang, H.; Sui, Y.; Hu, N.; Ding, D.; Ye, Y.; Li, G.; Wang, Y.; Dai, Z. Transformation of uranium species in soil during redox oscillations. *Chemosphere* **2018**, *208*, 846−853.

(151) Okur, H. I.; Hladilkova, J.; Rembert, K. B.; Cho, Y.; Heyda, J.; Dzubiella, J.; Cremer, P. S.; Jungwirth, P. Beyond the Hofmeister Series: Ion-Specific Effects on Proteins and Their Biological Functions. *J. Phys. Chem. B* **2017**, *121*, 1997−2014.

(152) Dominguez, A.; Fernandez, A.; Gonzalez, N.; Iglesias, E.; Montenegro, L. Determination of critical micelle concentration of some surfactants by three techniques. *J. Chem. Educ.* **1997**, *74*, 1227−1231.

(153) Rangachari, V.; Moore, B. D.; Reed, D. K.; Sonoda, L. K.; Bridges, A. W.; Conboy, E.; Hartigan, D.; Rosenberry, T. L. Amyloid-β(1−42) Rapidly Forms Protofibrils and Oligomers by Distinct Pathways in Low Concentrations of Sodium Dodecylsulfate. *Biochemistry* **2007**, *46*, 12451−12462.

(154) Glasoe, P. K.; Long, F. A. Use of glass electrodes to measure acidities in deuterium oxide. *J. Phys. Chem.* **1960**, *64*, 188−190.

(155) Edelhoch, H. Spectroscopic determination of tryptophan and tyrosine in proteins. *Biochemistry* **1967**, *6*, 1948−1954.

(156) Anachkov, S. E.; Danov, K. D.; Basheva, E. S.; Kralchevsky, P. A.; Ananthapadmanabhan, K. P. Determination of the aggregation number and charge of ionic surfactant micelles from the stepwise

thinning of foam films. *Adv. Colloid Interface Sci.* **2012**, *183−184*, 55−67.

(157) Danielsson, J.; Andersson, A.; Jarvet, J.; Gräslund, A. 15N relaxation study of the amyloid beta-peptide: structural propensities and persistence length. *Magn. Reson. Chem.* **2006**, *44*, S114−S121.

(158) Roche, J.; Shen, Y.; Lee, J. H.; Ying, J.; Bax, A. Monomeric Aβ$^{1−40}$ and Aβ$^{1−42}$ Peptides in Solution Adopt Very Similar Ramachandran Map Distributions That Closely Resemble Random Coil. *Biochemistry* **2016**, *55*, 762−775.

(159) Yamaguchi, T.; Matsuzaki, K.; Hoshino, M. Transient formation of intermediate conformational states of amyloid-beta peptide revealed by heteronuclear magnetic resonance spectroscopy. *FEBS Lett.* **2011**, *585*, 1097−1102.

(160) Kuzmic, P. *History, Variants and Usage of the "Morrison Equation" in Enzyme Inhibition Kinetics*; BioKin Ltd., 2015. Technical Note TN-2015-01 [Online]. www.biokin.com/TN/2015/01.

(161) Bitan, G.; Fradinger, E. A.; Spring, S. M.; Teplow, D. B. Neurotoxic protein oligomers−what you see is not always what you get. *Amyloid* **2005**, *12*, 88−95.

(162) Baldassarre, M.; Barth, A. Pushing the detection limit of infrared spectroscopy for structural analysis of dilute protein samples. *Analyst* **2014**, *139*, 5393−5399.

Curriculum vitae

Personal data

Name:	Elina Berntsson
Date of birth:	29.03.1993
Place of birth:	Stockholm, Sweden
Citizenship:	Swedish

Contact data

E-mail: elinaberntsson@gmail.com ; ebernt@taltech.ee

Education

2020–2025	Tallinn University of Technology, Estonia, PhD Student
2018–2019	Uppsala University, Sweden, MSC
2015–2018	Uppsala University, Sweden, BSC
2008–2011	High school

Language competence

Swedish	Native
English	Fluent

Professional employment

2019–2020	Research Traineeship, Stockholm University, Sweden
2018–2018	Laboratory Assistant, Karolinska Institute, Sweden

List of publications

Berntsson, E., Sardis, M., Noormägi, A., Jarvet, J., Roos, P. M., Tõugu, V., Gräslund, A., Palumaa, P., & Wärmländer, S. (2022). Mercury Ion Binding to Apolipoprotein E Variants ApoE2, ApoE3, and ApoE4: Similar Binding Affinities but Different Structure Induction Effects. *ACS Omega*, *7*(33), 28924-28931.

Berntsson, E., Vosough, F., Svantesson, T., Pansieri, J., Iashchishyn, I. A., Ostojic, L., Dong, X., Paul, S., Jarvet, J., Roos, P. M., Barth, A., Morozova-Roche, L. A., Gräslund, A., & Wärmländer, S. (2023). Residue-specific binding of Ni(II) ions influences the structure and aggregation of amyloid beta (Abeta) peptides. *Scientific Reports*, *13*(1), 3341.

Noormägi, A., Golubeva, T., **Berntsson, E**., Wärmländer, S., Tõugu, V., & Palumaa, P. (2023). Direct Competition of ATCUN Peptides with Human Serum Albumin for Copper(II) Ions Determined by LC-ICP MS. *ACS Omega*, *8*(37), 33912-33919.

Berntsson, E., Vosough, F., Noormägi, A., Padari, K., Asplund, F., Gielnik, M., Paul, S., Jarvet, J., Tõugu, V., Roos, P. M., Kozak, M., Gräslund, A., Barth, A., Pooga, M., Palumaa, P., & Wärmländer, S. (2023). Characterization of Uranyl (UO(2)(2+)) Ion Binding to Amyloid Beta (Abeta) Peptides: Effects on Abeta Structure and Aggregation. *ACS Chem Neurosci*, *14*(15), 2618-2633.

Berntsson, E., Paul, S., Vosough, F., Sholts, S. B., Jarvet, J., Roos, P. M., Barth, A., Gräslund, A., & Wärmländer, S. (2021). Lithium ions display weak interaction with amyloid-beta (Abeta) peptides and have minor effects on their aggregation. Acta Biochimica Polonica, 68(2), 169-179.

Koski, L., Ronnevi, C., **Berntsson, E**., Wärmländer, S., & Roos, P. M. (2021). Metals in ALS TDP-43 Pathology. International Journal of Molecular Sciences, 22(22).

Paul, S., Jenistova, A., Vosough, F., **Berntsson, E**., Mörman, C., Jarvet, J., Gräslund, A., Wärmländer, S., & Barth, A. (2023). (13)C- and (15)N-labeling of amyloid-beta and inhibitory peptides to study their interaction via nanoscale infrared spectroscopy. Commun Chem, 6(1), 163.

Koski, L., **Berntsson, E**., Vikström, M., Wärmländer, S., & Roos, P. M. (2023). Metal ratios as possible biomarkers for amyotrophic lateral sclerosis. J Trace Elem Med Biol, 78, 127163.

Lakela, A., **Berntsson, E**., Jarvet, J., Gräslund, A., Wärmländer, S. (2024). Secondary structures of human calcitonin at different temperatures and in different membrane-mimicking environments, characterized by circular dichroism (CD) spectroscopy. *Accepted for publication in ACS Omega.*

Lakela, A., **Berntsson, E**., Vosough, F., Jarvet, J., Paul, S., Barth, A., Gräslund, A., Roos, P., Wärmländer, S. (2024). Molecular interactions, structural effects, and binding affinities between silver ions (Ag$^+$) and amyloid beta (Aβ) peptides. *Accepted for publication in Scientific Reports*.

Elulookirjeldus

Isikuandmed

Nimi:	Elina Berntsson
Sünniaeg:	29.03.1993
Sünnikoht:	Stockholm, Rootsi
Kodakondsus:	Rootsi

Kontaktandmed

E-post: elina.berntsson@dbb.su.se ; ebernt@taltech.ee

Hariduskäik

2020–2025	Tallinna Tehnikaülikool, PhD
2018–2019	Uppsala Ülikool, MSC
2015–2018	Uppsala Ülikool, BSC
2008–2011	Keskharidus

Keelteoskus

Rootsi keel	emakeel
Inglise keel	kõrgtase

Teenistuskäik

2019–2020	Praktikant, Stockholmi Ülikool, Rootsi
2018–2018	Laborant, Karolinska instituut, Rootsi

Publikatsioonid

Berntsson, E., Sardis, M., Noormägi, A., Jarvet, J., Roos, P. M., Tõugu, V., Gräslund, A., Palumaa, P., & Wärmländer, S. (2022). Mercury Ion Binding to Apolipoprotein E Variants ApoE2, ApoE3, and ApoE4: Similar Binding Affinities but Different Structure Induction Effects. *ACS Omega*, *7*(33), 28924-28931.

Berntsson, E., Vosough, F., Svantesson, T., Pansieri, J., Iashchishyn, I. A., Ostojic, L., Dong, X., Paul, S., Jarvet, J., Roos, P. M., Barth, A., Morozova-Roche, L. A., Gräslund, A., & Wärmländer, S. (2023). Residue-specific binding of Ni(II) ions influences the structure and aggregation of amyloid beta (Abeta) peptides. *Scientific Reports*, *13*(1), 3341.

Noormägi, A., Golubeva, T., **Berntsson, E**., Wärmländer, S., Tõugu, V., & Palumaa, P. (2023). Direct Competition of ATCUN Peptides with Human Serum Albumin for Copper(II) Ions Determined by LC-ICP MS. *ACS Omega*, *8*(37), 33912-33919.

Berntsson, E., Vosough, F., Noormägi, A., Padari, K., Asplund, F., Gielnik, M., Paul, S., Jarvet, J., Tõugu, V., Roos, P. M., Kozak, M., Gräslund, A., Barth, A., Pooga, M., Palumaa, P., & Wärmländer, S. (2023). Characterization of Uranyl (UO(2)(2+)) Ion Binding to Amyloid Beta (Abeta) Peptides: Effects on Abeta Structure and Aggregation. *ACS Chem Neurosci*, *14*(15), 2618-2633.

Berntsson, E., Paul, S., Vosough, F., Sholts, S. B., Jarvet, J., Roos, P. M., Barth, A., Gräslund, A., & Wärmländer, S. (2021). Lithium ions display weak interaction with amyloid-beta (Abeta) peptides and have minor effects on their aggregation. Acta Biochimica Polonica, 68(2), 169-179.

Koski, L., Ronnevi, C., **Berntsson, E**., Wärmländer, S., & Roos, P. M. (2021). Metals in ALS TDP-43 Pathology. International Journal of Molecular Sciences, 22(22).

Paul, S., Jenistova, A., Vosough, F., **Berntsson, E**., Mörman, C., Jarvet, J., Gräslund, A., Wärmländer, S., & Barth, A. (2023). (13)C- and (15)N-labeling of amyloid-beta and inhibitory peptides to study their interaction via nanoscale infrared spectroscopy. Commun Chem, 6(1), 163.

Koski, L., **Berntsson, E**., Vikström, M., Wärmländer, S., & Roos, P. M. (2023). Metal ratios as possible biomarkers for amyotrophic lateral sclerosis. J Trace Elem Med Biol, 78, 127163.

Lakela, A., **Berntsson, E**., Jarvet, J., Gräslund, A., Wärmländer, S. (2024). Secondary structures of human calcitonin at different temperatures and in different membrane-mimicking environments, characterized by circular dichroism (CD) spectroscopy. *Accepted for publication in ACS Omega.*

Lakela, A., **Berntsson, E**., Vosough, F., Jarvet, J., Paul, S., Barth, A., Gräslund, A., Roos, P., Wärmländer, S. (2024). Molecular interactions, structural effects, and binding affinities between silver ions (Ag$^+$) and amyloid beta (Aβ) peptides. *Accepted for publication in Scientific Reports*.